Order Number 9402449

Modes of nonlinear optical fibers

Hassan, Mohamed Adel, Ph.D.

King Fahd University of Petroleum and Minerals (Saudi Arabia), 1993

U·M·I
300 N. Zeeb Rd.
Ann Arbor, MI 48106

MODES OF NONLINEAR OPTICAL FIBERS

BY

Mohamed Adel Hassan

A Thesis Presented to the

FACULTY OF THE COLLEGE OF GRADUATE STUDIES

KING FAHD UNIVERSITY OF PETROLEUM & MINERALS

DHAHRAN, SAUDI ARABIA

In Partial Fulfillment of the
Requirements for the Degree of

DOCTOR OF PHILOSOPHY

In

Electrical Engineering

January 1993

KING FAHD UNIVERSITY OF PETROLEUM AND MINERALS

DHAHRAN 31261, SAUDI ARABIA

COLLEGE OF GRADUATE STUDIES

This Dissertation, written by **Mohamed Adel Hassan Hassan Aly,** under the direction of his Dissertation Advisor and approved by his Dissertation Committee, has been presented to and accepted by the Dean of the College of Graduate Studies, in partial fulfillment of the requirements for the degree of **DOCTOR OF PHILOSOPHY DEGREE** in **ELECTRICAL ENGINEERING.**

Dissertation Committee

S. Bader

Dr. Samir J. Al-Bader (Chairman)

Dr. Samir H. Abdul-Jauwad (Member)

Essam E. M. Hassan

Dr. Essam E. M. Hassan (Member)

Dr. Hussain A. Jamid (Member)

Mohamad A. Chaudary 15-5-93

Dr. Mohamad A. Chaudary (Member)

15-5-93

Department Chairman

Dean, College of Graduate Studies

Date 16-5-93

Dedicated to the memory

of my parents

ACKNOWLEDGEMENT

All praises and thanks be to the Almighty, Allah who blessed me with courage and wisdom to accomplish this research work.

I greatly owe my success to my beloved family, my wife, son, daughter, brother and sisters for their patience, encouragement and continuous prayers.

Acknowledgement is due to King Fahad University of Petroleum and Minerals and the department of electrical engineering for supporting this work.

I wish to express my deep appreciation to Dr. Samir J. Al-Bader, my advisor for his patience, careful attention, advice, guidance and continuous help.

My thanks and appreciation extend to Dr. Hussain A. Jamid, thesis committee member for his valuable assistance and suggestions during the study. I am also grateful to the other thesis committee members Dr. samir H. Abdul-Jauwad, Dr. Essam E. M. Hassan and Dr. Mohamed A. Chaudary for their support and helpful suggestions.

Thanks are also due to Mr. M. Imtar, King Faisal University, for writing the computer subroutines used for evaluating Bessel's functions.

Last, but of course not least, I am sincerely grateful to all my colleagues and friends who enriched me with moral support, inspiration and motivation.

TABLE OF CONTENTS

LIST OF FIGURES

LIST OF TABLES

DISSERTATION ABSTRACT

FULL NAME OF STUDENT: Mohamed Adel Hassan Hassan Aly

TITLE OF STUDY: Modes of Nonlinear Optical Fibers

MAJOR FIELD: Electrical Engineering

DATE OF DEGREE: January 1993

The research work presented in this thesis solves the nonlinear wave equation for electromagnetic fields and finds the guided modes in the nonlinear optical fiber. The nonlinear materials in optoelectronics are characterized by dielectric constants which are functions of the light intensity. The dispersion characteristics of the nonlinear fiber are accordingly functions of the light intensity. The solution of the problem has been carried out using a multilayer numerical approach in which the nonlinear wave equation is piecewise linearized by dividing the fiber into a large number of layers. In each layer the local field is determined and used to evaluate the dielectric constant of that layer. The dispersion relations, field profiles and dielectric constant distributions have been evaluated for different types of polarization including TE, TM and hybrid modes. Two waveguide structures have been considered for which either the core or cladding material is taken to be nonlinear while the other is linear. The nonlinear fiber results have been checked against the linear ones in the limiting cases of very low and very high power. Another numerical scheme based on a self-consistent solution of electromagnetic field, has also been used to confirm the results obtained using the multilayer scheme. The stability of the nonlinear guided modes has been discussed based on the resultant .dispersion relations. The recursive scheme has also been used to study the metal-clad optical fiber consisting of two, three or four layers. The attenuation characteristics of these fiber structures have been found. These results are relevant in the design of mode filters and fiber polarizers.

DOCTOR OF PLILOSOPHY DEGREE

KING FAHD UNIVERSITY OF PETROLEUM AND MENIRALS

Dhahran, Saudi Arabia

January 1993

خلاصة الرسالة

إسم الطالب الكامل : محمد عادل حسن حسن علي

عنوان الدراســـــة : الأنماط الموجية في الألياف البصرية غير الخطية

التخصـــــــــص : هندسة كهربائية

تاريـــخ الشـــهادة : ينايـــر ١٩٩٣م

يتناول البحث المقدّم في هذه الرسالة حل المعادلة الموجية الغير خطية للمجالات الكهرومغناطيسية وإيجاد الأنماط الموجية داخل الألياف البصرية غير الخطية .

إن المواد غير الخطية المستخدمة في الإلكترونيات البصرية تتميز بمعامل إنكسار ضوئي يعتمد على شدة الضوء المار في تلك المواد ، وعليه فإن الخواص الموجية للألياف البصرية المصنوعة من تلك المواد تكون أيضاً معتمدة على شدة الضوء المار داخل هذه الألياف البصرية . إن طريقة الحل المستخدمة تعتمد على تقسيم أحد هذه الألياف البصرية إلى عدد كبير من الطبقات التي تختلف فيها شدة الضوء ثم تستخدم شدة الضوء المحسوبة لكل طبقة لإيجاد معامل الإنكسار الخاص بهذه الطبقة، ومن ثم يتم تحويل المعادلة الموجية غير الخطية إلى معادلة موجية خطية تختلف من طبقة إلى أخرى تبعاً لاختلاف معامل الإنكسار الضوئي ، هذه المعادلات الخطية يمكن حلها بالطرق المعروفة .

لقد تم إيجاد وحساب الخواص الموجية وتوزيعات شدة الضوء المار في الألياف البصرية وكذلك تغير معامل الإنكسار داخل هذه الألياف نتيجة لإعتماده اللاخطي على شدة الضوء . وقد غطت الدراسة الأنواع المختلفة للموجات الكهرومغناطيسية في قوائد الموجات الإسطوانية والتي تشمل الموجات ذات إستقطاب المجال الكهربي وأخرى ذات إستقطاب المجال المغناطيسي وثالثة مختلطة الإستقطاب . وقد شملت الدراسة نموذجين مختلفين لقوائد الموجات غير الخطية يكون في إحداها مادة اللب لقائد الموجات غير خطية بينما مادة الغطاء المحيط خطية . وفي النموذج الآخر يكون اللب مصنوعاً من مادة خطية بينما الغطاء المحيط من مادة غير خطية .

هذا وقد تم تحقيق النتائج المستنبطة بإستخدام طريقة رقمية أخرى للحل تعتمد على التطابق الذاتي للمجالات الكهرومغناطيسية . وقد ساعدت النتائج المستنبطة للخواص الموجية في تحديد مدى إستقرارالموجات أثناء إنتشارها داخل الألياف البصرية غير الخطية . وقد تم أيضاً إستخدام نموذج الحل التتابعي متعدد الطبقات في دراسة قوائد الموجات الإسطوانية المغطاة خارجياً بطبقة من المعدن والمكونة من طبقتين أو ثلاث أو أربع طبقات . ومن المعروف أن لقوائد الموجات هذه أهمية خاصة في تصميم مرشحات الموجات الأحادية الإستقطاب .

درجة الدكتوراه في الفلسفة

جامعة الملك فهد للبترول والمعادن

الظهران - المملكة العربية السعودية

يناير ١٩٩٣م

CHAPTER 1

NONLINEAR SLAB AND CYLINDRICAL WAVEGUIDES

1.1 INTRODUCTION

The nonlinear effects in optical fibers and dielectric waveguides have received a growing interest in the last two decades. The nonlinear guided and surface waves have been investigated in many different respects particularly in planar waveguides.

A complete study of nonlinear phenomena in optical fibers and fiber devices requires the solution of nonlinear wave equations subject to the appropriate boundary conditions.

For the slab waveguide, the nonlinear wave equation in rectangular coordinates can be solved analytically for certain types of nonlinearities such as the Kerr-like nonlinearity. However, in fibers there have been no analytical solutions of the nonlinear wave equation and numerical techniques must be used to find the solution.

The research work proposed here uses a multilayered technique for solving nonlinear optical fiber problems. The nonlinearity under

consideration will be the third order Kerr-like nonlinearity with a single frequency input and a single frequency output. The saturation limit of the dielectric constant will also be considered.

The applications of nonlinear optical effects and nonlinear guided waves have been shown to cover wave mixing process, harmonic generation, parametric amplification, self-focusing, self-defocusing and a wide range of devices including bistable switches, logic gates, optical limiters, bandpass power filters, periodic structures, and optical filters.

In this thesis, we are interested in the guided modes of optical fibers. A considerable part of the recent work in guided waves is now directed to study the nonlinear fiber. The nonlinear fiber may be one of the three configurations, linear core-nonlinear cladding, nonlinear core-linear cladding or nonlinear core-nonlinear cladding.

In the following sub-sections we will study the research work related to the nonlinear guided waves in optical fibers as well as in slab waveguides. It can be shown that some of the nonlinear dispersion characteristics are common in both fiber and slab waveguide. The field distributions will also be investigated for both cases. The multi-layer technique adopted in this thesis is not only applicable to the nonlinear waveguide problems, but it is also applicable to any arbitrary refractive index profile. Thus it can be used to solve graded-index profiles and waveguide structures that involve a metallic

layer as the outer layer. In chapter 4 of this thesis an extensive work has been done to study the attenuation characteristics of metal-clad cylindrical waveguide. The objective of such a study is to check the recursive scheme in complicated waveguide structures and at the same time to report some of the important attenuation characteristics of cylindrical metal-clad waveguide. These attenuation characteristics have not been studied in literature as will be seen in chapter 4.

It can be seen from the literature review of section 1.3 that the nonlinear optical fiber has not been investigated in full, specially when the nonlinearity is of saturable type which is more practical and realistic than the Kerr nonlinearity. The research study presented in this thesis is devoted to the investigation of guided modes in nonlinear cylindrical waveguide. The nonlinearity of the waveguide media is considered of saturable type. There are two different structures of the nonlinear optical fiber. The first one consists of a nonlinear core and a linear cladding while the second structure is formed of a linear core and a nonlinear cladding. TE, TM and hybrid modes are to be studied in the proposed work. In the case of the fundamental HE_{11} mode all the six field components are utilized by the recursive scheme. It is thus considered more rigorous than those used in literature which involve the use of linearly polarized modes. In such LP approximation the problem reduces to only three field components and can

be treated using the recursive scheme in a manner similar to the TE modes.

The solution of the problem is carried out numerically using two different numerical schemes. The first scheme is a multilayer one in which the nonlinear fiber is divided into a large number of linear sub-layers. In each layer the wave equation is solved linearly by considering the effect of the local field on the dielectric constant. The second scheme is, however, based on the self-consistent behavior of electromagnetic fields. In this approach the solution of the nonlinear wave equation is obtained through a successive number of solutions for a linear graded-index profile problem. The two scheme will be explained in details in chapter 3.

1.2 THE NONLINEAR SLAB WAVEGUIDE

The nonlinear effects in slab waveguides have received a large attention in the last few years. Because our main objective is to study nonlinear guided modes in fibers, we will only concentrate on the relevant slab work which serves our purpose. In 1987, Al-Bader and Jamid [1] studied the nonlinear TE waves in a nonlinear thin film. The waveguide structure consists of a nonlinear self-focusing film cladded in both sides by linear media. The TE wave dispersion relations have been obtained for both symmetric and asymmetric solutions. Both Kerr and saturable nonlinearities were considered. The saturation limit has been considered in [1] for the first time. The research work preceding [1] accounts only for Kerr-nonlinearity.

The dispersion characteristics are shown in fig.(1.1a). The symmetric solutions (broken lines) show a multivalued dependence of the effective index on surface intensity. This is the case for relatively high saturation levels. This is an important feature of nonlinear guided waves. For low saturation levels the dependence of the effective index on surface intensity is monotonic. Only the fundamental TE mode has been studied. The relation between guided power and effective index has also been obtained for different saturation levels, as shown in fig.(1.1b). In this figure all curves start at the same asymptotic line which corresponds to the minimum value of the effective index. The field distribution corresponding to these dispersion characteristics are evaluated. The problem of Kerr nonlinearity has been solved analytically and numerically. The two solutions are consistent. For the saturable nonlinearity there is no analytical solutions available and only the numerical technique is used.

The TM polarized waves in a nonlinear thin film bounded by linear media is investigated in [2]. A multilayered scheme is introduced to study the problem. The nonlinear medium is divided into a large number of layers. Each layer is characterized by an isotropic linear dielectric constant. The value of the dielectric constant is determined from the information of the field distribution of the previous layer. Therefore, the nonlinear wave equation is treated for each layer as a linear wave equation with the dielectric constant calculated locally from the field information. A similar recursive multilayered

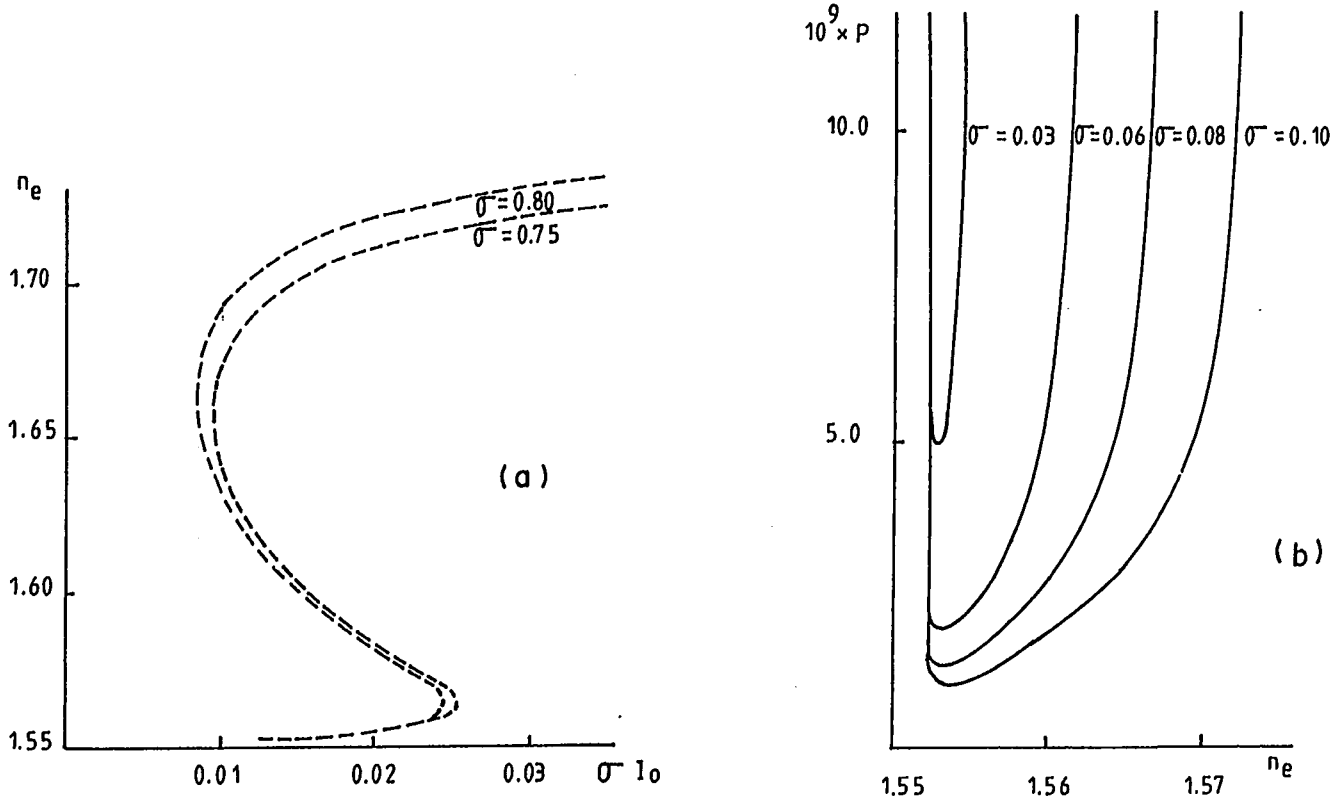

Fig.(1.1)
a) Mode index versus surface intensity for two saturation levels
b) Mode index versus guided power for four saturation levels [1] .

scheme is used to study the nonlinear fiber in our proposed work.

It must be noted that most of the research work in nonlinear guided waves has been devoted to the Kerr nonlinearity in which the dielectric constant is given by:

$$\varepsilon = \varepsilon_{bg} + \alpha|E|^2 \qquad (1.1)$$

Where ε_{bg} is the background dielectric constant with no field applied, α is the nonlinear coefficient of the material and $|E|^2$ is the local field intensity. The kerr model is relatively simple to analyse and the problem with Kerr nonlinearity can be solved analytically for some cases [2].

However, this model is not realistic. The nonlinear material always responds to the applied field up to a certain limit. Any further increase in the applied field will not affect the value of the dielectric constant. It may cause a complete breakdown of the dielectric material. The use of a saturable dielectric function is a result of this fact. The saturable expressions of the dielectric materials are more realistic and based on the fact that the dielectric function cannot grow indefinitely but must level off at a maximum value that depends on the nature of the nonlinear material. Two models have been shown in [3] as follows:

$$\varepsilon = \varepsilon_{bg} + \frac{\alpha|E|^2}{1+g\alpha|E|^2} \tag{1.2}$$

$$\varepsilon = \varepsilon_{bg} + \frac{1}{g}(1-e^{-\alpha|E|^2}) \tag{1.3}$$

where the maximum increase in the dielectric function is equal to $\frac{1}{g}$ for an infinitely intense field. These two models of saturation have also been used in [1].

The dispersion relations for the fundamental TM mode are obtained in terms of the mode index versus both guided power and surface intensity. They are shown in figs. (1.2.a) and (1.2.b) respectively. For low values of saturation level the mode index is a monotonic function of the intensity. For the Kerr nonlinearity and high level of saturation the relation is generally a multivalued i.e. for the same value of surface intensity there are two values of the effective index.

In the above citations we have considered one configuration of nonlinear planar waveguide in which the nonlinear thin film is surrounded on both sides by linear media. Another important nonlinear planar waveguide structure has been given by Sang-Yang Shin et al. [4] in 1989. This

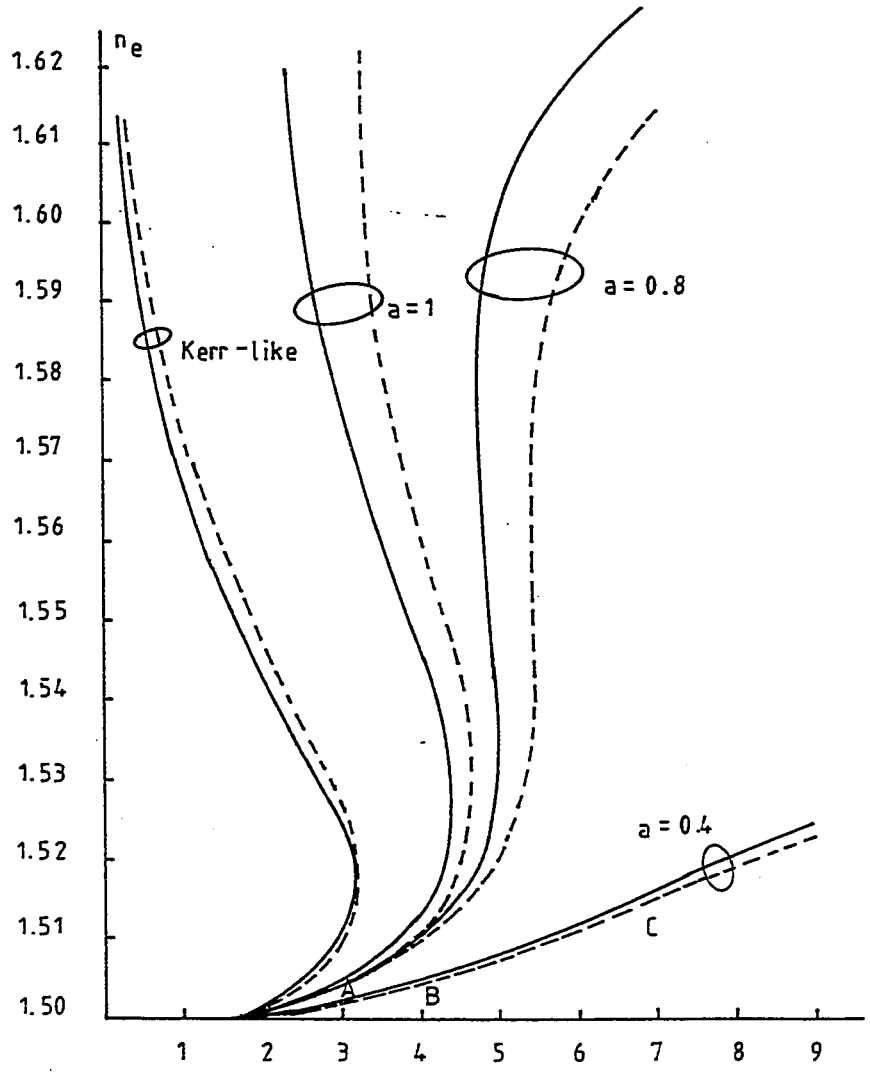

Fig.(1.2.a) The dispersion characteristic as a plot of n_e versus scaled intensity for different saturation levels. Solid lines, the nonlinearity due to thermal effect. Broken lines, the nonlinearity due to electronic distortion [2] .

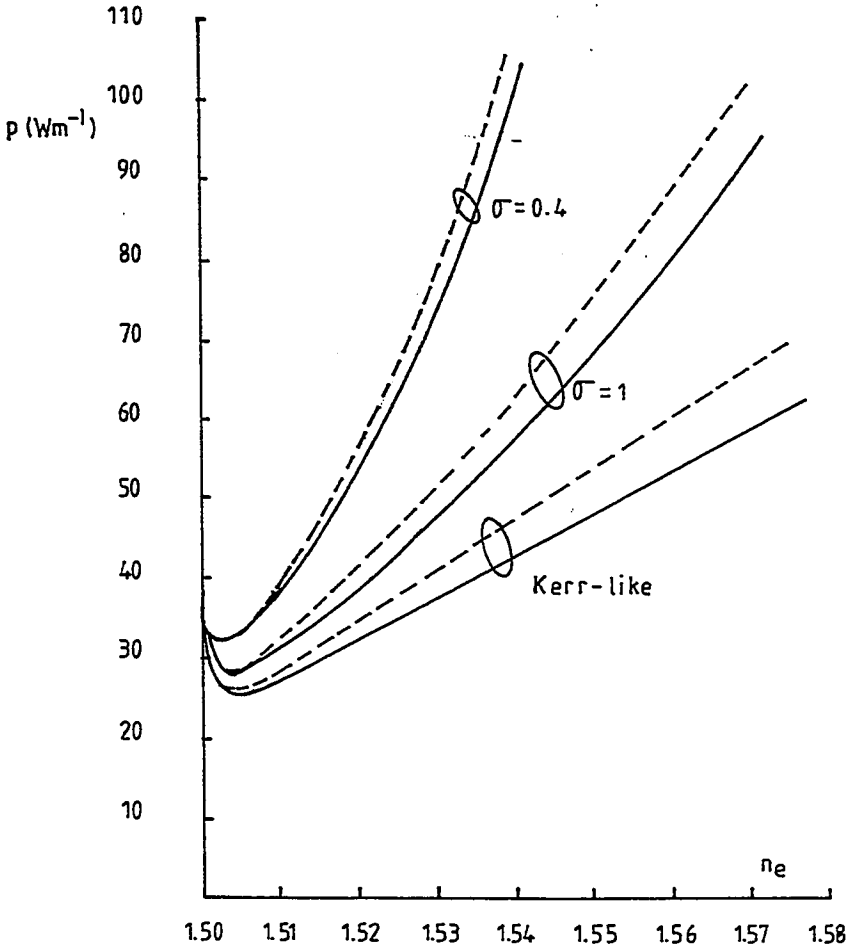

Fig.(1.2.b) The dispersion characteristic as a plot of n_e versus guided power for different saturation levels. Solid lines for, the nonlinearity due to thermal effect. Broken lines, the nonlinearity due to electronic distortion [2] .

waveguide consists of two parallel dielectric thin films separated by a layer of linear medium and bounded on both sides by a nonlinear Kerr medium. It is therefore considered a five layers structure forming a nonlinear directional coupler. In the nonlinear directional coupler the coupling between the two waveguide channels is controlled by the input power. This has an important application in the design of optical logic gates.

The technique of solution used in [4]. is based on integrating the wave equation in the nonlinear regions and imposing the condition that the transverse field vanishes at infinity. The wave equation in the nonlinear region is solved directly in terms of trigonometric functions. The solutions are then matched at each interface to obtain the propagation constant and the corresponding field profiles.

The dispersion characteristics for this directional coupler are shown in fig.(1.3.a) for a structure similar to that described above and in fig.(1.3.b) for a different structure in which one of the nonlinear outer layers is replaced by a linear medium. Figure (1.3.a) shows that both TE_0 and TE_1 modes have two solutions, symmetric and asymmetric. For the symmetric solution The field distribution has even symmetry with respect to the axis of the waveguide. At low power there are two field maxima, one in each guiding film. This is the linear state of the problem. As the power increases, each maximum moves towards the adjacent nonlinear interface. A further increase of the

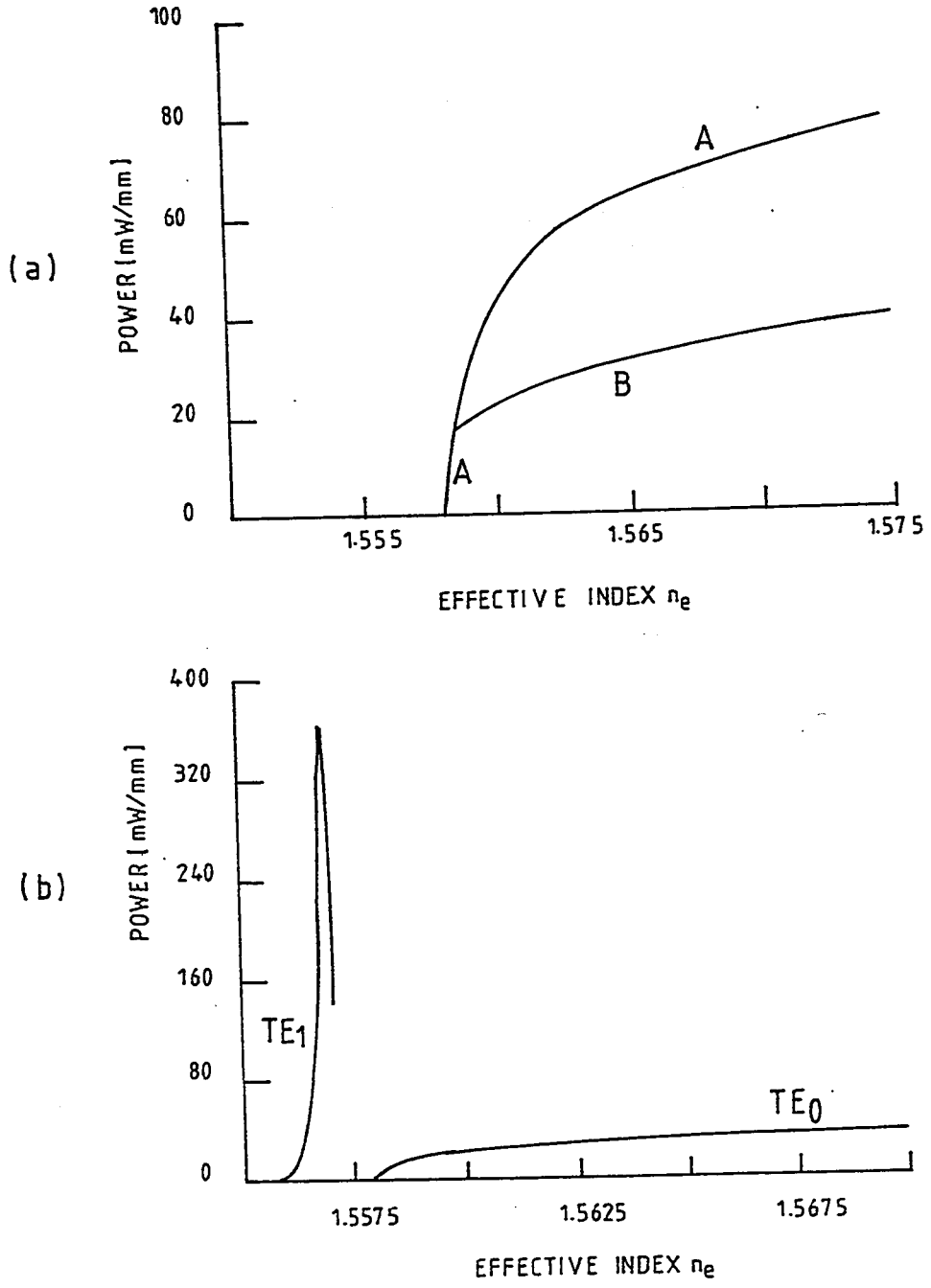

Fig.(1.3)
a) The power- n_e diagram for TE_0 nonlinear guided mode in a symmetric nonlinear coupled waveguide. Branch A, symmetric solution. Branch B, asymmetric solution.
b) The power- n_e diagram for TE_0 and TE_1 wave solutions in a nonlinear coupled waveguide [4] .

power forces these maxima to cross the interface and lie in the nonlinear regions. The dispersion relations shown in fig.(1.3.b) exhibits a peak power for TE_1 mode at a certain value of effective index. for the TE_0 the effective index varies monotonically with the power.

1.3 THE NONLINEAR FIBER

The work done to study wave propagation in nonlinear optical fibers is limited. The reason for this is that the theoretical analysis is difficult compared to the slab waveguide. The solution of the optical fiber problems in cylindrical coordinates system involves the use of Bessel functions which are more complicated compared to the trigonometric functions resulting from the solution of the slab waveguide problems. The simplest structure of a nonlinear fiber consists of two layers, a core and an unlimited cladding. Three configurations are considered, nonlinear core - linear cladding, linear core - nonlinear cladding and nonlinear core - nonlinear cladding. With the availability of fast computers and efficient numerical techniques, those analytical difficulties can be overcome.

1.3.1 Fiber with nonlinear core and linear cladding

The first attempt to find the modes of nonlinear cylindrical waveguides has been carried out by Garmire et al. in 1964 [5]. The wave equation with a nonlinear Kerr term is solved numerically for a single medium in cylindrical

coordinates. The conventional waveguide which has a core and a cladding is not treated here. The waveguide structure consists of unlimited core. The self-focusing action and the beam diameter will determine the physical dimension of the waveguide. The work in this reference is devoted to self-trapping of optical beam. The self trapping is a state in which the effects of self-focusing and scattering balance each other under a certain critical value of the applied power. This will be discussed in more details in chapter 2. The field profile for this waveguide resembles the fundamental LP mode of an optical fiber. It has a peak intensity at the beam axis and decays in the radial direction.

This work was followed by another investigation by Haus et al. in 1966, which includes the higher order modes [6]. The first five modes are analysed numerically. The field distributions corresponding to these modes have been evaluated and plotted. These field profiles exhibit self-focused rings. The number of rings is less than the radial mode number by one. For example, the fifth order mode has four self-focusing rings.

The chromatic dispersion of a nonlinear fiber has been investigated in [7] by Okamoto and Marcatili in 1989. The term chromatic dispersion refers to the dependence of the group velocity on the optical frequency. It arises from the interaction of an electromagnetic wave with the bound electrons of the dielectric [8]. Chromatic dispersion is used to determine the chirping

properties of an optical pulse. Pulses at different wavelengths propagate at different speeds inside the fiber because of the group velocity mismatch.

The chromatic dispersion characteristics are closely related to the index profile and hence they are expected to be different from linear fiber. The technique used in [7] is based on solving the nonlinear wave equation using a variational method. Two values of the total power flow have been chosen to represent the linear and nonlinear states of the fiber. These values are 1 mW and 200 KW respectively. The dispersion relations for the nonlinear fiber are compared to those of the linear fiber. The wave equation is assumed to have a Kerr nonlinearity and the fiber is considered circularly symmetric with no azimuthal dependence. The analysis is therefore an approximate one valid only for weakly guiding fibers. The scheme used in [7] divides the fiber into a nonlinear region, surrounding the core and spreading over a radial distance D equals five times the core radius, and a linear region for the radial distance greater than D . The nonlinear region is subdivided into N subregions. The finite element method is used to find the solution of this part. The solution of the linear region is given in terms of modified Bessel function.

The dispersion characteristics obtained in [7] as a plot of the normalized propagation constant versus the fiber V number have only a slight difference between the linear and the nonlinear waveguides shown in fig (1.4). For the

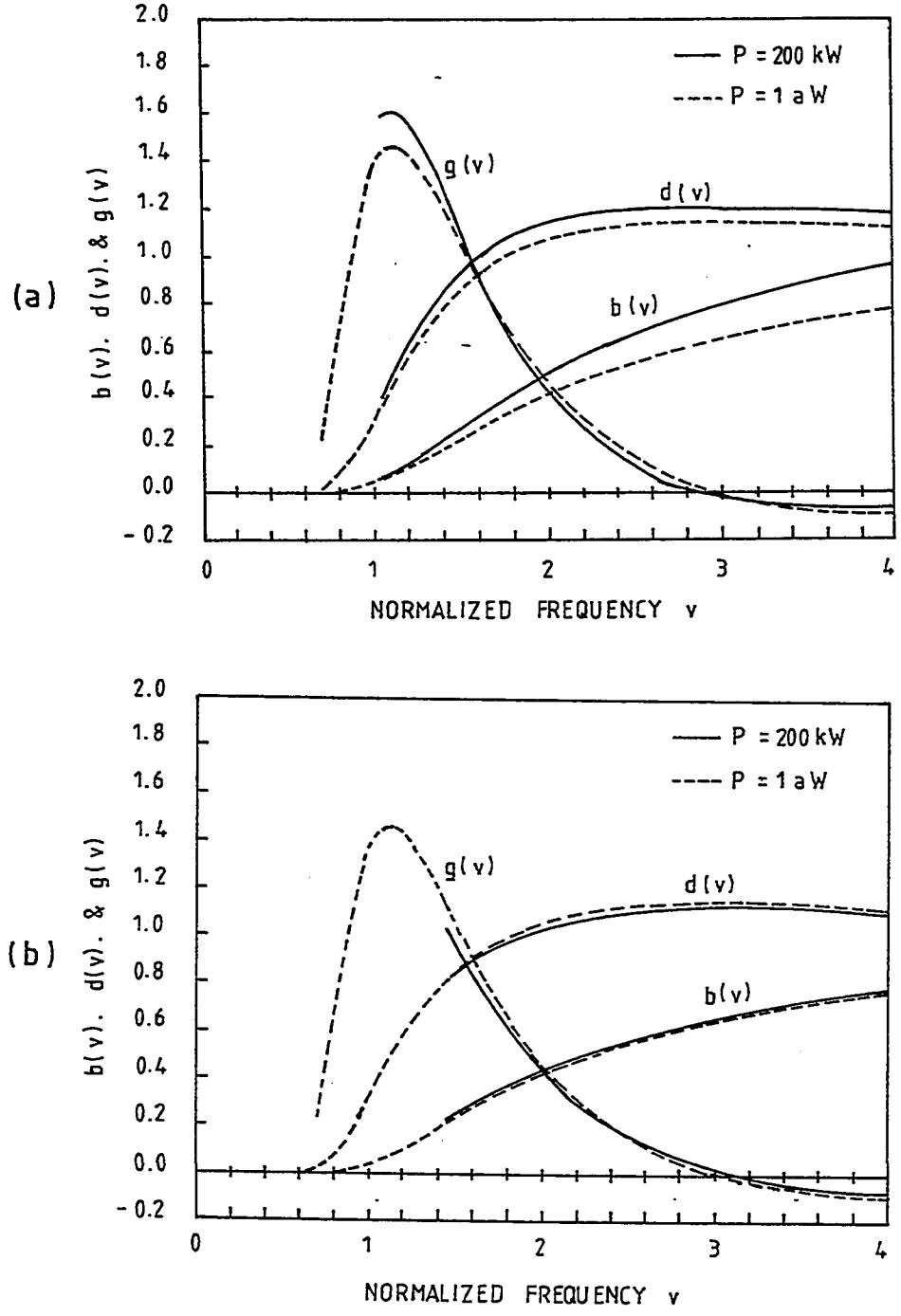

Fig.(1.4)
a) Dispersion characteristics of step-index fiber with core nonlinearity.
b) Dispersion characteristics of step-index fiber with cladding nonlinearity.
b(v) is the normalized propagation constant, d(v) is the normalized group delay and g(v) is the waveguide dispersion [7] .

nonlinear fiber with nonlinear core and linear cladding, the nonlinear propagation constant is relatively greater than the corresponding linear case for the same V number.

1.3.2 Fiber with linear core and nonlinear cladding

The case of linear core and nonlinear cladding is treated by Boardman et al. [9] in 1986. The field solutions for the fundamental mode HE_{11} are obtained from the scaler wave equation with no azimuthal dependence for a radially symmetric fiber. A new class of radially symmetric waves is reported. This class of waves creates self-focusing rings of energy flowing parallel to the fiber axis.

The investigation is done for the Kerr nonlinearity where the nonlinear cladding is assumed to have a refractive index of the form $n = n_c + \alpha|E|^2$. The wave equation used for this investigation is simplified representing only the weakly guiding fiber. The modes of such a fiber are linearly polarized. The linearly polarized (LP) modes are characterized by an electric field vector pointing in one direction in the transverse plane and a magnetic field vector perpendicular to that direction. The axial components are neglected with respect to the transverse component. Therefore LP modes are similar to TEM waves in parallel plates transmission lines. If the nonlinear term added to the dielectric constant is very small compared to the the background

value, the LP approximations can be used to solve the wave equation and find the nonlinear guided modes. On the other hand if the nonlinear term is relatively high, a complete rigorous solution of the wave equation should be obtained.

The important conclusion of this work is that unlike the linear fiber the field can have a maximum which takes place in the nonlinear region. Also the mode index can exceed the core value. For this case the guided waves are transformed into surface waves. The stability of these nonlinear waves is given in terms of the slope of the power versus mode index curve. If the slope is positive the solution is stable. If it is negative the solution needs more investigation to decide about its stability.

Akhamdiev et al. have investigated the linear cylindrical waveguide surrounded by nonlinear medium [10] in 1985. Only TE modes have been reported. The nonlinearity of the cladding is also Kerr-like with dielectric constant of the form $\varepsilon = \varepsilon_0 + \alpha|E|^2$. It has been shown in [10] that the dispersion relations as a plot of the energy flux versus the normalized mode index for this fiber configuration behave as an N curve. This means that for a single value of the field intensity there are three values for the mode index. For higher modes we may have more than one N curve depending on the mode number. Also for this investigation the nonlinearity has been assumed not to have a saturation limit i.e., Kerr-like nonlinearity.

An important observation here is that the nodes of the solution which represent the crossings of the field profile to the fiber axis can go beyond the core of the waveguide. This is a unique characteristic of the nonlinear waveguide and has no linear counterpart The technique of solution used in [10] is based on solving Maxwell's equations for the linear core in terms of Bessel functions and finding the solution of the wave equation for the nonlinear cladding using numerical methods. The boundary conditions are matched at the core cladding interface. The investigation also covers the case when the dielectric constant of the waveguide is smaller than or equal to the linear cladding value. In the linear sense, waveguide modes do not exist in such fiber configuration. In a linear waveguide, guidance takes place only if the core refractive index is greater than the cladding refractive index which can fulfill the condition for total internal reflection. However, for a nonlinear surrounding medium, waveguide modes exist only for values of power greater than a certain threshold. The main conclusion shows that a cylindrical waveguide immersed in a medium with a nonlinear permittivity has some important characteristics, in particular the multi-valued dependence of optical power on effective index. This nonlinear waveguide is used in the design of switches in optical communication devices, where the light intensity is used to switch the fiber between two guiding states or between a cutoff and a guiding state.

The waveguide of linear core and nonlinear cladding has also been studied by Akhmediev et al. in 1990 [11]. The dielectric function in [11] can account for both saturable and nonsaturable nonlinearities. To the best of our knowledge this is the first time a saturable dielectric is treated in optical fiber beside the ordinary Kerr nonlinearity. Two solutions are obtained, symmetrical and asymmetrical. For the asymmetrical solution the field distributions have no axial symmetry. The asymmetrical solutions occur only for values of effective index greater than a minimum value n_0. Below this value only the symmetric solutions exist. Above n_0 the asymmetric solutions branches from the symmetric ones.

For the fiber with linear core and nonlinear cladding studied in [7] the dispersion relation is almost the same for the linear and the nonlinear states.

CHAPTER 2

NONLINEAR MATERIAL IN OPTOELECTRONICS

2.1 INTRODUCTION

Many characteristics of extremely low-loss fibers, whose development points towards the feasibility of long-distance wide-band transmission systems, enhances the relevance of nonlinear phenomena in optical waveguide propagation. These characteristics are the long interaction length provided by the fiber itself, the small fiber diameter pertinent to monomode operation and the existence of narrow-linewidth single frequency lasers. In particular, the product of the fiber length L and the intensity $\frac{P}{(\pi a^2)}$, associated with a core radius a and an input power P can become large enough, compared with nonlinear propagation in an unbounded medium, to balance the intrinsically small nonlinearity of silica glass at relatively low power.

The third order nonlinear susceptibility $\chi^{(3)}$ is an important optical property of material because of its contribution to numerous nonlinear optical processes. Some of these processes are the self-focusing, self-defocusing,

self-trapping and self-bending of light. Degenerate four-wave mixing, and phase conjugation are also results of the third order nonlinear susceptibility.

2.2 CHARACTERISTICS OF NONLINEAR MATERIALS

Nonlinear optical processes are usually described in terms of the polarization vector $\overline{P}$ which is related to the $\overline{D}$ and the $\overline{E}$ vectors by the following equation:

$$\overline{D} = \varepsilon_0 \overline{E} + \overline{P} \qquad (2.1)$$

The polarization can be formally expanded in a power series of the electric field as *ith* component by:

$$P_i = \chi_{ij} E_j + 2\chi_{ijk} E_j E_k + 4\chi_{ijkl} E_j E_k E_l + \ldots\ldots \qquad (2.2)$$

where P_i is the *ith* component of $\overline{P}$ and χ is the susceptibility.

For linear materials only the first order susceptibility χ_{ij} is important. High rank susceptibility terms are negligible. For this type of materials the relative dielectric constant is represented by

$$\varepsilon_r = 1 + \chi_{ij} \qquad (2.3)$$

For nonlinear materials the higher order susceptibilities are not negligible

specially in the presence of strong electric field.

The second order nonlinear term $2\chi_{ijk}E_jE_K$ is responsible for the phenomena of second harmonic generation, parametric amplification and oscillation. It is however negligible in glasses because of inversion symmetry of the material, so that in practice all the nonlinear effects taking place inside the glass optical fiber are associated with the third term of the right hand side of in equation (2.2). These nonlinear effects can be roughly divided into two classes, according to whether the induced polarization vibrates at the same frequency as the incident field or not. The second class includes stimulated Raman scattering, stimulated Brillouin scattering and four-wave mixing, while the first concerns the so called induced field effects which can be described in terms of a nonlinear refractive index eg. the optical Kerr effect. Table 2.1 lists the values of $\chi^{(3)}$ for some optical nonlinear materials. It can be seen from the table that the value of $\chi^{(3)}$ is about 10^{-12} for most of the material at different optical wavelengths. Therefore, a field strength of the order $10^5\,(V/m)$ can make an increase of the dielectric constant equal to 0.01. The above field strength is roughly corresponding to a power density of $10^4\,(W/cm^2)$. This power density can be obtained form a Helium-Neon or a Yag laser source.

TABLE 2.1

Values of nonlinear polarizabily $\chi^{(3)}$ of some nonlinear materials [12], [13] .

Material	λ (μm)	$\chi^{(3)}$ $V^{-2}m^2$
Polydiacetylne	0.602	3.6(-9)
Poly-4-BCMU	0.585	3.6(-9)
Polythiophene	0.602	9.0(-9)
Polyacetylene	1.060	3.6(-9)
Polyacetylene	0.602	9.0(-9)
Polysilane	1.064	1.35(-11)
Polygermane	1.064	1.02(-10)
Poly(PBNSPhs)	1.064	4.68(-11)
Poly(PDN4S)	1.064	1.98(-11)
Poly(PDN14S)	1.064	4.68(-11)
silica	0.6328	4.68(-12)
fused silica	0.6328	2.1(-12)

2.3 SELF-INDUCED NONLINEAR EFFECTS

The third order polarizability corresponding to the third term of the right hand side of of equation (2.2) can be written by assuming the fiber material to be isotropic and its nonlinear response to be dominated by the fast response of electronic processes.

$$P^{(3)} = \varepsilon_0 \chi^{(3)} E \cdot EE \tag{2.4}$$

where the assumption that P and E are oscillating at the same frequency ω is considered. Equations (2.2) and (2.4) show that the $\chi^{(3)}$ is in general a fourth rank tensor which can be represented by 81 components in the three dimensional coordinate system. However, because of the isotropy of the nonlinear materials and other symmetry properties, the forth rank tensor can be reduced to a second rank tensor having 9 components and can be put in a 3×3 matrix. For a weakly guiding fiber where the transverse fields components are large compared to the longitudinal components, the 3×3 matrix is reduced to a 2×2 matrix. By further assuming that the fiber is a polarization-maintaining one, it can be shown that the susceptibility is only a function of a single field [3], and [8]. The nonlinear dielectric constant under the third order Kerr effect is given for homogeneous isotropic medium by:

$$\varepsilon = \varepsilon_{bg} + \alpha |E|^2 \tag{2.5}$$

where ε_{bg} is the background dielectric constant. It is in fact the linear part of the dielectric constant obtained at weak fields. The parameter α is the nonlinear coefficient of the material and E is the applied electric field strength. It has in general three components: E_r, E_φ and E_z. The kerr model is relatively simple to analyse and the problem with Kerr nonlinearity can be solved analytically for a slab waveguide for lossless media. However, the model given by equation (2.5) is not realistic. The nonlinear material always responds to the applied field in a limited way. At high applied electric field intensities saturation effects ensue. Moreover, high field intensities may cause complete breakdown of the dielectric material. Saturation effects suggest the use of more realistic model of the dielectric function. The model is Phenomenological and is based on the fact that the dielectric function cannot grow indefinitely but must level off at a maximum value that depends on the nature of the nonlinear material. Two forms have been proposed in [3] to account for saturation effects. They are given by the following expressions:

$$\varepsilon = \varepsilon_{bg} + \frac{\alpha |E|^2}{1 + g\alpha |E|^2} \tag{2.6}$$

$$\varepsilon = \varepsilon_{bg} + \frac{1}{g}(1 - e^{-\alpha |E|^2}) \tag{2.7}$$

where it is seen that the maximum increase in the dielectric function is seen to be equal to $\frac{1}{g}$ at very high field intensity. It must also be noted that for a weak electric field, equations (2.6) and (2.7) approximate the Kerr behavior.

The nonlinear effects have been widely used in the slab waveguide. There are important devices which have been implemented and tested in integrated optics such as directional coupler, Mach-Zender interferometers and prism coupler. These devices can be used in all-optical signal processing when at least one of the waveguide media exhibits an intensity independent refractive index.

2.4 PHYSICAL DESCRIPTION OF SELF-FOCUSING PHENOMENA

Self-focusing is an induced lens effect. It results from a wavefront distortion inflicted on the beam by itself while traversing a nonlinear medium. Consider a single mode laser beam with a Gaussian transverse profile propagating into a medium with refractive index n given by $n = n_0 + \Delta n(|E|^2)$ where $\Delta n(|E|^2)$ is the optical-field-induced refractive index change. If Δn is positive, the central part of the beam having a higher intensity will experience a larger refractive index than the edge and therefore travel at a slower velocity than the edge. Consequently, as the beam travels in the medium, the original plane wavefront gets progressively more distorted as shown in

fig.(2.1) [14]. The distortion is similar to that imposed on the beam by a positive lens. Since the optical ray propagation is in the direction perpendicular to the wavefront, the beam appears to focus by itself. However, a beam with a finite cross section should also diffract. Only when the self-focusing is greater than diffraction will the beam self-focus. The self-focusing is proportional to $\Delta n(|E|^2)$, while the diffraction action is inversely proportional to the square of the beam radius. Therefore, as the beam shrinks in self-focusing action the diffraction action become stronger. At some point, diffraction overcomes self-focusing and the beam after reaching a minimum cross section (the focal point) will diffract. The self trapping is a special case when both self-focusing action and diffraction action on the input beam just balance each other. It must be mentioned that self-defocusing effects also occur in third order nonlinear materials. These are associated with materials with negative third order nonlinearity.

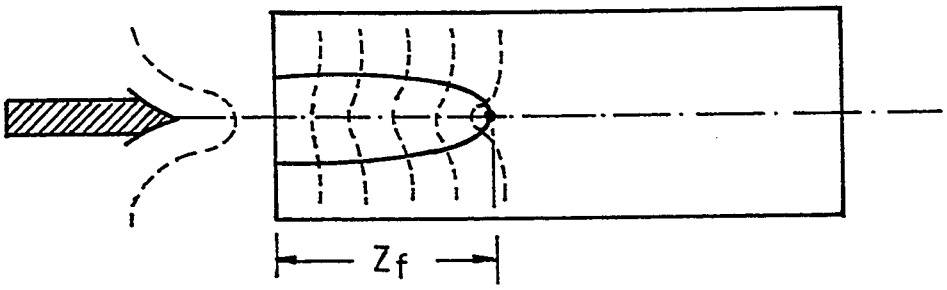

Fig.(2.1) Distortion of the wavefront of a laser beam leading to self-focusing in the nonlinear medium [14] .

CHAPTER 3

THEORETICAL STUDY OF MULTILAYER OPTICAL FIBER

3.1 INTRODUCTION

In this chapter Maxwell's equations are used to develop the general vector wave equation for the electric and magnetic fields. The simplified scalar wave equation is deduced from the vector wave equation under certain conditions. We always assume monochromatic field quantities. This means that the input and output frequencies are the same.

Although in the case of third order Kerr nonlinearity the interacting field components generate another field at the third harmonic of the input frequency [8], our interest in this thesis is concerned only with the fundamental frequency component. The basic theory of guided waves is developed for TE and TM guided modes as well as the fundamental HE_{11} hybrid mode. The approach used in this research is based on the linearization of the wave equation. The linearization is achieved by dividing the nonlinear fiber into a large number of layers. Each layer is treated as a linear, isotropic and homogeneous medium.

The electromagnetic theory in this chapter is developed using references [15]–[18]. The notations used for Bessel functions and their important properties are taken from [19] and [20].

3.2 MAXWELL'S EQUATIONS

The following four equations govern the propagation of electromagnetic fields in different media:

$$\nabla \times \bar{E} = -\frac{\partial \bar{B}}{\partial t} \tag{3.1}$$

$$\nabla \times \bar{H} = -\frac{\partial \bar{D}}{\partial t} + \bar{J} \tag{3.2}$$

$$\nabla \cdot \bar{B} = 0 \tag{3.3}$$

$$\nabla \cdot \bar{D} = \rho \tag{3.4}$$

where $\bar{E}$ and $\bar{H}$ are the electric and magnetic fields respectively, $\bar{B}$ is the magnetic flux density, $\frac{\partial \bar{D}}{\partial t}$ is the displacement current density, $\bar{J}$ is the conduction current density and ρ is the electric charge density. The bar on any quantity denotes a vector quantity.

Maxwell's equations can explain all macroscopic phenomenon in electromagnetic. There are four field vectors $\bar{E}, \bar{H}, \bar{B}, \bar{D}$, each of which has three components. Therefore, twelve scalar equations are needed to solve for all fields. These twelve equations are obtained by expanding the two vector curl equations and the two vector constitutive relations $\bar{D} = \varepsilon\bar{E}$ and $\bar{B} = \mu\bar{H}$ which will be discussed in a subsequent section of this chapter.

Under monochromatic time dependence all field quantities vary as $e^{-i\omega t}$ For vacuum and dielectric media both $\bar{J}$ and ρ are zeros.

Therefore Maxwell's equations can be written as:

$$\nabla \times \bar{E} = -i\omega\bar{B} \tag{3.5}$$

$$\nabla \times \bar{H} = i\omega\bar{D} \tag{3.6}$$

$$\nabla \cdot \bar{B} = 0 \tag{3.7}$$

$$\nabla \cdot \bar{D} = 0 \tag{3.8}$$

Because Maxwell's equations are not all independent, the constitutive relations must be used for a complete description of electromagnetic fields. This should be accomplished by applying the proper boundary conditions which is the subject of the next section.

3.3 BOUNDARY CONDITIONS

To solve Maxwell's equations in different media we must apply the appropriate boundary conditions at the interface separating any two different media. These boundary conditions are as follows:

$$\hat{n} \times (\bar{E}_1 - \bar{E}_2) = 0 \tag{3.9}$$

$$\hat{n} \times (\bar{H}_1 - \bar{H}_2) = \bar{J}_s \tag{3.10}$$

$$\hat{n}.(\bar{B}_1 - \bar{B}_2) = 0 \tag{3.11}$$

$$\hat{n}.(\bar{D}_1 - \bar{D}_2) = \rho_s \tag{3.12}$$

where $\hat{n}$ is the unit normal at the interface pointing outwards of medium 2, ρ_s is the surface charge density and J_s is the surface current density. They vanish for a source free medium.

Maxwell's equations do not include the properties of the medium under consideration. However, these properties are accounted for by the following constitutive relations:

$$\bar{D} = \varepsilon \bar{E} \tag{3.13}$$

$$\bar{B} = \mu \bar{H} \tag{3.14}$$

$$\bar{J} = \sigma \bar{E} \tag{3.15}$$

where ε is the permittivity, μ is the magnetic permeability and σ is the conductivity. For nonmagnetic materials μ is equal to μ_0, the free space value.

The dielectric constant is written in the following form for nonmagnetic media :

$$\varepsilon = \varepsilon_0 \varepsilon_r = \varepsilon_0 n^2 \tag{3.16}$$

where ε_r is the relative permittivity and n is the refractive index of the medium. The refractive index is real for a nonabsorbing (lossless) medium and complex for an absorbing or a lossy medium. For such lossy medium the dielectric constant and the refractive index are written as

$$\varepsilon_r = \varepsilon_1 + i\varepsilon_2 = n^2 \tag{3.17}$$

where ε_1 and ε_2 are the real and the imaginary parts of the dielectric constant and n is the complex refractive index.

When the constitutive relations are substituted in Maxwell's equations, the following forms are obtained:

$$\nabla \times \bar{E} = -i\omega\mu_0 \bar{H} \tag{3.18}$$

$$\nabla \times \bar{H} = i\omega\varepsilon_0 n^2 \bar{E} \tag{3.19}$$

$$\nabla . \bar{H} = 0 \tag{3.20}$$

$$\nabla . \varepsilon\bar{E} = 0 \tag{3.21}$$

These equations are valid for a nonmagnetic, isotropic, linear and source-free medium. Throughout this work, the nonlinear wave equation will be locally linearized by using a multi-layer structure. All layers share the same properties of the medium except for the value of the dielectric constant which is different for each layer. It is thus possible to use the known linear solution of the above Maxwell's equations for each layer.

3.4 THE VECTOR WAVE EQUATION

To derive the vector wave equation, either $\bar{E}$ or $\bar{H}$ must be eliminated from the above 4 equations. By applying the curl operator to equation (3.18) and using equation (3.19) the following equation is obtained:

$$\nabla^2 \bar{E} + \nabla(\bar{E} \cdot \nabla(\ln n^2)) + k_0^2 n^2 \bar{E} = 0 \tag{3.22}$$

where the vector identity:

$$\nabla \times (\nabla \times \overline{A}) = \nabla(\nabla \cdot \overline{A}) - \nabla^2 \overline{A} \tag{3.23}$$

has been used and $k_0 = (\omega^2 \mu_0 \varepsilon_0)^{\frac{1}{2}}$ is the free space wave number.

Equation (3.22) is the vector wave equation for the $\overline{E}$ field. In a similar manner the vector wave equation for the $\overline{H}$ field can be derived as:

$$\nabla^2 \overline{H} + \nabla(\ln n^2) \times (\nabla \times \overline{H}) + k_0^2 n^2 \overline{H} = 0 \tag{3.24}$$

These two vector wave equations are valid for any coordinate system. In a nonlinear medium the permittivity is a function of the electric field and hence it is also a function of space coordinates. When the multilayer approach is used, the dielectric function is evaluated locally at each layer and treated as constant for the entire layer. Under this condition the second terms of equations (3.22) and (3.24) vanish and the two vector wave equations for both $\overline{E}$ and $\overline{H}$ fields reduce to:

$$\nabla^2 \overline{E} + k_0^2 n^2 \overline{E} = 0 \tag{3.25}$$

$$\nabla^2 \overline{H} + k_0^2 n^2 \overline{H} = 0 \tag{3.26}$$

In cylindrical coordinates the vector Laplacian operator ∇^2 appearing in equations (3.25) and (3.26) is given by:

$$\bar{\nabla}^2\bar{A} = \left[\nabla^2 A_r - \frac{2}{r^2}\frac{\partial A_\varphi}{\partial \varphi} - \frac{A_r}{r^2}\right]\hat{r} + \left[\nabla^2 A_\varphi + \frac{2}{r^2}\frac{\partial A_\varphi}{\partial \varphi} - \frac{A_\varphi}{r^2}\right]\hat{\varphi} + \nabla^2 A_z \hat{z} \qquad (3.27)$$

where we introduce the bar in the left hand side to distinguish between the vector Laplace operator and the scalar Laplace operator on the right hand side of the equation. The scalar operator is given by:

$$\nabla^2 = \frac{\partial^2}{\partial r^2} + \frac{1}{r}\frac{\partial}{\partial r} + \frac{1}{r^2}\frac{\partial^2}{\partial \varphi^2} + \frac{\partial^2}{\partial z^2} \qquad (3.28)$$

Therefore, the z-component of the two vector wave equations (3.25) and (3.26) reduces to the same scalar form given by:

$$\nabla^2\Psi + k_0^2 n^2 \Psi = 0 \qquad (3.29)$$

where Ψ is either E_z or H_z. The variation in the z-direction is taken as $e^{i\beta z}$ where β is the propagation constant. Equation (3.29) now reduces to the form:

$$\frac{\partial^2\Psi}{\partial r^2} + \frac{1}{r}\frac{\partial\Psi}{\partial r} + \frac{1}{r^2}\frac{\partial^2\Psi}{\partial \varphi^2} + (k_0^2 n^2 - \beta^2)\Psi = 0 \qquad (3.30)$$

The solution of equation (3.30) is sought in the form:

$$\Psi(r,\varphi) = R(r)e^{iv\varphi} \qquad (3.31)$$

where v is an integer representing the azimuthal periodicity of the field solution. Substituting equation (3.31) into equation (3.30) the following equation is obtained:

$$\frac{\partial^2 R}{\partial r^2} + \frac{1}{r}\frac{\partial R}{\partial r} + \left(k_0^2 n^2 - \beta^2 - \frac{v^2}{r^2}\right)R = 0 \qquad (3.32)$$

Defining the parameter γ as:

$$\gamma^2 = k_0^2 n^2 - \beta^2 \qquad (3.33)$$

Equation (3.32) is the standard Bessel differential equation. The solution of this equation is given by:

$$R(r) = AJ_v(\gamma r) + BY_v(\gamma r) \qquad (3.34)$$

where J_v and Y_v are Bessel functions of the first and the second kind respectively and A and B are constants to be determined from the boundary conditions. Using Maxwell's equations, the transverse field components are expressed in terms of the axial components as:

$$E_r = -\frac{1}{\gamma^2}\left(\frac{v\omega\mu_0}{r}H_z - i\beta\frac{\partial E_z}{\partial r}\right) \qquad (3.35)$$

$$E_\varphi = -\frac{1}{\gamma^2}(i\omega\mu_0\frac{\partial H_z}{\partial r} + \frac{\beta\nu}{r}E_z) \qquad (3.36)$$

$$H_r = \frac{1}{\gamma^2}(\frac{\nu n^2\varepsilon_0\omega}{r}E_z + i\beta\frac{\partial H_z}{\partial r}) \qquad (3.37)$$

$$H_\varphi = \frac{1}{\gamma^2}(in^2\varepsilon_0\omega\frac{\partial E_z}{\partial r} - \frac{\nu\beta}{r}H_z) \qquad (3.38)$$

For a multilayer structure equations (3.34)-(3.38) are valid for each layer where A,B and n are replaced by the appropriate values corresponding to that layer

The above analysis is general and can be used to cover different types of polarization, namely the transverse electric (TE), the transverse magnetic (TM) and the hybrid modes. In the next sections each of the above cases is studied and the corresponding eigenvalue equation is derived.

3.5 TE EIGENVALUE EQUATION

For TE waves the electric field $\overline{E}=(0,E_\varphi,0)$ has only one field component which is transverse and the magnetic field $\overline{H}=(H_r,0,H_z)$ has one axial component and one transverse component. Also the value of ν for TE waves is zero which means that the fields do not have azimuthal dependence.

Fig.(3.1) shows the multilayer structure under investigation.

For any arbitrary layer, (except for the innermost layer), the field components are written in the form:

$$H_z^l = A_l J_0(\gamma_l r) + B_l Y_0(\gamma_l r) \qquad d_{l-1} \le r \le d_l \qquad (3.39)$$

$$E_\varphi^l = \frac{i\omega\mu_0}{\gamma_l}\{A_l J_1(\gamma_l r) + B_l Y_1(\gamma_l r)\} \qquad d_{l-1} \le r \le d_l \qquad (3.40)$$

$$H_r^l = \frac{-i\beta}{\gamma_l}\{A_l J_1(\gamma_l r) + B_l Y_1(\gamma_l r)\} \qquad d_{l-1} \le r \le d_l \qquad (3.41)$$

where γ_l is given by

$$\gamma_l = (\varepsilon_l k_0^2 - \beta^2)^{\frac{1}{2}} \qquad (3.42)$$

To evaluate ε_l we define the general nonlinear dielectric function as:

$$\varepsilon(r,E) = \varepsilon_{bg}(r) + \frac{\alpha|E|^2}{1 + g\alpha|E|^2} \qquad (3.43)$$

where $\varepsilon_{bg}(r)$ is the field-independent part of ε. The values of the constants α and g depend on the dielectric material. The above representation of the dielectric function gives a maximum change of ε equal to $\frac{1}{g}$. The term $|E|^2$

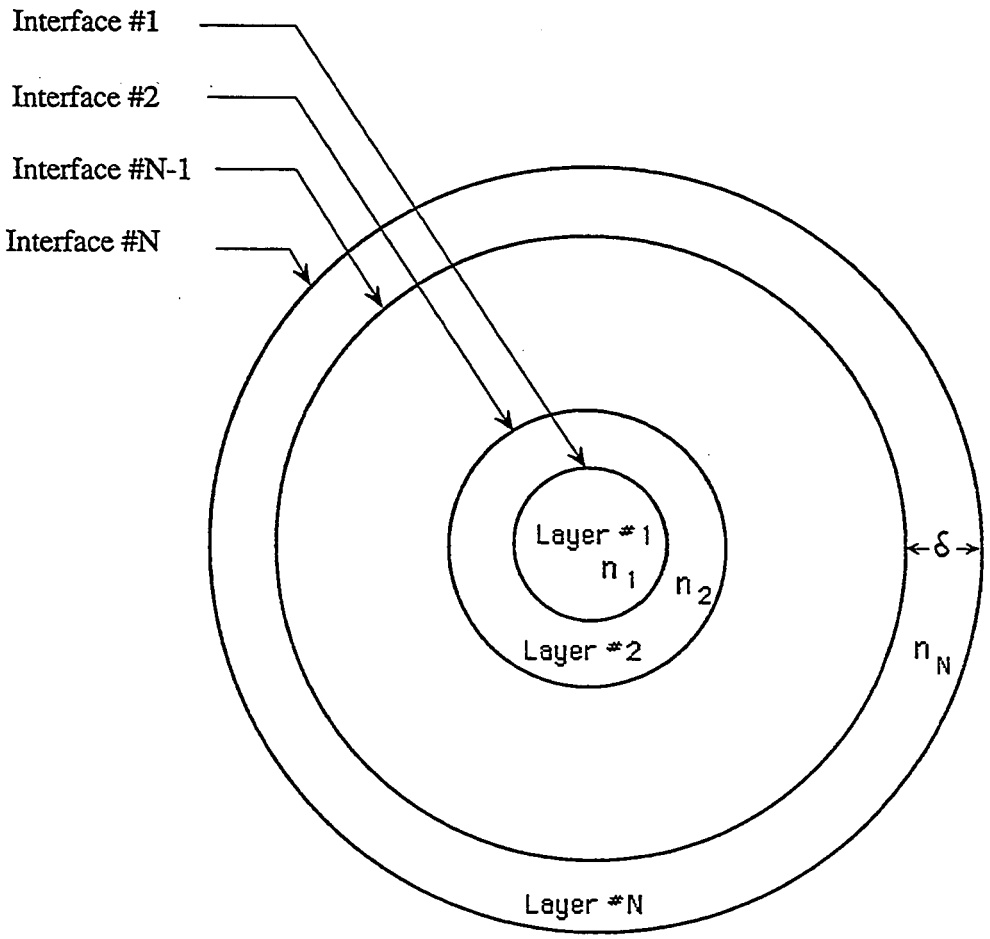

Fig.(3.1) The multi-layer structure in a cylindrical waveguide.

is given by

$$|E|^2 = |E_z|^2 + |E_r|^2 + |E_\varphi|^2 \qquad (3.44)$$

The technique for calculating the dielectric constant for any layer is based on evaluating the electric field at the inner boundary of that layer and then calculate the dielectric constant using equation (3.43). This can be represented mathematically as:

$$\varepsilon_l = \varepsilon_{bg} + \frac{\alpha|E_{l-1}|^2}{1+g\alpha|E_{l-1}|^2} \qquad (3.45)$$

where E_{l-1} is the electric field for the $(l-1)^{th}$ layer evaluated at $r = d_l$. For TE waves, there is only one electric field component E_φ contributing to the dielectric function.

It is well known that the standard Bessel differential equation (equation (3.32)) can be solved in terms of J and Y functions as given in equation (3.33) or in terms of the modified Bessel functions I and K as follows

$$R(r) = CI_\nu(i\gamma r) + DK_\nu(i\gamma r) \qquad (3.46)$$

where I and K are the modified Bessel functions of the first and the second kind respectively.

The recursive relations are expressed in terms of J and Y functions for TE guided waves. These recursive relations are used to derive the effective index and the modal fields of a given TE mode of the nonlinear optical fiber. The I and K functions are also used in the TM case.

To start the recursive scheme, the dielectric constant must be evaluated for the most inner layer (layer 1). The fields components for the first layer are given by:

$$H_z^{\,1} = A_1 J_0(\gamma_1 r) \qquad 0 \le r \le d_1 \qquad (3.47)$$

$$E_\varphi^{\,1} = \frac{i\omega\mu_0}{\gamma_1} A_1 J_1(\gamma_1 r) \qquad 0 \le r \le d_1 \qquad (3.48)$$

$$H_r^{\,1} = \frac{-i\beta}{\gamma_1} A_1 J_1(\gamma_1 r) \qquad 0 \le r \le d_1 \qquad (3.49)$$

where the coefficient B_1 has been set equal to zero because the Y function is infinite at the origin. The electric field of equation (3.48) is evaluated at the axis of the fiber and substituted into equation (2.45) to obtain the value of ε_1. The value of this field is zero since $J_1(\gamma r)$ vanishes at $r = 0$. This is also necessary to insure the continuity of E_φ at $r = 0$. The evaluated value of the dielectric constant ε_1 is used to calculate the field at position $r = d_1$ which

will in turn be used to evaluate ε_2, the dielectric constant of layer 2 and so on. Equations (3.39)-(3.41) can be repeated for the $(l+1)^{th}$ layer as follows:

$$H_z^{l+1} = A_{l+1}J_0(\gamma_{l+1}r) + B_{l+1}Y_0(\gamma_{l+1}r) \qquad d_l \le r \le d_{l+1} \qquad (3.50)$$

$$E_\varphi^{l+1} = \frac{i\omega\mu_0}{\gamma_{l+1}}\{A_{l+1}J_1(\gamma_{l+1}r) + B_{l+1}Y_1(\gamma_{l+1}r)\} \qquad d_l \le r \le d_{l+1} \qquad (3.51)$$

$$H_r^{l+1} = \frac{-i\beta}{\gamma_{l+1}}\{A_{l+1}J_1(\gamma_{l+1}r) + B_{l+1}Y_1(\gamma_{l+1}r)\} \qquad d_l \le r \le d_{l+1} \qquad (3.52)$$

At the interface $r = d_l$, the continuous tangential fields H_z and E_φ are matched on both sides of the interface in order to express the field amplitudes A_{l+1} and B_{l+1} in terms of A_l and B_l. In so doing, the following two equations are obtained

$$A_lJ_0(\gamma_l d_l) + B_lY_0(\gamma_l d_l) = A_{l+1}J_0(\gamma_{l+1}d_l) + B_{l+1}Y_0(\gamma_{l+1}d_l) \qquad (3.53)$$

$$\frac{1}{\gamma_l}\{A_lJ_1(\gamma_l d_l) + B_lY_1(\gamma_l d_l)\} = \frac{1}{\gamma_{l+1}}\{A_{l+1}J_1(\gamma_{l+1}d_l) + B_{l+1}Y_1(\gamma_{l+1}d_l)\} \qquad (3.54)$$

Equations (3.53) and (3.54) are now solved for A_{l+1} and B_{l+1} in terms of A_l and B_l. The two recurrence relations for the amplitude coefficients are given by:

$$A_{l+1} = \frac{C_1}{C_2} A_l + \frac{C_3}{C_2} B_l \qquad (3.55)$$

where C_1,C_2 and C_3 are given by:

$$C_1 = \frac{\gamma_{l+1}}{\gamma_l} J_1(\gamma_l d_l)\, Y_0(\gamma_{l+1} d_l) - J_0(\gamma_l d_l)\, Y_1(\gamma_{l+1} d_l)$$

$$C_2 = J_1(\gamma_{l+1} d_l)\, Y_0(\gamma_{l+1} d_l) - J_0(\gamma_{l+1} d_l)\, Y_1(\gamma_{l+1} d_l)$$

$$C_3 = \frac{\gamma_{l+1}}{\gamma_l} Y_1(\gamma_l d_l)\, Y_0(\gamma_{l+1} d_l) - Y_0(\gamma_l d_l) Y_1(\gamma_{l+1} d_l)$$

After determining A_{l+1} using equation (3.55), B_{l+1} is obtained from equation (3.53) :

$$B_{l+1} = \frac{1}{Y_0(\gamma_{l+1} d_l)} \{A_l J_0(\gamma_l d_l) + B_l Y_0(\gamma_l d_l) - A_{l+1} J_0(\gamma_{l+1} d_l)\} \qquad (3.56)$$

Considering an N-layers fiber surrounded by an unlimited cladding as shown in fig.(3.1), the eigenvalue equation is obtained by writing the fields of the last layer (layer N) as:

$$H_z^N = A_N J_0(\gamma_N r) + B_N Y_0(\gamma_N r) \qquad d_{N-1} \le r \le d_N \qquad (3.57)$$

$$E_{\varphi}^{N} = \frac{i\omega\mu_0}{\gamma_N} \{A_N J_1(\gamma_N r) + B_N Y_1(\gamma_N r)\} \qquad d_{N-1} \le r \le d_N \qquad (3.58)$$

For the open cladding region the fields should be a decaying function of r. This is satisfied by the modified Bessel function of the second kind (the K function). The tangential fields are given by:

$$H_z^c = A_c K_0(\gamma_c r) \qquad d_N \le r \le \infty \qquad (3.59)$$

$$E_{\varphi}^{c} = \frac{i\omega\mu_0}{\gamma_c} A_c K_1(\gamma_c r) \qquad d_N \le r \le \infty \qquad (3.60)$$

The subscript c denotes the cladding. Equating the tangential fields H_z and E_φ at the cladding interface $r = d_N$, the required eigenvalue equation is obtained as follows:

$$A_N J_0(\gamma_N d_N) + B_N Y_0(\gamma_N d_N) = A_c K_0(\gamma_c d_N) \qquad r = d_N \qquad (3.61)$$

$$\frac{1}{\gamma_N} \{A_N J_1(\gamma_N d_N) + B_N Y_1(\gamma_N d_N)\} = -\frac{1}{\gamma_c} A_c k_1(\gamma_c d_N) \qquad at\ r = d_N \qquad (3.62)$$

where γ_c is given by:

$$\gamma_c = (\beta^2 - n_c^2 k_0^2)^{\frac{1}{2}} \qquad (3.63)$$

where n_c is the cladding refractive index. Eliminating A_c, the following equation is obtained

$$K_0(\gamma_c d_N)\left[A_N J_1(\gamma_N d_N) + B_N Y_1(\gamma_N d_N)\right] + \frac{\gamma_N}{\gamma_c} K_1(\gamma_c d_N)$$
$$\left[A_N J_0(\gamma_N d_N) + B_N Y_0(\gamma_N d_N)\right] = 0 \qquad at\ r = d_N \qquad (3.64)$$

Equation (3.64) is based on assuming a given axial electric field amplitude at the axis of the fiber and then, propagating this field recursively through the fiber by expressing the field amplitudes of any layer in terms of the amplitudes of the previous layer. At $r = d_N$, the tangential fields are matched at the core cladding interface to obtain this equation. The only unknown in this equation is the propagation constant β or equivalently the mode effective index n_e. Equation (3.64) can be solved numerically using a zero finding routine which can handle both real and complex functions. In our computer work, the routine based on Muller's method is used [21].

It must be noted that our recursive scheme is similar to that reported by C. Yeh and G. Lindgren in 1977 [22] and applied to a linear fiber. The two schemes are based on stratifying the fiber into a large number of layers. The latter utilizes matrix operations for eliminating all field coefficients and can handle any linear arbitrary refractive index profile. Our scheme is however applicable to linear as well as nonlinear fibers. For the nonlinear case, we

use the electric field intensity at the boundary of the innermost layer ($r=d_1$) as a parameter. The propagation constant in this case, will be a function of the electric field at $r=d_1$.

3.6 TM EIGENVALUE EQUATION

The field components associated with the TM polarization are E_z, E_r, and H_φ. There are therefore, two electric field components contributing to the dielectric function of the nonlinear medium given by equation (3.43). The analysis of the TM case is carried out in a manner similar to that used for the TE guided waves. Modified Bessel functions are used in region $r>d_1$ for the description of the field components. The tangential field components E_z and H_φ are expressed for the different layers as:

$$E_z^1 = A_1 J_0(\gamma_1 r) \qquad 0\le r\le d_1 \qquad (3.65)$$

$$E_z^l = A_l I_0(\gamma_l r) + B_l K_0(\gamma_l r) \qquad d_{l-1}\le r\le d_l \qquad (3.66)$$

$$E_z^c = A_c K_0(\gamma_c r) \qquad d_N\le r\le \infty \qquad (3.67)$$

The parameters γ_1 and γ_c are the same as those given in equations (3.42) and (3.63) respectively. While γ_l is given by:

$$\gamma_l = (\beta^2 - k_0^2 n_l^2)^{\frac{1}{2}} \tag{3.68}$$

Also the tangential magnetic field H_φ is given by:

$$H_\varphi^1 = \frac{-i\varepsilon_0 n_1^2 \omega}{\gamma_1} A_1 J_1(\gamma_1 r) \qquad 0 \le r \le d_1 \tag{3.69}$$

$$H_\varphi^l = \frac{i\varepsilon_0 n_l^2 \omega}{\gamma_l} \{ A_l I_1(\gamma_l r) - B_l K_1(\gamma_l r) \} \qquad d_{l-1} \le r \le d_l \tag{3.70}$$

$$H_\varphi^c = \frac{-i\varepsilon_0 n_c^2 \omega}{\gamma_c} A_c K_1(\gamma_c r) \qquad d_N \le r \le \infty \tag{3.71}$$

The radial component of electric field E_r is written as:

$$E_r^1 = \frac{-i\beta}{\gamma_1} A_1 J_1(\gamma_1 r) \qquad 0 \le r \le d_1 \tag{3.72}$$

$$E_r^l = \frac{-i\beta}{\gamma_l} r \{ A_l I_1(\gamma_l r) - B_l K_1(\gamma_l r) \} \qquad d_{l-1} \le r \le d_l \tag{3.73}$$

$$E_r^c = \frac{-i\beta}{\gamma_c} A_c K_1(\gamma_c r) \qquad d_N \le r \le \infty \tag{3.74}$$

To start the recursive scheme, the dielectric function must be evaluated for the first layer. By examining the two electric field components at the axis of

the fiber, it is clear that E_r vanishes at r = 0 and E_z is maximum at r = 0 and equal to A_1 . Therefore, ε_1 is given by:

$$\varepsilon_1 = \varepsilon_{bg} + \frac{\alpha|A_1|^2}{1+g\alpha|A_1|^2} \qquad 0 \le r \le d_1 \qquad (3.75)$$

Following the same procedure used in the TE case and matching the tangential field components E_z and H_φ, we derive the recurrence relations at an arbitrary interface $(r=d_l)$. These relations are given by:

$$A_{l+1} = \frac{X_1}{X_2} A_l + \frac{X_3}{X_2} B_l \qquad (3.76)$$

where X_1, X_2, X_3 are given as follows:

$$X_1 = \frac{\gamma_{l+1}}{\gamma_l} \frac{\varepsilon_l}{\varepsilon_{l+1}} I_1(\gamma_l d_l) K_0(\gamma_{l+1} d_l) + I_0(\gamma_l d_l) K_1(\gamma_{l+1} d_l)$$

$$X_2 = I_1(\gamma_{l+1} d_l) K_0(\gamma_{l+1} d_l) - I_0(\gamma_{l+1} d_l) K_1(\gamma_{l+1} d_l)$$

$$X_3 = K_0(\gamma_l d_l) K_1(\gamma_{l+1} d_l) - \frac{\gamma_{l+1}}{\gamma_l} \frac{\varepsilon_l}{\varepsilon_{l+1}} K_1(\gamma_l d_l) K_0(\gamma_{l+1} d_l)$$

Using equation (3.76) for A_{l+1}, the amplitude coefficient B_{l+1} is then evaluated.

It is given by:

$$B_{l+1} = \frac{1}{K_0(\gamma_{l+1}d_l)} \{A_l I_0(\gamma_l d_l) + B_l K_0(\gamma_l d_l) - A_{l+1} I_0(\gamma_{l+1} d_l)\} \tag{3.77}$$

The boundary conditions are applied at $r = d_N$ to obtain the following equation:

$$\frac{\varepsilon_N \gamma_c}{\varepsilon_c \gamma_N} K_0(\gamma_c d_N)\left[A_N I_1(\gamma_N d_N) - B_N K_1(\gamma_N d_N)\right] + K_1(\gamma_c d_N)$$
$$\left[A_N I_0(\gamma_N d_N) + B_N K_0(\gamma_N d_N)\right] = 0 \qquad at\ r = d_N \tag{3.78}$$

After assuming the amplitude of the electric field E_z at the axis of the optical fiber, the only unknown in equation (3.78) is the effective index n_e. Therefore, it is considered as the TM eigenvalue equation for an N-layer fiber. If the fiber is linear and weak guidance is assumed, equations (3.63) and (3.78) will result in almost the same eigenvalues. In this case the TE modes and their corresponding TM modes become almost degenerate. However, for the nonlinear fiber the eigenvalues depend on the field intensity as well as the refractive index difference.

3.7 FUNDAMENTAL HE_{11} EIGENVALUE EQUATION

The derivation of the eigenvalue equation for the hybrid modes requires a complete solution of Maxwell's equations assuming that both E_z and H_z exist. The other four field components E_φ,H_φ,E_r and H_r are evaluated as usual from equations (3.35)-(3.38). The strategy for solving the problem is based on assuming different coefficients for E_z and H_z at r=0. The next step is to find the recurrence relations of all field coefficients in terms of these two coefficients. The last step is to relate the coefficient of H_z to that of E_z through the computer program. The evaluation of ε_1 for the innermost layer is discussed in the end of this section. The axial electric field components in the different layers are given by:

$$E_z^1 = A_1 J_1(\gamma_1 r)\cos\varphi \qquad 0 \le r \le d_1 \qquad (3.79)$$

$$E_z^l = \{A_l I_1(\gamma_l r) + B_l K_1(\gamma_l r)\}\cos\varphi \qquad d_{l-1} \le r \le d_l \qquad (3.80)$$

$$E_z^c = A_c K_1(\gamma_c r)\cos\varphi \qquad d_N \le r \le \infty \qquad (3.81)$$

and the axial magnetic field components are given as follows:

$$H_z^1 = C_1 J_1(\gamma_1 r)\sin\varphi \qquad 0 \le r \le d_1 \qquad (3.82)$$

$$H_z^l = \{C_l I_1(\gamma_l r) + D_l K_1(\bar{\gamma}_l r)\}\sin\varphi \qquad d_{l-1} \le r \le d_l \qquad (3.83)$$

$$H_z^c = C_c K_1(\gamma_c r)\sin\varphi \qquad d_N \le r \le \infty \qquad (3.84)$$

The other field components E_φ, H_φ and E_r are given for the different layers by:

$$E_\varphi^1 = -\frac{i}{\gamma_1^2}\{-\frac{\beta}{r}A_1 J_1(\gamma_1 r) - \omega\mu_0 C_1\gamma_1 J_1'(\gamma_1 r)\}\sin\varphi$$

$$0 \le r \le d_1 \qquad (3.85)$$

$$E_\varphi^l = i\frac{\beta}{\gamma_l^2} r\left[A_l I_1(\gamma_l r) - B_l K_1(\gamma_l r)\right]\sin\varphi + i\omega\frac{\mu_0}{\gamma_l}$$

$$\left[C_l I_1'(\gamma_l r) + D_l K_1'(\gamma_l r)\right]\sin\varphi \qquad d_{l-1} \le r \le d_l \qquad (3.86)$$

$$E_\varphi^c = -\frac{i}{\gamma_c^2}\{-\frac{\beta}{r}A_c K_1(\gamma_c r) - \omega\mu_0 C_c\gamma_c K_1'(\gamma_c r)\}\sin\varphi$$

$$d_N \le r \le \infty \qquad (3.87)$$

$$H_\varphi^1 = -\frac{i}{\gamma_1^2}\{\frac{\beta}{r}C_1 J_1(\gamma_1 r) + \omega\varepsilon_0 n_1^2 A_1\gamma_1 J_1'(\gamma_1 r)\}\cos\varphi$$

$$0 \le r \le d_1 \qquad (3.88)$$

$$H_{\varphi}^{l} = -i\frac{\beta}{\gamma_l^2 r}\left[C_l I_1(\gamma_l r) + D_l K_1(\gamma_l r)\right]\cos\varphi + i\omega\varepsilon_0\frac{n_l^2}{\gamma_l}$$

$$\left[A_l I_1'(\gamma_l r) + B_l K_1'(\gamma_l r)\right]\cos\varphi \qquad d_{l-1}\le r\le d_l \qquad (3.89)$$

$$H_{\varphi}^{c} = -\frac{i}{\gamma_c^2}\{\frac{\beta}{r}C_c K_1(\gamma_c r) + \omega\varepsilon_0 n_c^2 A_c\gamma_c K_1'(\gamma_c r)\}\sin\varphi$$

$$d_N\le r\le\infty \qquad (3.90)$$

$$E_r^1 = -\frac{i}{\gamma_1^2}\{\beta\gamma_1 A_1 J_1'(\gamma_1 r) + \frac{\omega\mu_0 C_1}{r} J_1(\gamma_1 r)\}\cos\varphi$$

$$0\le r\le d_1 \qquad (3.91)$$

$$E_r^l = -i\frac{\beta}{\gamma_l}\left[A_l I_1'(\gamma_l r) + B_l K_1'(\gamma_l r)\right]\cos\varphi + \frac{i\omega\mu_0}{r\gamma_l^2}$$

$$\left[C_l I_1(\gamma_l r) + D_l K_1(\gamma_l r)\right]\cos\varphi \qquad d_{l-1}\le r\le d_l \qquad (3.92)$$

$$E_r^c = -\frac{i}{\gamma_c^2}\{\beta\gamma_c A_c K_1'(\gamma_c r) + \frac{\omega\mu_0}{r}C_c K_1(\gamma_c r)\}\sin\varphi$$

$$d_N\le r\le\infty \qquad (3.93)$$

$$H_r^1 = \frac{i}{\gamma_1^2}\{\beta\gamma_1 C_1 J_1'(\gamma_1 r) + \frac{\omega\varepsilon_0 n^2 A_1}{r} J_1(\gamma_1 r)\}\cos\varphi$$

$$0\le r\le d_1 \qquad (3.94)$$

$$H_r^l = -i\frac{\beta}{\gamma_l}\left[C_l I_1'(\gamma_l r) + D_l K_1'(\gamma_l r)\right]\cos\varphi + \frac{i\omega\varepsilon_0 n^2}{r\gamma_l^2}$$

$$\left[A_l I_1(\gamma_l r) + B_l K_1(\gamma_l r)\right]\cos\varphi \qquad d_{l-1} \le r \le d_l \qquad (3.95)$$

$$H_r^c = -\frac{i}{\gamma_c^2}\{\beta\gamma_c C_c K_1'(\gamma_c r) + \frac{\omega\varepsilon_0 n^2}{r} A_c K_1(\gamma_c r)\}\sin\varphi$$

$$d_N \le r \le \infty \qquad (3.96)$$

In equations (3.85)-(3.96) the prime on Bessel functions denotes a differentiation with respect to the argument. After writing the field components for the different layers, the next step is to derive the recurrence relations for the amplitude coefficients and the eigenvalue equation. In order to to simplify the notation of the next section the abbreviation $\Psi_x(m)$, is introduced where Ψ is used to denote any field component while x denotes the coordinate of that field component and m indicates that this field is evaluated for the m^{th} layer at a distance $r=d_m$ from the axis of the fiber. Choosing an arbitrary interface $r=d_l$ and matching the four tangential fields components E_z, H_z, E_φ and H_φ, we obtain the four recurrence relations which relate the coefficients of the $(l+1)^{th}$ layer to those of the l^{th} layer as follows:

$$A_{l+1} = \frac{X_1}{X_2} \qquad at\ r=d_l \qquad (3.97)$$

where X_1 and X_2 are given by:-

$$X_1 = i\gamma_{l+1}^2 H_\varphi(l)\, K_1(\gamma_{l+1}d_l) - \omega\varepsilon_0 n_{l+1}^2 \gamma_{l+1}\, E_z(l) K_1'(\gamma_{l+1}d_l) - \frac{\beta}{d_l} H_z(l)\, K_1(\gamma_{l+1}d_l)$$

$$X_2 = \omega\varepsilon_0 n_{l+1}^2 \gamma_{l+1}\, \{I_1'(\gamma_{l+1}d_l)\, K_1(\gamma_{l+1}d_l) - I_1(\gamma_{l+1}d_l)\, K_1'(\gamma_{l+1}d_l)\}$$

After determining A_{l+1}, the second electric field coefficient B_{l+1} is obtained from the following equation

$$B_{l+1} = \frac{1}{K_1(\gamma_{l+1}d_l)} \{E_z(l) - A_{l+1} I_1(\gamma_{l+1}d_l)\} \qquad (3.98)$$

The magnetic field coefficients are determined in a similar way as:

$$C_{l+1} = \frac{X_3}{X_3} \qquad at\ r = d_l \qquad (3.99)$$

where X_3 and X_4 are given by:

$$X_3 = i\gamma_{l+1}^2 E_\varphi(l)\, K_1(\gamma_{l+1}d_l) + \omega\mu_0 \gamma_{l+1}\, H_z(l) K_1'(\gamma_{l+1}d_l) + \frac{\beta}{d_l} E_z(l)\, K_1(\gamma_{l+1}d_l)$$

$$X_4 = -\omega\mu_0\gamma_{l+1}\{I_1'(\gamma_{l+1}d_l)K_1(\gamma_{l+1}d_l) - I_1(\gamma_{l+1}d_l)K_1'(\gamma_{l+1}d_l)\}$$

After determining C_{l+1}, the second magnetic field coefficient D_{l+1} is found to be:

$$D_{l+1} = \frac{1}{K_1(\gamma_{l+1}d_l)}\{H_z(l) - C_{l+1}I_1(\gamma_{l+1}d_l)\} \tag{3.100}$$

For the N-layer fiber shown in fig.(3.1), matching the azimuthal tangential field components E_φ and H_φ at the core/cladding interface results in the following two equations:

$$E_\varphi(N) + \frac{i}{\gamma_c^2}\{-\frac{\beta}{d_N}E_z(N) - \omega\mu_0\gamma_c H_z(N)\frac{K_1'(\gamma_c d_N)}{K_1(\gamma_c d_N)}\} = 0 \tag{3.101}$$

$$H_\varphi(N) + \frac{i}{\gamma_c^2}\{\frac{\beta}{d_N}H_z(N) + \omega\varepsilon_0 n_c^2\gamma_c E_z(N)\frac{K_1'(\gamma_c d_N)}{K_1(\gamma_c d_N)}\} = 0 \tag{3.102}$$

It is to be noted that equations (3.101) and (3.102) must give the same eigenvalue if the ratio of the axial electric field to the axial magnetic field coefficients, A_1/C_1 assumed for the first layer is correct. To start the recursive scheme, an initial value is taken to be the same as that of the

weakly guiding fiber namely, $\frac{\eta_0}{n_1}$, where η_0 is the free space intrinsic impedance equals to 120π and n_1 is the core refractive index.

The first run will produce two different eigenvalues. By changing the ratio $\frac{A_1}{C_1}$ in small increments, the two eigenvalues can be made as close to each other as desired until the proper ratio $\frac{A_1}{C_1}$ corresponding to the solution is captured. It is thus seen that the recursive scheme for the HE_{11} mode, not only solves the effective index but also results in the proper electric to magnetic field ratio.

In order to start the recursive scheme for the case of nonlinear core and linear cladding, the dielectric constant of the innermost layer ε_1 must be evaluated at the axis of the fiber. By examining the three electric field components contributing to the dielectric function, the following value for electric field intensity is obtained at r = 0

$$|E_0|^2 = |E_r|^2 + |E_\varphi|^2 = \left(\frac{\beta A_1}{\gamma_1}\right)^2 + \left(\frac{\omega\mu_0 C_1}{\gamma_1}\right)^2 \qquad r=0 \qquad (3.103)$$

It is noted that E_z vanishes at r = 0. The dielectric constant ε_1 is found

from equation (3.45) as

$$\varepsilon_1 = \varepsilon_{bg} + \frac{\alpha|E_0|^2}{1+g\alpha|E_0|^2} \qquad 0 \le r \le d_1 \qquad (3.104)$$

It must be noted that ε_1 is also embedded in γ_1. After substituting and arranging the terms, the following quadratic equation is obtained:

$$\gamma_1^2\varepsilon_1\,(\gamma_1^2 + F_1) = \gamma_1^2\varepsilon_{bg}\,(\gamma_1^2 + F_1) + F_2 \qquad (3.105)$$

Where F_1,F_2 and γ_1 are given by:

$$F_1 = g\alpha\left[\left(\frac{\beta A_1}{\gamma_1}\right)^2 + \left(\frac{\omega\mu_0 C_1}{\gamma_1}\right)^2\right]$$

$$F_2 = \alpha\left[\left(\frac{\beta A_1}{\gamma_1}\right)^2 + \left(\frac{\omega\mu_0 C_1}{\gamma_1}\right)^2\right]$$

$$\gamma_1 = (\varepsilon_1 k_0^2 - \beta^2)^{\frac{1}{2}}$$

By solving this quadratic equation ,the value of ε_1 is found. This value is necessary for starting the recursive scheme. To check the results obtained using the multilayer scheme, another numerical scheme is to be used. This

is the self-consistent scheme which is represented in the next section.

3.8 THE SELF-CONSISTENT SOLUTION NUMERICAL SCHEME

Because the solution of the nonlinear fiber adopted in this thesis is purely numerical, it is necessary to use another numerical scheme to compare the results. It is also of interest to show the advantages and disadvantages of each numerical scheme. The convergence and computational time are two important factors in comparing the two schemes.

The numerical scheme presented here is based on the method of the self-consistent solution of the nonlinear wave equation. This scheme has been reported by Fedrico Dois et al in 1989 [23]. It makes use of the self-consistent nature of the electromagnetic fields. The application of this method requires first the solution of the linear wave equation. The eigen field produced by this solution is taken to modify the dielectric function of the nonlinear fiber through the relation

$$\varepsilon(r) = \varepsilon_{bg} + \frac{\alpha|E(r)|^2}{1 + g\alpha|E(r)|^2} \qquad (3.106)$$

This results in a linear graded index profile which can be solved by a suitable multilayer scheme. The eigen field of the graded index fiber is then taken to produce another graded index profile which can be solved linearly. After

a certain number of iterations, the field distribution and the effective index are stabilized because of the self-consistent nature of the field. The final field is taken as the solution of the nonlinear problem. The method is simple and straightforward, but it suffers from some drawbacks. From the point of view of computational time the scheme requires much more time than the recursive scheme. The ratio between the two computation times is roughly equal to the number of iterations required for the self-consistent scheme to converge.

The convergence in the recursive scheme depends mainly on the number of layers. We found that 100 layers give good convergence (six significant digits) in most cases. The self-consistent routine requires at least 10 iterations for convergence in most cases. When the dispersion relation is multivalued (interface intensity versus mode index), the convergence of the self-consistent scheme is slow in the negative slope region. Because there are three values of n_e sharing the same intensity value, The routine sometimes fails to converge to the required value of n_e (located in the negative slope region) which is the closest solution to the input field. To overcome this difficulty the increment between intensity values should be very small. Another difficulty arises when the fiber with nonlinear core and linear cladding is cut-off at low power ($\varepsilon_{bq} < \varepsilon_2$). For such a case there is no linear solution corresponding to the cut-off fiber to start with. However, the

dispersion curve in this case can be traced from the saturable solution corresponding to $\varepsilon_1 = \varepsilon_{bg} + \frac{1}{g}$. The turning points on the dispersion curve, when the slope changes its sign, are also difficult to obtain.

In each run of the self-consistent routine, the effective index and the corresponding field distribution are obtained for a certain value of surface intensity. If this field profile is not stored it cannot be retrieved from knowledge of the effective index and surface intensity. In our recursive scheme, knowing a point on the dispersion relation curve is enough to obtain its corresponding field profile. The recursive scheme is also superior in the case of multivalued solution. The reason for this comes from the fact that the recursive scheme is governed by the value of the input field at the fiber axis which produces a unique value of n_e .

CHAPTER 4

DISPERSION CHARACTERISTICS OF METAL-CLAD OPTICAL FIBER

4.1 INTRODUCTION

Having developed the mathematical formulation of the recursive scheme in chapter 3 and checked it in the solution of eigenvalue equation for different types of lossless fiber structures consisting of two or three layers, the scheme can be applied to more complicated structures containing a metal as the outer layer. These structures are of importance particularly because of their attenuation that leads to application in mode filtering and the design of polarizers.

The fiber configurations that will be studied are: 1) hollow metallic step-index metal-clad fiber, 2) step index metal-clad fiber with a buffer layer between the core and the metal cladding and 3) a four-layer structure which has a very thin buffer layer separating the cladding layer form the metal cladding The first structure is covered in section (4.5.1). Section (4.5.2) is devoted to the second three-layer structure. The four layer structure which exhibits a thin dielectric buffer layer between the cladding and the outer

metallic jacket is investigated in section (4.5.3). The two important cases of a low-index buffer and a high-index buffer will be considered.

For the two layer step-index metal-clad fiber, the TE and the TM lowest order modes are to be investigated as well as the hybrid HE_{11} mode. However, for the three and four layer structures the study essentially concentrates on the TE and the TM modes because the main practical objective of this investigation is to use the waveguide as a polarizer or a mode filter. Also, there are some basic results reported for the planar metal-clad waveguide with structures similar to those mentioned for the fiber. We expect the cylindrical structure to behave in some respects the same as the planar waveguide specially when the fiber radius is large enough compared to the wavelength. When the radius of the cylindrical waveguide becomes very large it can be treated as a planar waveguide.

The hybrid mode HE_{11} is to be studied also in a multilayer structure for a special case of a single TE mode fiber. This fiber also supports TM_{01} as well as HE_{11} . In so doing, it is possible to compare the attenuation of the lowest order modes having different polarizations. This is the subject of section (4.5.4) of this chapter.

In the next sub-section (4.2), some of the important optical properties of metals are discussed. The investigation of metal-clad slab and cylindrical

waveguides will follow in sections (4.3) and (4.4) respectively.

4.2 OPTICAL PROPERTIES OF METALS

The permittivity of a lossy dielectric or a metal can be represented by:

$$\varepsilon = \varepsilon_0 \varepsilon_r = \varepsilon_0 \left(\varepsilon' + \frac{i\sigma}{\omega \varepsilon_0}\right) = \varepsilon_0 \left(\varepsilon' + i\,\varepsilon''\right) \tag{4.1}$$

where σ is conductivity, ε_r is the relative permittivity and ε' and ε'' are the real and imaginary parts of ε_r respectively. The refractive index is defined in terms of the relative permittivity as:

$$n = \varepsilon_r^{\frac{1}{2}} = n' + i\,n'' \tag{4.2}$$

where n' and n'' are the real and the imaginary parts of n . The extinction factor of the metal is represented by n'' . The values of the dielectric constant and refractive index for some of the most commonly used metals are listed in table 4.1 at $\lambda = 0.6328\ \mu m$ [24] . It is clear from the table that most of the metals exhibit a permittivity with a negative real part at the optical frequencies. The factor n'' compared to n' determines how lossy the metal is. It is shown in [24] that the three-layer structure consisting of a dielectric substrate, a dielectric core and a metal cladding can support guided modes when the metal has a permittivity with a positive real part,

TABLE 4.1

The relative permittivities and refractive indices of some important metals at a wavelength = 0.6328 μm [24].

Metal	ε'	ε''	n'	n''
Aluminum	-47.0	16.3	1.172	6.955
Copper	-10.0	1.0	0.158	3.166
Gold	-10.3	1.0	0.156	3.213
Silver	-16.3	0.51	0.063	4.04
Chromium	5.07	14.9	3.226	2.309
Germanium	17.4	15.3	4.504	1.698

under certain conditions. However, in this chapter only metals having permittivities with negative real parts are to be considered. This will enable guidance to occur with no restrictions on the metal used.

4.3 PLANAR METAL-CLAD WAVEGUIDE

For the metal-clad slab waveguide the extensive reported work covers different structures involving the metal as the outer layer. The three-layer waveguide consisting of a dielectric core, a metal cladding and a dielectric or air substrate exhibits a strong attenuation difference between TE and TM modes. The TM modes are attenuated about one order of magnitude greater than the TE modes. Also the higher order modes are strongly attenuated in comparison to lower order modes. The choice of the metal affects the attenuation characteristics. Metals with a large value of n'' lead to modes that have higher attenuation factors than those with a small value of n''. Mode attenuation can also be increased by reducing the guide thickness.

A technique to reduce the guided-mode attenuation is obtained by introducing a thick buffer layer between the core layer and the metallic cladding. For this case the guided energy absorbed by the metal is decreased because of the buffer layer. The thickness of the buffer layer controls the amount of attenuation for the waveguide. It should be chosen in such a way that the metal has a considerable effect on guided modes within

the core region. Reduction in the attenuation of the three-layer waveguide is also obtainable by increasing the waveguide thickness.

One important waveguide structure was studied by Yamamoto et al. in 1978 [25]. The waveguide is shown in fig. (4.1.a). The thickness of the buffer layer is very small compared to waveguide thickness and its refractive index is less than the guide indices n_1 and n_2. The attenuation of this waveguide depends on four factors, namely the waveguide thickness, the buffer layer thickness, the refractive index of each layer and the type of metal used as a cladding. Some of these factors, for instance, the guide thickness and the type of metal used have been discussed in the above sections. However, the thickness of the buffer layer has a great importance in the attenuation process. It will be studied for slab waveguide in the next paragraph and for the fibers in section 4.5.3

It has been shown in [25] that the attenuation of the TM_0 guided mode exhibits an absorption peak at a specific thickness of the buffer layer. This feature is important in the design of TE-TM mode filter with a high extinction ratio. Focusing attention on the TE_0 and TM_0 modes, at the absorption peak, the TM losses are about three orders of magnitude greater than the TE losses. This is shown in fig.(4.1.b). The losses of the TE modes are decreasing with the increase of the buffer layer thickness. Also, higher order

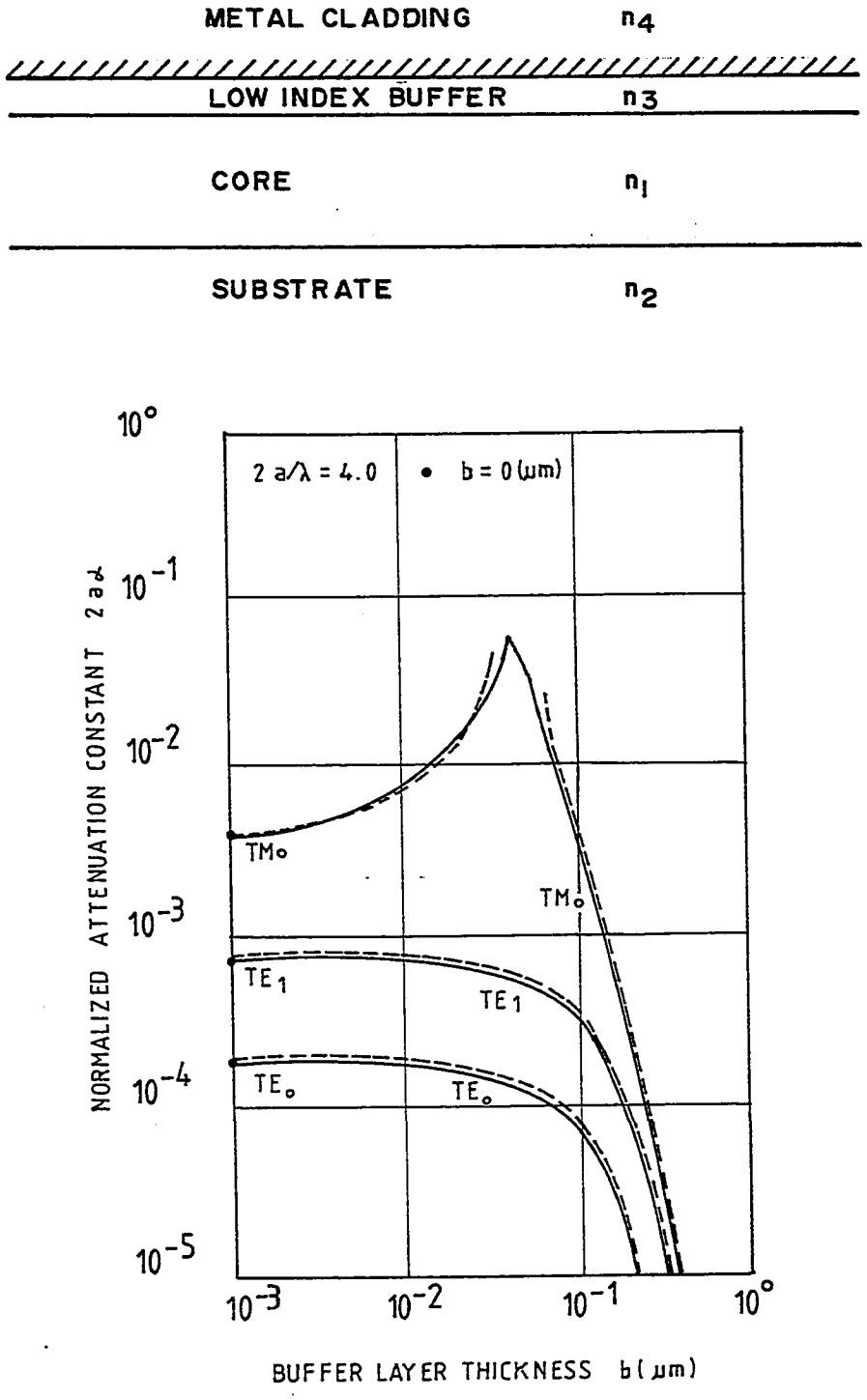

Fig.(4.1)
a) Multilayer metal-clad planar waveguide
b) Variation of attenuation factor with buffer thickness [25] .

modes have higher attenuation than lower order modes. Another four-layer structure different from that of reference [25] was reported by Jamid and Al-Bader in 1987 [26]. The waveguide structure uses a high-index buffer-layer instead of the low-index buffer used in reference [25]. It has been shown that this high-index buffer structure operates in dual mode as that of [25] and in fact discriminates against TE polarization.

4.4 METAL-CLAD OPTICAL FIBER

The reported work on metal-clad optical fibers is much less than that on planar optical waveguides. The reasons for this is that the optical fiber are normally used for long distance transmission with lossless materials used for core and cladding. Lossy jackets are kept at appreciable distance from the fiber axis for the purpose of loss reduction.

Most of the reported work on three-layer fiber structures treats the third layer (jacket) as a lossy dielectric [27]−[30]. The attenuation produced by a lossy dielectric is much less than that of a real metal, and therefore, perturbation analysis can be used to find the attenuation characteristics of these fiber structures [27] and [28].

The picture is completely different if the metal-clad fiber is to be used for specific applications involving mode filtering and the designing of TM or TE polarizers [31]−[32]. In this case, a real metal with considerable attenuation

properties must be used as a direct cladding or outer jacket. In such a case, the metallic jacket should be close enough to the core to influence the propagational characteristics of the waveguide. A complete exact solution of the guided modes must be obtained for the multilayer cylindrical waveguide without applying any approximation such as perturbation theory.

In 1989 Blok and Gorbulsky studied the hollow metallic waveguide [33]. They approximated the metal permittivity by a negative real number and considered a model having the following parameters: $\varepsilon_{co}=1$, $\varepsilon_{cl}=-1$ and $\lambda=2\pi a$ where a is the core radius. The dispersion characteristics for the proposed model have been obtained as a relation between the real propagation constant β and the fiber V number defined as:

$$V = ak_0(n_1^2 - n_2^2)^{1/2} \tag{4.3}$$

Where a is the core radius, k_0 is the free space wavenumber, n_1 is the core refractive index and n_2 is the cladding refractive index. The attenuation characteristics for such waveguide structure cannot be studied in this approximation. A real metal should be assumed which has both a negative real part and an imaginary part. It has been shown in [33] that the hybrid mode HE_{11} for this hypothetical structure has a cut-off frequency different from zero. This is contrary to the case of a dielectric-clad fiber where the

fundamental mode HE_{11} has a zero cutoff frequency. The fundamental mode in [33] is the TM_{01} mode which has the lowest cutoff frequency. Both the hybrid mode HE_{11} and the TE_{01} mode have the same cutoff frequency which is higher than that of TM_{01}. Also the cutoff values of the guided modes are shifted towards the higher frequency region (higher V number).

The three-layer radially stratified metal-clad optical fiber has also been studied by Charles Y. H. et al. in 1989 [34]. The eigenvalue equation for this structure is derived and solved numerically for TM and TE modes. This investigation facilitates the solution of D-shaped metal-clad fiber which can be reduced under conformal mapping transformation to the three layer cylindrical waveguide. The results obtained in this investigation show that for the D-shaped metal-clad fiber the attenuation of TM modes is greater than the attenuation of TE modes while the effective index of a certain TE mode is greater than that of the corresponding TM mode. These conclusions are common in both the planar and the cylindrical waveguides.

4.5 NUMERICAL RESULTS AND CONCLUSIONS

In this section, all the attenuation characteristics of metal-clad cylindrical waveguide are developed. The section is divided into three sub-sections covering two-layer, three-layer and four-layers metal-clad cylindrical waveguide. The different waveguide structures are shown in fig.(4.2)

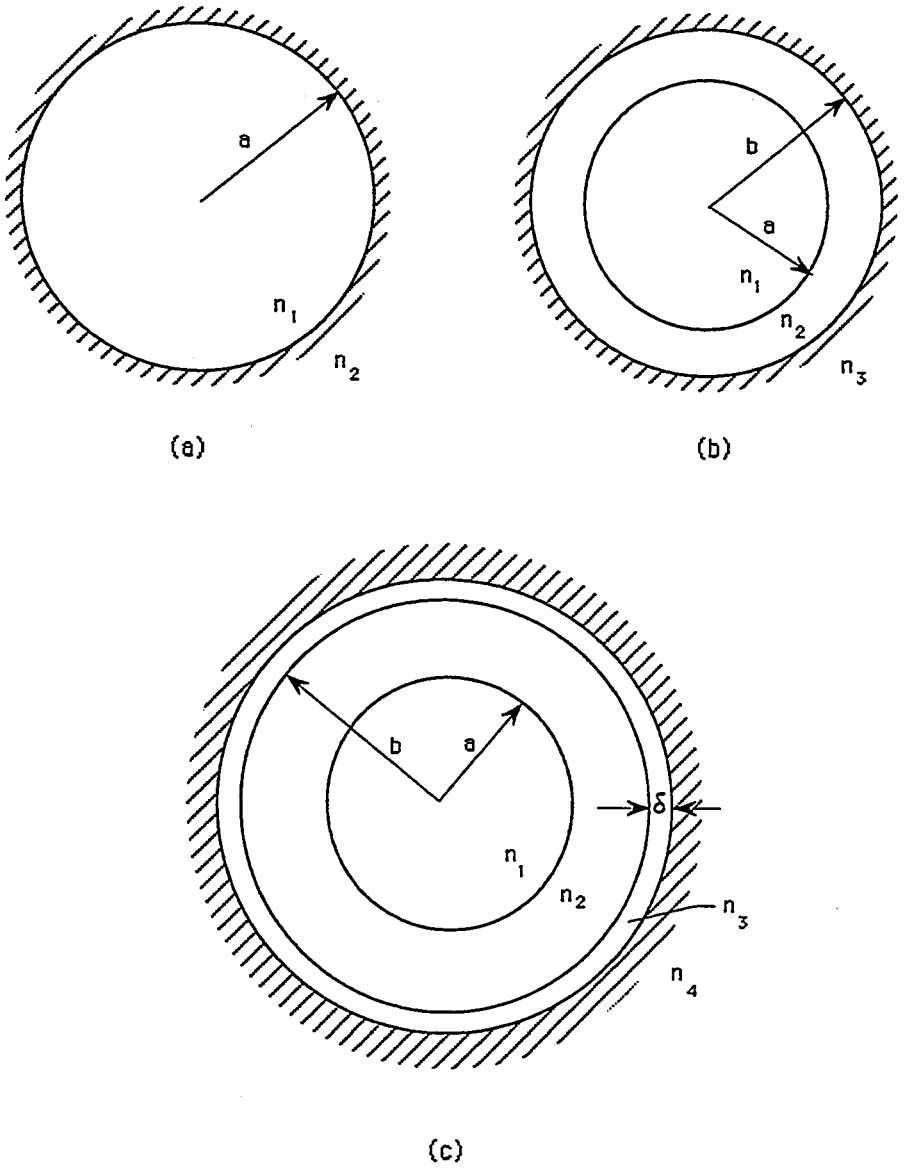

Fig.(4.2) a) Two-layer metal-clad optical fiber

b) Three-layer metal-clad optical fiber

c) four-layer metal-clad optical fiber

4.5.1 Dielectric-Metal Cylindrical Waveguide

The first cylindrical structure investigated is shown in fig.(4.2.a). The waveguide consists of dielectric core surrounded by a metal cladding. The waveguide parameters are as follows: $n_1^2 = (1.51)^2$, $\lambda = 0.6328\ \mu m$, $a = 6\ \mu m$ and $n_2^2 = -10.3 + j1$ (*gold*)

The dispersion and attenuation characteristics of this waveguide for fundamental TE, TM and HE modes have been studied. The results obtained by solving the direct eigenvalue equation and by using the recursive scheme are identical. These values are shown in table 4.2. The reason for this consistence arises from the fact that the recursive scheme indirectly generates the same eigenvalue of linear fiber regardless of the number of layers used. Fig.(4.3) shows a plot of the effective index versus the fiber radius. It can be seen that the fundamental mode is HE_{11}. Unlike the dielectric-clad fiber, the HE_{11} mode has a nonzero finite cut-off frequency. Another observation drawn from fig.(4.3) is the shift of cut-off frequencies of both TE_{01} and TM_{01} towards the lower frequency range (smaller core radius). For example, if the metal-clad of fig.(4.2.a) is replaced by a dielectric with $n_2^2 = (1.50)^2$, the resultant cutoff core radius of both TE_{01} and TM_{01} is 1.394 μm, which is equivalent to a V number equal to 2.405. It can be shown from

TABLE 4.2

The effective indices of the TE_{01}, TM_{01} and HE_{11} modes in a two-layer metal-clad fiber, obtained from the direct solution of the eigenvalue equation and the recursive scheme.

Mode	Solution	n_e'	n_e''
TE_{01}	recursive scheme	1.508654	0.497621(-6)
TE_{01}	eigenvalue equation	1.508654	0.497621(-6)
TM_{01}	recursive scheme	1.508581	0.358786(-5)
TM_{01}	eigenvalue equation	1.508581	0.358786(-5)
HE_{11}	recursive scheme	1.509456	0.806624(-6)
HE_{11}	eigenvalue equation	1.509456	0.806624(-6)

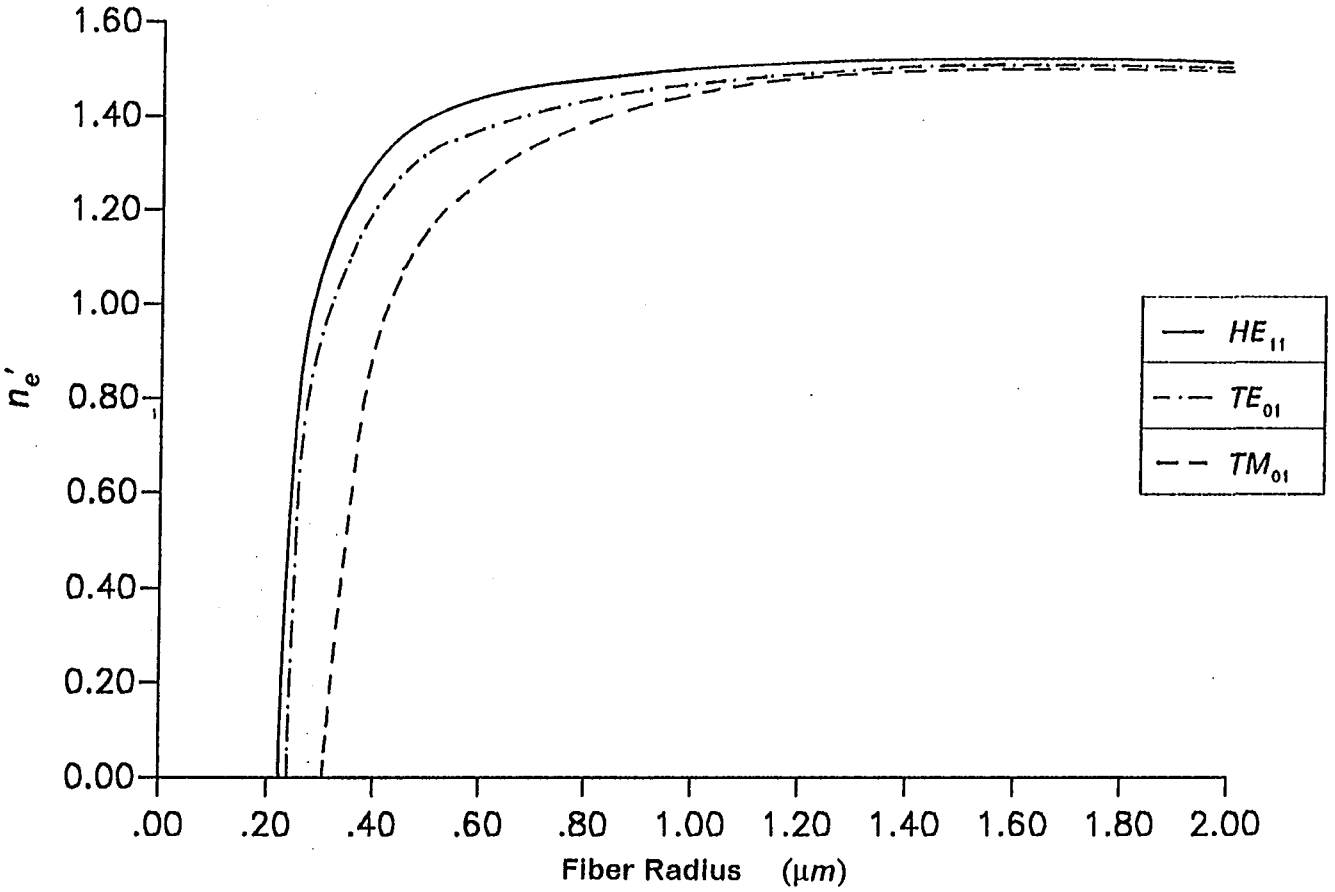

Fig.(4.3) Variation of n_e' with fiber radius

fig.(4.3) that these values for a metal-clad fiber are 0.22 μm and 0.27 μm for the TE_{01} and the TM_{01} respectively. The third conclusion that can be drawn from fig.(4.3), is that the effective index for the three investigated modes has an asymptotic value equal to the core index value as the fiber radius becomes very large. This feature is similar to that of the dielectric-clad fiber. One of the above conclusions has been obtained in [33], which is the nonzero cutoff frequency of the HE_{11} mode. All other conclusions contradict the results obtained in [33]. As has been mentioned in the previous section they reported in [33] that the fundamental mode is TM_{01} and the cutoff values move towards higher frequency region. Also the dispersion characteristic obtained in [33], shows that the effective index can exceed the core index value for all modes. The reason for these discrepancies is the use of hypothetical model in [33] which does not represent a real metal.

The attenuation characteristics of the dielectric-metal cylindrical waveguide are shown in fig.(4.4) as a plot of n_e'' versus the core radius. The actual attenuation coefficient is defined as $\alpha = k_0 n_e''$. All field components are attenuated with rate $e^{-\alpha z}$. However the attenuation coefficient for power is 2α since the power is proportional to the square of electric or magnetic field. Throughout the work of this chapter the attenuation will be represented by n_e'' which is considered as the normalized attenuation factor.

It is seen from fig.(4.4) that the attenuation of the TM_{01} mode is larger than

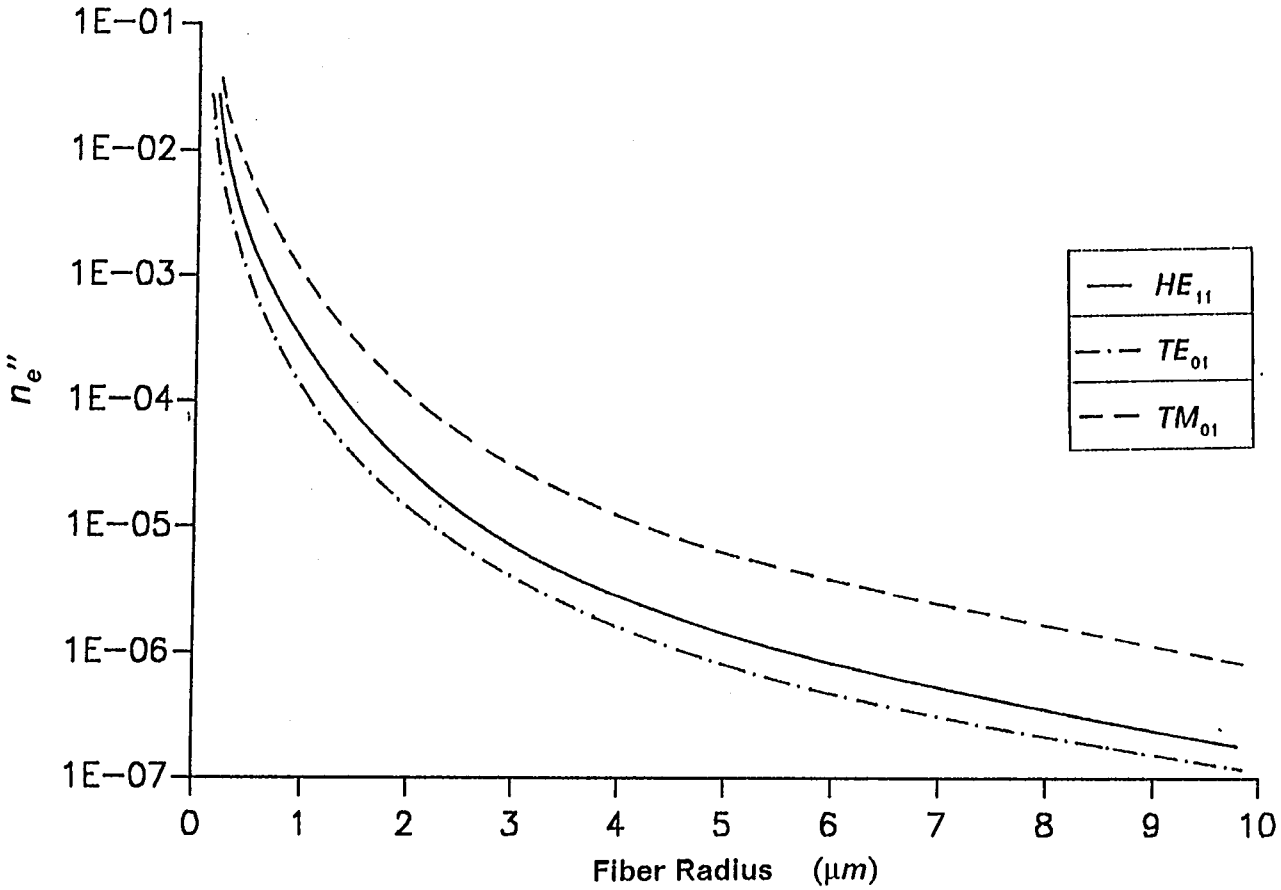

Fig.(4.4) Variation of n_e'' with fiber radius

that corresponding to TE_{01} mode by about an order of magnitude. The HE_{11} mode has a moderate attenuation which is greater than that of the TE_{01} mode and smaller than that of the TM_{01} mode. In addition the attenuation is a decreasing function of the fiber radius. The interaction between the metallic cladding and the guided field inside the core, decreases as the radius becomes larger.

4.5.2 THE THREE-LAYER METAL-CLAD FIBER

The waveguide is shown in fig.(4.2.b). The metal is used as a jacket surrounding the dielectric cladding. The waveguide parameters are as follows: $n_1^2 = (1.51)^2$, $n_2^2 = (1.50)^2$, $n_3^2 = -10.3 + j1$ (*gold*), $\lambda = 0.6328\ \mu m$, $a = 6\ \mu m$ and $b = 7.2\ \mu m$.

The modes of this waveguide have in general a smaller attenuation compared to the corresponding modes of the previous section. The reason for this reduction in mode attenuation is the reduced interaction between the guided field (which resides mostly in the core) and the metallic layer. A parameter c=b/a has been defined in the description of the performance of the structure. There are two limiting cases of this parameter. The first one for c=1, the fiber is reduced to the two layer cylindrical waveguide of section (4.4.1). The second limiting value is $c = \infty$ and the fiber in this case reduces to dielectric step-index fiber. In practice c should not be much

greater than 1 in order that the influence of metal on guided modes be of appreciable magnitude. The value of c has been chosen to be 1.2 in the study of the three-layer cylindrical waveguide. The direct eigenvalue equation derived by Unger [15] has been solved numerically for the above fiber parameters. Solution of the problem has also been obtained by using the recursive scheme. Table 4.3 lists the values of the effective index of the two solutions for both TE_{01} and TM_{01} modes. It is seen from table 4.3 that the two methods of solution exhibit agreement to six significant digits. the recursive scheme generates indirectly the same closed form eigenvalue equation.

4.5.3 THE FOUR-LAYER STRUCTURE

It must be stated from the outset that the objective of the study of three-layer structure shown in fig.(4.2.b) is in order to check our recursive scheme against the solution of the exact eigenvalue equation. Confidence in the recursive scheme enables us to apply it in the solution of more important waveguide structures. The four-layer waveguide shown in fig.(4.2.c) contains a thin dielectric buffer layer between the cladding and the metallic layer. An eigenvalue equation can be derived for this four layers structure. However, the effort involved is large. The three-layer structure can, however, be represented by 8×8 matrix [15]. The representation of the four-layer structure requires a 12×12 matrix containing different kinds of

TABLE 4.3

The effective indices of the TE_{01} and TM_{01} modes in a three-layer metal-clad fiber, obtained from the direct solution of the eigenvalue equation and the recursive scheme.

Mode	Solution	n_e'	n_e''
TE_{01}	recursive scheme	1.508867	0.240928(-7)
TE_{01}	eigenvalue equation	1.508867	0.240928(-7)
TM_{01}	recursive scheme	1.508860	0.282922(-6)
TM_{01}	eigenvalue equation	1.508860	0.282922(-6)

Bessel functions. Also, numerical techniques are required to solve the resulting 12×12 determinant to obtain the eigenvalues of the structure.

The recursive scheme adopted here relies on the elimination of field coefficients for each layer. As we have seen in chapter 3, this reduces the mathematical effort to dealing with 2×2 matrix operations for TE and TM modes and a 4×4 matrix operations for the hybrid modes irrespective of the number of layers of the waveguide structure. It must be noted that the same recursive scheme can be used to solve inhomogeneous fiber problems as well. In such a case, the inhomogeneous index profile is used to generate the values of ε for each layer.

As indicated in the case of the slab waveguide, the factors involving in the guided mode attenuation are many. The most important one for the four-layer structure is the buffer layer thickness. For this reason all waveguide parameters are going to be fixed and only the thickness of the buffer layer will be varied in order that its effect on the attenuation characteristics be indicated.

4.5.3.1 THE FOUR-LAYER STRUCTURE WITH A LOW-INDEX BUFFER LAYER

The waveguide model is shown in fig.(4.2.c). The metal used is gold and the fiber parameters are as follows: $n_1^2 = (1.51)^2$, $n_2^2 = (1.50)^2$,

$n_3^2=(1.30)^2$, $n_4^2=-10.3+j1(gold)$, $a=6\ \mu m$, $c=1.2$ and $\lambda=0.6328\ \mu m$.

The mode attenuation represented by the imaginary part of the effective index n_e'' is plotted versus the buffer-layer thickness for the three lowest order TE modes, see fig.(4.5). It is maximum for zero buffer thickness and decreases with increasing buffer-layer thickness. However, the TM modes for the same waveguide structure have a different attenuation characteristics. These attenuation characteristics are shown in fig.(4.6) as a plot of n_e'' versus the buffer thickness. Each mode exhibits an absorption peak at a specific critical buffer layer thickness. This absorption peak is caused by resonance coupling to the lossy TM surface mode. At these absorption peaks the attenuation of the TM modes is about 2-3 orders of magnitude greater than the TE modes. In such cases the extinction ratio will be large enough to design a good TE pass polarizer. Numerical values of extinction ratio for different fiber configurations, with the corresponding transmission losses will be given at the end of this chapter.

It must be noted that the type of metal used affects the amount of attenuation for both TE and TM modes. For example, if the gold (which has been used in our investigation) is replaced by Aluminium the attenuation will increase because Aluminium has permittivity with a relatively large imaginary part as shown in table 4.1. However, the general characteristics of figs.(4.5)

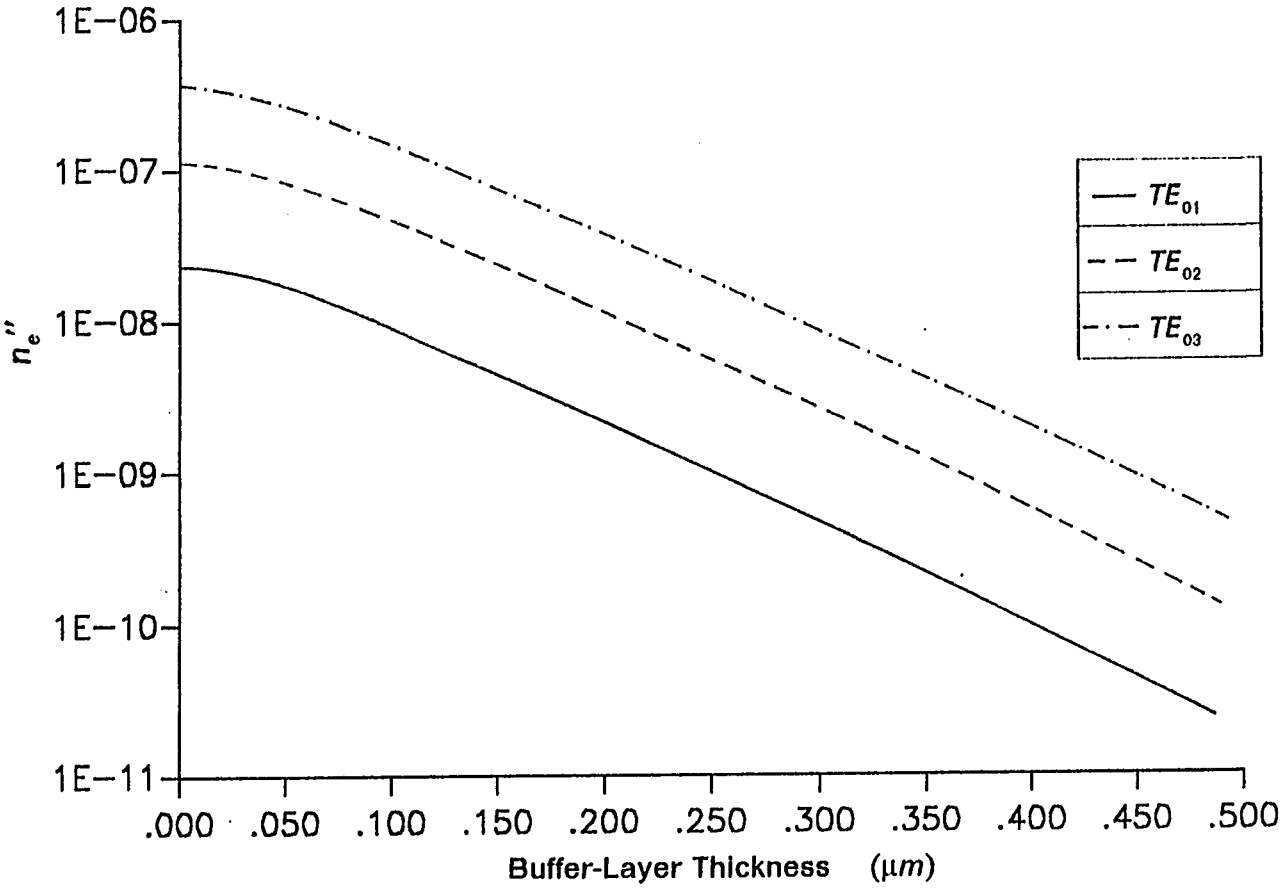

Fig.(4.5) Variation of n_e'' with buffer-layer thickness for TE modes

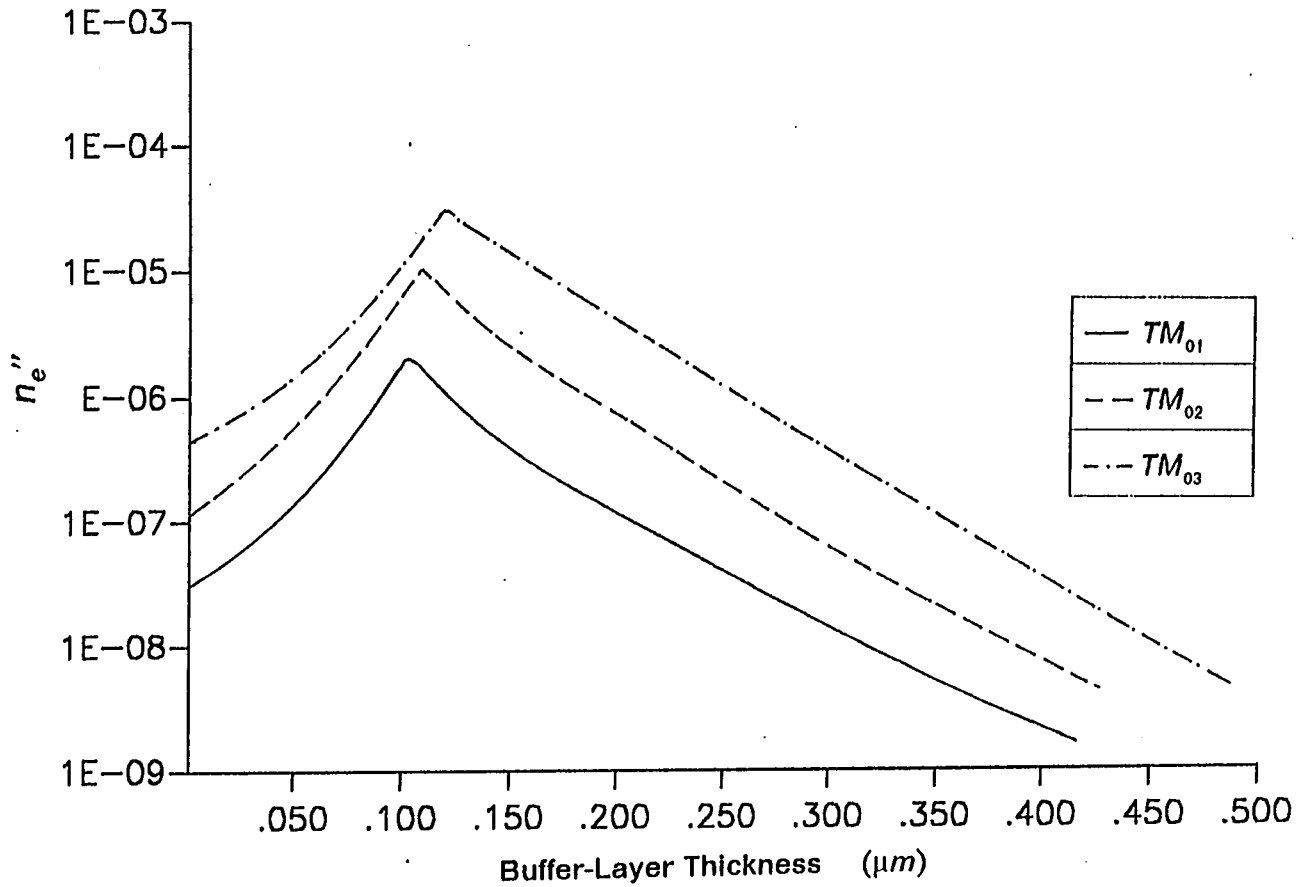

Fig.(4.6) Variation of n_e'' with buffer-layer thickness for TM modes

and (4.6) will remain unchanged. The attenuation plots will in this case exhibit a shift of the attenuation peak to higher values. Another important factor in designing polarizers is the insertion loss which should be minimized to have an efficient polarizer. The insertion loss is mainly the sum of three losses, two of them are due to the coupling at the input and output sections of the polarizer and the third one is the transmission loss through the length of the polarizer. The coupling losses are generally difficult to calculate. The insertion loss is usually measured experimentally. The coupling losses can be minimized when the polarizer used is of in-line type. This type of polarizer will be explained in some details at the end of this chapter. Therefore, the transmission loss can only be considered. As a matter of fact the TE normalized attenuation factor at the TM absorption peaks are between 10^{-5} and 10^{-6} which enable the TE waves to move a relatively large distance through the guide before being substantially attenuated. Table 4.4 shows the values of n_e for the first three lowest order TM modes at the absorption peaks and the corresponding TE values.

4.5.3.2 THE FOUR-LAYER STRUCTURE WITH A HIGH-INDEX BUFFER LAYER

The model used for this case is similar to the low-index buffer case except the value n_3 is now $(1.7)^2$. For this waveguide structure the attenuation of both TE and TM waves exhibit an oscillating behavior over the

TABLE 4.4

The effective indices of the three lowest order TM modes at the absorbing peaks and the corresponding TE values for the same low-buffer thickness in a four-layer waveguide structure.

Mode	δ (μm)	n_e'	n_e''
TM_{01}	0.105	1.508853	0.250770(-4)
TM_{02}	0.110	1.506175	0.110831(-3)
TM_{03}	0.120	1.502076	0.373227(-3)
TE_{01}	0.105	1.508859	0.919616(-8)
TE_{02}	0.110	1.506198	0.427356(-7)
TE_{03}	0.120	1.502097	0.150879(-6)

range of buffer layer thickness investigated between 0 and 1 μm . Fig.(4.7) illustrates this oscillating behavior for the TE_{01} and TM_{01} modes. There are two absorption peaks on each side of a minimum for this range of buffer-layer thickness. The important observation is that the peaks of the TE and the TM absorption are well separated. It is thus possible to discriminate against TE or TM polarization by the appropriate choice of the buffer-layer thickness.

This oscillating feature of the loss has been reported in [26] for the slab waveguide. In [26] the buffer-layer thickness nas been varied to cover the first absorption peak of both TE_0 and TE_1 modes as well as the minimum absorption of the TM_0 mode. In our investigation the buffer thickness has been extended to include two maximum attenuation points on each side of a minimum attenuation point for both TE_{01} and TM_{01} modes.

It must be noted that the attenuation of the slab structure mentioned above is about two orders of magnitude greater than that of the cylindrical waveguide. The reason for this is the strong influence of the metal on the guided fields inside the thin film compared to the cylindrical waveguide. The attenuation behavior of higher order modes is similar to that of the first mode shown in fig.(4.7). Table 4.5 gives the values of n_e'' at the first two absorption peaks and the corresponding high-index buffer-thicknesses for the first three lowest order TE and TM modes.

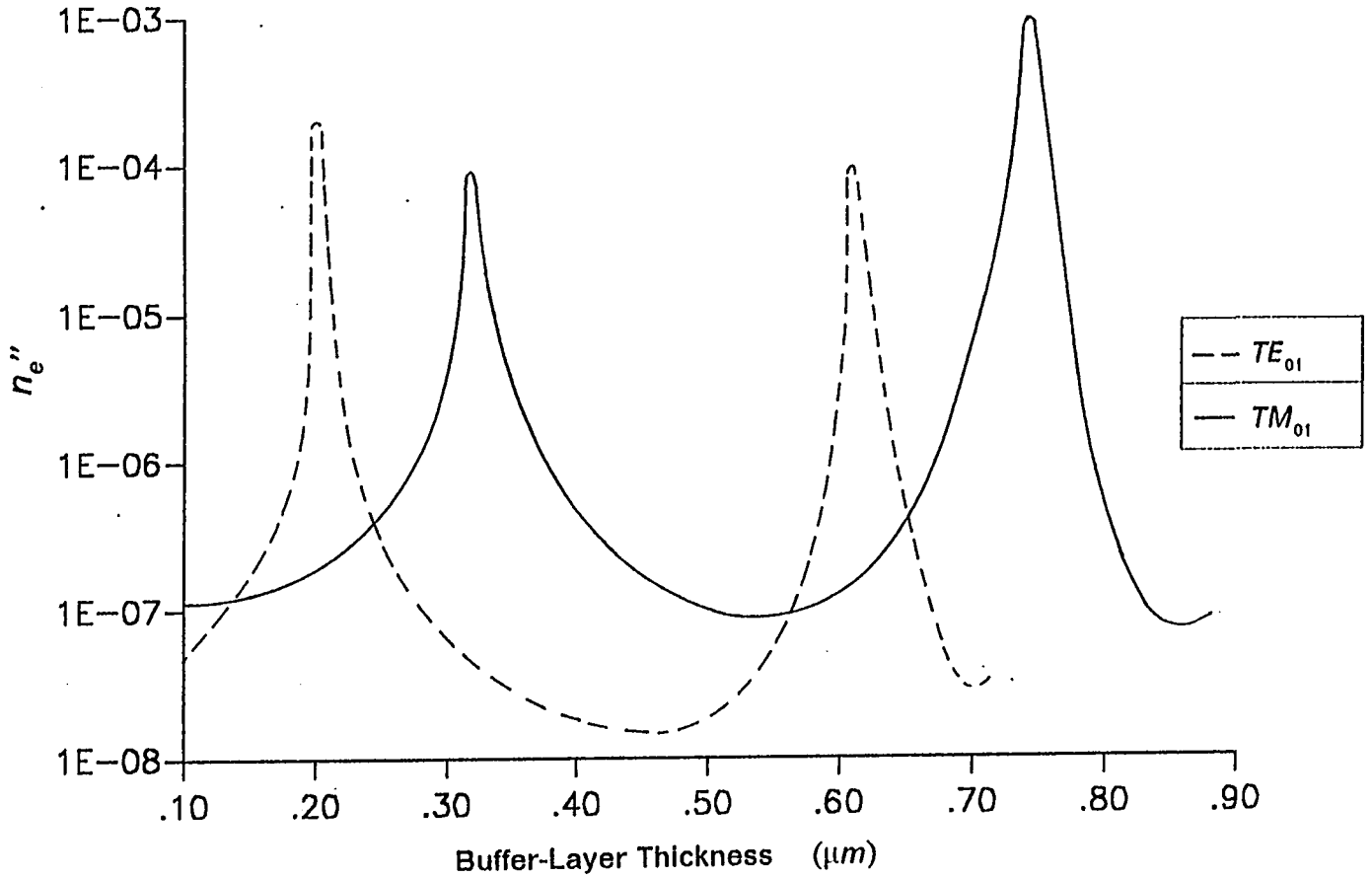

Fig.(4.7) Variation of n_e'' with buffer-layer thickness for TE_{01} and TM_{01} modes

TABLE 4.5

The effective indices of the three lowest order TE and TM modes at the first two apsorbtion peaks and the corresponding high buffer thickness in the four-layer waveguide structure.

Mode	δ (μm)	n_e'	n_e''
TE_{01}	0.200	1.50848	0.24561(-3)
TE_{01}	0.605	1.50865	0.10218(-3)
TE_{02}	0.195	1.50543	0.19482(-3)
TE_{02}	0.595	1.50671	0.11239(-3)
TE_{03}	0.185	1.50320	0.15340(-3)
TE_{03}	0.585	1.50340	0.15854(-3)
TM_{01}	0.320	1.50892	0.10736(-3)
TM_{01}	0.725	1.50890	0.14218(-3)
TM_{02}	0.320	1.50589	0.16168(-3)
TM_{02}	0.715	1.50660	0.29195(-3)
TM_{03}	0.300	1.50286	0.26584(-3)
TM_{03}	0.700	1.50300	0.30735(-3)

4.5.4 THE FUNDAMENTAL HYBRID MODE IN THE FOUR-LAYER STRUCTURE

To complete the study of loss of the lowest order TE and TM modes it is important to study the influence of the buffer layer on the HE_{11} mode. This mode is particularly important because it is the fundamental mode of the optical fiber. We have chosen a fiber radius of 3 μm which at $\lambda = 0.6328$ μm allows the support of TE_{01} and TM_{01} modes in addition to the HE_{11} mode.

For the case of low-index buffer, the HE_{11} mode behaves in a manner similar to that of TM_{01} mode. Only the attenuation of the hybrid mode is slightly less than that of the TM_{01} mode. This result is illustrated in fig.(4.8). It is also clear that the attenuation of both TM_{01} and HE_{11} modes is much higher than of that of TE_{01} mode. The attenuation difference reaches its maximum value when either TM_{01} mode or HE_{11} mode exhibit an absorption peak.

For the high-index buffer case, the attenuation factor (n_e'') is shown in fig.(4.9). The HE_{11} exhibits an oscillating behavior similar to the TE and the TM modes. For a buffer thickness between 0.0 and 0.3 μm the HE_{11} has an absorption peak which is located very close to the absorption peak of the TE_{01} mode. It can also be shown that there are some points of equal attenuation

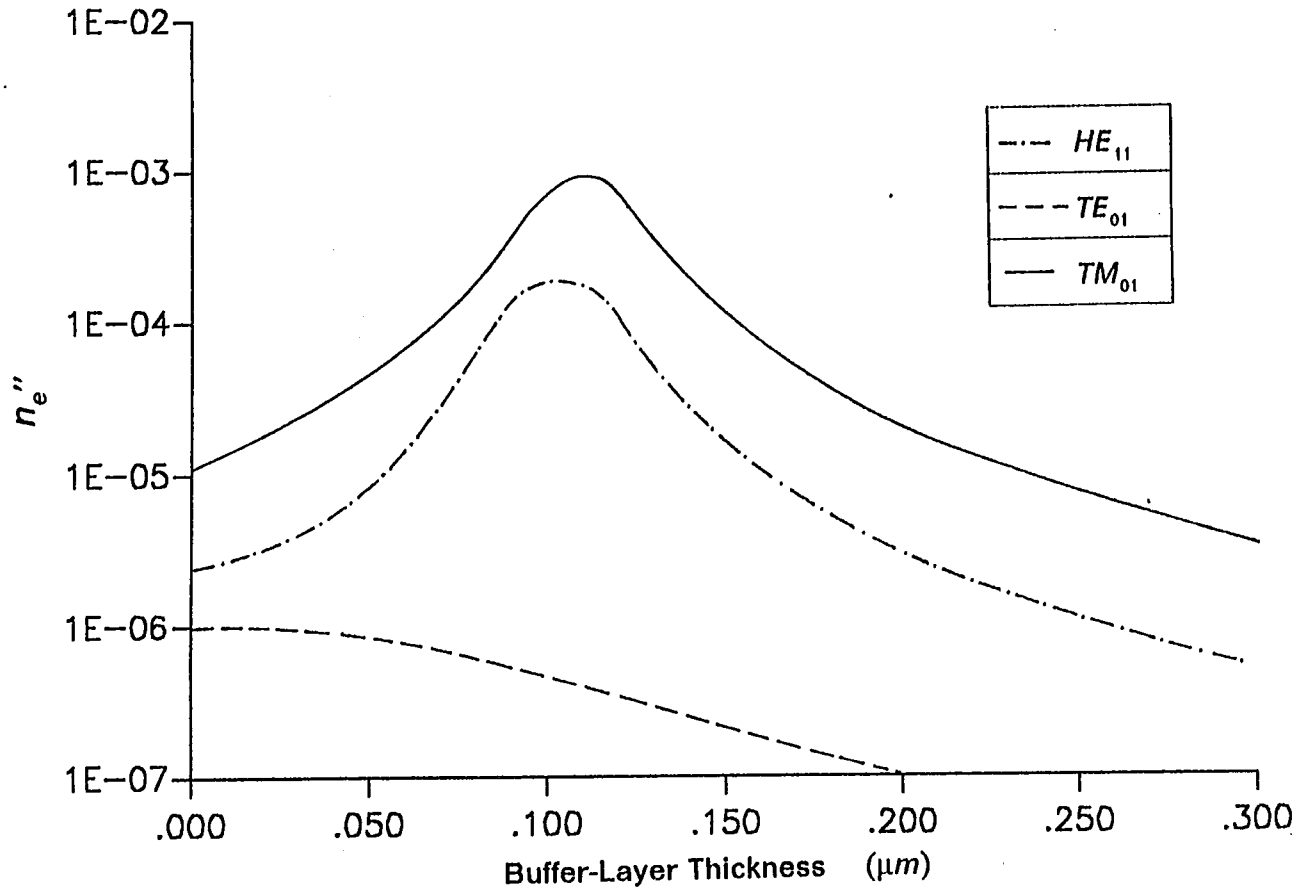

Fig.(4.8) Variation of n_e'' with buffer-layer thickness for HE_{11}, TE_{01} and TM_{01} modes

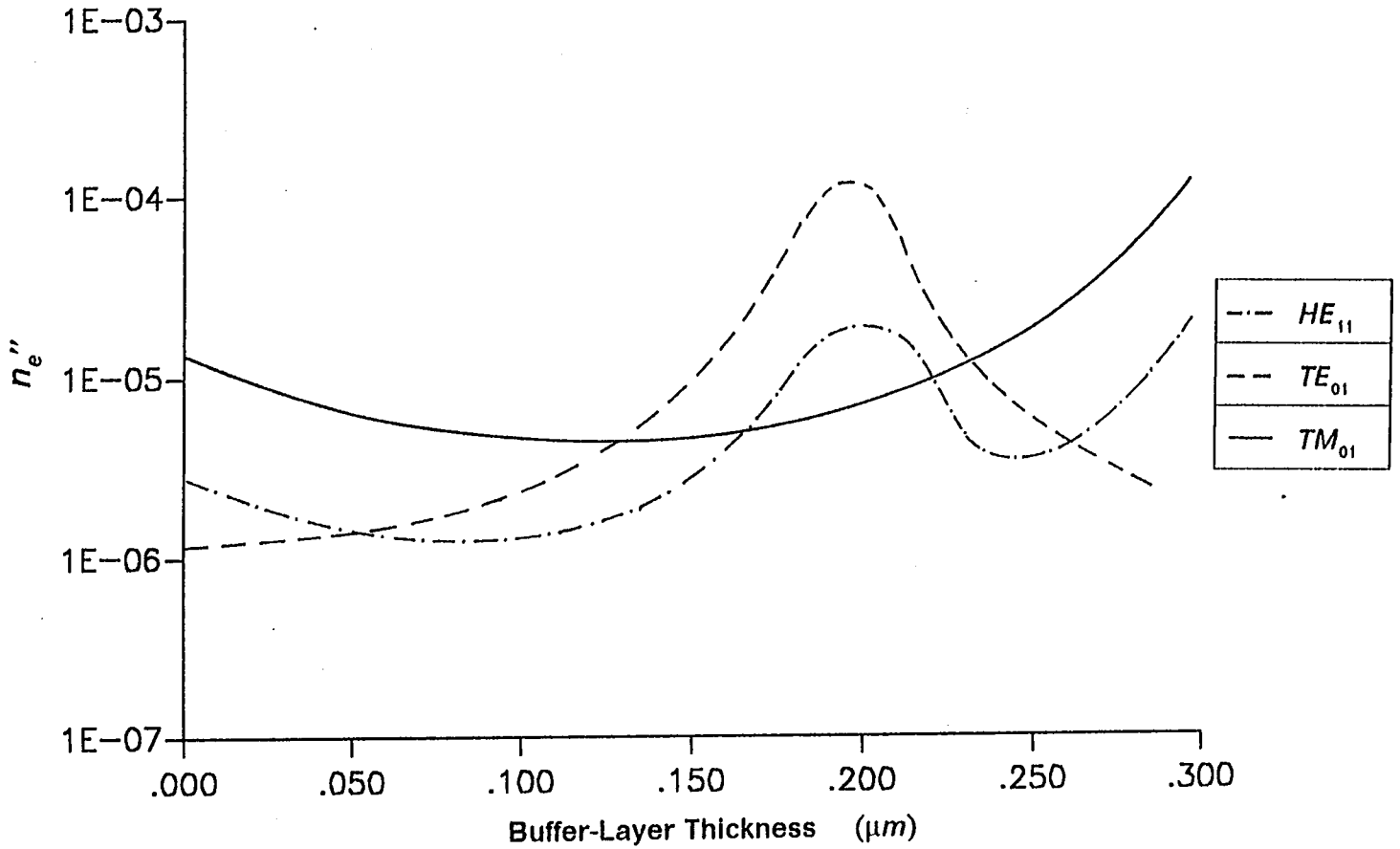

Fig.(4.9) Variation of n_e'' with buffer-layer thickness for HE_{11}, TE_{01} and TM_{01} modes

for different modes. For example, the HE_{11} and the TE_{01} modes have the same attenuation for some specific buffer thicknesses (0.05 μm and 0.26 μm).

The maximum attenuation occurs for The TE_{01} at a buffer thickness ($\delta = 0.19\ \mu m$). The imaginary part of effective index n_e'' for this maximum attenuation is 0.12380(-3) which means an equivalent loss of 106.77 db/cm at a wavelength of 0.6328 μm.

4.6 APPLICATIONS OF THE METAL-CLAD OPTICAL FIBER

The design of metal-clad fiber polarizers has received a large attention in the last few years [27]-[37]. The technique used in these references is essentially based on forming a metal-clad D-fiber. The polarizer is formed by grinding off the cladding on one side of the fiber and evaporating metals onto the polished surface. Figure (4.10) shows the cross-section and side view of such a fiber polarizer. It is called an in-line fiber polarizer because the metal-cladded area is formed on the main fiber. This helps to reduce the coupling losses. The structure shown in fig.(4.10) works as a polarizer by utilizing the attenuation difference between the TM_{01} and TE_{01}. It can also work as a TM-pass polarizer by utilizing the cutoff of the TE mode. The operation of some polarizers is based on the interaction between TM_{01} and the surface plasma waves inside the metallic coated region [40]-[42]. It is known that a single mode fiber can support two different perpendicular polarizations for

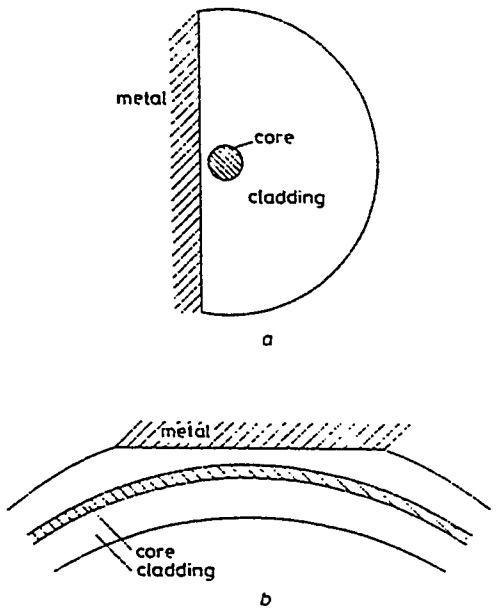

Fig.(4.10)
Structure of in-line D-fiber polarizer
a) cross-section b) Side view [37] .

the HE_{11} mode. The D-fiber can easily separate these two polarizations by the proper orientation of the flat edge of the D. This is important feature of the D-fiber. However the recursive scheme adopted in this thesis is only applied for circularly symmetric waveguide. In such a waveguide the two HE_{11} polarizations exist. The design of all the D-fiber polarizers depends on experimental testing. There is no rigorous analytical solution for the D-fiber configuration. The expected attenuation characteristics are taken qualitatively from the similar slab structure. Our recursive scheme is capable of solving different configurations of metal-clad optical fiber. This is an advantage which facilitates the choice of polarizer parameters to achieve certain design requirements. The extinction ratio and the transmission loss for different fiber structures have been calculated and listed in table 4.6. The extinction ratio is defined as the ratio between the attenuation of two different modes. The polarizer length is taken to be 3 cm for calculating the transmission loss. It is seen from table 4.6 that the low-index buffer structure is only suitable for a TE-pass polarizer with a high extinction ratio and a very low transmission loss. However, the high-index buffer structure can work as a TE-pass or TM-pass polarizer.

TABLE 4.6

The Extinction ratio and transmission loss of a four-layer metal-clad fiber

a) Low-index buffer-layer

Polarizer	δ (μm)	n_e''	*E.R.* (*db*)	*T.L.* (*db*)
TE-pass	0.10	0.411779(-6)	53.776	1.065

b) High-index buffer-layer

Polarizer	δ (μm)	n_e''	*E.R.* (*db*)	*T.L.* (*db*)
TE_{01}-*pass*	0.30	0.197180(-5)	24.195	5.102
TM_{01}-*pass*	0.20	0.721767(-5)	9.265	3.823
HE_{11}-*pass*	0.10	0.147750(-5)	9.727	18.674

CHAPTER 5

TE AND TM NONLINEAR GUIDED WAVES IN AN OPTICAL FIBER

5.1 INTRODUCTION

In this chapter and the next, the results on the behavior of the nonlinear guided modes in an optical fiber are given. The TE and TM nonlinear guided modes are presented in chapter 5 while the fundamental hybrid mode HE_{11} is investigated in chapter 6. The present chapter is divided into two main parts covering the lowest order TE and TM modes respectively.

In sections 5.2 and 5.3, the TE nonlinear guided waves are investigated. Two important fiber geometries are considered. In the first the core is nonlinear while the cladding is linear and in the second the core is linear while the cladding is nonlinear. In all cases, only self-focusing materials are considered. For these materials, the nonlinear coefficient is positive which means that the refractive index of the nonlinear material increases with the applied power.

In the case of a the cutoff fiber, the fiber will not transmit guided power at

low power levels because the background core refractive index is less than or equal to the cladding refractive index. This case is investigated in section 5.2. Guidance for this fiber can only take place when the applied field intensity exceeds a certain threshold value. The interface (surface) intensity means the value of light intensity evaluated at the core-cladding interface. It will be used frequently in this chapter and the next chapter.

When the cladding is nonlinear, the behavior of guided waves is considerably changed. The number of modes which can be supported by the fiber at low power increases with the applied intensity. The characteristics of the guided waves can be modified for this fiber with the shifting of the peak value of the field towards the nonlinear cladding.

The second part of this chapter (sections 5.4 and 5.5) is dedicated to TM nonlinear guided waves. All the investigations made for TE modes are repeated for the TM case. For the TM waves, there are two field components, E_z and E_r, contributing to the nonlinear dielectric constant while in the TE case only one electric field, E_{ph}, is affecting the dielectric constant.

All the results of this chapter have been obtained by the recursive scheme and checked using the self-consistent numerical scheme discussed in chapter 3. This is shown in section 5.6. The use of two numerical approaches is necessary because of the absence of analytical solution of the

problems at hand.

5.2 TE WAVES IN OPTICAL FIBERS WITH A NONLINEAR CORE AND A LINEAR CLADDING

The model used for this fiber structure is shown in fig.(5.1) where the nonlinear dielectric function is given by equation (2.43). Accordingly the dielectric function of the core material can be written as:

$$\varepsilon_1 = \varepsilon_{bg} + \Delta\varepsilon_{NL} \qquad (5.1)$$

where $\Delta\varepsilon_{NL}$ is the increment in the dielectric function due to the action of the field. This increment has a maximum value of $\frac{1}{g}$ for very large field. Three different cases have been studied. These are the fiber with $\varepsilon_{bg} > \varepsilon_2$, the cutoff fiber with $\varepsilon_{bg} = \varepsilon_2$ and the cutoff fiber with $\varepsilon_{bg} < \varepsilon_2$.

The first case investigated is a fiber which supports guided modes at low power. The fiber parameters used in the numerical investigation are as follows: $\varepsilon_{bg} = 2.255$, $\varepsilon_2 = 2.25$, $\alpha = 10^{-8}\ V^{2}m^{2}$, $g = 20$, $\lambda = 0.6328\ \mu m$ and $a = 4\ \mu m$. The values of α and λ are kept fixed at the above mentioned values for all investigations. The remaining parameters are changed for the individual cases of nonlinear optical fibers. For the present case, however, the fiber is made to be of the TE_{01} mode regardless of the amount of power

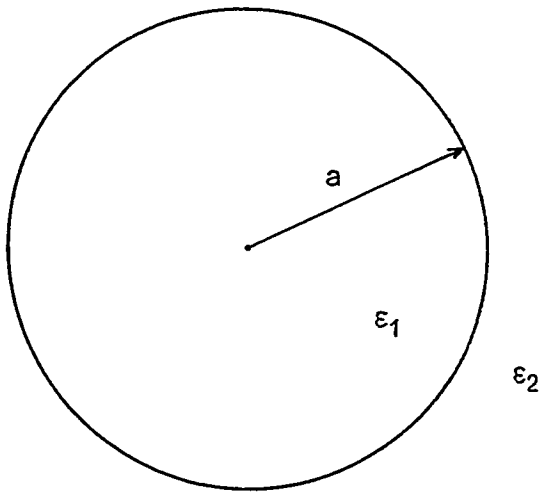

Fig.(5.1) Structure of nonlinear cylindrical waveguide

applied. Fig.(5.2) illustrates the dispersion characteristics for this fiber structure. The mode index is plotted versus the the surface intensity $|E_\varphi|^2$ at the core cladding interface. As seen from the figure, There are three distinct regions constituting the so called N curve. For low values of field intensity (represented here by the value at the core-cladding interface), there is only a single valued solution. There is one value of the mode index corresponding to one value of the interface intensity. As seen from the plot of fig.(5.2), the high intensity region has also a single valued solution. At intermediate values of surface intensity a multivalued solution is obtained. In this case a single value of surface intensity corresponds to three values of mode index.

The field profiles for interface value of E_φ equals to 410 V/m and corresponding to three mode index values are shown in figure (5.3). The plot shows the variation of E_φ across the fiber radius. The actual values of the electric field E_φ have been multiplied by a scaling factor SF to have the same value for all field maxima. This makes the comparison between field profiles more feasible. To retrieve the actual field profiles the plotted field values should be divided by the corresponding scaling factor SF. This method of comparing field profiles will frequently be used in this chapter and the next chapter. It is seen from fig.(5.3) that as the mode index increases, the field becomes better guided and confined in the core region. The

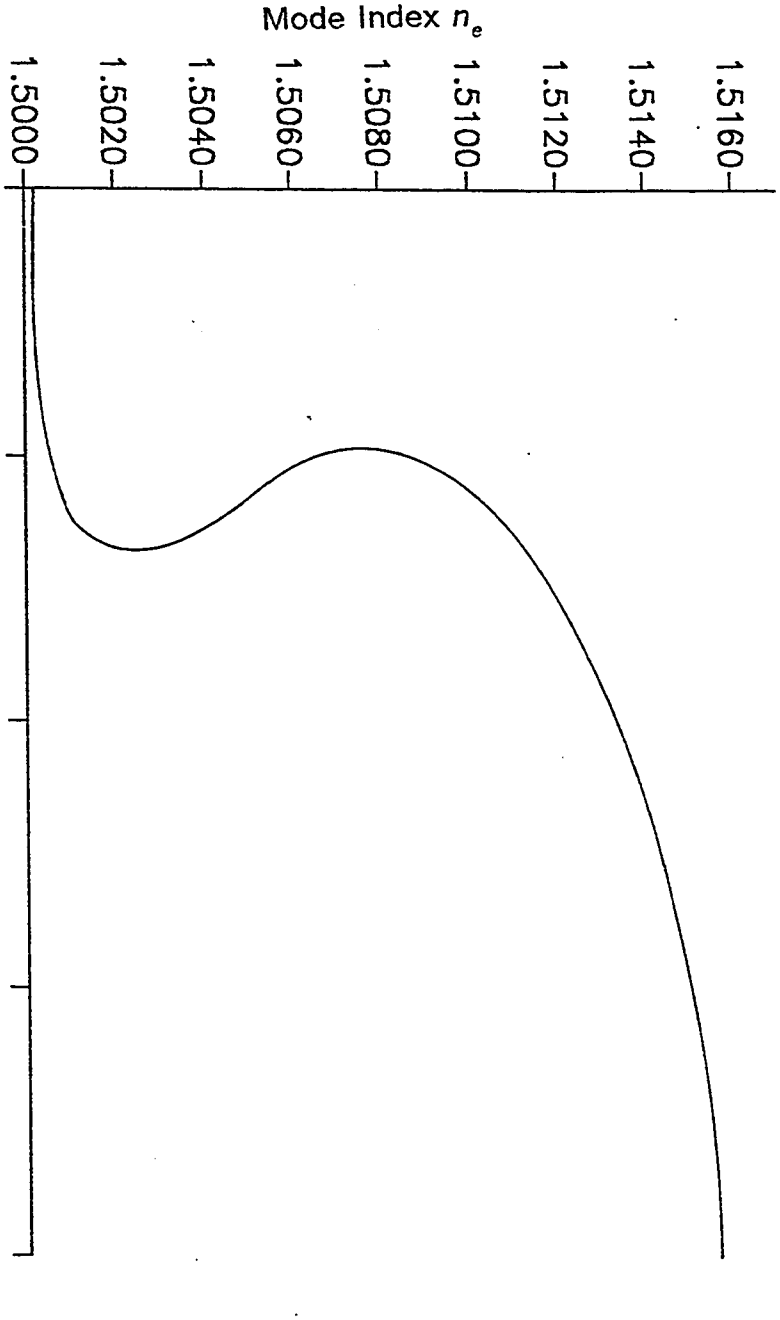

Fig.(5.2) Variation of n_e with the interface intensity for TE_{01} mode

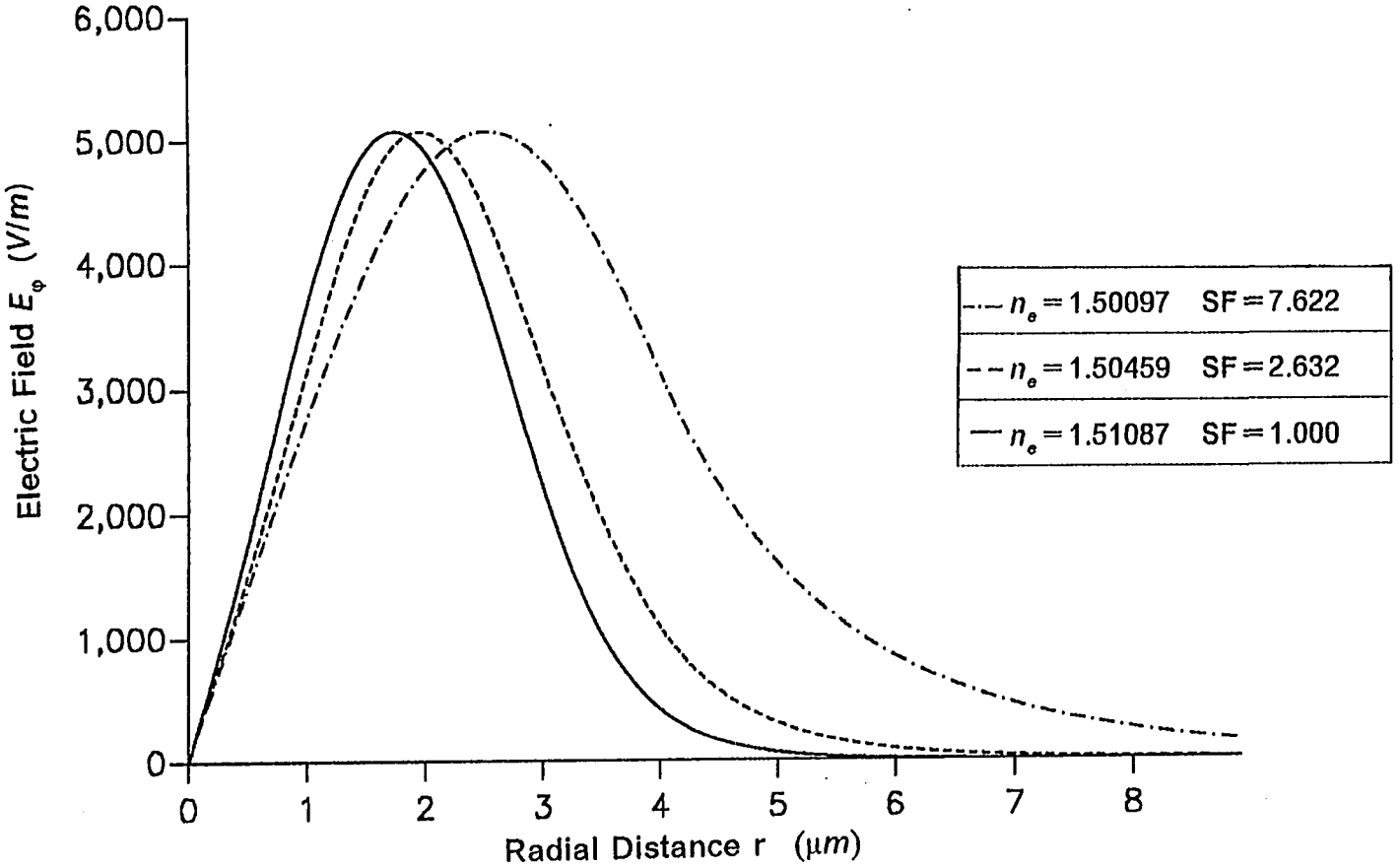

Fig.(5.3) Three field plots corresponding to three values of n_e taken from fig.(5.2)

distributions of the dielectric functions corresponding to these values of mode index are shown in fig.(5.4). The dielectric constant increases gradually from the background value at r=0 to a maximum value inside the core. It is then decreases gradually to the linear cladding value.

The self-focusing action is clearly illustrated by the plot of fig.(5.3). As the applied intensity increases, the value of the refractive index increases and the peak intensity moves towards the center of the fiber where the refractive index has a maximum value. This means that the width of the light beam becomes smaller as the applied field intensity increases.

For very low intensity values, the fiber operates as a linear step-index fiber with $\varepsilon_1 = \varepsilon_{bg}$. The value of the mode index of the TE_{01} mode obtained by the recursive scheme, has been checked by the direct solution of the eigenvalue equation :

$$\frac{J_1(u)}{uJ_0(u)} + \frac{K_1(w)}{wK_0(w)} = 0 \qquad (5.2)$$

where u and w are defined as:

$$u = a(n_{co}^2 k_0^2 - \beta^2)^{\frac{1}{2}}, \quad w = a(\beta^2 - n_{cl}^2 k_0^2)^{\frac{1}{2}}$$

where a is the core radius and n_{co} and n_{cl} are the core and cladding refractive

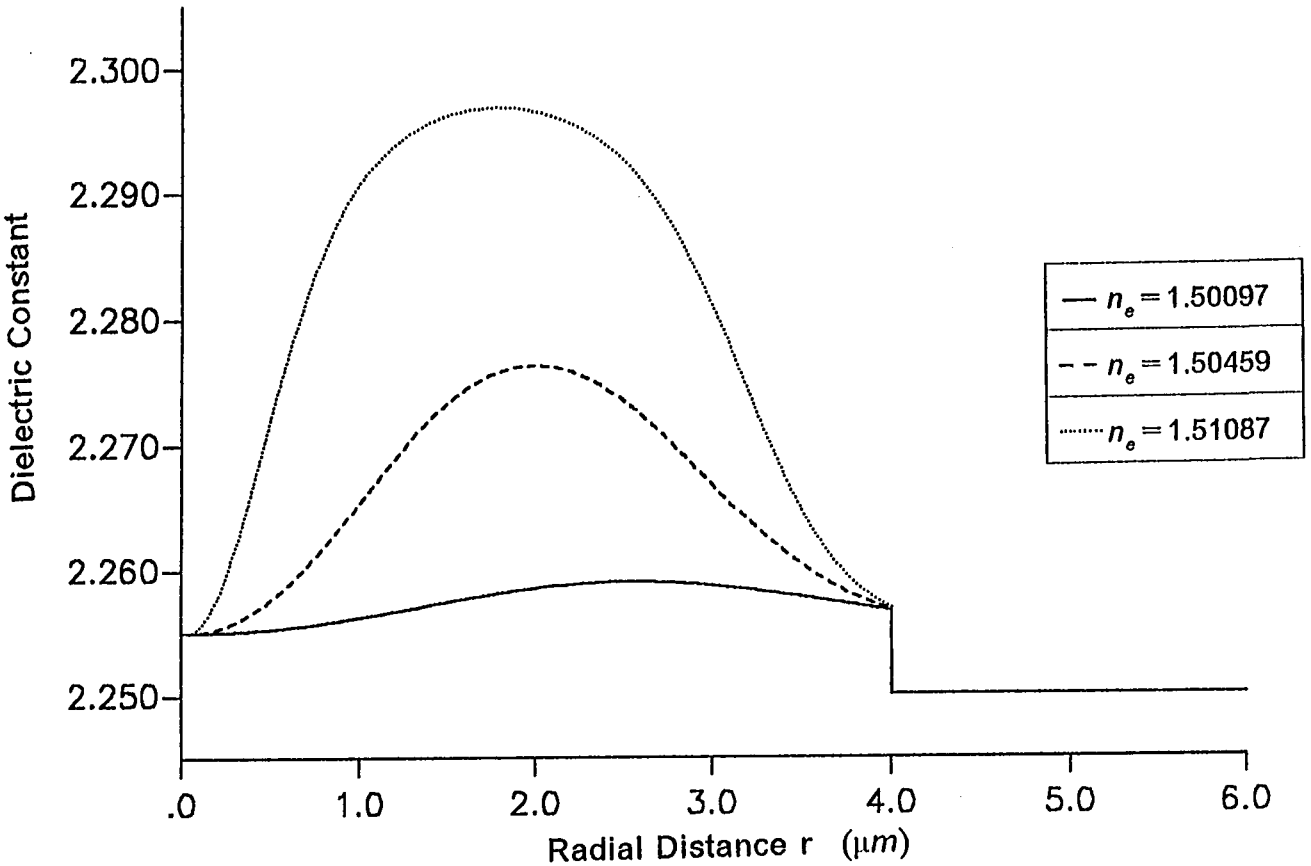

Fig.(5.4) Variation of the dielectric constant with the radial distance for three values of n_e taken from fig.(5.2)

indices respectively. Values obtained by the two solutions are found to be in agreement to six significant digits as shown in table 5.1. At the high intensity end of the dispersion characteristics, the fiber becomes saturated and behaves as a linear step-index fiber with $\varepsilon_1 = \varepsilon_{bg} + \Delta\varepsilon_{NLmax}$. This can also be seen in fig.(5.5). The value of n_e for the saturated fiber is checked against the one obtained from the closed form eigenvalue equation. The two values are in very good agreement as shown in table 5.1. Fig.(5.5) shows two plots of the nonlinear dielectric constant distribution for very high and very low intensity values. The fiber in these cases acts as a linear step-index fiber.

It must be noted that the same nonlinear guided wave characteristics have been obtained for the planar waveguide in the case of a nonlinear film surrounded by a linear medium on both sides [1].

The second case is devoted to a fiber which is cutoff for guided modes at low power The fiber parameters for this model are the same as the previous case except ε_{bg} is now changed to 2.25, thus making $\varepsilon_{bg} = \varepsilon_2$. In the linear sense, this fiber cannot support guided waves. In fact at low power level it resembles a uniform medium. However, if the core material is nonlinear and the applied field intensity exceeds a threshold value, the fiber can support nonlinear guided waves. To achieve this the recursive scheme starts by assuming a very low magnetic field ($H_z(0)$) value at the center of the

TABLE 5.1

Checking the values of n_e in the linear limit of the recursive scheme against the direct solution of the closed form eigenvalue equation for TE_{01} mode

Structure	Figure	Method	n_e	$A_{H_z}(0)$	$\|E_s\|^2$
$NL_{co}-L_{cl}$	(5.2)	recursive	1.500194	0.001	6.75
$NL_{co}-L_{cl}$		eigenvalue equation	1.500194		
$NL_{co}-L_{cl}$	(5.2)	recursive	1.515730	100	68.42(3)
$NL_{co}-L_{cl}$		eigenvalue equation	1.515732		
$NL_{co}-L_{cl}$	(5.6)	recursive	1.514105	100	1.3(9)
$NL_{co}-L_{cl}$		eigenvalue equation	1.514107		
$NL_{co}-L_{cl}$	(5.7)	recursive	1.512483	200	2.31(10)
$NL_{co}-L_{cl}$		eigenvalue equation	1.512484		
$L_{co}-NL_{cl}$	(5.10)	recursive	1.506044	0.1	10797
$L_{co}-NL_{cl}$		eigenvalue equation	1.506043		
$L_{co}-NL_{cl}$	(5.15)	recursive	1.501447	0.01	296.9
$L_{co}-NL_{cl}$		eigenvalue equation	1.501447		

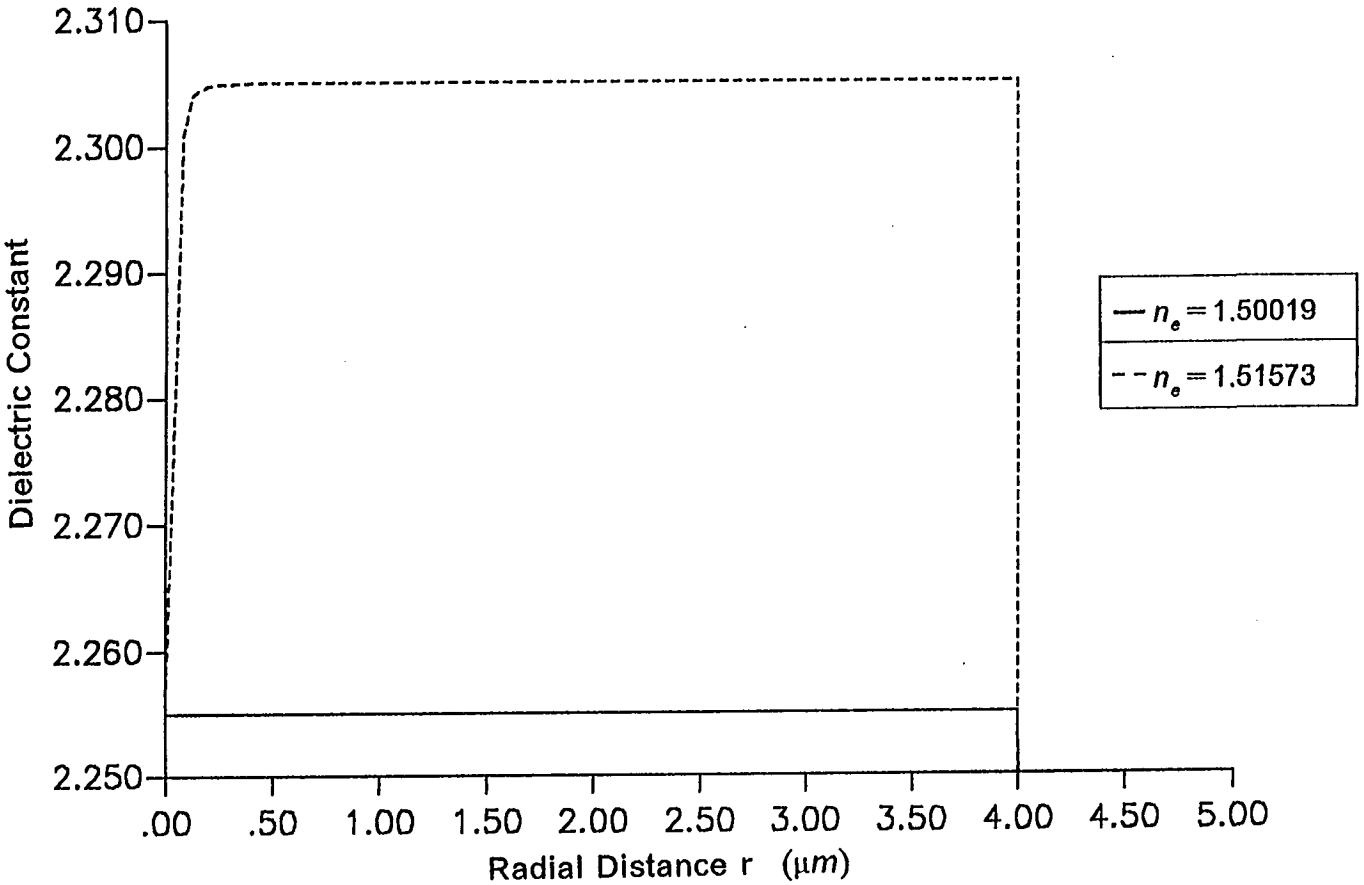

Fig.(5.5) The dielectric constant distribution for two values of n_e corresponding to linear and saturated waveguide

fiber. This will not probably lead to a solution of equation (3.64). By increasing the value of the magnetic field slowly, a solution of equation (3.64) is obtained when this magnetic field exceeds a threshold value.

The dispersion curve for this fiber is shown in fig.(5.6). The three operating regions discussed in section 5.2 in the case of the guiding fiber (fig.(5.2)) are also observed in this case. However, the low intensity region of fig.(5.2) is seen to be confined to a very small portion of the curve. There is a minimum value of intensity required to switch the fiber on. The mode index increases with the intensity at the core-cladding interface but soon the intensity undergoes a decrease with a further increase of the mode index.

The value of the mode index of a saturated fiber has been checked by the direct solution of the eigenvalue equation of the step-index fiber with $\varepsilon_1 = \varepsilon_{bg} + \Delta\varepsilon_{NLmax}$. The results are compared in table 5.1. It must be noted that the fully saturable nonlinear fiber requires an infinitely large field. If the field is not large enough there will be some discrepancies between the eigenvalues obtained using the closed form eigenvalue equation and those obtained using the the recursive scheme.

The third case is for a fiber which is cutoff at low field intensity. For this fiber structure ε_{bg} is taken to be 2.245 and all other fiber parameters

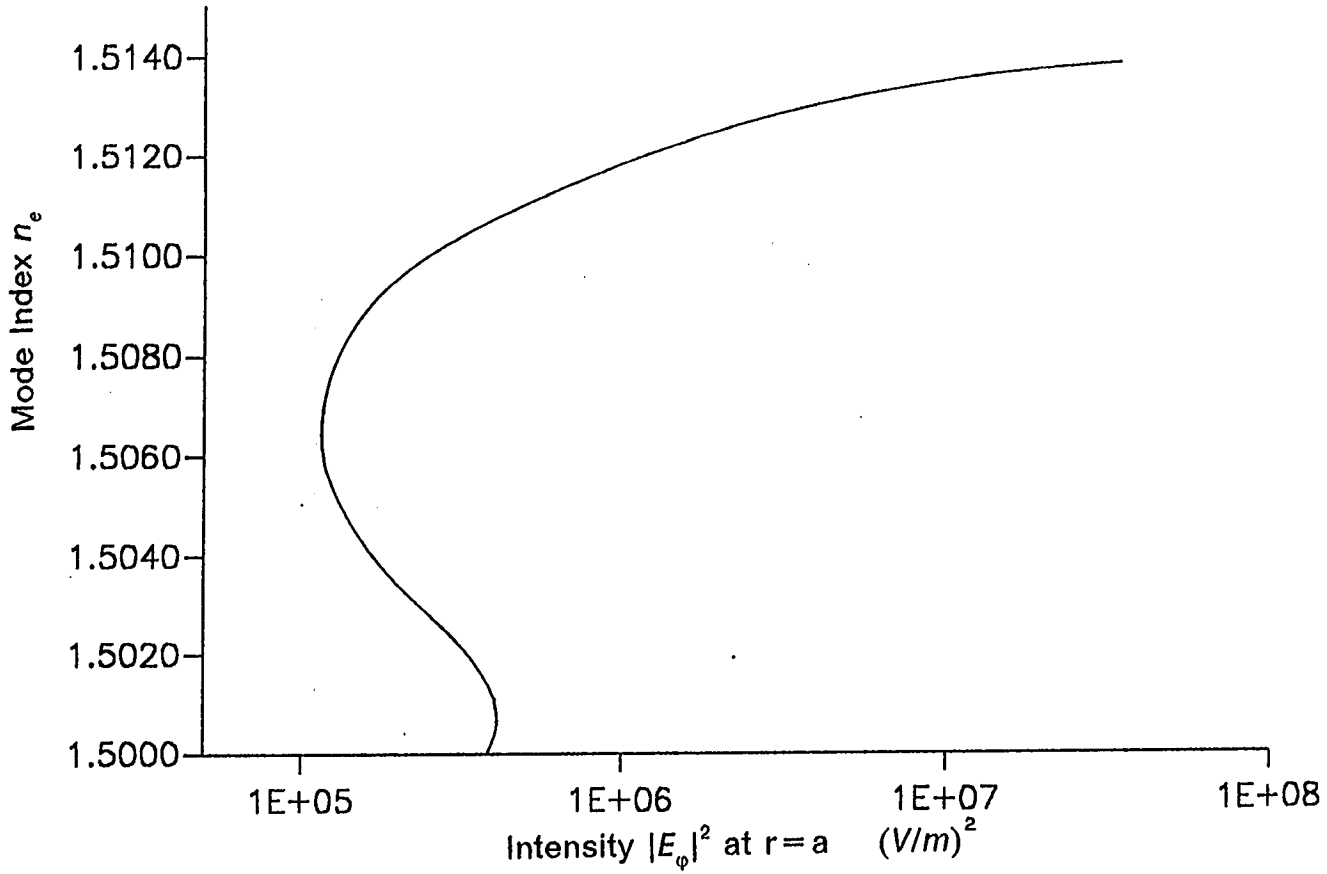

Fig.(5.6) Variation of n_e with the interface intensity for TE_{01}

remain the same as those used in previous case. The structure is cutoff in the linear sense. By increasing the applied power above a threshold value, the fiber will be turned on and the TE_{01} mode is supported. The dispersion characteristic of this mode is illustrated in fig.(5.7). It is seen that there are two main regions identified in the dispersion curve, the low input power region (above the threshold value) and the high input power region. In the low power region, as the power exceeds the threshold to turn the fiber on, the resulting field distribution has a large value of intensity at the core-cladding interface but relatively low peak value. This is indeed a feature of fibers working close to cutoff. By increasing the input power the field becomes more confined in the core region, causing the interface intensity to decrease and the peak value to increase.

For the second portion of the dispersion curve where the fiber is approaching saturation, both the interface intensity and the peak field value increase with the input power. It must be noted that in all of the dispersion curves, the ratio of the peak value of intensity to the interface intensity increases with the mode index. The value of the mode index for saturable medium with $\varepsilon_1 = \varepsilon_{bg} + \Delta\varepsilon_{NLmax}$ has also been checked against the direct solution of the eigenvalue equation (5.2). The results are shown in table 5.1.

The dispersion of the cutoff nonlinear fiber as a relation between the total propagated power and the mode index n_e, has been studied for the first TE

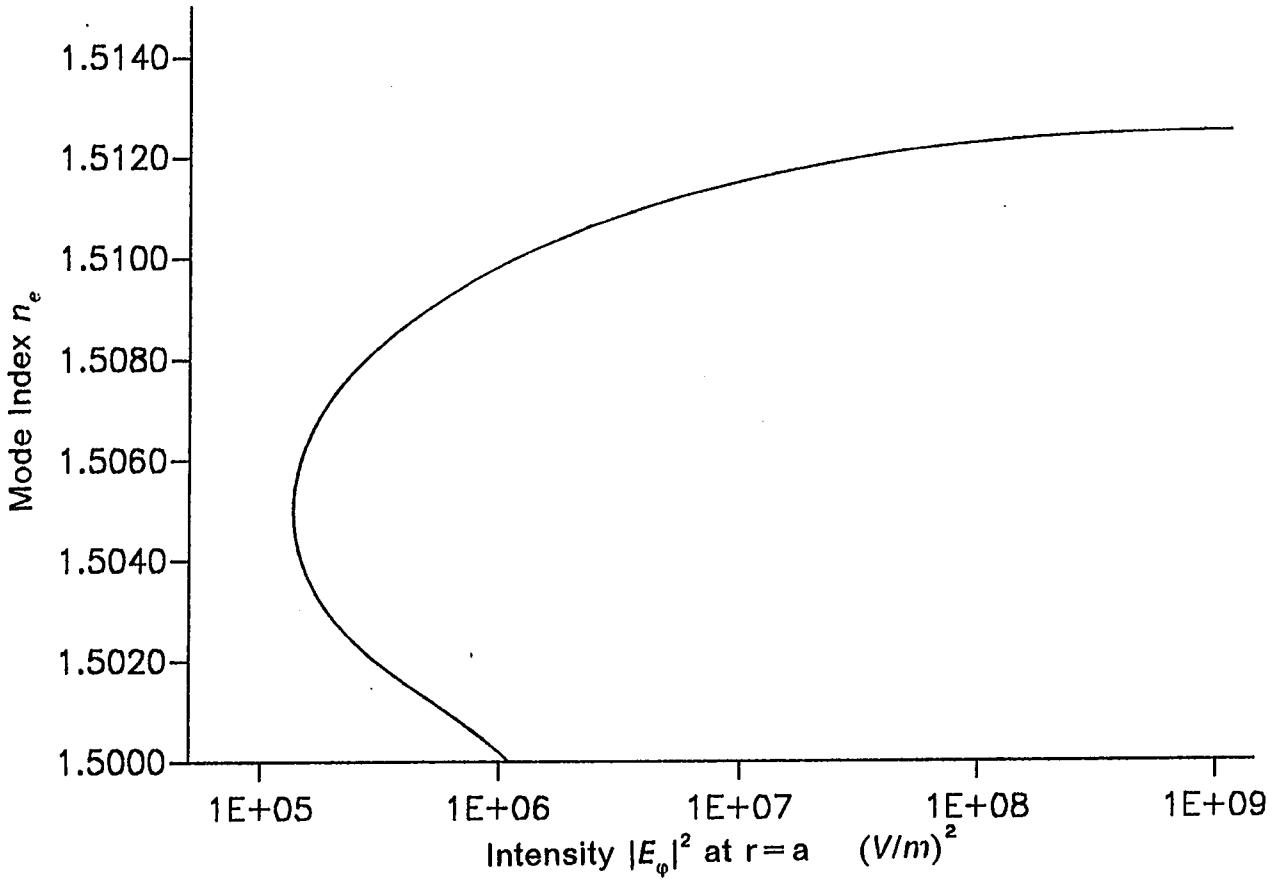

Fig.(5.7) Variation of n_e with the interface intensity for TE_{01} $(\varepsilon_{bg} < \varepsilon_2)$

mode for two different saturation levels. Fig.(5.8.a) shows this relation. The first portion of the dispersion curve has a negative slope which is considered unstable. However, the second portion has a positive slope. This portion is characterized by stable operation where, n_e increases with the input power.

The two values for the saturation parameter g are taken to be 20 and 40 . This makes a contribution to the dielectric constant equal to 0.05 and 0.025 respectively. The amount of power required to turn the fiber on is not the same for both levels of saturation. It can be seen from fig.(5.8.a) that the high saturation level requires less power for the fiber to support guided modes. The power can be calculated from the integral of the Poynting vector as follows:

$$P = \frac{1}{2}\,\mathrm{Re}\int_{-\infty}^{\infty} \bar{E}\times\vec{H}^{*}\cdot\overline{ds} \qquad (5.3)$$

where $\overline{ds}$ is the element of area given in cylindrical coordinates by $\overline{ds} = r\,dr\,d\varphi\hat{z}$. In the case of TE modes this expression reduces to

$$P = -\frac{1}{2}\,\mathrm{Re}\int_{0}^{\infty}\int_{0}^{2\pi} E_{\varphi}H_{r}^{*}\,d\varphi\,r\,dr \qquad (5.4)$$

The direction of propagation in equation (5.4) is the positive z direction. Figure (5.8.b) shows the dispersion relation as a plot of interface intensity

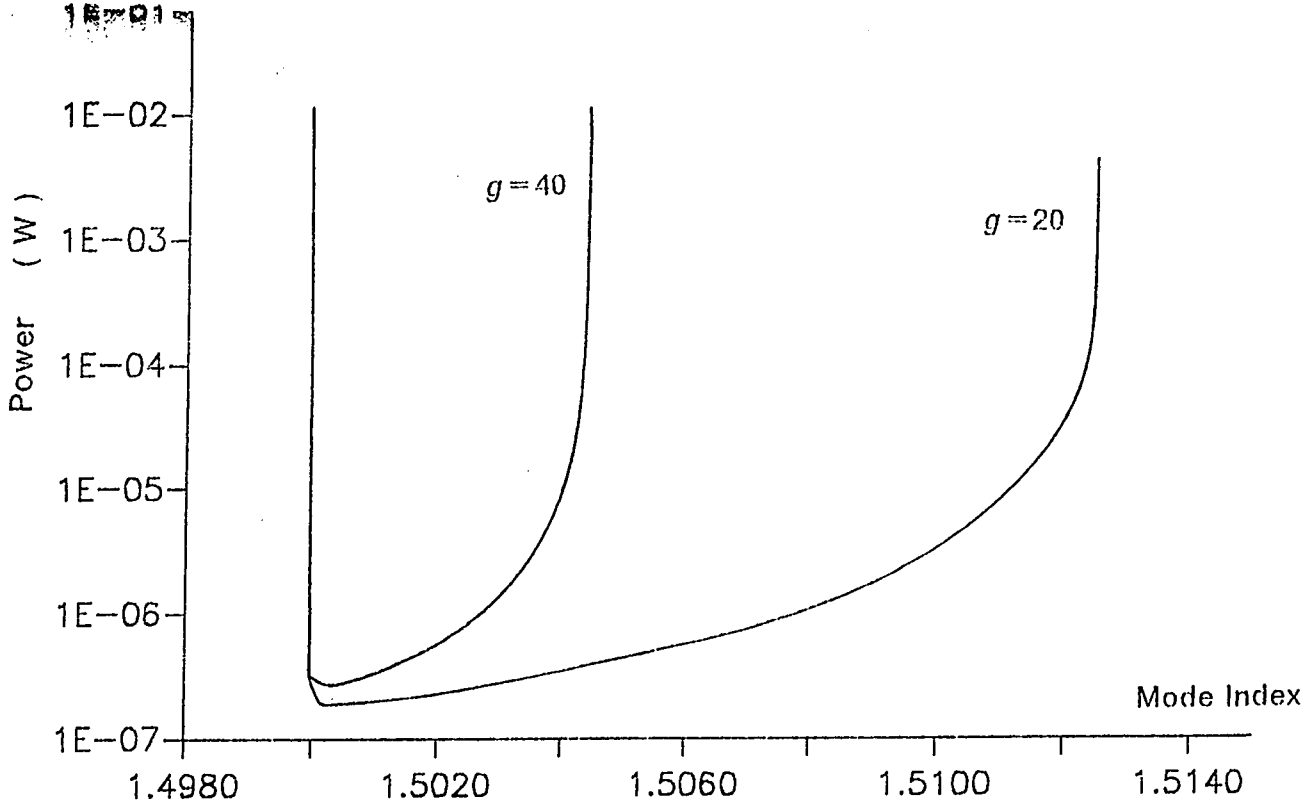

Fig.(5.8.a) Variation of n_e with the total power for TE_{01} mode in a waveguide having two different saturation levels

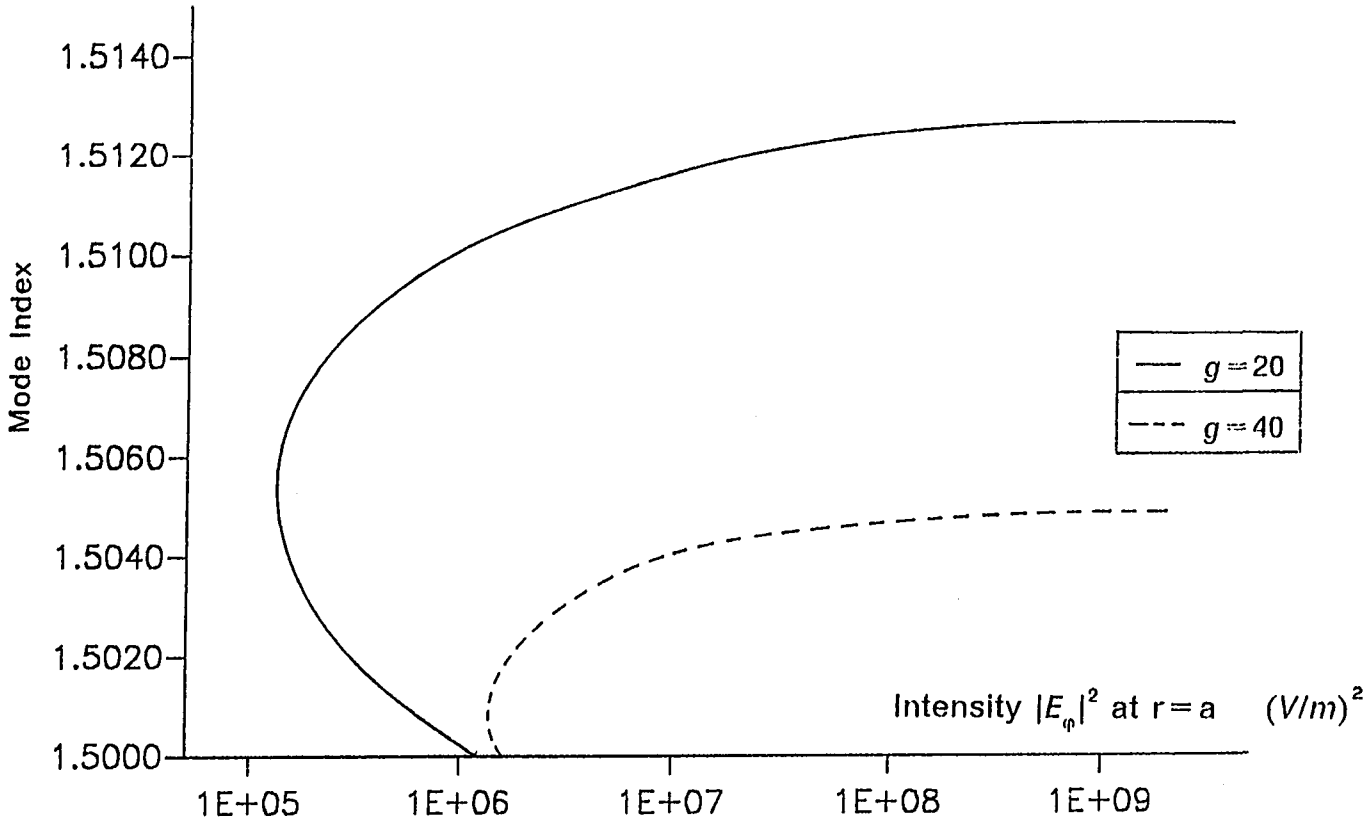

Fig.(5.8.b) Variation of n_e with the interface intensity for TE_{01} mode in a waveguide having two different saturation levels

versus the mode index, for the same two saturation levels. As a matter of fact the threshold interface intensity depends on the difference between ε_{bg} and ε_2 as well as the maximum level of saturation used.

The important application of the cutoff fiber is the limiting process where the intensity of light acts as a limiter to control the operation of the fiber. If this intensity is above the threshold value, the fiber is on and and supports guided modes. and if it is below the threshold the fiber is cutoff.

It is important to have an insight into the behavior of higher order modes. For this purpose the radius of the fiber has been increased to 5 μm. This radius can support the first three lowest order TE modes TE_{01}, TE_{02} and TE_{03} for high intensity values. The dispersion relation of this waveguide as a plot of power versus mode index is shown in fig.(5.9.a). It can be seen from this figure that the higher order modes require more power to be supported by the waveguide. However, the general behavior of the dispersion curve is unchanged. Supporting higher order modes depends on the way of excitation and coupling the fiber to the laser source. It is also of interest to show the field profiles and dielectric constant distributions for the three lowest order modes. Figure (5.9.b) illustrates three field profiles corresponding to an input magnetic field amplitude of 5.1 A/m. For this value of magnetic field the first mode TE_{01} is approaching saturation while the third mode TE_{03} is close to cutoff. The field profiles are seemed to be

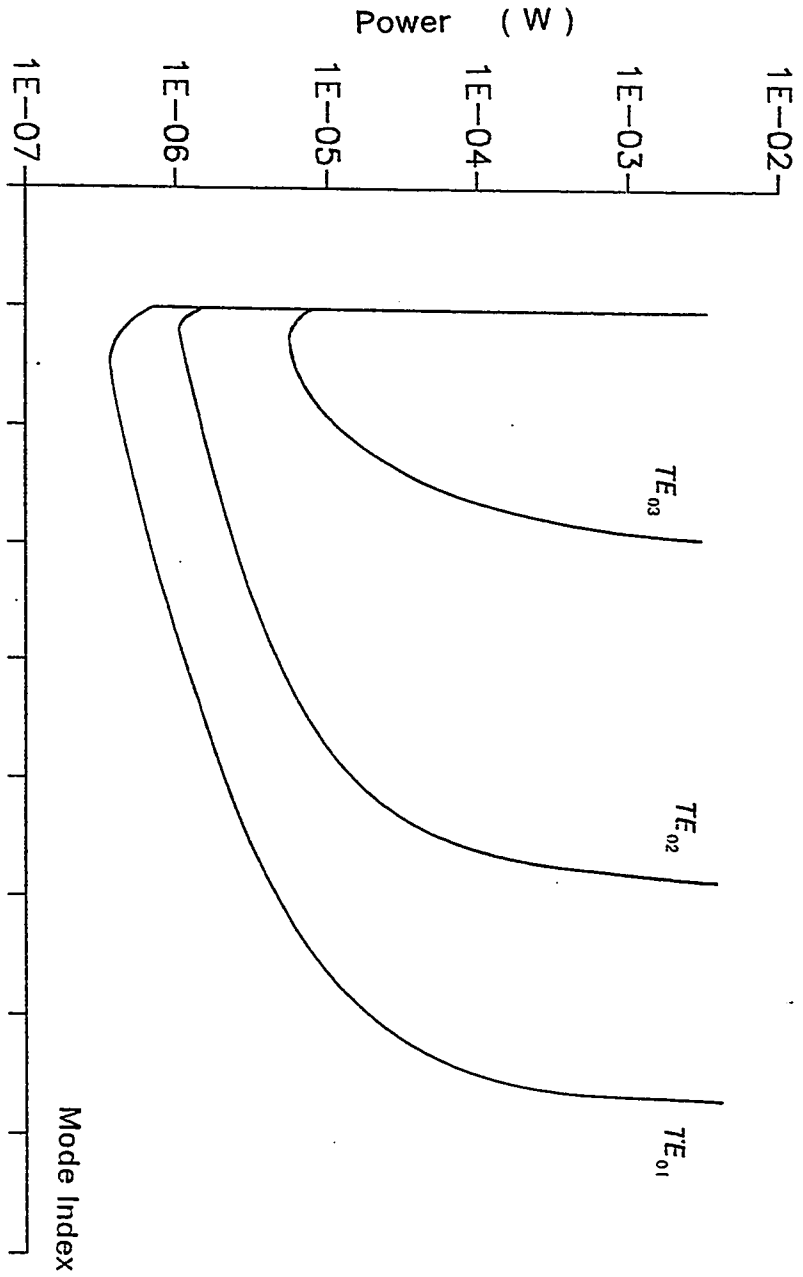

Fig.(5.9.a) Variation of n_e with the modal power for TE_{01}, TE_{02} and TE_{03} modes

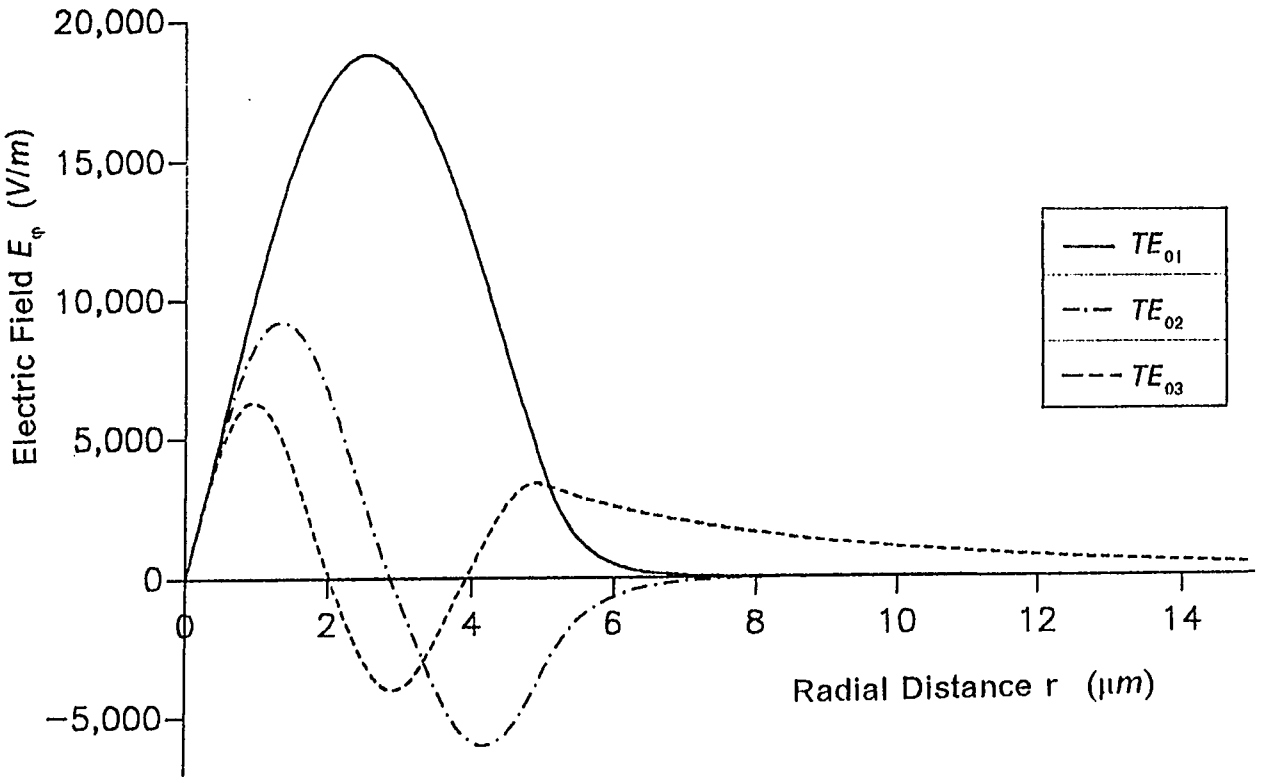

Fig.(5.9.b) Three field plots for TE_{01}, TE_{02} and TE_{03} modes corresponding to the same input value of axial magnetic field H_z

similar to their linear counterpart. As the mode index increases, the confinement of the light improves in the nonlinear core. The dielectric constant distribution corresponding to the same input magnetic field is shown in fig.(5.9.c). It is clearly seen that the dielectric constant for higher order modes drops to the background value ε_{bg} wherever the corresponding field profile has a node (zero crossing).

5.3 TE WAVES IN OPTICAL FIBERS WITH A LINEAR CORE AND A NONLINEAR CLADDING

The model studied for this case is shown in fig.(5.1). The cladding dielectric function has the general form given by equation (3.43). Two important cases are to be considered. The first one is characterized by $\varepsilon_{bg}+\Delta\varepsilon_{NLmax}<\varepsilon_1$ and the second case has $\varepsilon_{bg}+\Delta\varepsilon_{NLmax}=\varepsilon_1$

The first case is a fiber which supports guided modes at low power. The fiber parameters used in this case are as follows: $\varepsilon_1=2.275$, $\varepsilon_{bg}=2.25$, $\alpha=10^{-8}V^{-2}m^2$, $g=50$, $\lambda=0.6328\,\mu m$ and $a=4\,\mu m$. The optical fiber in this case supports the TE_{01} mode regardless of the amount of the applied power. The dispersion relation of the TE_{01} is shown in fig (5.10) where n_e is seen to increase with the interface field intensity. The effect of the nonlinearity is to modify the field profiles. For low intensity levels $\Delta\varepsilon_{NL}$

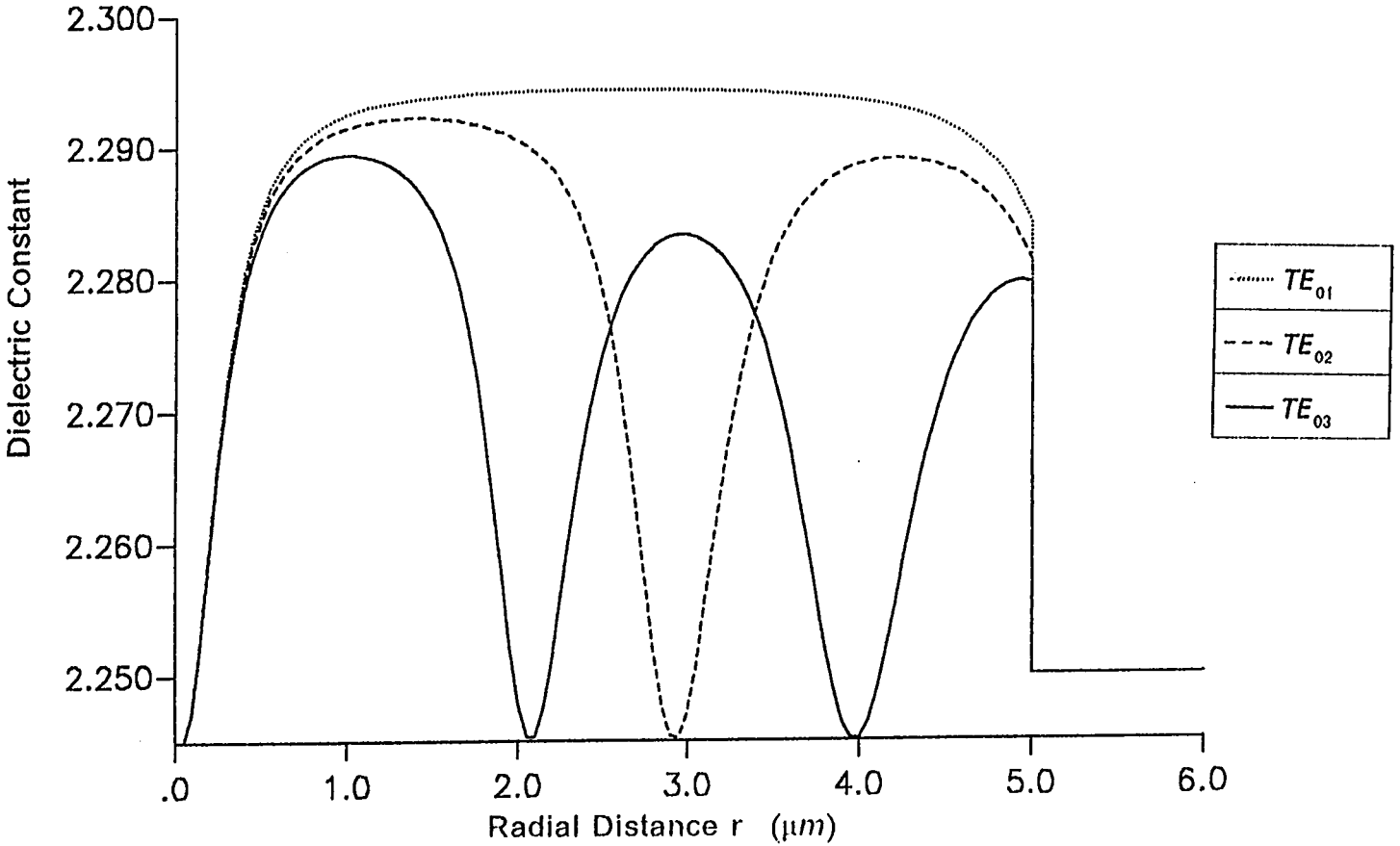

Fig.(5.9.c) Variation of the dielectric constant with the radial distance for TE_{01}, TE_{02} and TE_{03} modes.

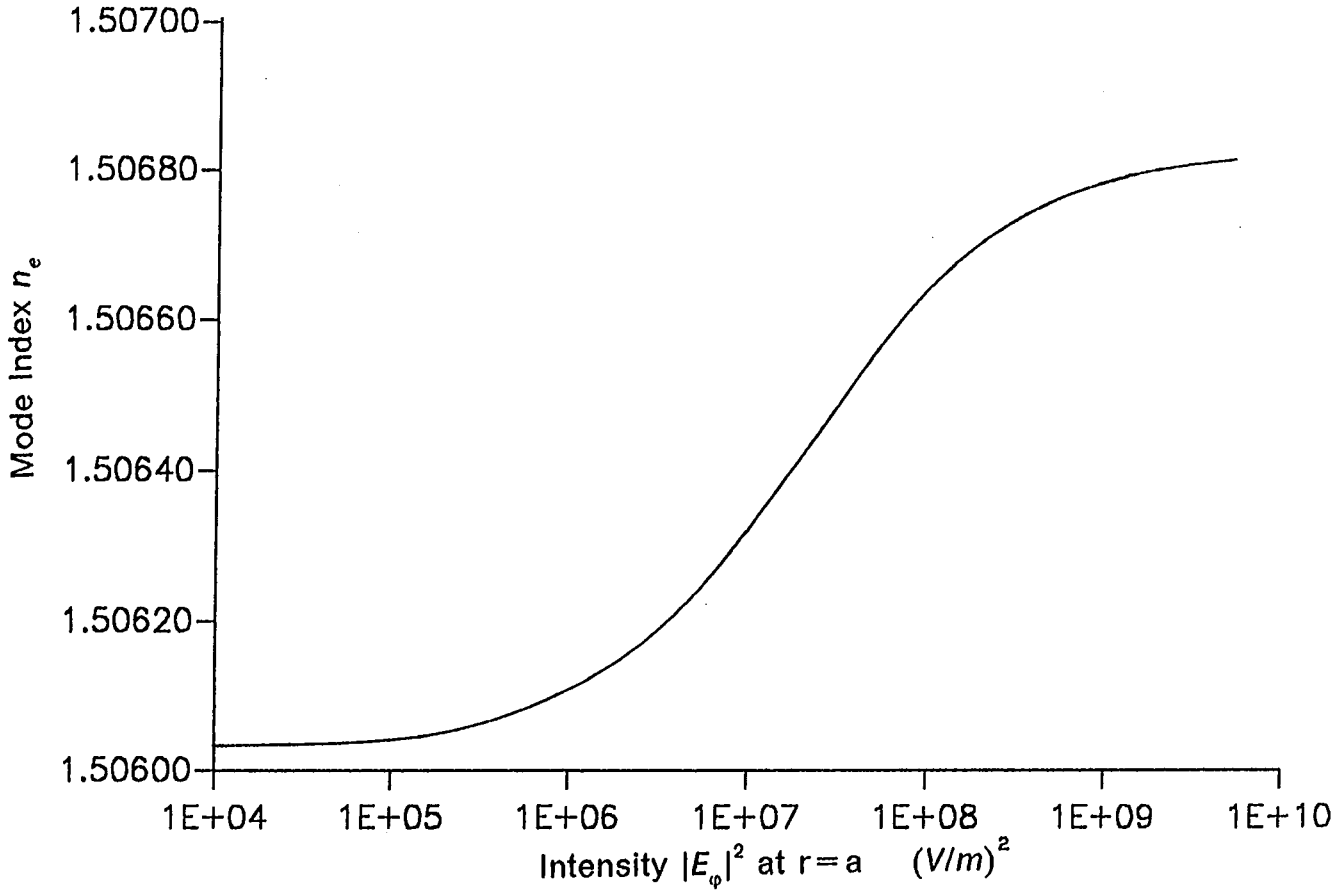

Fig.(5.10) Variation of n_e with the interface intensity for TE_{01} in a waveguide having linear core and nonlinear cladding

is small and the field distribution represents the linear solution of the fiber. However, for high intensity levels the peak of the first TE mode moves towards the nonlinear cladding. This behavior illustrates the self-focusing action of the nonlinear medium. Figure (5.11) shows three field distributions for three values of the mode index to show the shift of the peak of field profile. The first value of n_e is the linear value where $\Delta\varepsilon_{NL}=0$ and it is corresponding to curve (A). The second value corresponding to curve (B) is taken for $\Delta\varepsilon_{NL}=0.5\Delta\varepsilon_{NLmax}$. The third value for fully a saturated medium where $\Delta\varepsilon_{NL}=\Delta\varepsilon_{NLmax}$. It is represented by curve (C). As the intensity increases the field maximum moves towards the nonlinear cladding. This makes the field less confined in the core region. A considerable part of propagated power is concentrated in the cladding region. It must be noted that the peak of the field will not cross the core cladding interface as long as $\varepsilon_{bg}+\Delta\varepsilon_{NLmax}<\varepsilon_1$ The distribution of the dielectric function versus the radial distance for the three values of the mode index used is shown in fig.(5.12). The distribution for low intensity resemble the step-index profile. For the moderate and high intensity values there is a graded-index decaying portion between $\varepsilon_{bg}+\Delta\varepsilon_{NL}$ and ε_{bg}

It is important to explain the application of the numerical recursive scheme for this fiber structure. The linear core is taken as the first layer and the field at the core cladding interface (evaluated in the linear region) is used

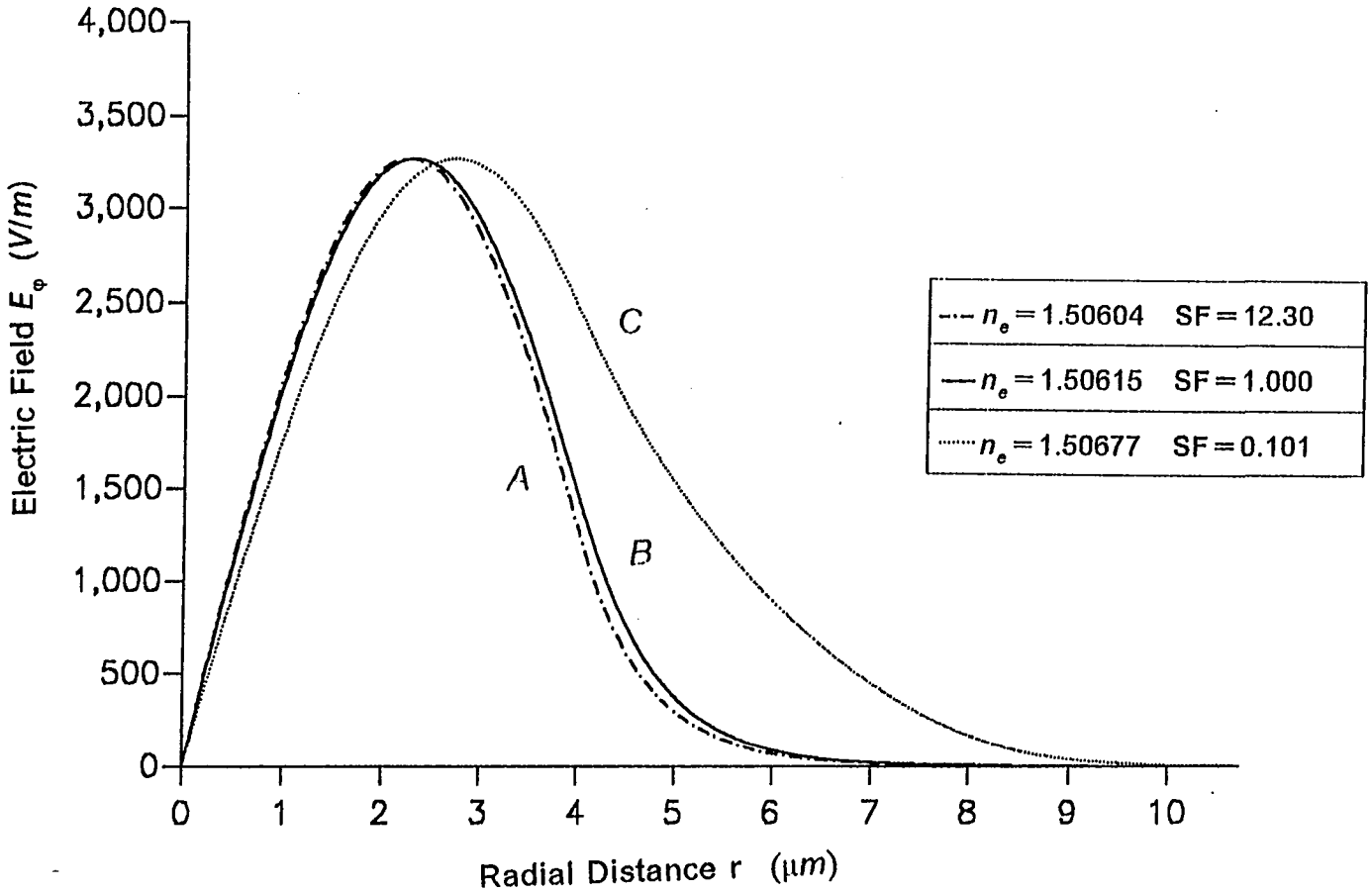

Fig.(5.11) Three field plots corresponding to three values of n_e taken from fig.(5.10)

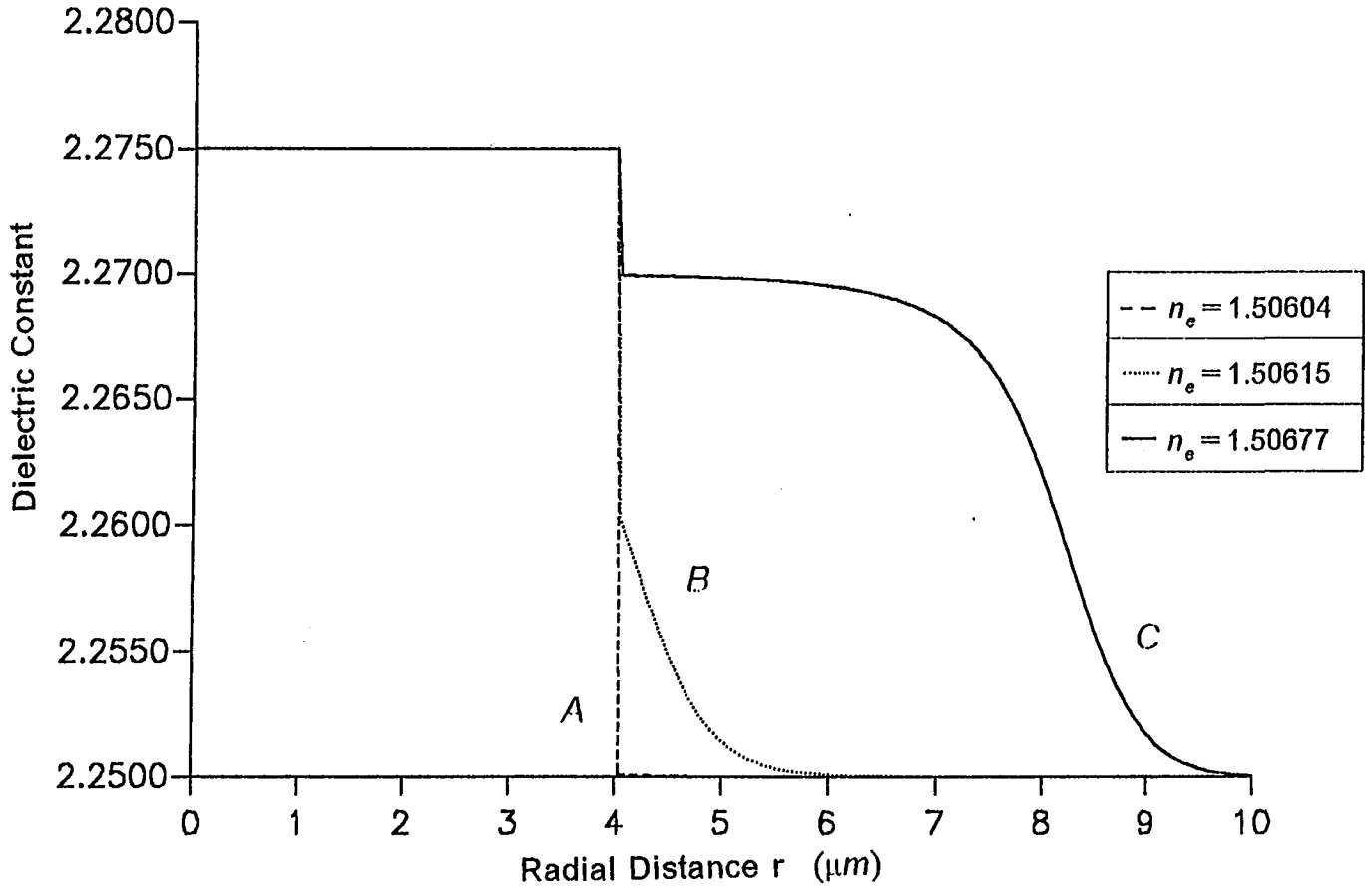

Fig.(5.12) Variation of the dielectric constant with the radial distance for three values of n_e taken from fig.(5.10)

to modify the first nonlinear layer. The cladding is divided into a large number of layers. The boundary condition is applied at a distance far enough into the cladding such that the effect of the field is neglected. Accordingly the nonlinear medium is treated as a linear one with a dielectric constant equal ε_{bg}. However, this boundary point should not be taken far away from core-cladding interface to have a solution of equation (3.64). If the fields values at the boundary point are too small, the zero finding routine will not be able to obtain the correct eigenvalue. In such a case, the expression for evaluating the mode index will suffer from overflow or underflow. if the increment added to the dielectric constant due to the field is equal to or less than 10^{-4}, the effect of the field is considered negligible.

The second case represents a fiber which supports variable number of modes according to the value of intensity. The parameters of this optical fiber are: $\varepsilon_1 = 2.26$, $\varepsilon_{bg} = 2.25$, $\alpha = 10^{-8} V^{-2} m^2$, $g = 100$, $\lambda = 0.6328\ \mu m$ and $a = 4\ \mu m$. For this case the fiber can support only the TE_{01} mode for low power values. As the applied field increases the peak value of the field distribution of the TE_{01} mode moves towards the nonlinear medium and crosses the core cladding interface. Three field distributions are shown in fig.(5.13) for low, intermediate and high intensity levels. It is clear that the field maximum corresponding to the highest chosen surface intensity (curve C), is located in the cladding region. This is a feature of nonlinear guided waves in this

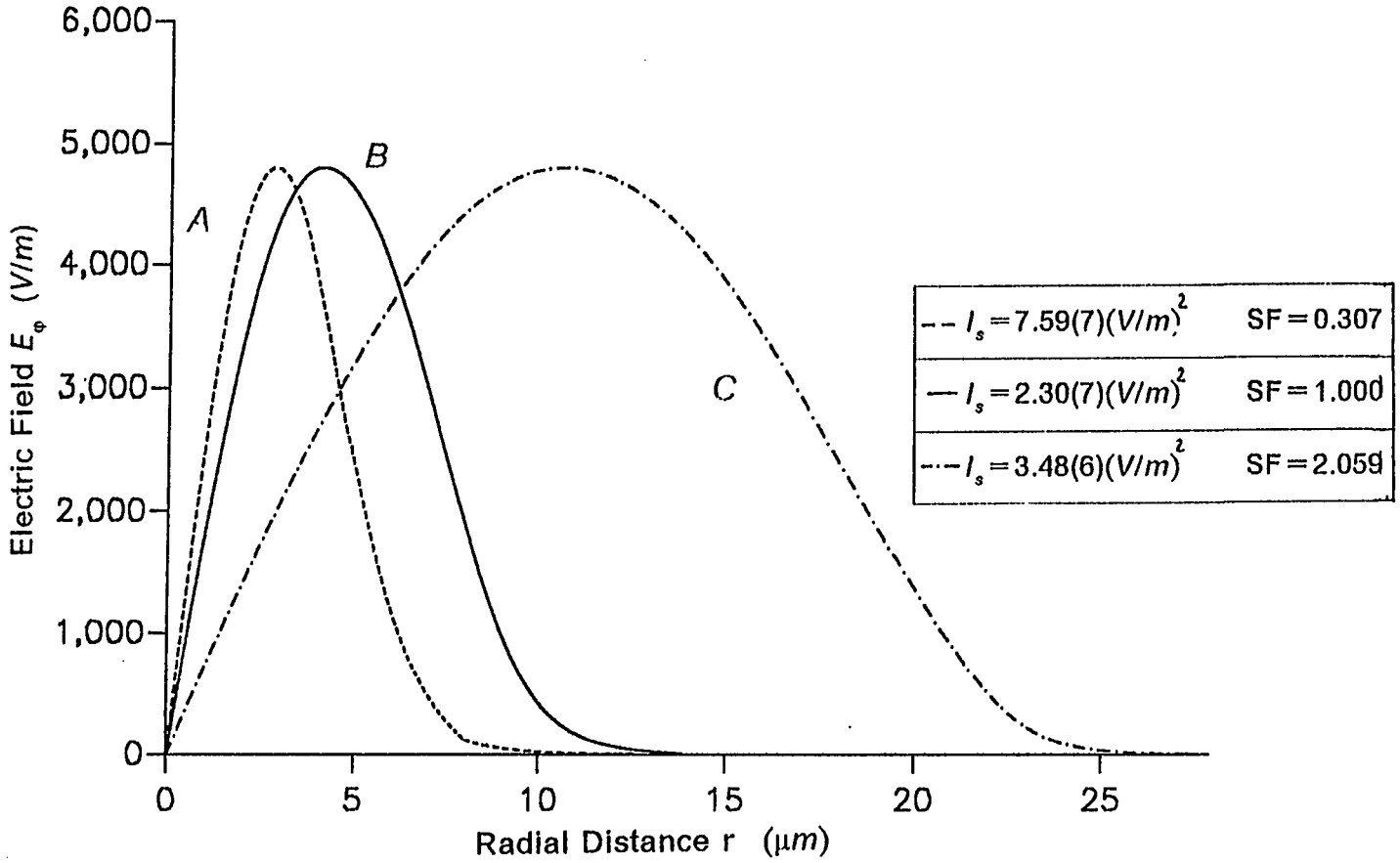

Fig.(5.13) Three field plots corresponding to low, moderate and high intensity values

waveguide structure and has no linear counterpart. For such a case most of the propagated power is located in the cladding region. Eventually the TE_{01} mode will be mainly guided by the nonlinear cladding. Another important conclusion can be drawn from fig.(5.13) (curve C), when the fiber approaches the saturation, the physical radius of the fiber becomes greater than the actual core radius ($4\,\mu m$). The higher order modes of weak intensities can be supported by the dielectric constant profile corresponding to TE_{01} mode. However, if their intensities are large the modes will interact and the wave propagation process inside the fiber will be complicated. The dielectric constant variations corresponding to the three field distributions of fig.(5.13) are shown in fig.(5.14). When the fiber approaches saturation ($\varepsilon_{bg}+\Delta\varepsilon_{NL}\approx\varepsilon_1$), the refractive index profile resembles a step-index profile with a physical radius of about $25\,\mu m$. This can be seen from fig.(5.14). This physical radius is about six times the actual core radius ($4\,\mu m$). The next higher order mode TE_{02} has also been investigated This mode is cut-off at low power values. However, for high power values the saturated fiber supports this mode among the higher order modes. The fiber in this case resembles a linear fiber with a large radius and a refractive index difference between the core and the cladding equal to $\varepsilon_1-\varepsilon_{bg}$. The fiber thus has a large value of V number which allows the support of many modes.

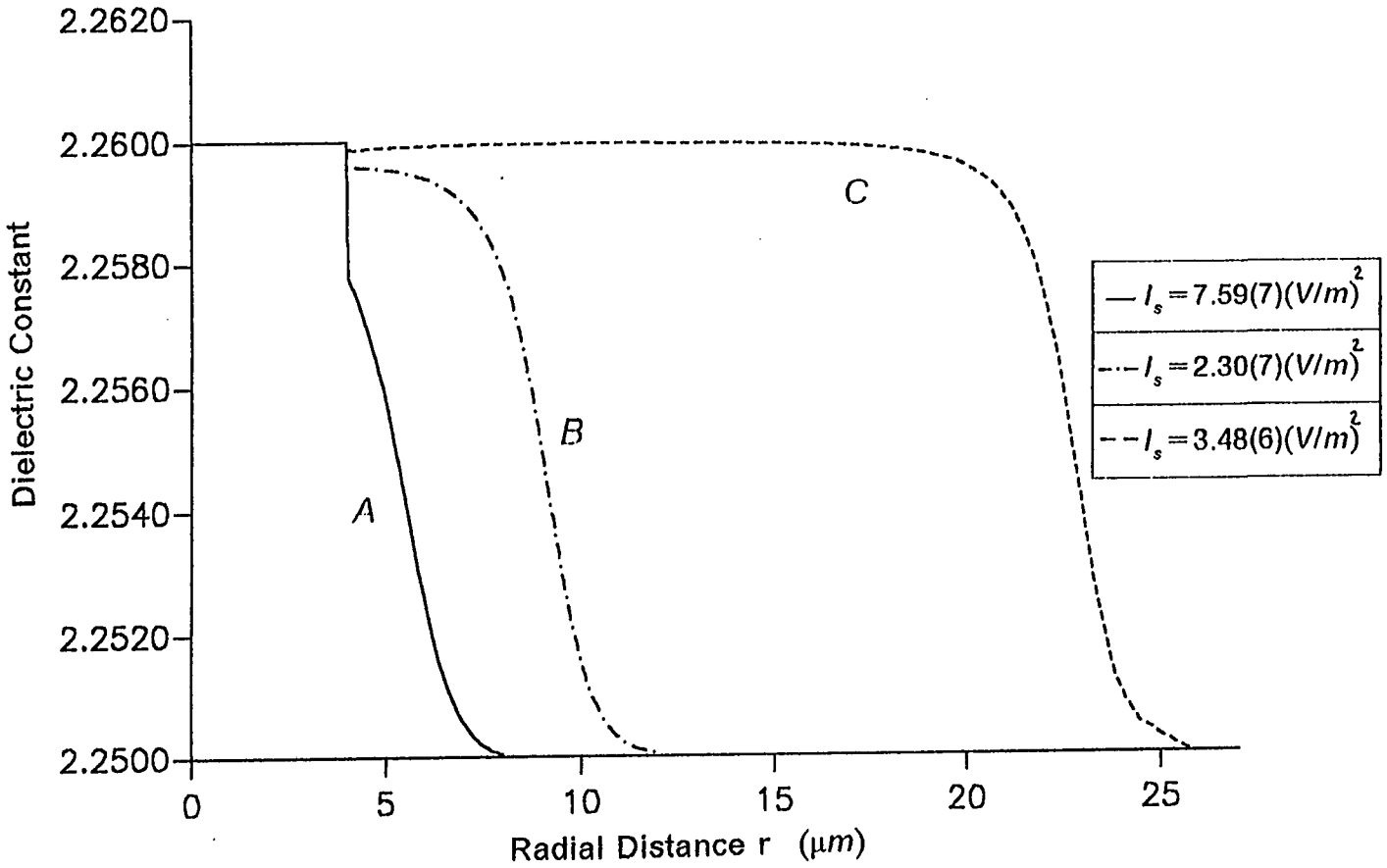

Fig.(5.14) The dielectric constant distributions for the three intensity values used in fig.(5.13)

The TE_{02} mode reaches cutoff as the applied intensity becomes lower than a threshold value. The value of the threshold intensity depends on the physical parameters of the fiber, mode order, and the nonlinear coefficient of the cladding material. An important application for the fiber of this type is as a power limiter. At high power levels, the fiber can support higher order modes in addition to the TE_{01} mode. However, these modes may interact if their intensity is large. As the power decreases gradually the higher order modes are made cut-off and eventually only the TE_{01} mode will be supported by the fiber. The dispersion curve for this fiber is shown in fig.(5.15.a) where the power is plotted versus the mode index. for the first order mode TE_{01} It can be seen that, for low power values, the fiber behaves as a linear fiber and the mode index is power independent. However, for high power values the mode index increases with the power. The variation of the n_e of the TE_{02} with the interface intensity is shown in fig.(5.15.b). It is seen that there is a small threshold value above which the mode is supported and below this value the mode is cut-off.

5.4 TM WAVES IN FIBERS WITH A NONLINEAR CORE AND A LINEAR CLADDING

TM guided waves are characterized by the field vectors $\overline{E}=(E_r, 0, E_z)$ and $\overline{H}=(0, H_\varphi, 0)$. There are thus two electric fields components contributing to

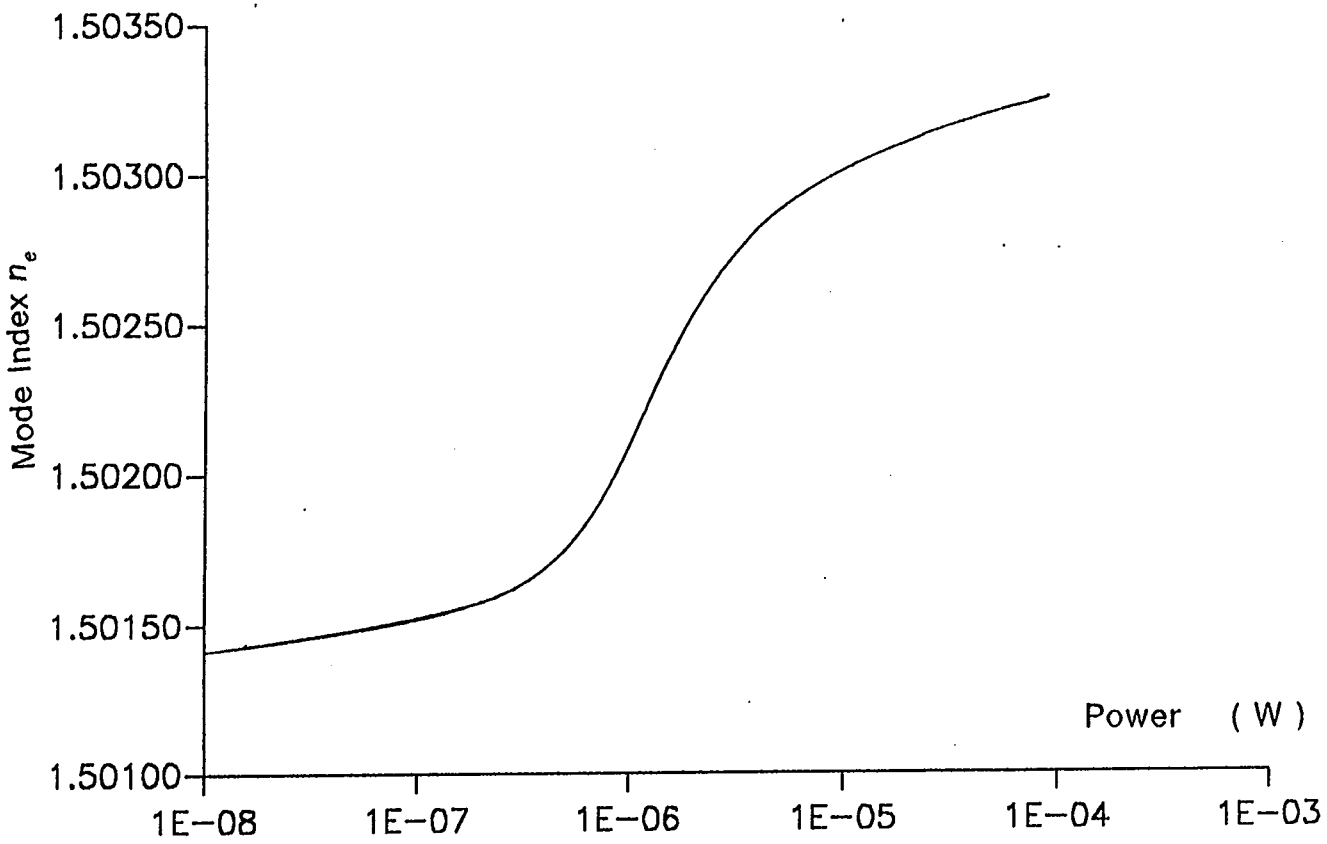

Fig.(5.15.a) Variation of n_e with the total power for TE_{01} mode in a waveguide having linear core and nonlinear cladding

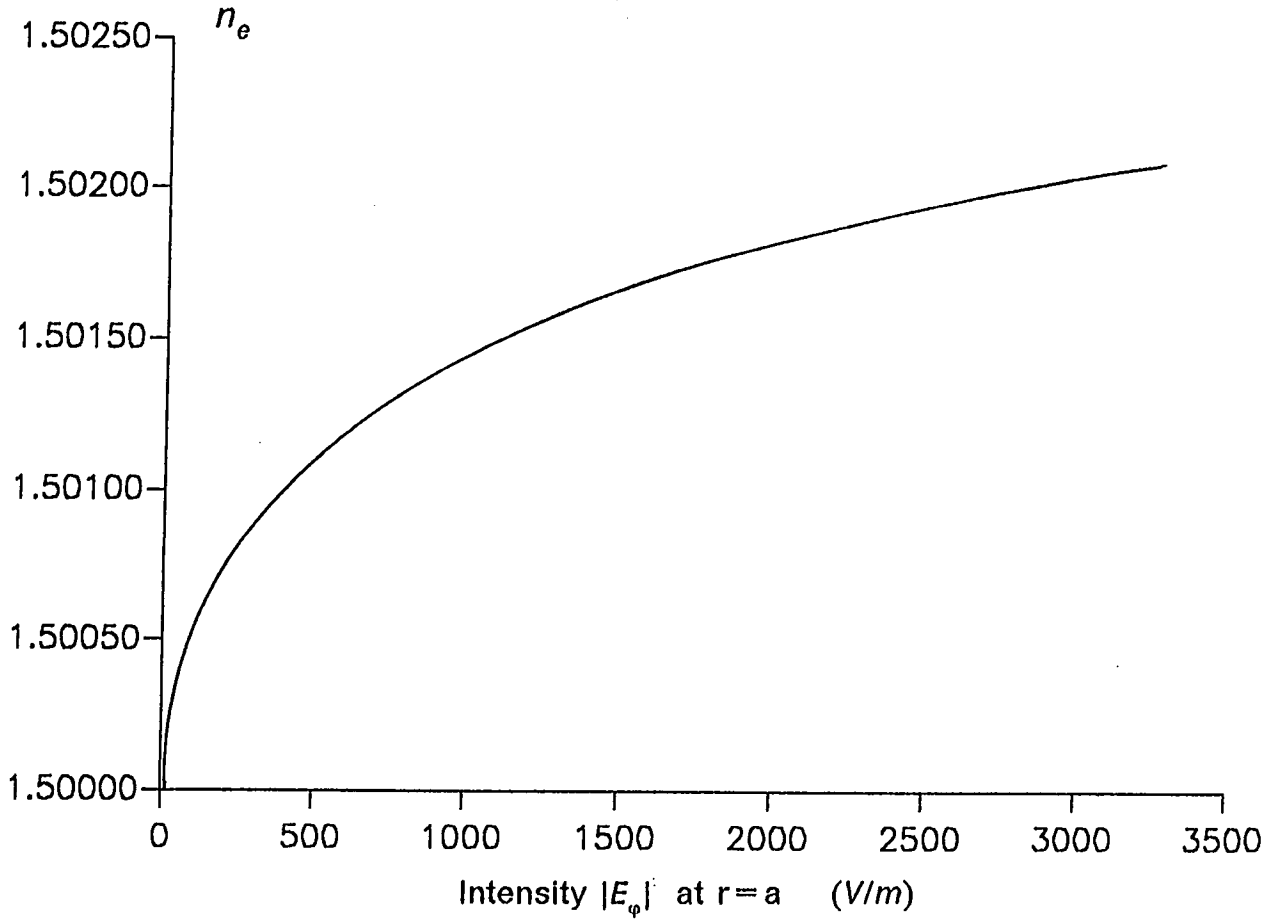

Fig.(5.15.b) Variation of n_e with the interface value of E_φ for TE_{02} mode in a waveguide having linear core and nonlinear cladding

the dielectric function of the nonlinear medium. The wave equation is solved, in this case, for E_z and H_φ is obtained form E_z using equation (3.38). the dispersion relations are described for convenience in terms of the tangential magnetic field intensity $|H_\varphi|^2$ measured at the core cladding interface. The magnetic field H_φ in the TM modes is considered the dual of the electric field E_φ in the TE modes. Also it is the only magnetic field component and at the same time it is transverse to the fiber axis. Therefore, it is the component meant by transverse magnetic. As all boundaries, this magnetic field component is also continuous at the core cladding interface. It is noted that most of the dispersion characteristics of TM modes of nonlinear fiber are similar from the outset to their TE counterparts. This will be clearly shown in the next subsections. However, the distribution of the dielectric constant of the nonlinear medium is different from that of TE case. In the case of TE modes in nonlinear waveguide (nonlinear core-linear cladding) the value of ε_1 at the fiber axis (r=0) is constant independent of the field E_φ and equal to the background value ε_{bg}. However, for TM case it is field dependent and given by equation (3.75). Two cases are to be studied corresponding to whether the fiber is supporting guided modes at low power or not.

The first case is a fiber which supports guided modes at low power. The

parameters used for this case are as follows: $\varepsilon_{bg}=2.255$, $\varepsilon_{2}=2.25$, $\alpha=10^{-8}\,V^{-2}m^{2}$, $g=20$, $\lambda=0.6328\,\mu m$ and $a=4\,\mu m$. The dispersion characteristic is shown in fig.(5.16) as a plot of mode index versus the magnetic field intensity $|H_{c}|^{2}$ evaluated at the core-cladding interface. As in the TE case there are three regions of interest for the first order TM mode (TM_{01}) depending on the field intensity. The first region has a positive slope and represent the low intensity behavior. In this region the mode index becomes an increasing function of the surface intensity. A similar behavior is also obtained in the high intensity region. The mode index becomes independent of the the applied field and equal to the linear case corresponding to $\varepsilon_{1} = \varepsilon_{sat.}$ as the intensity becomes very large. The high intensity and low intensity results obtained by the recursive scheme have been checked by solving the eigenvalue equation given bellow

$$\frac{\varepsilon_{co}J_{1}(u)}{uJ_{0}(u)} + \frac{\varepsilon_{cl}K_{1}(w)}{wK_{0}(w)} = 0 \qquad (5.3)$$

where u,w are defined in equation (5.2) and ε_{co} is taken equal to ε_{bg} for the low power case and equal to $\varepsilon_{bg} + \Delta\varepsilon_{NLmax}$ for the high power case. These results are shown in table 5.2. The agreement between the two results is up to the sixth digit.

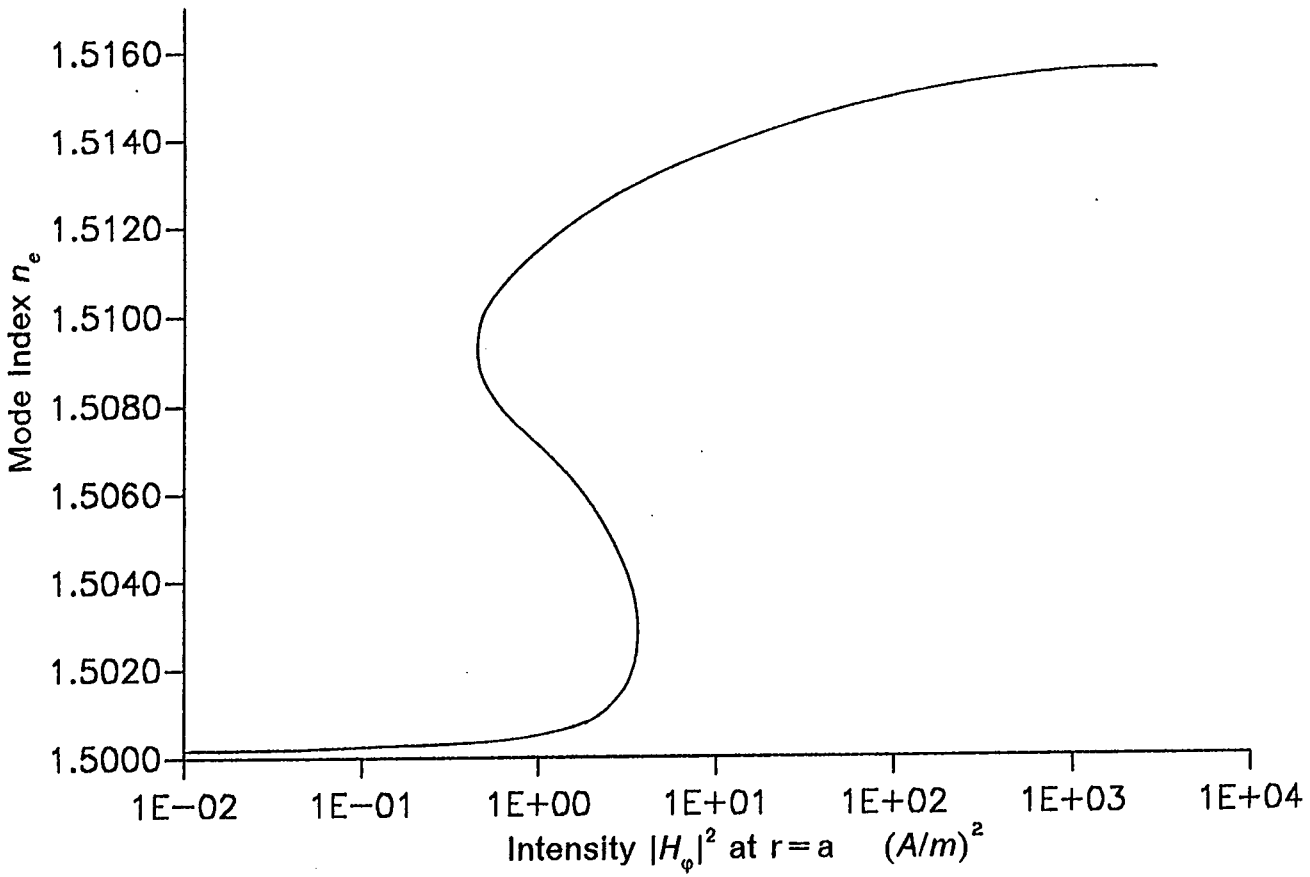

Fig.(5.16) Variation of n_e with the interface intensity for TM_{01} mode

TABLE 5.2

Checking the values of n_e in the linear limit of the recursive scheme against the direct solution of the closed form E.V.E. for TM_{01} mode. scheme.

Structure	Figure	Method	n_e	$A_{H_z}(0)$	$\|H_s\|^2$
$NL_{co}-L_{cl}$	(5.16)	recursive	1.500194	0.01	1.7(-7)
$NL_{co}-L_{cl}$		eigenvalue equation	1.500194		
$NL_{co}-L_{cl}$	(5.16)	recursive	1.515722	10000	11767.9
$NL_{co}-L_{cl}$		eigenvalue equation	1.515709		
$NL_{co}-L_{cl}$	(5.20)	recursive	1.512473	30000	130610
$NL_{co}-L_{cl}$		eigenvalue equation	1.512475		
$L_{co}-NL_{cl}$	(5.22)	recursive	1.506038	10	2.2(-2)
$L_{co}-NL_{cl}$		eigenvalue equation	1.506038		
$L_{co}-NL_{cl}$	(5.25)	recursive	1.501446	10	7.497(-2)
$L_{co}-NL_{cl}$		eigenvalue equation	1.501445		

The second region of the dispersion relation shown in fig.(5.16) is characterized by a negative slope where the mode index increases with the surface intensity. The multivalued solution is clear. For the same value of surface intensity there are three values of the mode index. The field profiles in fig.(5.17) are shown for three values of n_e covering different region of fig.(5.16) and chosen in the region of multivalued solution. As the modal power increases, the magnetic field becomes more confined in the core region and the field maximum moves towards the axis of the fiber. The distributions of the dielectric constant corresponding to the three values of n_e is illustrated in fig.(5.18). As has been mentioned before, the value of ε at $r=0$ is not equal to the background value as TE case, but it has an increment due to the value of E_z at $r=0$. This fact is clearly seen in fig.(5.18).

Figure (5.19) shows this dispersion relation as a plot of mode index versus total power. The power is calculated from equation (5.3). For the TM modes the expression for calculating the power is given by:

$$P = \frac{1}{2}\mathrm{Re}\int_0^{2\pi}\int_0^{\infty} E_r H_\varphi^{*}\, r\, dr\, d\varphi \qquad (5.5)$$

The dispersion curve has three regions of operation, corresponding to low, moderate and high power. The first region is the low power region in which, n_e is almost constant and independent of power. This is also the case for the high power (saturation) region. For moderate values of power,

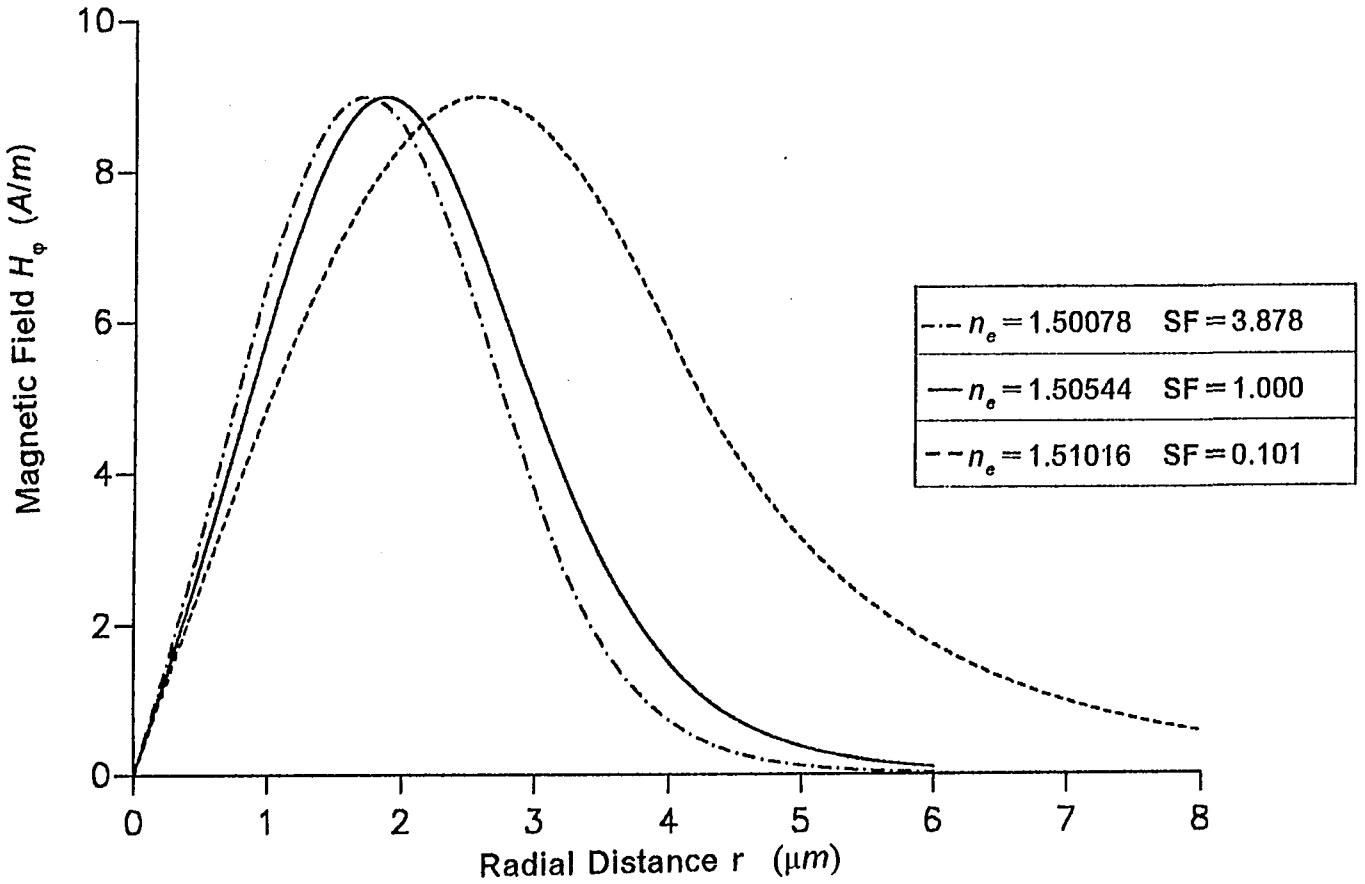

Fig.(5.17) Three field plots corresponding to three values of n_e taken from fig.(5.16)

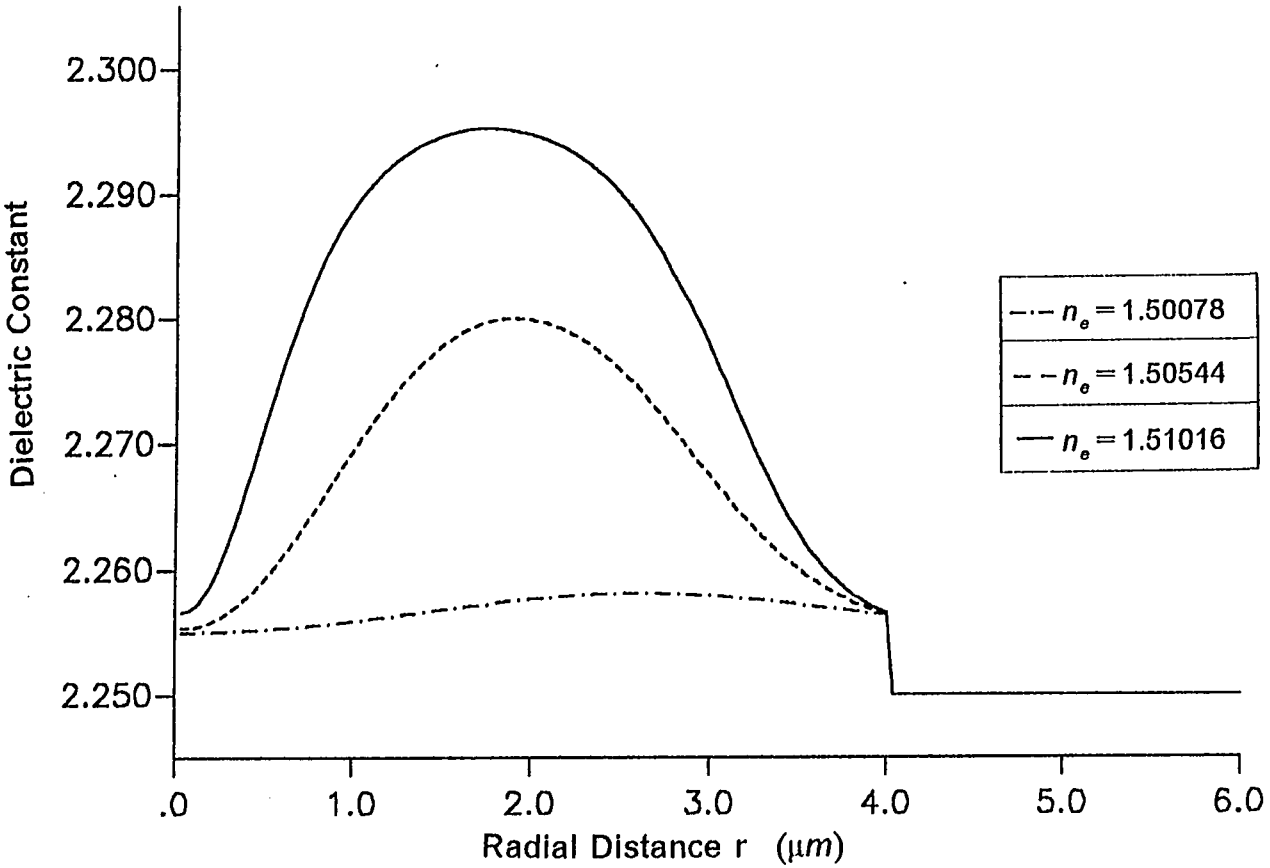

Fig.(5.18) Variation of the dielectric constant with the radial distance for the three values of n_e taken from fig.(5.16)

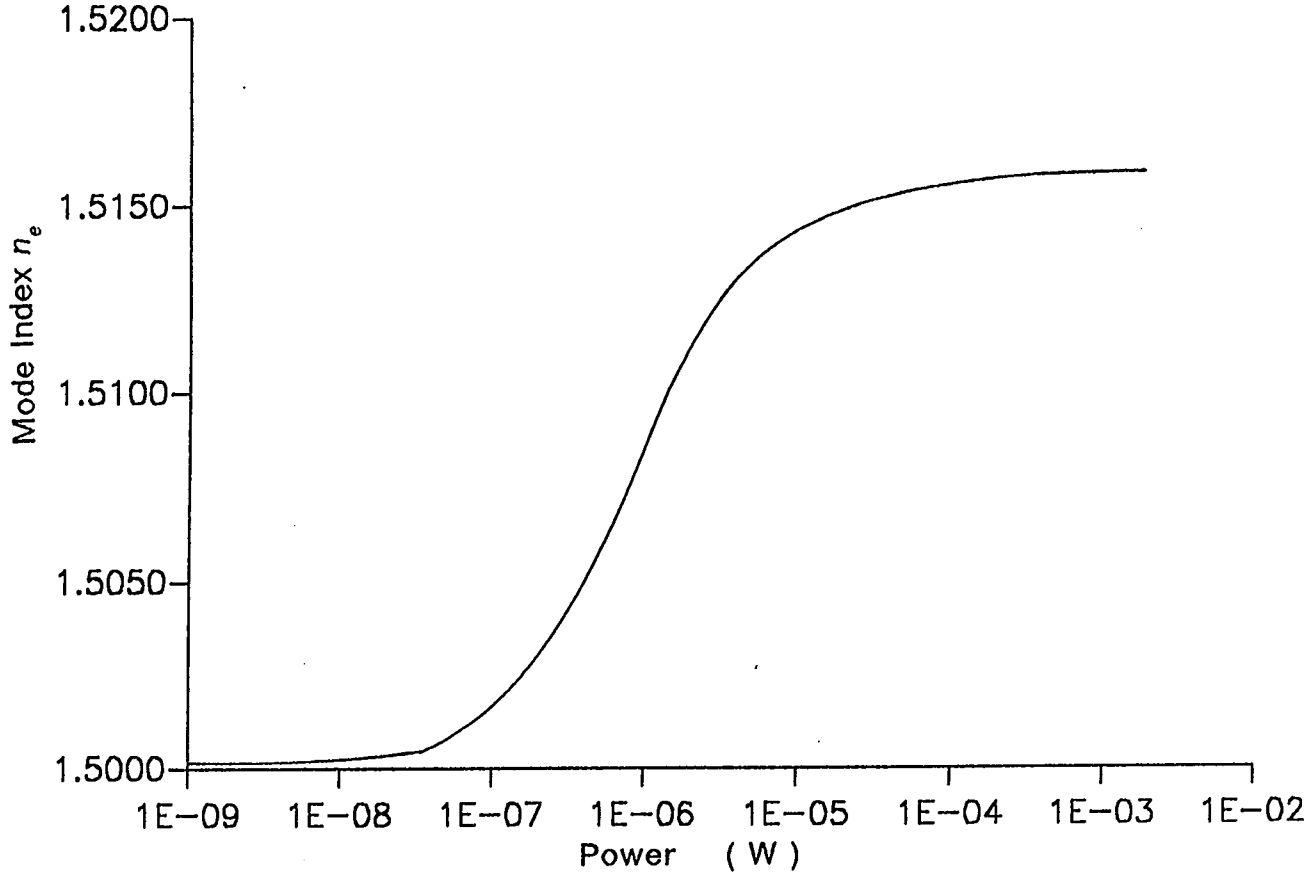

Fig.(5.19) Variation of n_e with the total power for TM_{01} in a waveguide having nonlinear core and linear cladding

it can be seen from this figure that n_e increases with the modal power. This is shown in the second region of the dispersion curve.

The second case is devoted to an optical fiber which is cut-off at low power. This fiber is characterized by $\varepsilon_{bg} \leq \varepsilon_2$. Two cases similar to those discussed in section 5.2, (second and third cases), for the TE_{01} mode have been investigated and studied. All the fiber parameters are also the same as those used in section 5.2. The dispersion characteristic for the fiber with $\varepsilon_{bg} < \varepsilon_2$ is shown in fig.(5.20) as a plot of n_e versus $|H_\infty|^2$ Similar to TE case the cutoff fiber requires a minimum surface intensity to be turned on. This threshold intensity depends on the refractive index difference, the nonlinear coefficient and the mode order. For the case of $\varepsilon_{bg} = \varepsilon_2$, the dispersion characteristic is similar to fig.(5.6) of the TE case.

5.5 TM WAVES IN OPTICAL FIBERS WITH A LINEAR CORE AND A NONLINEAR CLADDING

Two cases are to be considered. The first one is the fiber which supports the $TM_{01}$for all intensity values and characterized by $\varepsilon_1 > \varepsilon_{bg} + \Delta\varepsilon_{NLmax}$. The second case is devoted to a fiber which also supports the same mode, however, the saturation limit is such that $\varepsilon_1 = \varepsilon_{bg} + \Delta\varepsilon_{NLmax}$.

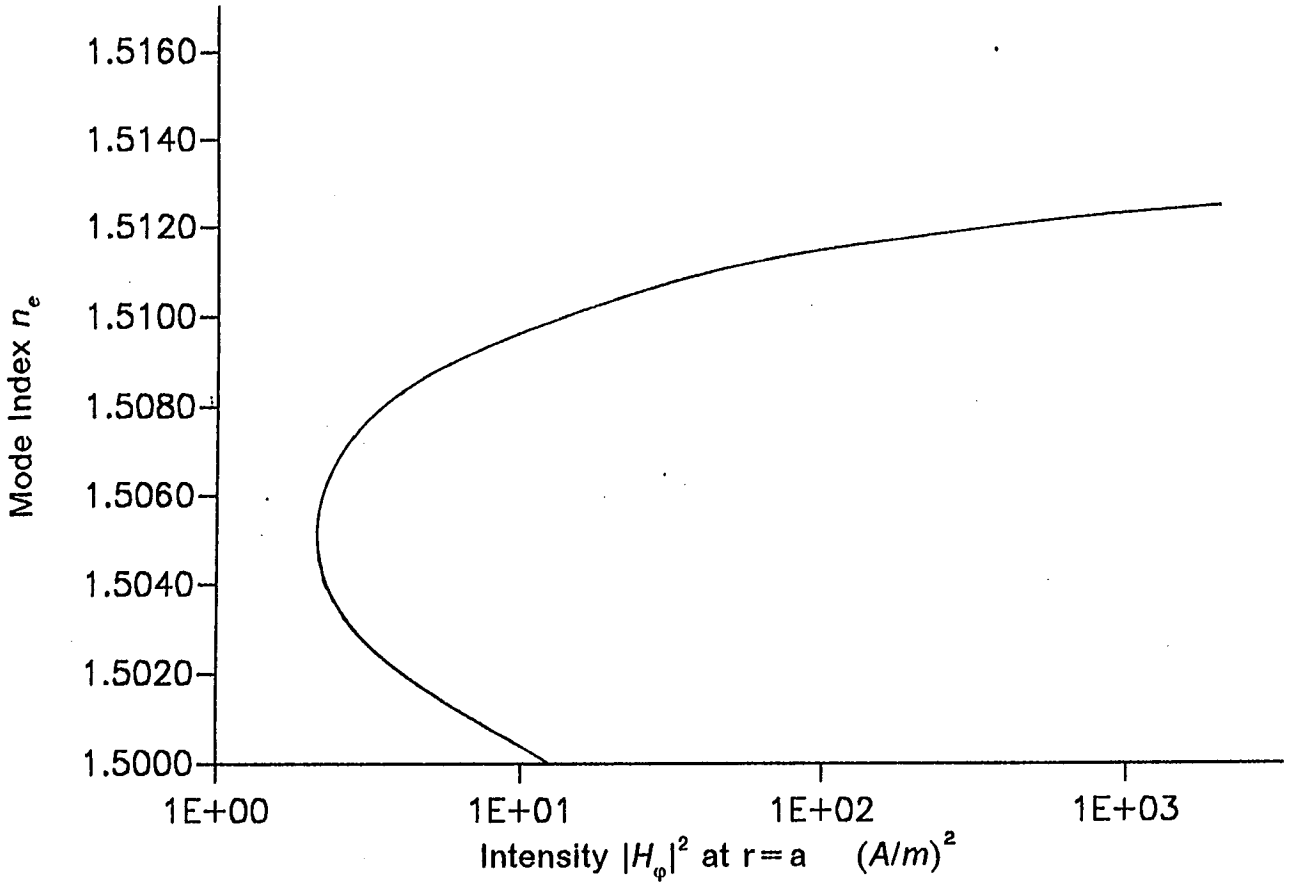

Fig.(5.20) Variation of n_e with the interface intensity for TM_{01} mode in a waveguide having nonlinear core and linear cladding

In the first case, the fiber parameters are the same as those of section (5.3). The reason for choosing the same parameters is to have a basis of comparison between different polarization, Particularly between TE_{01} and HE_{11} modes which will be shown in the next chapter. The dispersion characteristics are expressed here in two ways. In the first representation the total power is plotted against n_e as shown in fig.(5.21). The second one is illustrated in fig.(5.22) as a plot of surface intensity versus the mode index. Comparing the two plots of fig.(5.10) and fig.(5.22), there is a clear similarity between TE and TM dispersion characteristics. In fig.(5.22), for very low and very high intensity values the mode index is independent of the interface magnetic field intensity. The transition between these two states occurs monotonically. This is also the case in fig.(5.10).

It is seen from fig.(5.21) that the fiber can support the TE_{01} mode for any value of the input intensity. Three mode indices covering different regions of fig.(5.22) have been chosen and their corresponding field profiles are shown in fig.(5.23). The shift of maximum field amplitude towards the nonlinear medium is clear.

Unlike the fiber with a nonlinear core and a linear cladding in which most of the field energy is concentrated in the core, a considerable part of the field energy is propagated in the cladding where the core is linear and the cladding is nonlinear. This is also the case of TE modes. It is seen from

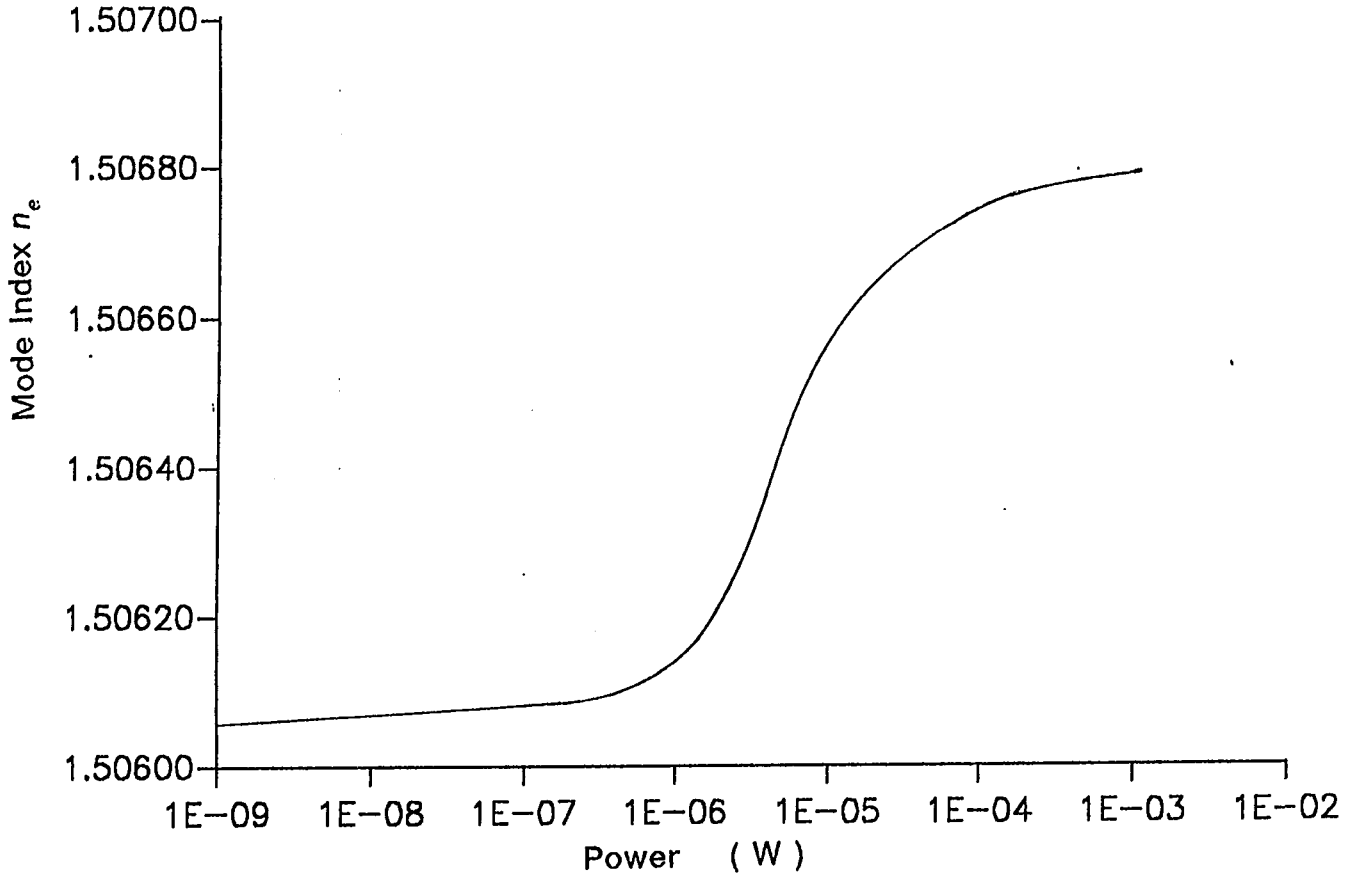

Fig.(5.21) Variation of n_e with the total power for TM_{01} in a waveguide having linear core and nonlinear cladding

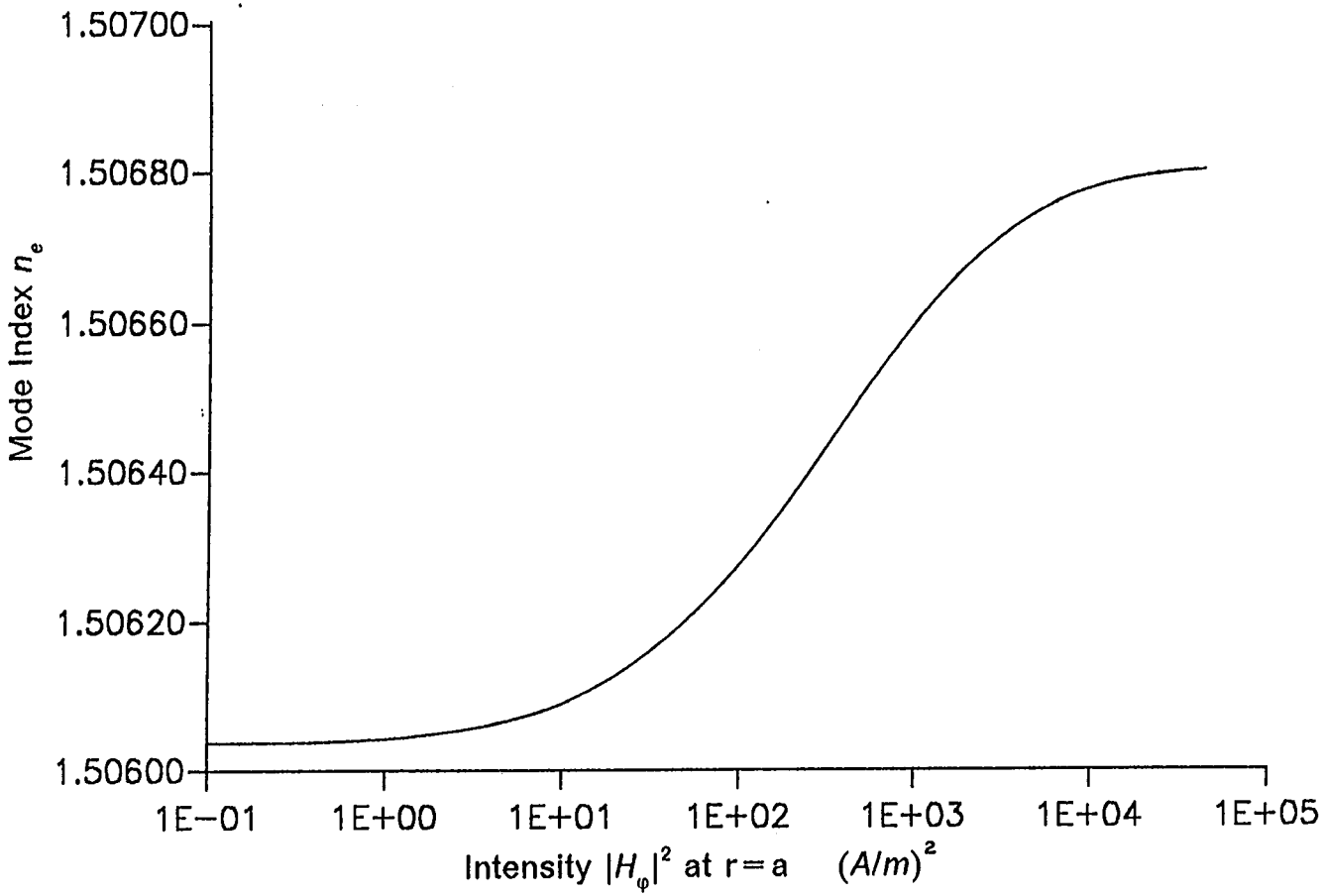

Fig.(5.22) Variation of n_e with the interface intensity for TM_{01} in a waveguide having linear core and nonlinear cladding

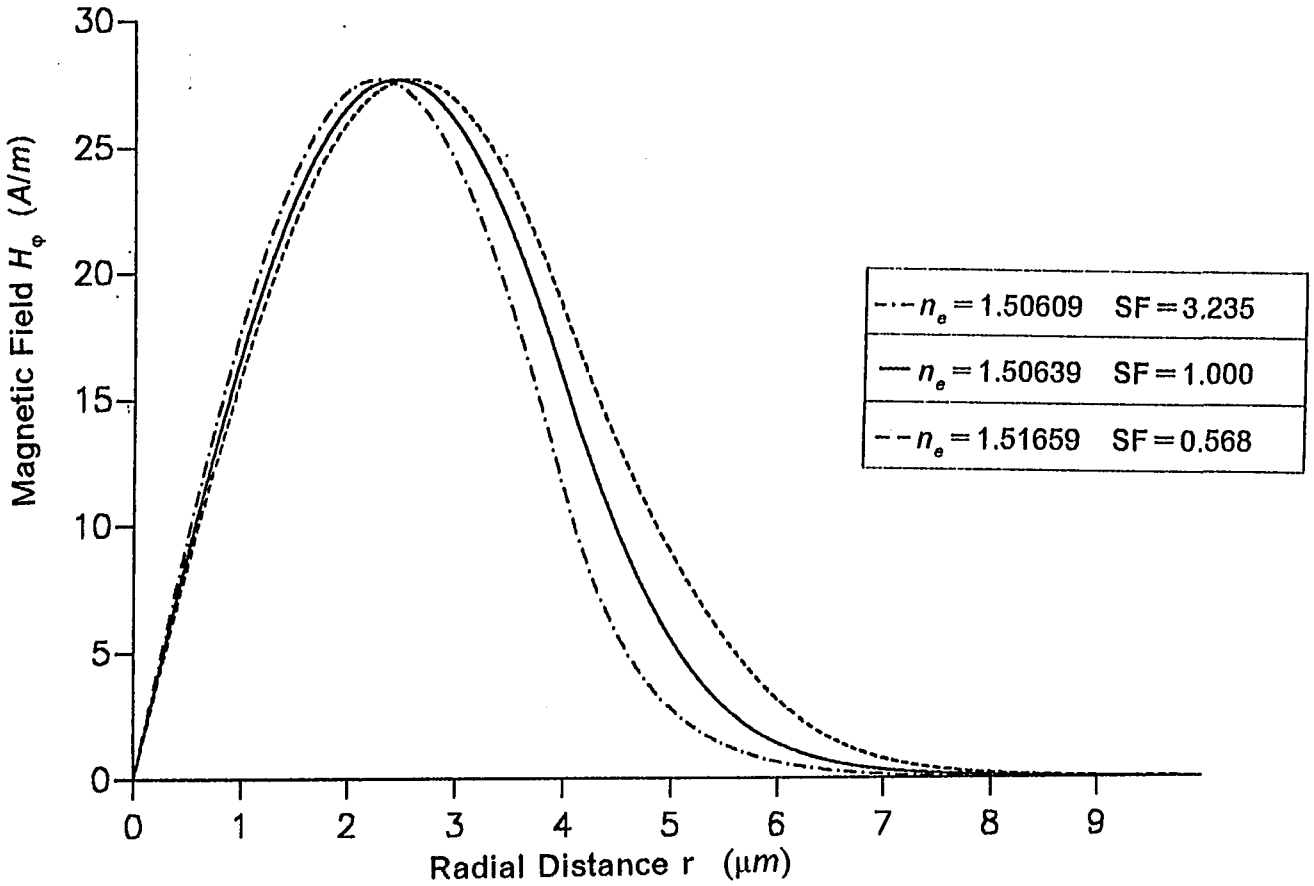

Fig.(5.23) Three field plots corresponding to three values of n_e taken from fig.(5.22)

fig.(5.23) that as the medium is approaching saturation, the field peak becomes more closer to the core cladding interface.

The distribution of the dielectric constant corresponding to the above three values of mode index is illustrated in fig.(5.24). For this fiber structure the index profile is similar to that of the TE case shown in fig.(5.12). As can be seen from fig.(5.24),there is a graded-index distribution in the cladding region depending of the amount of power applied, the larger the power the more penetration of the graded-index profile in the cladding region.

As has been done for the TE case, the solutions of the linear states of the waveguide are checked against the corresponding direct solution of the eigenvalue equation These Two linear states are characterized by $\varepsilon_2 = \varepsilon_{bg}$ and $\varepsilon_2 = \varepsilon_{bg} + \Delta\varepsilon_{NLmax}$ respectively. The results are identical as shown in table 5.2

The second case under consideration is characterized by $\varepsilon_1 = \varepsilon_{bg} + \Delta\varepsilon_{NLmax}$. This optical fiber supports the TM_{01} mode for low intensity levels which makes $\varepsilon_1 > \varepsilon_{bg} + \Delta\varepsilon_{NL}$. However, for high input power, the fiber approaches saturation for which $\varepsilon_1 \approx \varepsilon_{bg} + \Delta\varepsilon_{NLmax}$. In this case the fiber resembles a linear step-index with a large radius. This enables the fiber to support the next higher order modes. The parameters taken for this

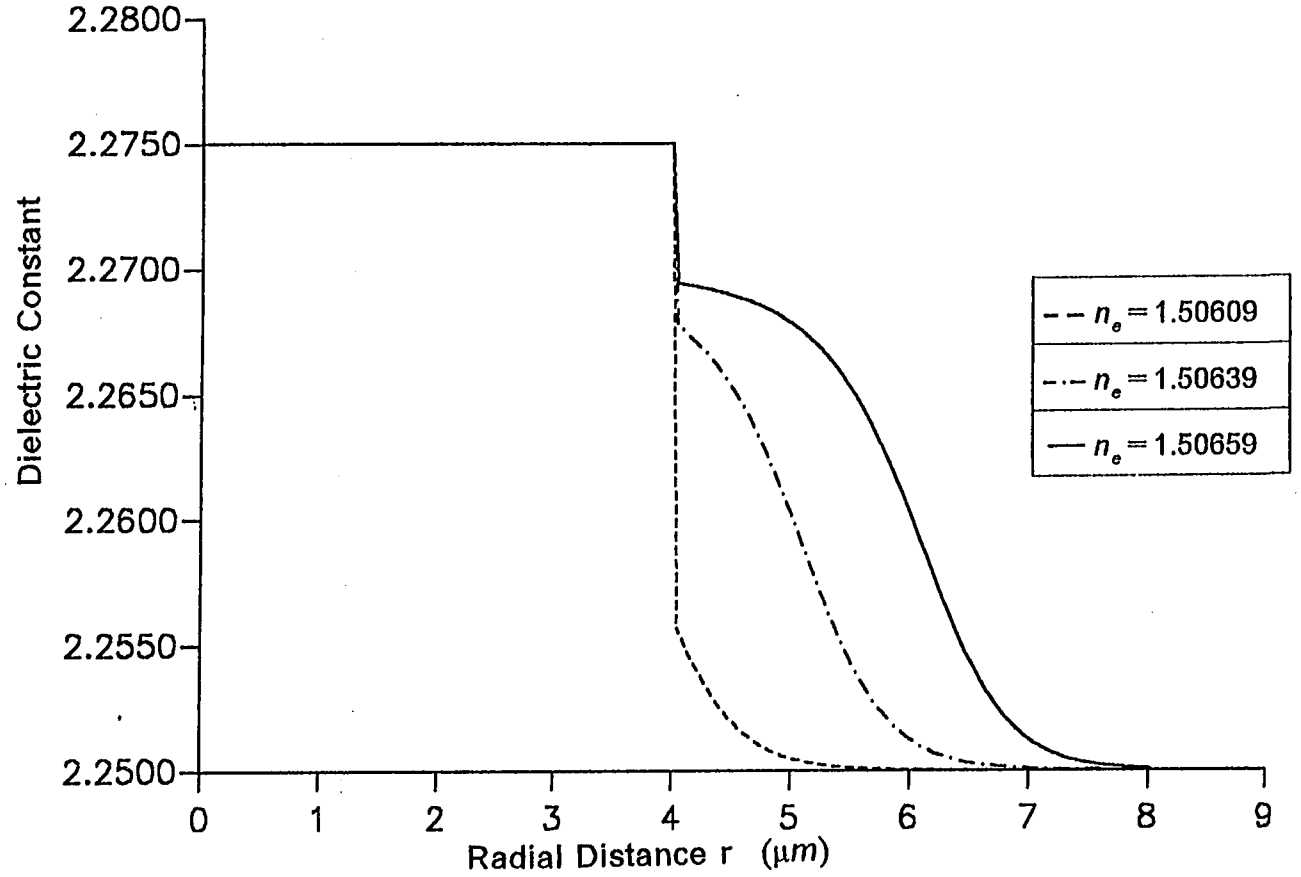

Fig.(5.24) Variation of the dielectric constant with the radial distance for the three values of n_e taken from fig.(5.22)

waveguide are similar to those given in section (5.3). The dispersion characteristic is shown in fig.(5.25) as a plot of the modal power of the TM_{01} mode versus the mode index. It is seen that n_e is independent of power for low power values. However, for moderate and high power values, n_e increases with power until the fiber reaches saturation. Three values of the mode index are chosen corresponding to close to linear, close to saturation, and an intermediate value. The field profiles associated with these three values are shown in fig.(5.26). It is clear that as the nonlinearity becomes stronger, the field is guided mainly in the nonlinear region (cladding) and only a small amount of energy is confined in the core region. This unique characteristic of the waveguide with nonlinear cladding also occurs in the TE case. The distribution of the dielectric constant for the same values of the mode indices is shown in fig.(5.27). It is similar to fig.(5.14) of the TE case. The physical radius of the fiber increases at saturation to about five times the the actual radius.

5.6 CHECKING THE RESULTS USING THE SELF-CONSISTENT SCHEME

After applying the recursive scheme to different nonlinear waveguide structure, it is instructive to check the obtained results using the self-consistent routine. The strategy for doing this is based on choosing three different values of the mode index from the dispersion curve. The intensity profiles for these values of n_e are known from the recursive solution. The

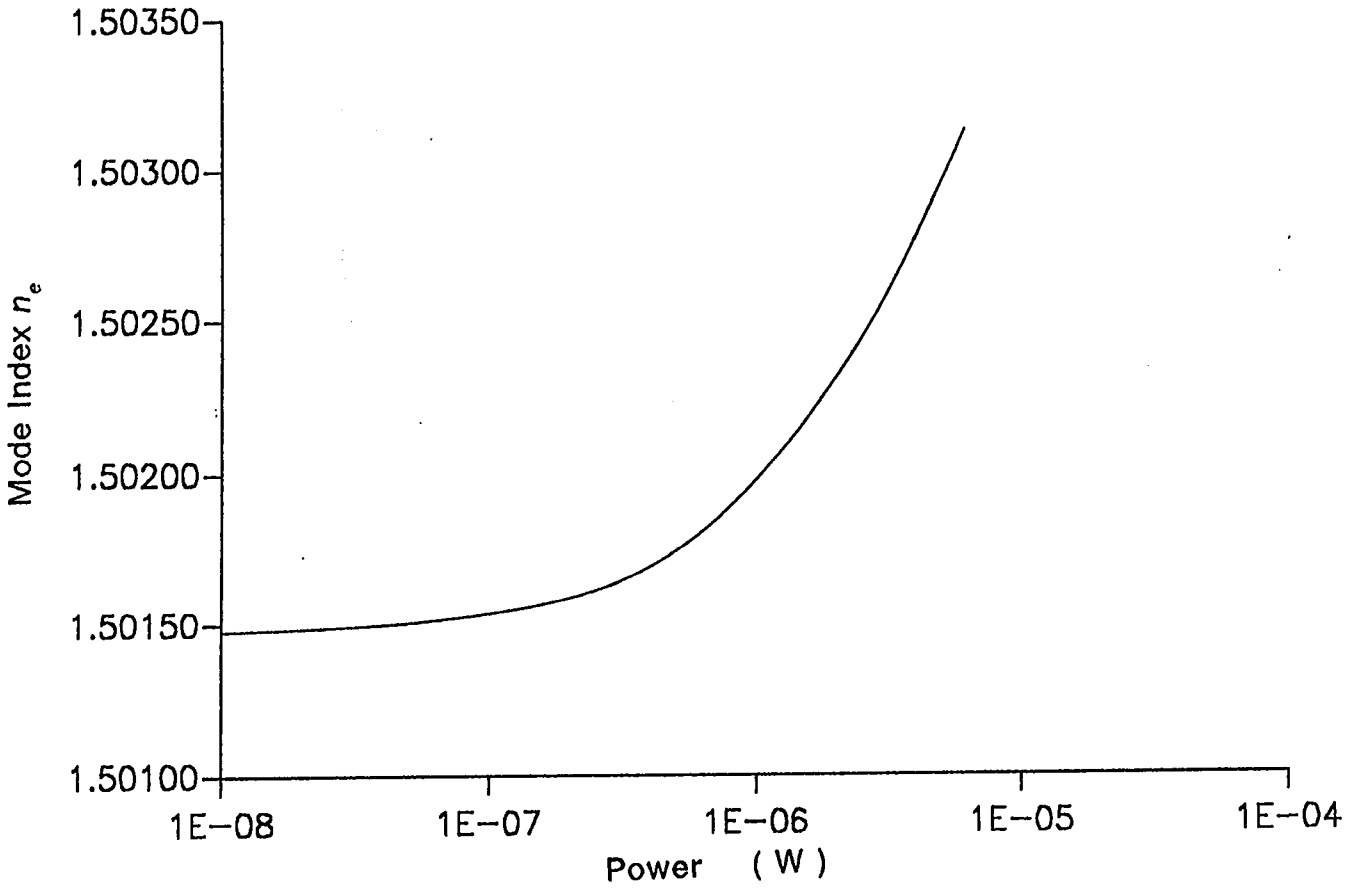

Fig.(5.25) Variation of n_e with the total power for TM_{01} in a waveguide having linear core and nonlinear cladding

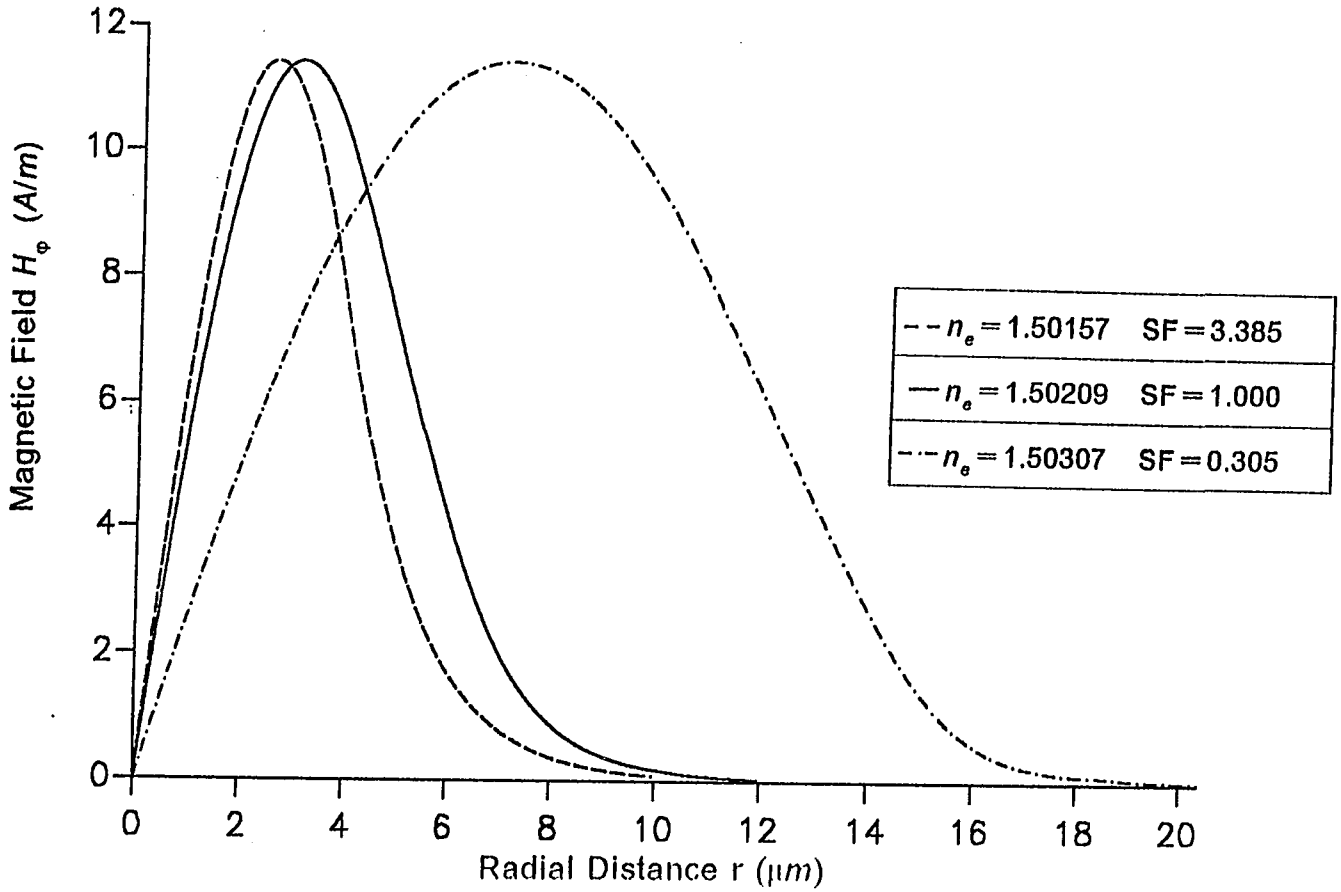

Fig.(5.26) Three field plots corresponding to three values of n_e taken from fig.(5.25)

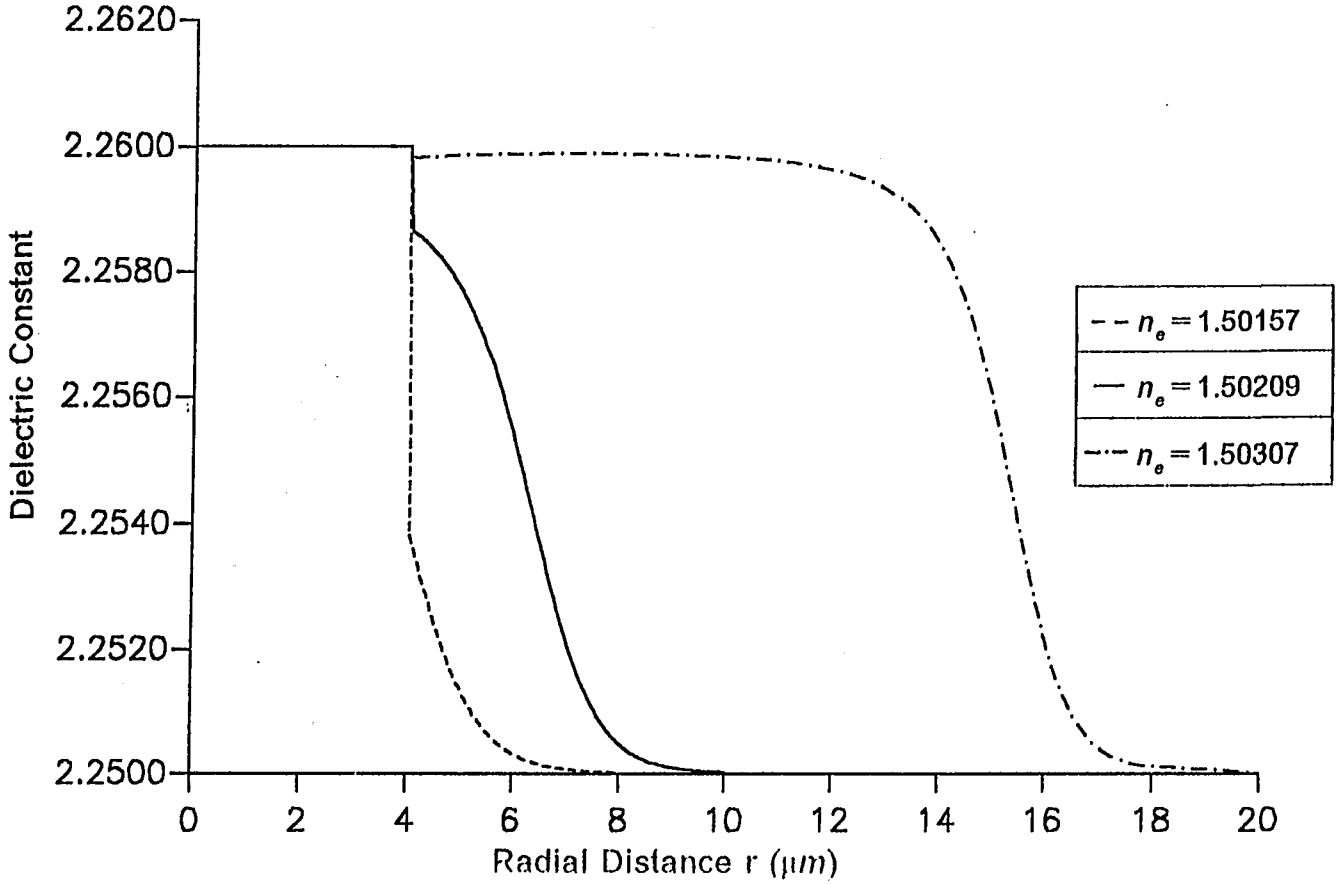

Fig.(5.27) Variation of the dielectric constant with the radial distance for three values of n_e taken from fig.(5.25)

intensity $|E|^2$ has the general definition given in equation (3.44). For each value of the n_e, the corresponding intensity profile is used as an input to the self-consistent scheme. This intensity profile modifies the dielectric constant according to equation (3.45) and generates a graded-index profile. The self-consistent scheme solves linearly the graded-index profile and produce the corresponding mode index and its associated intensity profile. If the input to the recursive scheme is a correct solution to the nonlinear problem, the first run of the scheme will produce the same mode index and the same intensity profile. This will guarantee a quick convergence of the self-consistent scheme. Table 5.3 lists the results obtained from the two methods in the case of TE waves. The figure number shown in the second column gives the dispersion curve, which has been checked. The fifth column in the table is assign to the amplitude of H_z at r=0. This amplitude is necessary to start the recursive scheme. The value of n_e, the field profile and the surface intensity will be function of this amplitude. However, in the self-consistent routine, the solution is independent of this field amplitude. The same field amplitude has been used in both routines in order to obtain the same surface intensity $|E_s|^2$ directly without normalizing the results. the values of n_e in both methods are the same since the self-consistent scheme is initiated with the proper solution of the nonlinear problem. Table 5.4 is similar to table 5.3 and is devoted to TM waves. To start the TM

TABLE 5.3

The effective indices of the fundamental TE mode obtained from the recursive solution and the solution using self-consistent scheme.

Structure	Figure	Method	n_e	$A_{H_z}(0)$	$\lvert E_s\rvert^2$
$NL_{co}-L_{cl}$	(5.2)	recursive	1.500969	0.2	167329
$NL_{co}-L_{cl}$		self-cons.	1.500969	0.2	167329
$NL_{co}-L_{cl}$	(5.2)	recursive	1.507101	1.0	101049
$NL_{co}-L_{cl}$		self-cons.	1.507101	1.0	101049
$NL_{co}-L_{cl}$	(5.2)	recursive	1.515087	5.0	1.165(7)
$NL_{co}-L_{cl}$		self-cons.	1.515087	5.0	1.165(7)
$L_{co}-NL_{cl}$	(5.10)	recursive	1.506063	0.5	286475
$L_{co}-NL_{cl}$		self-cons.	1.506063	0.5	286475
$L_{co}-NL_{cl}$	(5.10)	recursive	1.506311	2.0	8923126
$L_{co}-NL_{cl}$		self-cons.	1.506311	2.0	8923126
$L_{co}-NL_{cl}$	(5.10)	recursive	1.506655	5.0	1.184(8)
$L_{co}-NL_{cl}$		self-cons.	1.506655	5.0	1.184(8)

TABLE 5.4

The effective indices of the first order TM mode obtained from the recursive solution and the self-consistent scheme.

Structure	Figure	Method	n_e	$A_{E_z}(0)$	$\lvert E_s\rvert^2$
$NL_{co}-L_{cl}$	(5.16)	recursive	1.500958	50	166011
$NL_{co}-L_{cl}$		self-cons.	1.500958	50	166011
$NL_{co}-L_{cl}$	(5.16)	recursive	1.503624	120	216292
$NL_{co}-L_{cl}$		self-cons.	1.503624	120	216292
$NL_{co}-L_{cl}$	(5.16)	recursive	1.512957	600	759226
$NL_{co}-L_{cl}$		self-cons.	1.512957	600	759226
$L_{co}-NL_{cl}$	(5.22)	recursive	1.506088	200	790890
$L_{co}-NL_{cl}$		self-cons.	1.506088	200	790890
$L_{co}-NL_{cl}$	(5.22)	recursive	1.506227	400	4616806
$L_{co}-NL_{cl}$		self-cons.	1.506227	400	4616806
$L_{co}-NL_{cl}$	(5.22)	recursive	1.506509	800	3.583(7)
$L_{co}-NL_{cl}$		self-cons.	1.506509	800	3.583(7)

recursive scheme, the value of E_z at r=0 is required. This value is given in the fifth column. The same comment on the TE case is valid for the TM case.

It must be noted that the self-consistent scheme can be used to solve the nonlinear optical fiber completely. However,it is very time consuming. The convergence of the routine differs from one region to another on the dispersion curve. For example, in fig.(5.2), the convergence of the single-valued solution regions is faster than that of the multi-valued region. Also the convergence is slower in the negative slope region than that in the positive slope regions. The objective of using the self-consistent routine is only to check the obtained results using the recursive scheme.

CHAPTER 6

THE FUNDAMENTAL HYBRID MODE IN A NONLINEAR OPTICAL FIBER

6.1 INTRODUCTION

The hybrid HE_{11} mode is the most important mode of an optical fiber. It has a zero cut-off frequency and therefore can be supported by any optical fiber regardless of its core size and refractive index difference. Single mode fibers which are characterized by a fiber V number less than 2.405 have superior dispersion performance in communication systems than multimode fibers. This results in the single mode optical fiber having a much higher bandwidth compared to multimode optical fibers.

The nature of the hybrid mode HE_{11} is explained for a linear optical fiber and then is considered in a nonlinear fiber. As in the case of TE and TM modes discussed in chapter 5, the field profiles of a nonlinear fiber are similar to those of a linear fiber except for a power dependent change in the field profile. This results in a change of the distribution of total power over the core and the cladding regions.

For the fundamental mode in saturable media, there is no shift of the field maximum towards the nonlinear region, because it is always located at the origin. However, the distribution of power is changed.

In step-index optical fiber, the hybrid modes are designated HE modes and EH modes. The designation HE modes and EH modes has been explained by Unger [10] as follows: HE_{11} and EH_{11} modes are the lowest order hybrid modes in optical waveguide. One of them HE_{11} gives field profiles inside the core which are similar to those of the round hollow metallic waveguide operating in the H_{11} (TE_{11}) mode. Because the H_{11} is the fundamental mode in the metallic waveguide, the fundamental mode of the fiber has been designated HE_{11}. The hybrid nature of the HE modes results from the fact that the mode is not a pure H-mode, but has also an axial E_z component. Accordingly HE modes are H-like modes or (TE-like modes) when related to the equivalent metallic waveguide modes. As there is another mode sharing the same subscript 11 with the HE_{11} mode the designation EH_{11} has been allotted to it. This designation fixes the classification of higher order modes.

The fundamental Hybrid mode HE_{11} is characterized by some important features. For instance, it is linearly polarized when the refractive index difference between the core and cladding is very small. The optical fiber in

this case, is called a weakly guiding fiber. It is well-known that the linearly polarized modes of the weakly guiding fiber are in general a superposition of degenerate modes which share the same propagation constant β. However, the HE_{11} is linearly polarized by itself which is a distinguishing characteristic of all HE_{1m} modes. The linear polarization feature means briefly that the important electric and magnetic fields are in the transverse plane normal to each other while the axial fields components are negligible compared to the transverse components. This makes the field inside the fiber similar to that of TEM plane wave.

By examining the values of the field components for HE_{11} (equations (3.85)-(3.96)) in the case of weak guidance ($n_1 \approx n_2$), two important conclusions are obtained. The first one is that the transverse electric fields E_φ and E_r are equal in magnitude and in their radial dependence, but are different in their azimuthal dependence. If one of them is taken to vary as $\cos\varphi$ the other varies as $\sin\varphi$. This feature is also found for the transverse magnetic field components H_φ and H_r. The second feature is that the axial field components E_z and H_z have the same radial dependence. Their azimuthal variations differ by $\frac{\pi}{2}$. The amplitudes ratio $\frac{A_{E_z}}{A_{H_z}}$ is the ratio between the amplitudes of axial electric field E_z and the amplitude of the axial

magnetic field H_z. It is equal to the ratio $\frac{A_1}{C_1}$ obtained from equations (3.79) and (3.82). This ratio is also equal to the intrinsic impedance of the core material. This fact is considered because for weak guidance, both the core and the cladding have almost the same refractive index. Wave propagation in this case is similar to the one in a single unbounded medium. In the subsections (6.2) and (6.3) the dispersion characteristics of the hybrid mode HE_{11} in a nonlinear optical fiber are presented. The nonlinear optical fiber with nonlinear core and linear cladding is discussed in section 6.2. Section 6.3 is devoted to the the optical fiber with linear core and nonlinear cladding. Checking of the results obtained by the recursive scheme in sections 6.2 and 6.3 is made by using the self-consistent scheme (discussed in section (3.8)). The results are given in section 6.4.

6.2 THE OPTICAL FIBER WITH A NONLINEAR CORE AND A LINEAR CLADDING

Two cases have been studied, the first one is for a fiber which supports guided modes at low power and has $\varepsilon_{bg} > \varepsilon_2$. The second one is the case of a cut-off fiber characterized by $\varepsilon_{bg} < \varepsilon_2$. For the first case the fiber parameters are as follows: $\varepsilon_{bg} = 2.255$, $\varepsilon_2 = 2.25$, $\alpha = 10^{-8}\, V^{-2} m^2$, $g = 20$, $\lambda = 0.6328\ \mu m$ and $a = 4\ \mu m$. The dispersion characteristics are expressed

as plots of the mode index, n_e versus the tangential field component $|E_\varphi|^2$ evaluated at the core-cladding interface as has been done in the TE case. The dispersion plots can alternatively be given as plots of $|E|^2$ versus the mode index or plots of mode power versus the mode index.

Figure (6.1) shows the dispersion relation of the HE_{11} mode of this waveguide as a plot of surface intensity $|E|^2$ versus n_e for two saturation levels. In the case of high saturation level (g=20), the multivalued dependence of n_e on the surface intensity is clear for a range of the surface intensity. However, if the surface intensity is outside this range, the relation is single valued. For the case of low saturation level (g=100), there is no optical bistability and the relation is monotonic. It must be noted that in the regions where the dependence is single valued for g=20, the fiber behaves in a manner similar to that of a linear fiber with $\varepsilon_1 = \varepsilon_{bg}$ or $\varepsilon_1 = \varepsilon_{bg} + \Delta\varepsilon_{NLmax}$ depending on whether the intensity is very low or very high respectively The values of n_e for these two cases have been compared with the results of the solution of the eigenvalue equation given in reference [10]. Table 6.1 lists the eigenvalues obtained by the two methods.

Figure (6.2) shows the field profiles for three values of the effective index covering different regions of operation. (points A, B and C in fig.(6.1)). It can be seen from fig.(6.2) that as the input power increases the field becomes

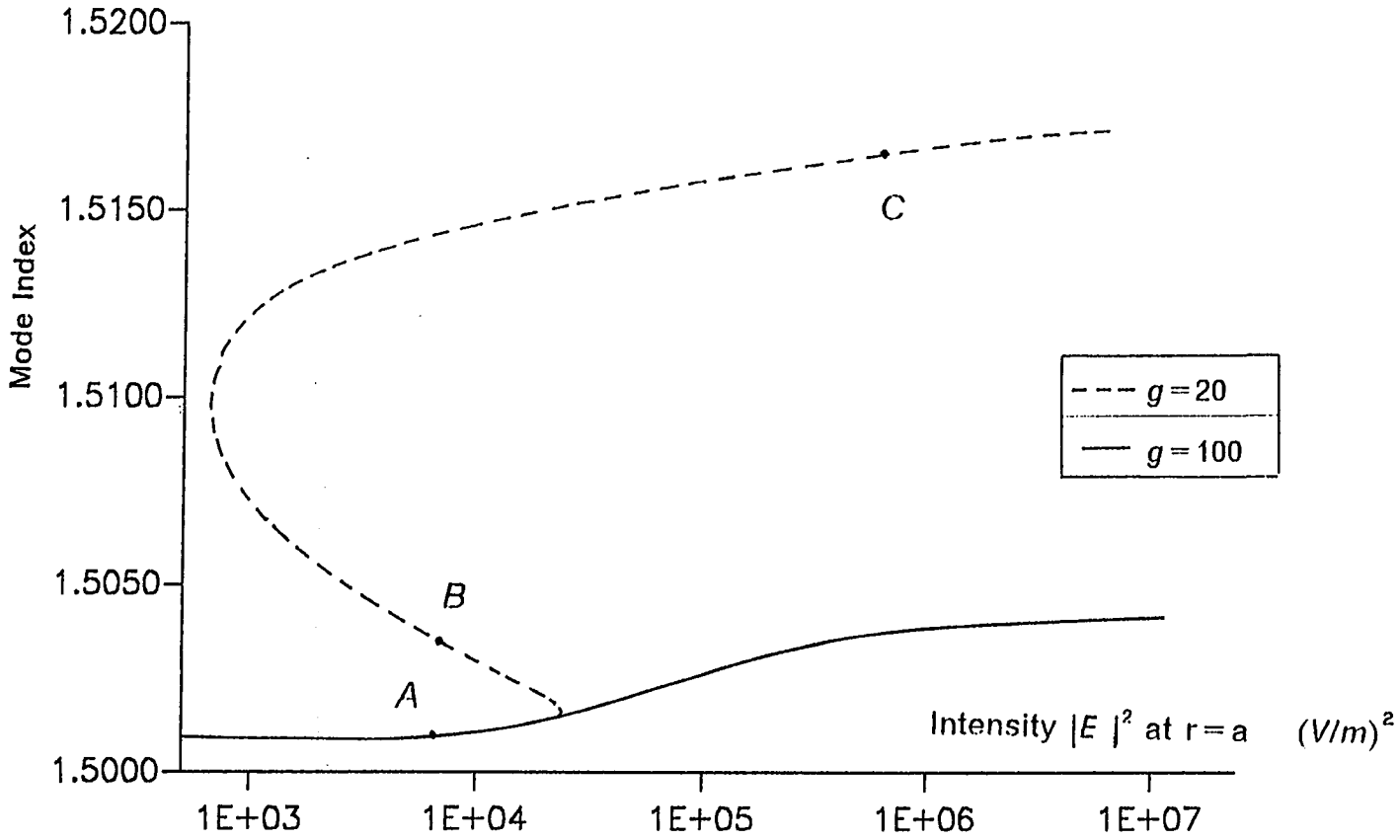

Fig.(6.1) Variation of n_e with the surface intensity for HE_{11} mode in a waveguide having two different saturation levels

TABLE 6.1

The effective indices of the fundamental HE mode obtained from the recursive solution and the closed form eigenvalue equation

Structure	Figure	Method	n_e	$A_{E_z}(0)$	$\lvert E_s\rvert^2$
$NL_{co}-L_{cl}$	(6.2)	recursive	1.501033	1.0	335.40
$NL_{co}-L_{cl}$		eigenvalue equation	1.501029		
$NL_{co}-L_{cl}$	(6.2)	recursive	1.517209	10000	15.44(7)
$NL_{co}-L_{cl}$		eigenvalue equation	1.517237		
$NL_{co}-L_{cl}$	(6.4)	recursive	1.505779	5000	17.92(8)
$NL_{co}-L_{cl}$		eigenvalue equation	1.515780		
$L_{co}-NL_{cl}$	(6.8)	recursive	1.507409	10	5654.15
$L_{co}-NL_{cl}$		eigenvalue equation	1.507409		
$L_{co}-NL_{cl}$	(6.8)	recursive	1.507645	1000	2.817(8)
$L_{co}-NL_{cl}$		eigenvalue equation	1.507677		
$L_{co}-NL_{cl}$	(6.12)	recursive	1.502564	1.0	152.96
$L_{co}-NL_{cl}$		eigenvalue equation	1.502564		

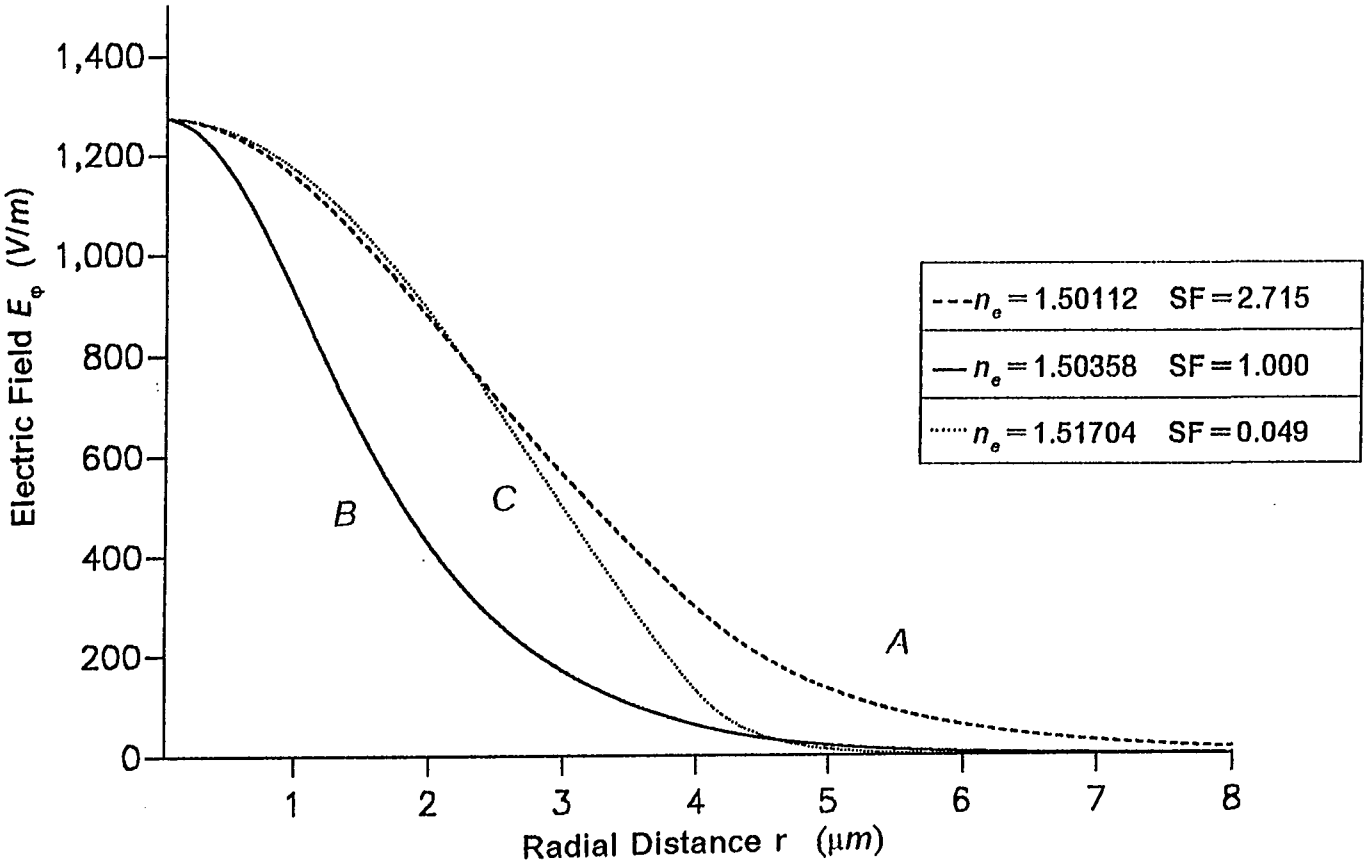

Fig.(6.2) Three field plots corresponding to three values of n_e taken from fig.(6.1)

more confined in the core region and the field penetration in the cladding decreases. The corresponding dielectric constant distributions for points A, B and C is illustrated in fig.(6.3).

It can be shown by comparing fig.(6.3) to the corresponding TE and TM cases in figs.(5.4) and (5.18), that the HE_{11} has a different dielectric constant profile. In the case of the HE_{11} mode, the dielectric constant has a maximum at the axis of the fiber and is in general a graded index distribution. However, in both the TE and the TM cases, the dielectric constant has a distribution which is completely different form that occurring in the HE_{11} case. The maximum value of the dielectric constant occurs inside the core but, not at the center of the fiber. The profile in general resembles the letter M.

The cutoff fiber investigated here is similar to that used in section 5.2 with all waveguide parameters are taken the same. The dispersion relation for this fiber is shown in fig.(6.4) as a plot of interface value of $|E_n|^2$ versus n_e. The fiber requires a minimum amount of intensity to support the HE_{11} mode. As the guidance takes place with more power propagated along the fiber the interface intensity decreases and the field maximum increases which represents the negative slope part of fig.(6.4). For the positive slope part of the same figure, both interface intensity and n_e increase with the mode power

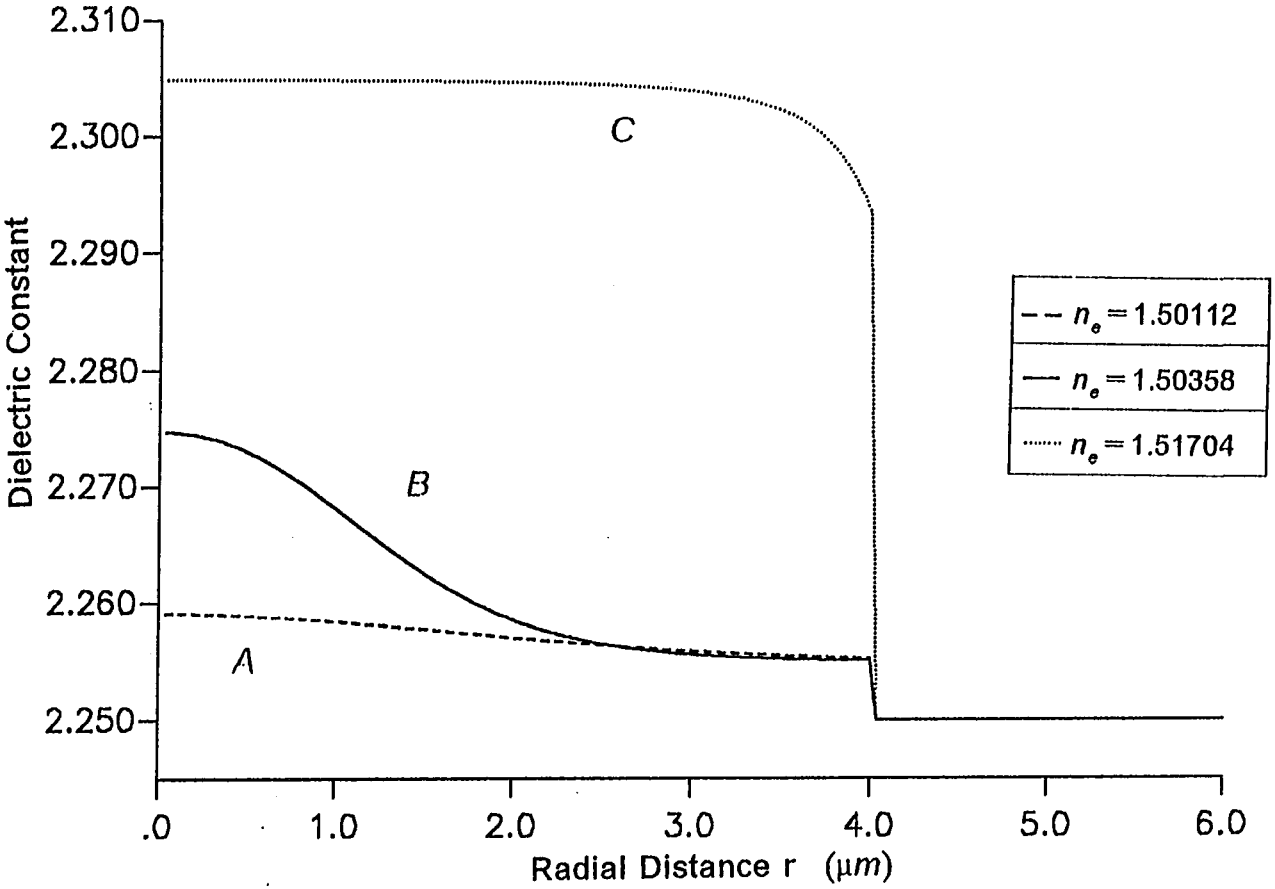

Fig.(6.3) Variation of the dielectric constant with the radial distance for three values of n_e taken from fig.(6.1)

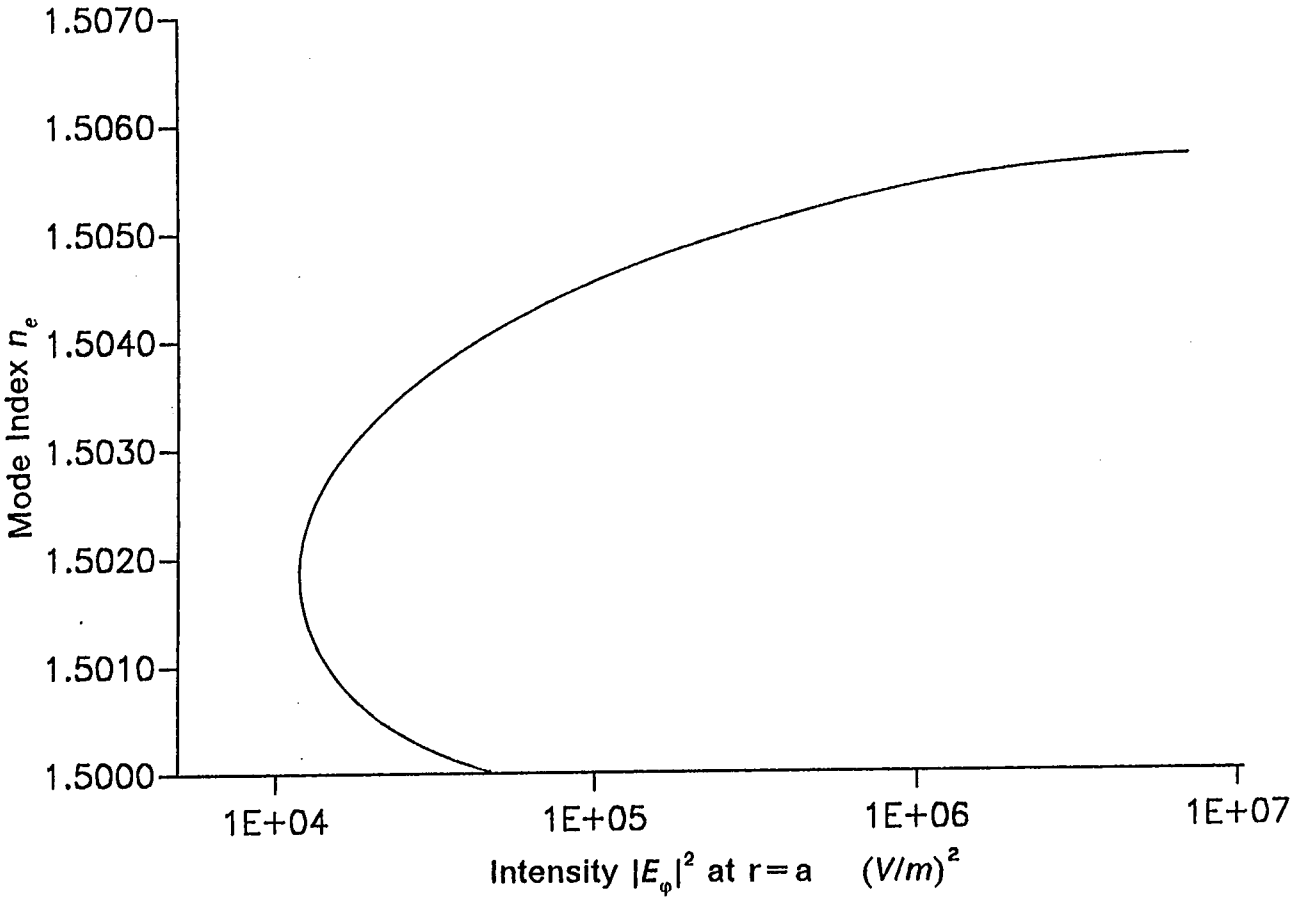

Fig.(6.4) Variation of n_e with the interface intensity for HE_{11} mode in a waveguide having $\varepsilon_{bg} < \varepsilon_2$

and the fiber is driven into saturation. The same dispersion characteristic is illustrated in fig.(6.5.a) with the surface intensity replaced by the modal power. The power can be calculated form the integral of the Poynting vector given in equation (5.3). For the HE_{11} mode, this integral reduces to:

$$P = \frac{1}{2}\mathrm{Re}\int_0^{2\pi}\int_0^{\infty}\{E_r H_\varphi^{*} - E_\varphi H_r^{*}\}\; r\,dr\,d\varphi \qquad (6.1)$$

In equation (6.1), the power flow is considered in the positive z direction. The minimum threshold power required for the fiber to support the HE_{11} mode can be seen from fig.(6.5.b). There is a small negative slope part corresponding to unstable operation. The remaining part of the dispersion curve with positive slope is considered stable. When the fiber approaches saturation the effective index n_e becomes constant independent of the modal power.

Figure (6.5.b) is similar to fig.(6.5.a) and showing at the same time the behavior of the TE_{01} mode compared to the HE_{11} mode. The comparison is important because it gives the power range in which the fiber can support only the HE_{11} mode and works as a single mode fiber. This type of fiber is commonly used in long distance communication and has low dispersion compared to multimode fiber.

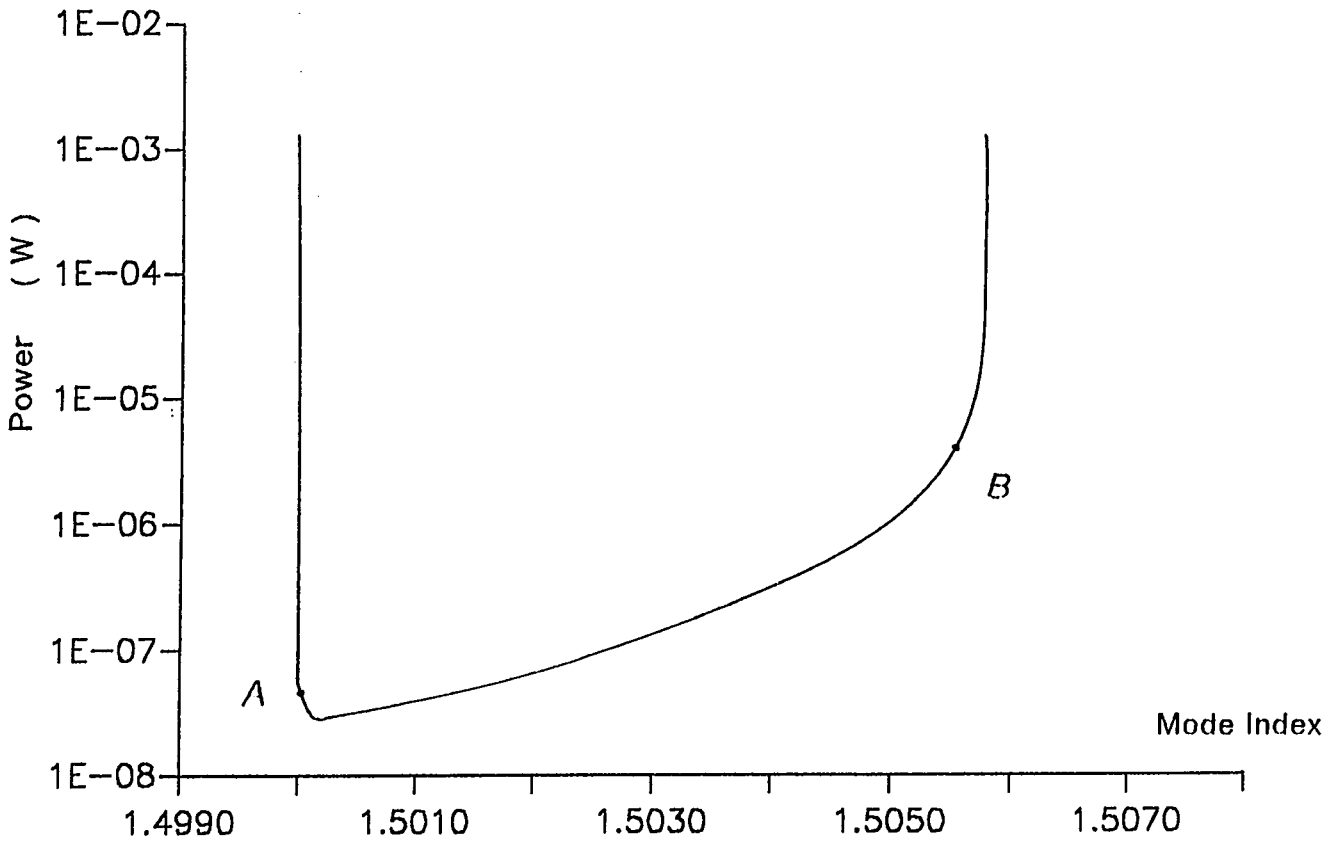

Fig.(6.5.a) Variation of n_e with the guided power for HE_{11} mode

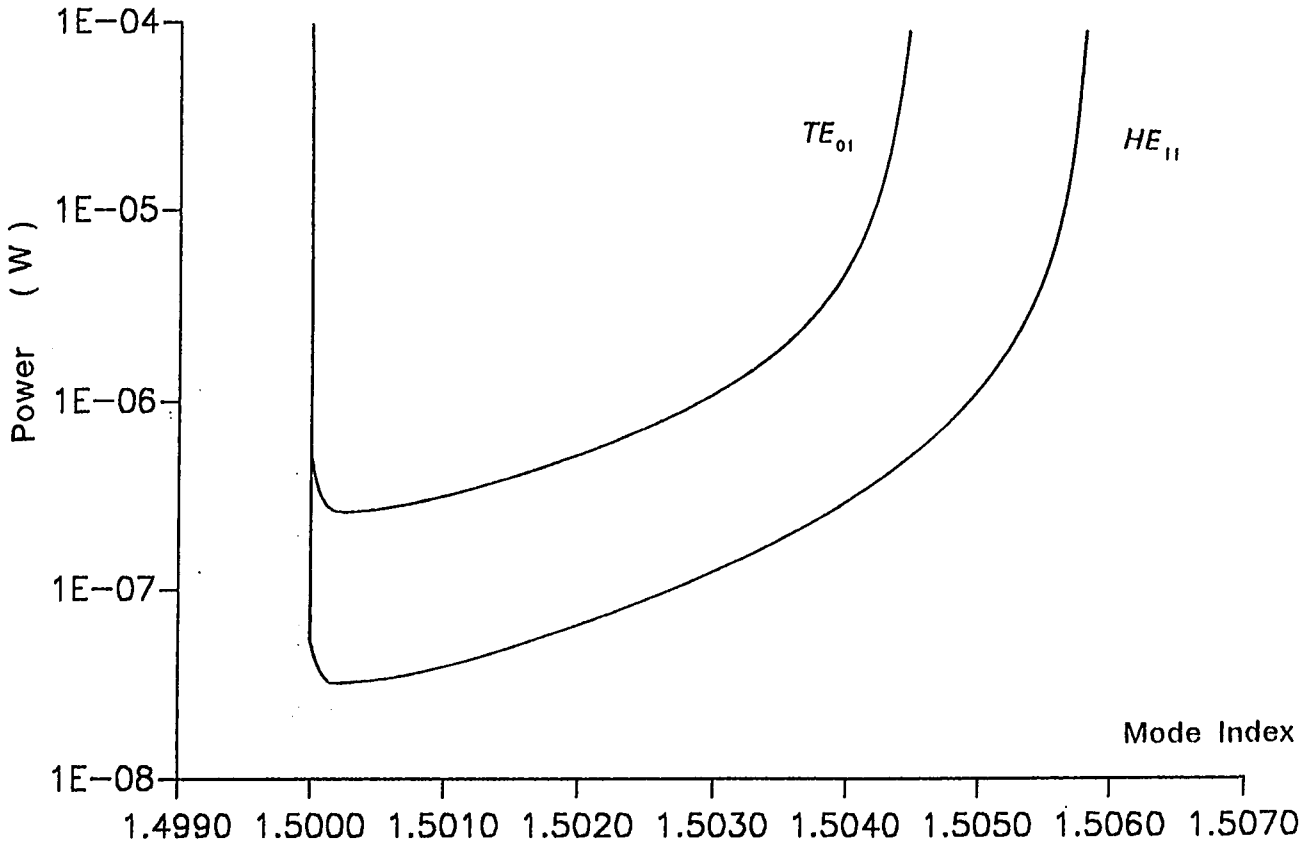

Fig.(6.5.b) Variation of n_e with the modal power for HE_{11} and TE_{01} modes

Two field distributions are shown in fig (6.6) corresponding to points A and B in fig.(6.5.a). The confinement of light increases with the mode index. This improves the performance of the waveguide since the light intensity is concentrated in the core. The dielectric constant distribution corresponding to the same two points is shown in fig.(6.7). For point B, the nonlinear optical fiber approaches saturation and the distribution is close to step-index profile. However, the profile corresponding to point A is similar to W-fiber.

6.3 OPTICAL FIBER WITH A LINEAR CORE AND A NONLINEAR CLADDING

The nonlinearity can affect this fiber structure in two ways: the first one is to modify the field profile according to the amount of input power. A considerable part of the propagated energy will be concentrated in the nonlinear cladding. The second effect of the nonlinearity is to support the higher order modes which are cutoff at low power levels. This case has been investigated in [8] for LP modes. The field profile nodes of the higher order modes are located in the nonlinear cladding which is in contrast with the linear case in which all the field nodes are in the core region. Another important feature which has been shown in [9] is the existence of surface modes when the value of the nonlinear cladding refractive index exceeds the linear core value. The peak of such modes is located at the core-cladding interface.

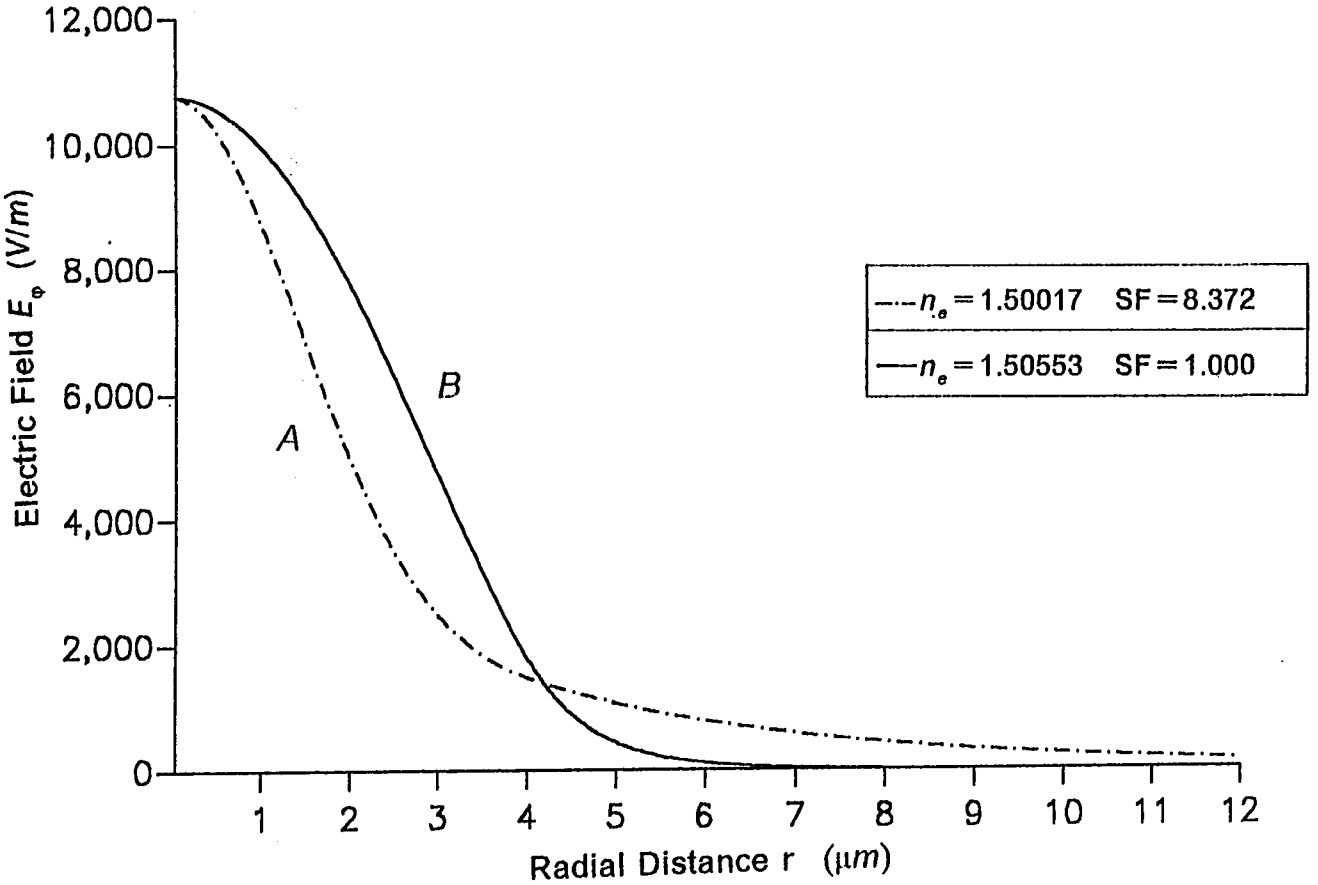

Fig.(6.6) Two field plots for HE_{11} corresponding to low and high power values

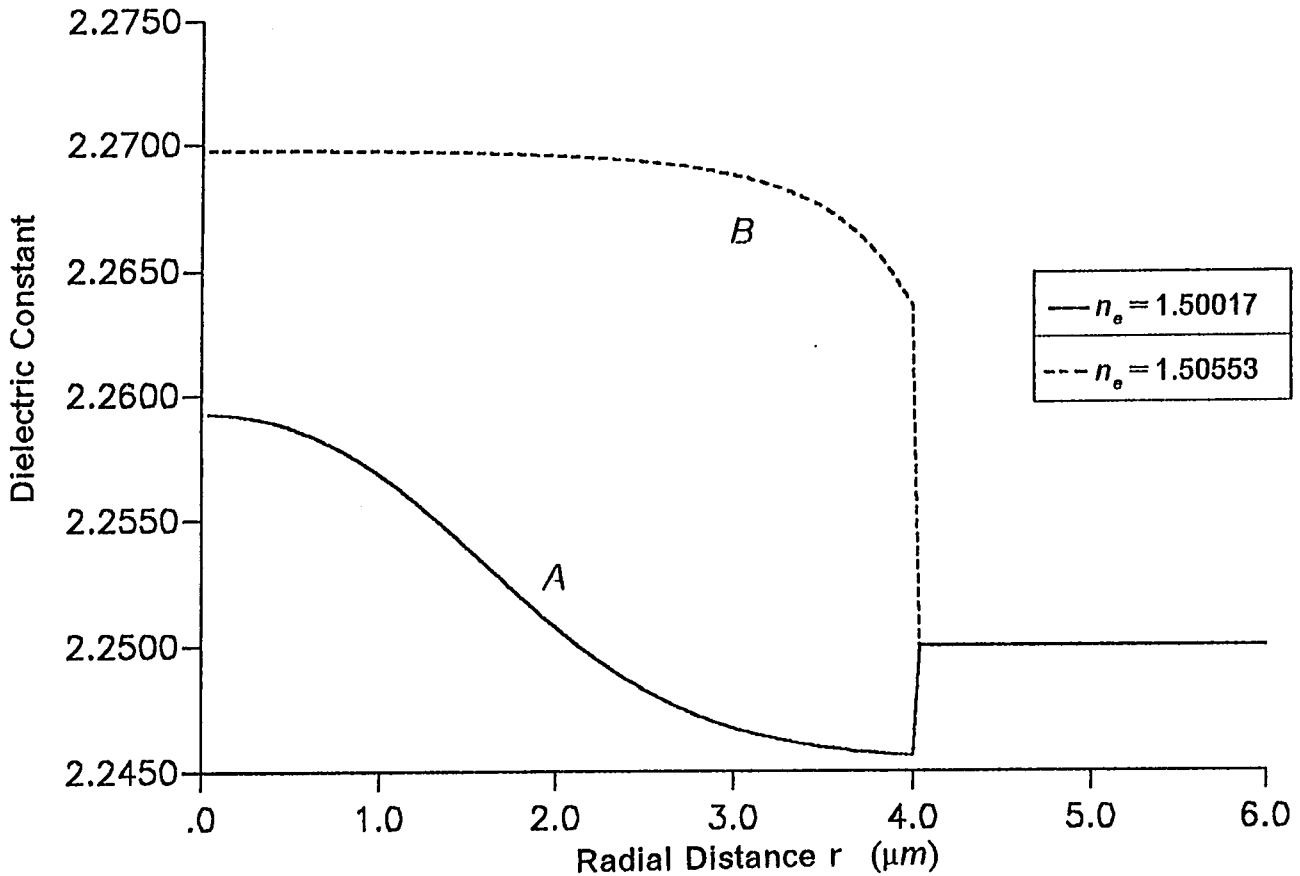

Fig.(6.7) The dielectric constant distribution for low and high power values

The first case to be treated here is the fiber which supports the HE_{11} mode regardless of the amount of power propagated. In this case the nonlinearity changes the features of the field. The saturation level is taken such that the saturable cladding refractive index is less than linear core refractive index. The parameters chosen are the same as those used for the TE case in section 5.3. The dispersion curve is shown in fig.(6.8). The surface intensity is plotted versus n_e. It is similar to those of TE and TM waves shown in figs.(5.10) and (5.19) respectively. The waveguide behaves as linear waveguide for low and high intensity. The effect of nonlinearity is clear for moderate values of intensity, where the mode index increases with the interface intensity Figure (6.9) shows two fields profiles corresponding to two different points A and B. As the nonlinearity increases the field becomes less confined in the core region. In this case a considerable amount of the propagated energy is located in the cladding region. The dielectric constant distributions for point A and B are given in fig.(6.10). The index profile is similar to the corresponding TE and TM cases. It must be noted that the dispersion relation in fig.(6.9) can also be expressed as a plot of modal power versus mode index. This plot is shown in fig.(6.11). The mode index is independent of power for low and high power values and increases with power for moderate power values.

The second case under consideration is the fiber which supports the HE_{11}

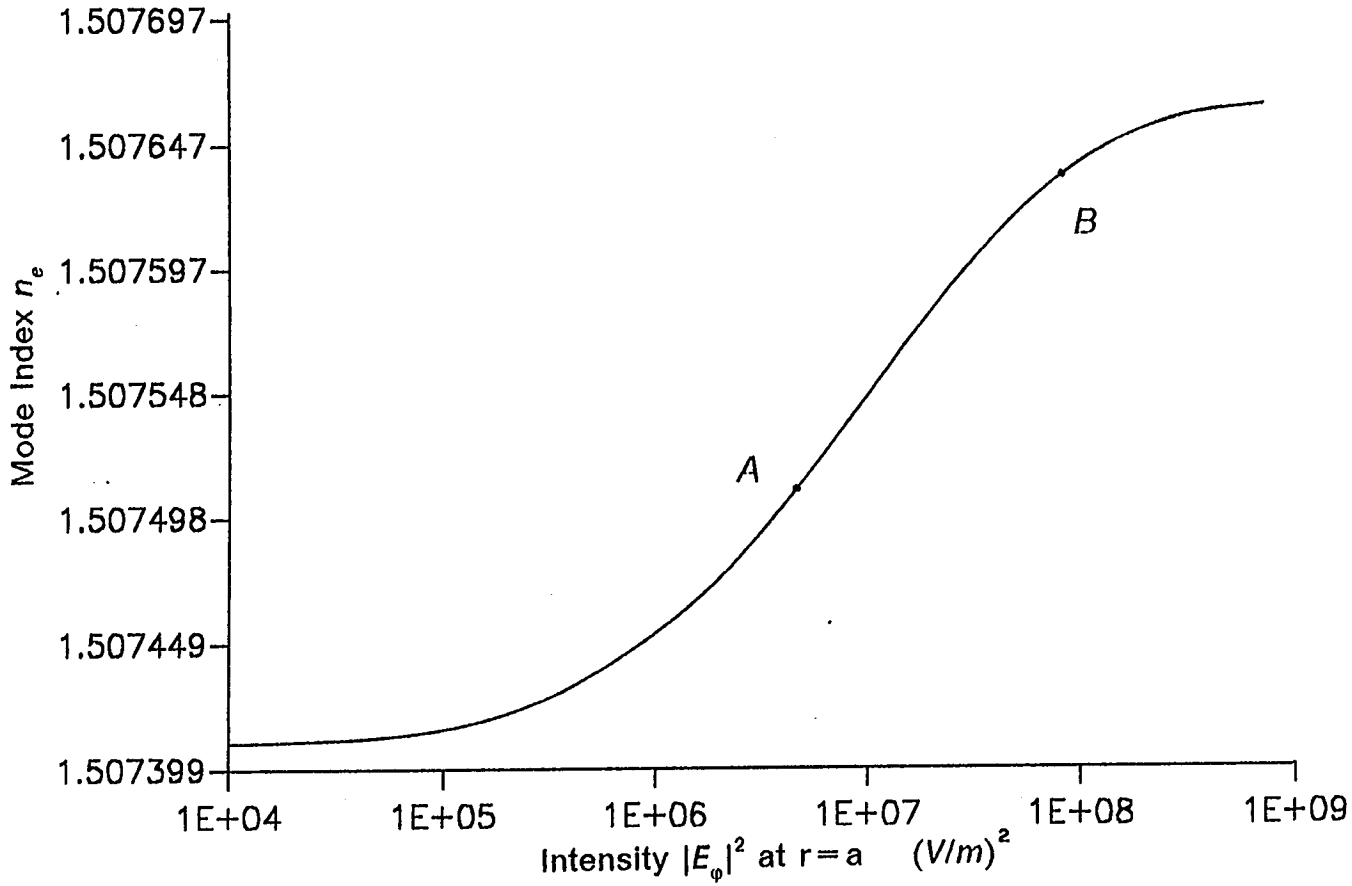

Fig.(6.8) Variation of n_e with the interface intensity for HE_{11} mode in a waveguide having linear core and nonlinear cladding

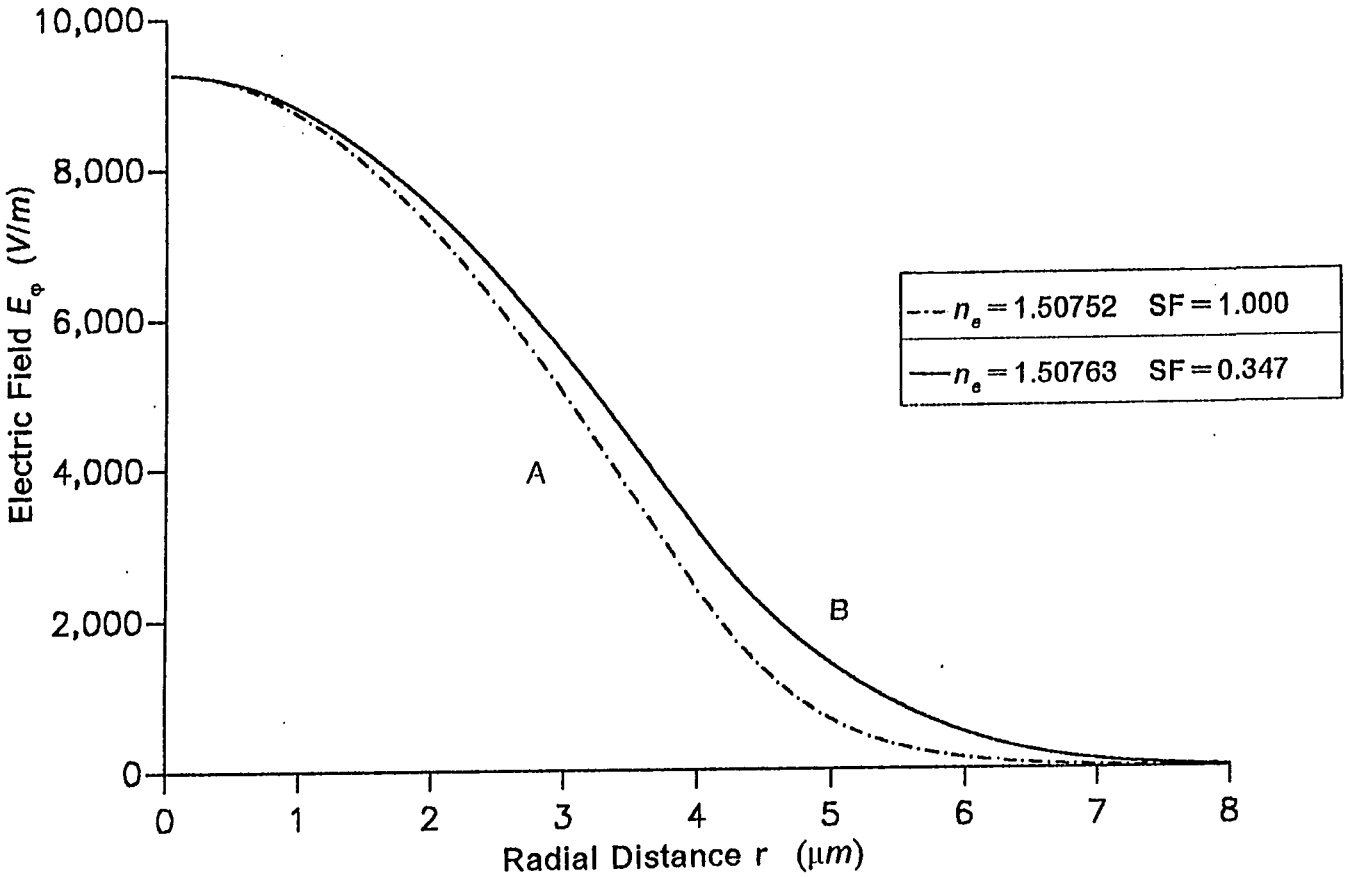

Fig.(6.9) Two field plots corresponding to two values of n_e taken from fig.(6.8)

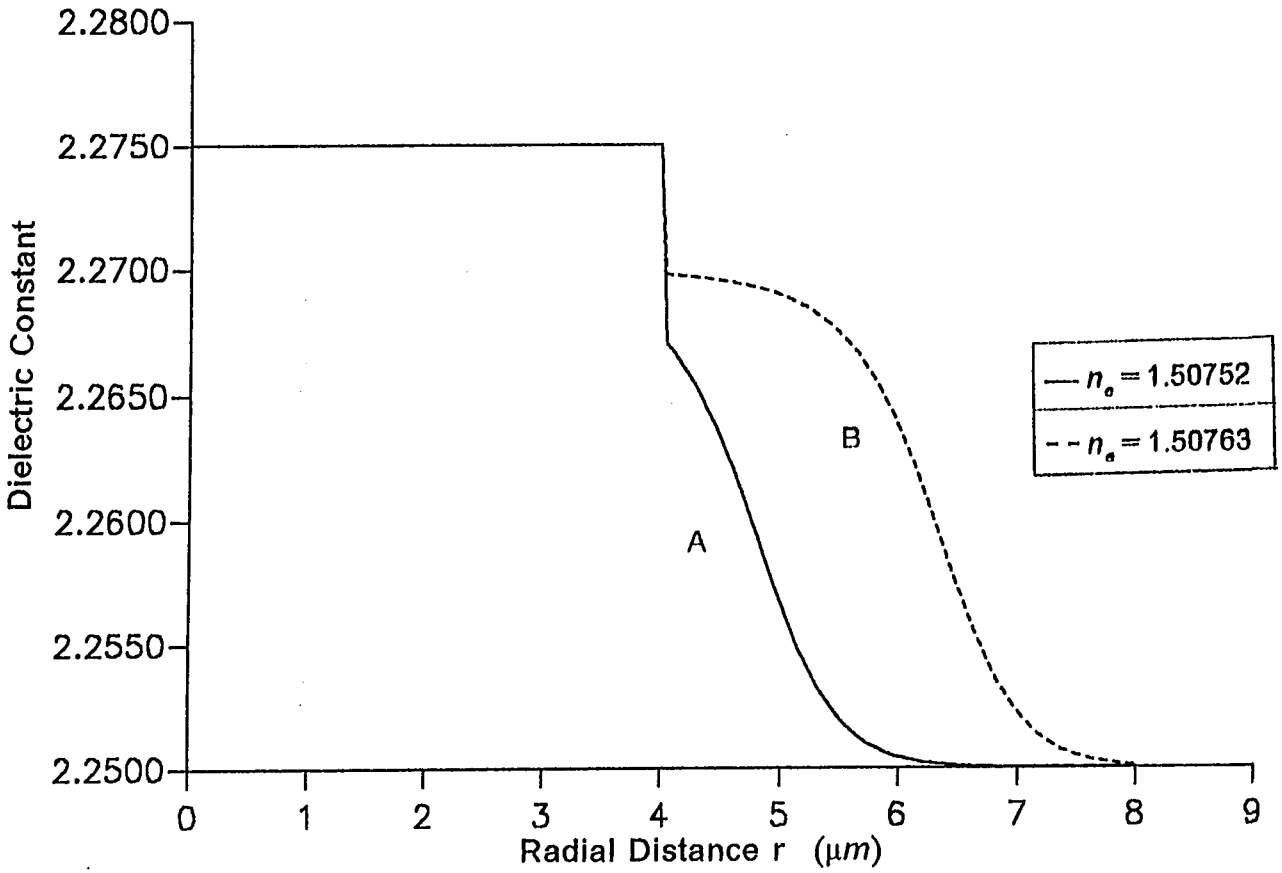

Fig.(6.10) Variation of the dielectric constant with the radial distance for the values of n_e taken from fig.(6.8)

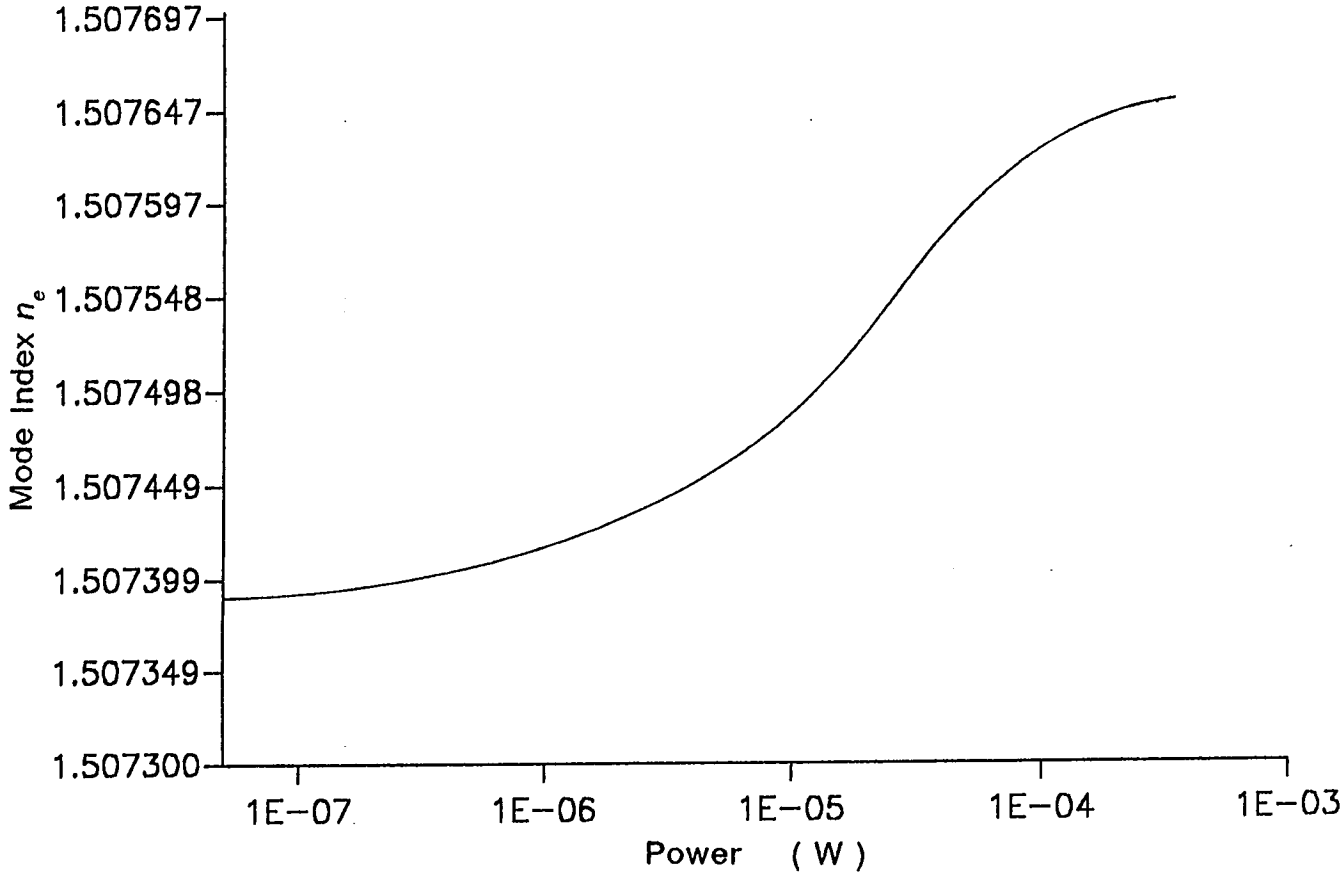

Fig.(6.11) Variation of n_e with the total power for HE_{11} mode in a waveguide having linear core and nonlinear cladding

mode at low power and its saturation limit is such that $\varepsilon_{bg}+\Delta\varepsilon_{NLmax}=\varepsilon_1$. The fiber parameters used are identical to those mentioned in section 5.3. The dispersion characteristic is shown in fig.(6.12) as a power-mode index relationship. The mode index increases with power until it reaches its saturation value. Any further increase in power will not cause an increase in the mode index. The field profiles corresponding to three points (A, B and C) on the dispersion curve are plotted in fig.(6.13). The penetration of the field in the nonlinear cladding can be seen clearly. A considerable part of the propagated power is concentrated in the cladding region. The dielectric function distributions for the same three points A, B and C are given in fig.(6.14). Point C represents the fiber approaching saturation. The physical radius of the fiber increases when the waveguide approaches saturation. The profile in this case resemble a step-index profile, However, the physical radius of the fiber in this case is several times the actual core radius ($4\ \mu m$) . This enables the fiber to support a large number of higher order modes.

6.4 VERIFYING THE RESULTS USING THE SELF-CONSISTENT SCHEME

The results obtained form the recursive scheme have been checked against the self consistent scheme and tabulated in table 6.2. The recursive scheme is applied the same way explained in section 5.6. The agreement between the schemes can be seen clearly from table 6.2. There is a very

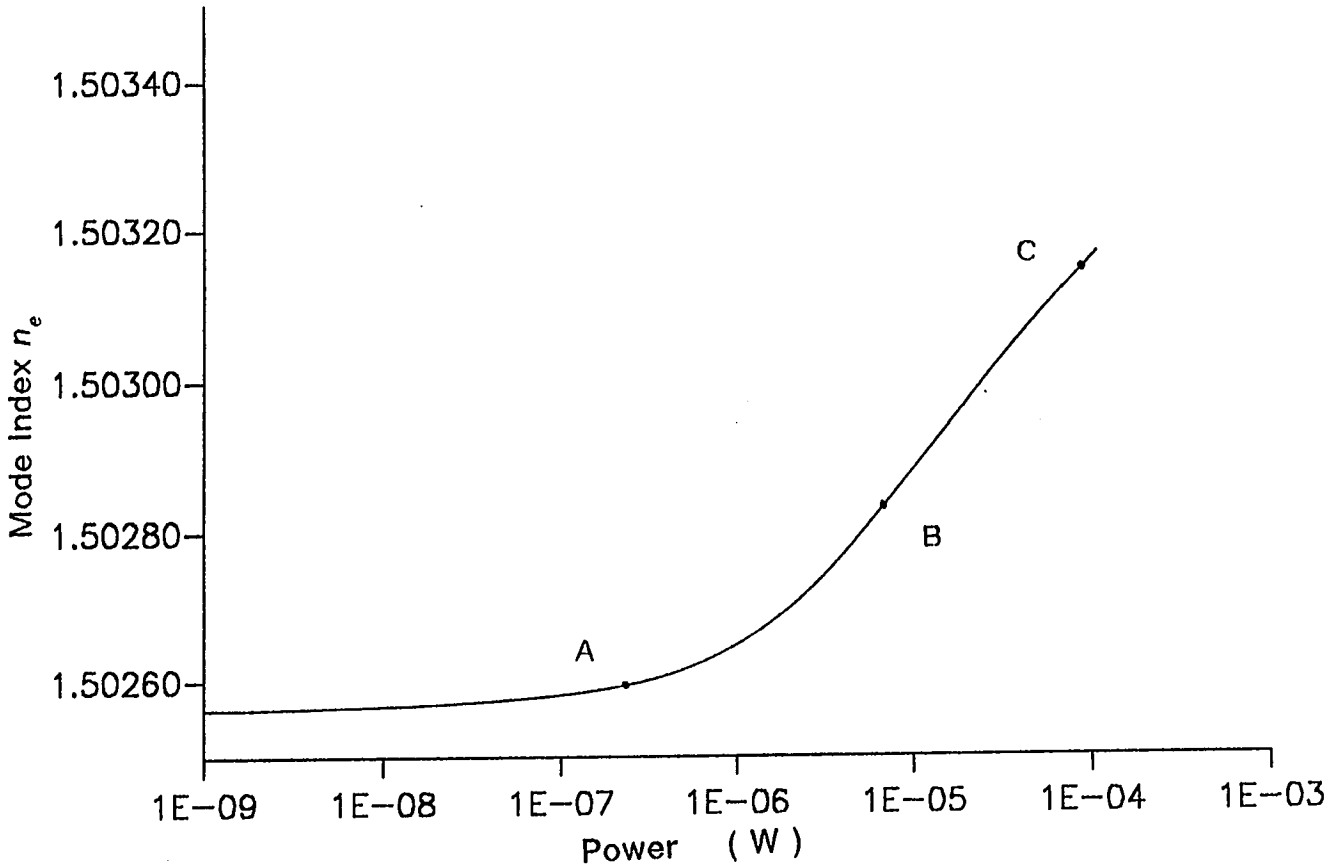

Fig.(6.12) Variation of n_e with the total power for HE_{11} mode

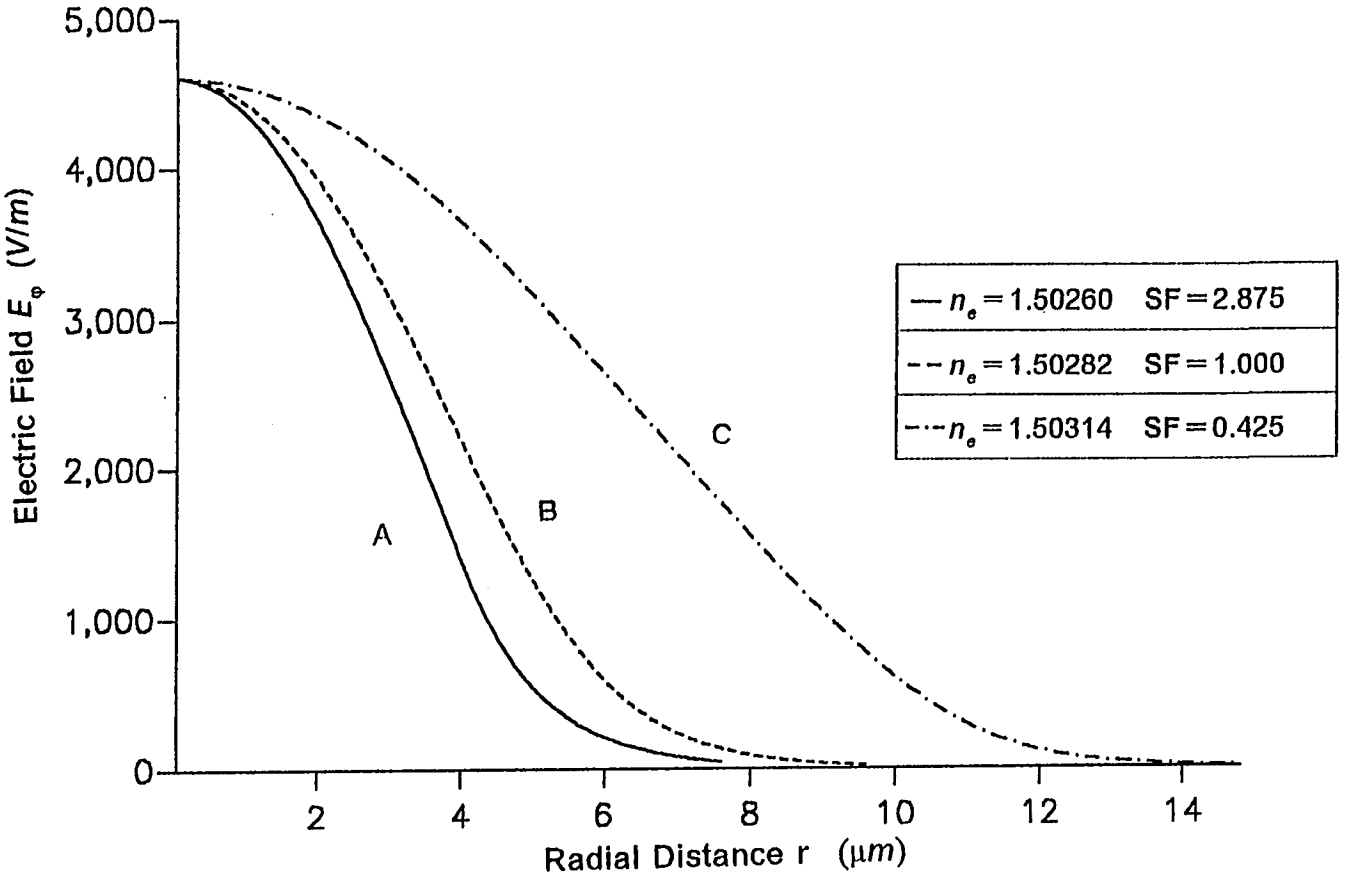

Fig.(6.13) Three field plots corresponding to three values of n_e taken from fig.(6.12)

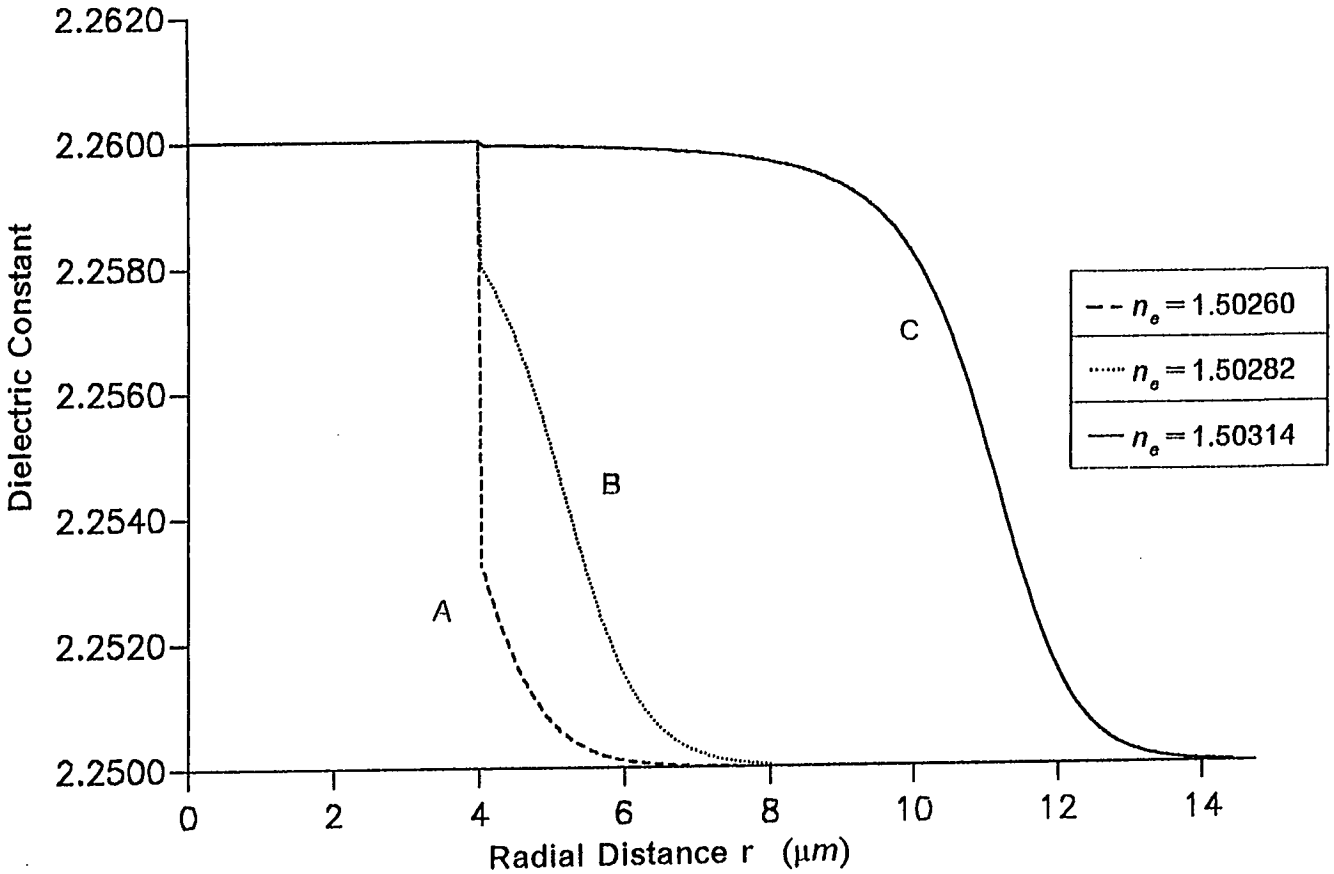

Fig.(6.14) Variation of the dielectric constant with the radial distance for three values of n_e taken from fig.(6.12)

TABLE 6.2

The effective indices of the fundamental HE mode obtained from the recursive solution and the self-consistent scheme.

Structure	Figure	Method	n_e	$A_{E_z}(0)$	$\|E_s\|^2$
$NL_{co}-L_{cl}$	(6.2)	recursive	1.501297	10	15810
$NL_{co}-L_{cl}$		self-cons.	1.501297	10	158101
$NL_{co}-L_{cl}$	(6.2)	recursive	1.503384	100	7489
$NL_{co}-L_{cl}$		self-cons.	1.503384	100	7489
$NL_{co}-L_{cl}$	(6.2)	recursive	1.516834	800	4445478
$NL_{co}-L_{cl}$		self-cons.	1.516834	800	4445478
$L_{co}-NL_{cl}$	(6.8)	recursive	1.507425	100	640137
$L_{co}-NL_{cl}$		self-cons.	1.507425	100	640137
$L_{co}-NL_{cl}$	(6.8)	recursive	1.507562	400	2.7(7)
$L_{co}-NL_{cl}$		self-cons.	1.507562	400	2.7(7)
$L_{co}-NL_{cl}$	(6.8)	recursive	1.507633	800	1.674(7)
$L_{co}-NL_{cl}$		self-cons.	1.507633	800	1.674(7)

good agreement between the two results. It must be noted that the amplitude of the electric field $A_{E_z}(0)$ is required to start the recursive scheme which produces the corresponding eigenvalue and eigen field. However, this amplitude is arbitrary in the self-consistent scheme because the problem is linear and the solution does not depend on the input filed amplitude.

To show the effect of nonlinearity on the guided field, a comparison between linear and nonlinear waveguides has been made. the nonlinear fiber is identical to the one studied in the above section. The linear fiber has the same parameters with the nonlinear coefficient α equal to zero. The recursive computer program has been ran two times, the first one for nonlinear fiber with input $A_{E_z}(0) = 170 v/m$. The second run is made for the linear fiber with the input unchanged. The resultant field profiles are shown in fig.(6.15). Because the linear mode index is much less than the nonlinear one, the field amplitude of the linear guide is less than that of the nonlinear guide. However the linear field is more confined in the core region. Also the power propagated in the linear guide is less than that of the nonlinear guide although they have the same input $A_{E_z}(0)$.

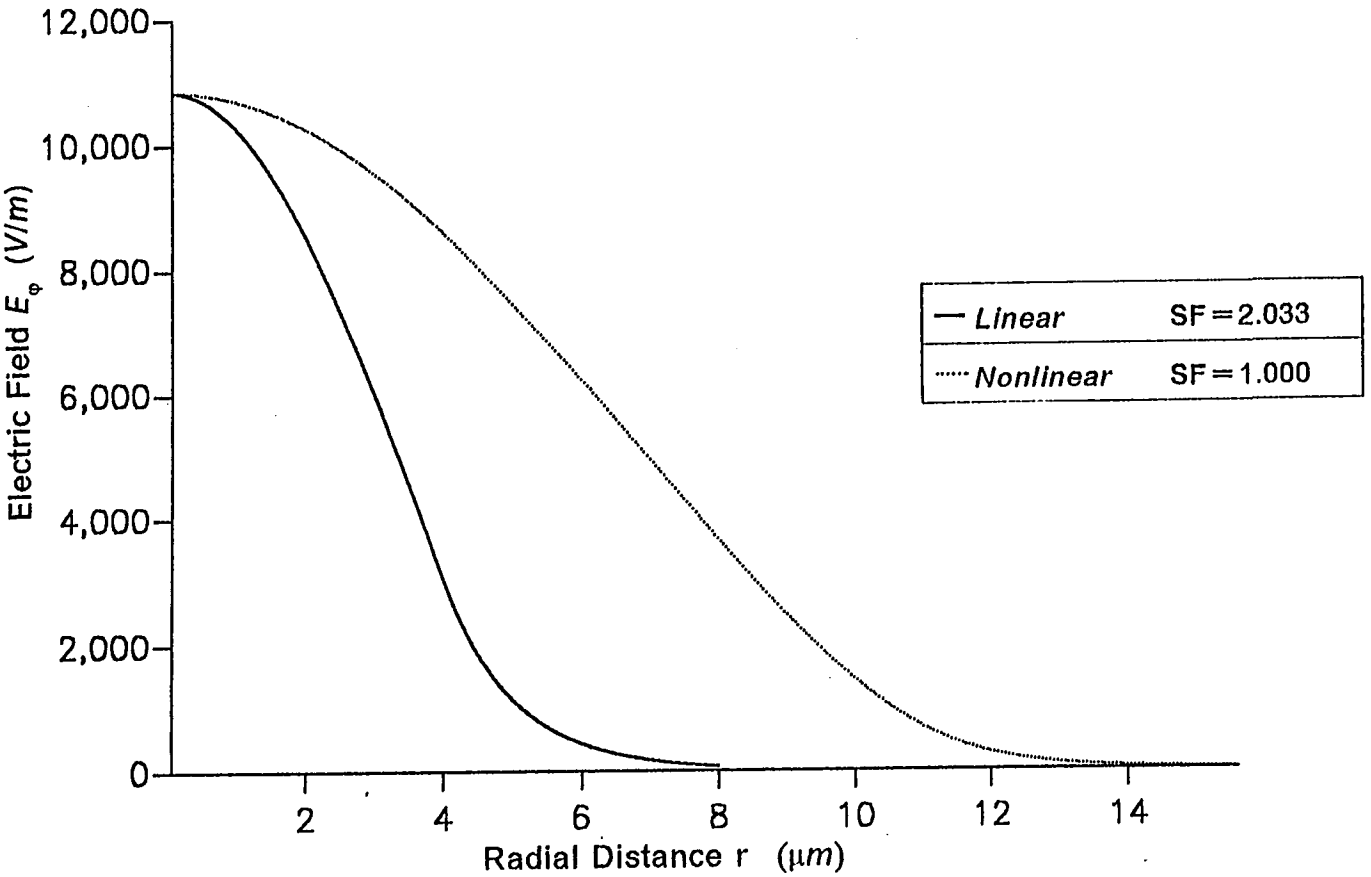

Fig.(6.15) Comparison between two field plots of linear and nonlinear waveguides having the same axial field amplitude $A_{E_z}(0)$ at r = 0

CHAPTER 7

CONCLUSIONS AND FUTURE WORK

CONCLUSIONS

The checking of the multilayer scheme against the closed form eigenvalue equation shows a complete consistency between the eigenvalues obtained from the two methods. The multilayer scheme reduces indirectly to the same eigenvalue equation in the case of linear fiber. For a fiber consisting of more than three layers, the use of the recursive scheme is essential to obtain the eigenvalues. The utilization of complex Bessel function is preferable to overcome the problems arise when the argument of Bessel function changes from real to imaginary or vice versa. Also it has another advantage in treating the problems involving metallic layer or lossy dielectric.

The metal-clad optical fiber studied in chapter 4 exhibits some important features. For the two-layer fiber consisting of a dielectric core and a metal-clad, The hybrid mode HE_{11} is the fundamental mode. However it has a finite cutoff frequency different from zero which is the case of the dielectric-clad. For the TE_{01} and TM_{01} the cutoff frequencies are shifted towards the low

frequency region compared to the dielectric-clad fiber. The attenuation of the TM_{01} is greater than that of the TE_{01} by about an order of magnitude. The attenuation of the hybrid mode HE_{11} is located between the two and slightly close to that of the TM_{01}. In general the attenuation is a decreasing function of the core radius. The four-layer structures involving a thin dielectric buffer layer between the dielectric-clad and the metallic jacket have some important attenuation characteristics. In the case of low-index buffer, The TM modes exhibit an absorption peak located at some critical buffer thickness. However the attenuation of the TE modes is a decreasing function of the buffer thickness. In general the highest order modes are attenuated more than the lowest order modes. In the case of high-index buffer, the attenuation of both TE and TM modes has an oscillating behavior function of the buffer thickness. The absorption peaks are well separated which facilitate the design of a good fiber polarizer with high extinction ratio.

The dispersion relations of nonlinear optical fiber are similar for TE_{01}, TM_{01} and HE_{11}. The following discussion is valid for any one of these modes unless mentioned otherwise. The dispersion relation is obtained as a plot of the mode index versus the surface intensity measured at the core-cladding interface. For a fiber with nonlinear core and linear cladding, the shape of the dispersion curve depends on the initial state of the fiber (at zero applied intensity). If the fiber is initially guiding, the dispersion curve will be similar

to that shown in fig.(5.2). It exhibits a negative slope region for which a single value of surface intensity corresponds to three values of the mode index. If the fiber is initially cutoff the dispersion curve will be similar to fig.(5.7). The fiber in this case requires a threshold surface intensity to support guided modes. The switching action in this case can be used in the design of logic gates and limiters. In both cases of guiding and cutoff fiber the nonlinearity will cause the field to be more confined in the core region. It must be noted that the distribution of the dielectric constant over the core region is not the same for the three modes under consideration. For the HE_{11} mode, it has a maximum value at the center and decreases gradually with distance. This gives in general a graded index distribution as shown in fig.(6.3). However for the TE_{01} and TM_{01} modes, the maximum value of the dielectric constant is located between the center of the fiber and the surface of the core. The general distribution is shown in fig.(5.4). The field profiles of the HE_{11} mode forms a spot of light which has a maximum value at the center and decreases with the radial distance. However for both TE_{01} and TM_{01} the field profile resembles a ring of light which has a zero intensity at the origin and a maximum value inside the core.

The other important waveguide structure is a fiber with linear core and nonlinear cladding . For this fiber, the dispersion relation is monotonic. The mode index increases with the surface intensity. This will cause the

peak of both TE_{01} and TM_{01} to move towards the nonlinear cladding. If the induced dielectric constant of the nonlinear cladding is less than the core value, the peak of the field will remain inside the core region. However if $\varepsilon_{NL} > \varepsilon_{co}$, the peak of the field will cross the core cladding interface and position in the cladding region. The nonlinear field in this case is different from its linear counterpart. Although they have the same field profiles, the nonlinear field is mainly guided by the nonlinear cladding and its peak is located in the cladding region. This reduces the effect of the linear core on the guidance process. It also causes most of the field energy to concentrate in the nonlinear cladding. For the HE_{11}, the peak of the field remains at the origin. However the confinement of the field inside the core region decreases as the intensity increases.

The nonlinear fiber models used throughout the thesis can be tested experimentally. The value of nonlinear coefficient α used in the numerical examples is larger than the practical values of the nonlinear materials (table 2.1). However, this can be compensated through the term $\alpha|E|^2$. The important observation is that the total power required is limited and can be delivered by practical laser sources.

FUTURE WORK

The recursive scheme developed in this thesis is applicable to graded-

index as well as nonlinear fiber. This solves a large number of fiber problems in which the core or the cladding can be taken nonlinear, linear or graded-index. A combination of nonlinearity and inhomogeinity can also be treated with the same algorithm after making the necessary modification in the array containing the dielectric constant.

Another class of important problems is the one in which the metal is used as a cladding or an outer jacket, with the core considered nonlinear. In this thesis different linear structures have been covered including two, three and four layers cylindrical waveguide. The future investigation should replace one of the dielectric layers by a nonlinear materials and study the effect of nonlinearity on the attenuation characteristics of metal-clad optical fiber.

This thesis covers mainly the first three lowest order modes HE_{11}, TE_{01} and TM_{01}. Although the higher order TE modes have been investigated in some cases, the work should be extended to cover highest order modes. In the nonlinear optical fiber, light intensity will control the number of modes supported by the fiber.

The nonlinear materials used in this thesis are characterized by a self-focusing effect, in which the nonlinear coefficient is positive. This gives rise to the dielectric constant as the intensity increases. The same computer programs can be used to treat materials featuring a self-defocusing effect. It

is of interest to study a fiber in which the core material is self-focusing and the cladding material is self-defocusing. A fiber with this configuration is expected to have field profiles which are very well confined in the core region.

REFERENCES

1) S. J. Al-Bader and H. A. Jamid, "Guided Waves in Nonlinear Saturable Self-Focusing Thin Films", IEEE J. Quant. Elect., Vol. 23, No. 11, pp. 1948-1955, 1987.

2) S. J. Al-Bader, "TM Waves in Nonlinear Saturable Thin Film: A Multilayer Approach", IEEE J. Light Wave Technology, Vol. 7, No. 4, pp. 717-725, April 1989.

3) A. A. Maradudin, " Nonlinear Surface Electromagnetic Waves" in Optical and Acoustic Waves in Solids - Modern Topics, M. porisov, Ed. Singapore World Scientific Publ., P. 72, 1983.

4) Sang-Yang Shin, E. M. Wright and G. I. Stegeman, "Nonlinear TE Waves in Coupled Waveguides Bounded by Nonlinear Media", IEEE J. Light Wave Technology Vol. 8, No. 6 PP. 977-983, June 1989.

5) R. Y. Chiao, E. Garmire and C. H. Townes, "Self Trapping of Optical Beams", Phys. Rev. Lett., Vol. 13, No. 15, PP. 479-482, (1964).

6) H. A. Haus, "Higher Order Trapped Light Beam Solutions", Applied Physics Letters, Vol. 8, No. 5, PP. 128-129, Mar. 1966.

7) Katsunar Okamoto and A. J. Marcatile, "Chromatic Dispersion Characteristics of Fibers with Optical Kerr-Effect Nonlinearity", IEEE J. Light Wave Technology Vol. 7, No. 12, PP. 1988-1994, Dec. 1989.

8) Govind P. Agrawal, "Nonlinear Fiber Optics", Academic Press, Inc., 1989.

9) A. D. Boardman, G. S. Cooper and R. D. Robbins, "Novel Nonlinear Waves in Optical Fibers", Optics Letters, Vol. 11, No. 2, pp. 112-114, 1986.

10) V. I. Korneev, N. N. Akhmediev and T. D. Shermergor, "Normal Modes of a Cylindrical Waveguide in a Medium with Nonlinear Dielectric Constant", Radiofizika, Vol. 27, No. 12, pp. 1525-1529, 1984.

11) N. N. Akhmediev, R. F. Nabiev and Y. M. Popov, "Angel Dependent Nonlinear Modes of Cylindrical Waveguides", J. Opt. Soc. Am. B., Vol. 7, No. 6, PP. 975-980, June 1990.

12) "Material for Nonlinear Optics - Chemical Perspectives" Edited by S. R.

Marder, J. E. Sohn and G. D. Stacky, ACS Symposium Series 455, 1991.

13) "Nonlinear Optical Properties of Organic and Polymeric Materials" Edited by David J. Williams, ACS Symposium Series 233, 1983. ACS Symposium Series 455, 1991.

14) Y. R. Shen, "The Principles of Nonlinear Optics", John Wiley and Sons. Inc., 1984.

15) Unger, H. G., "Planar Optical Waveguides and Fibers", Oxford, New York, Galrendon Press, 1972.

16) M. J. Adams, "An Introduction to Optical Waveguides", Chechester, England, Wieley, 1981.

17) A. W. Snyder and J. D. Love, "Optical Waveguide Theory", Chapman and Hall, England, 1983.

18) Jin Au kong, "Electromagnetic Wave Theory", John Wiley and Sons. Inc., 1986.

19) M. Abramowitz and I. Stegun, "Handbook of Mathematical Functions", Dover, New York, 1965.

20) G. N. Watson, "A Treatise of the Theory of Bessel Functions", Cambridge, England, 1966.

21) D. E. Muller, "A Method for Solving Algebraic Equations Using an Automatic Computer", MTAC, Vol. 10, pp. 208-215, 1956.

22) C. Yeh and G. Lindgren, "Computing the Propagation Characteristics of Radially Stratified Fibers: an Efficient Method", Applied Optics, Vol. 16 No. 2, PP. 483-493, Feb. 1977

23) Fedrico Dios, Luis Torner and Fernando Canal, "Self consistent solution for general nonlinear slab waveguides"Optics Communications, Vol. 72, No. 1/2, JUL. 1989.

24) T. A. Batchman and K. A. McMillan, "Measurement on Positive-Permittivity Metal-Clad Waveguides", IEEE J. of Quant. Elect., Vol. 13, No. 4, PP. 187-192, April 1977.

25) Y. Yamamoto, T. Kmiya and H. Yanai, "Characteristics of Optical Guided Modes in Multilayer Metal-Clad Planar Optical Guide with Low-Index

Dielectric Buffer Layer", IEEE J: of Quant. Elect., Vol. 11, No. 9, PP. 729-736, Sep. 1975.

26) H. A. Jamid and S. J. Al-Bader, "TM-Pass Polariser Using Metal-Clad Waveguide with High-Index Buffer Layer", Elect. Lett., Vol. 24, No. 4, PP. 229-230, Feb. 1988.

27) Norio Kashima and Naoya Uchida, "Excess Loss Caused by a Lossy Outer Layer in Multimode Step-Index Fibers", Applied Optics, Vol. 16, No. 4, PP. 1038-1040, April 1977.

28) Ronald Roberts, "Attenuation Characteristics of Multimode Optical Fiber with Lossy Cladding and Lossy Jacket", Elect. Lett., Vol. 11, No. 22, PP. 529-530, Oct. 1975.

29) Norio Kashima and Naoya Uchida, "Transmission Characteristics of Graded-Index Optical Fibers with a Lossy Outer Layer", Applied Optics, Vol. 17, No. 8, PP. 1199-1207, April 1978.

30) A. H. Cherin and E. J Murphy, "An Analysis of the Effect of Lossy Coatings on the Transmission Energy in a Multimode Optical Fiber", The Bell System Technical Journal, PP. 1531-1546, Nov. 1975.

31) Toshihito Hosaka, K. Okamoto and J. Noda, "Single Mode Fiber Type Polarizer", IEEE J. of Quant. Elect. Vol. 18, No. 10, PP 1569-1572, Oct. 1982.

32) Yu Tong and Wu Yizun, " Theoretical Study of Metal-Clad Optical Waveguide Polarizer", IEEE J. of Quant. Elect., Vol. 25, No. 6, PP. 1209-1213, June 1989.

33) V. R. Blok and P. Gorbulsky, "Dispersion Characteristics of Cylindrical Metal-Clad Optical Waveguides", IEEE J. of Quant. Elect., Vol. 25, No. 8, PP. 1763-1766, Aug. 1989.

34) Charles Y.H. Taso, David N. Payne and Luksun Li, "Modal Propagation Characteristics of Radially Stratified and D-Shaped Optical Fibers", Applied Optics, Vol. 28, No. 3, PP. 588-594, Feb. 1989.

35) J. Hamasaki and K. Nosu, "A Partially Metal-Clad-Dielectric-Slab Waveguide for Integrated Optics", IEEE J. of Quant. Elect. Vol., 10 No. 10, PP. 822-825, Oct. 1974.

36) S. C. Lee and Jen-i Chen, "New Metal-Clad Fiber Polarizer", Applied Optics, Vol. 29, No. 18, PP. 2667-2668, June 1990.

37) W. Eickhoff, "In-Line Fiber-Optic Polarizer", Elect. Lett., Vol. 16, No. 20, PP. 762-763, Sep. 1980.

38) W. Johnstone, G. Stewart, B. Culshaw and T. Hart, "Fiber-Optic Polarisers and Polarising Couplers", Elect. Lett., Vol. 24, No. 14, PP. 866-868, Sep. 1988.

39) J. R. Feth and C. L. Chang, "Metal-Clad Fiber-Optic Cutoff Polarizer", Opt. Lett., Vol. 11, No. 6, PP. 386-388, June 1986.

40) M. N. Zervas and I. P. Giles, "Performance of Surface-Plasma-Wave Fiber-Optic Polarizers", Opt. Lett., Vol. 15, No. 9, PP. 313-315, May 1990.

41) S. Carey and W. Johnstone, "Characteristics of Surface Plasmon Wave Polarising Devices", Elect. Lett., Vol. 27, No. 11, PP. 988-990, May 1991.

42) W. Johnstone, G. Stewart, T. Hart and B. Culshaw, "Surface Plasmon Polaritons in Thin Metal Films and Their Role in Fiber Optic Polarising Devices", IEEE J. Light Wave Technology, Vol. 8, No. 4, PP. 538-543, April 1990.

43) R. Willsch, "High Performance Metal-Clad Fiber-Optic Polarizers", Elect. lett., Vol. 26, No. 15, PP. 1113-1115, July 1990.

44) F. A. Burton and T. K. White, "Fabrication and Assessment of a D-Fiber Polarization Spletter", Elect. lett., Vol. 27, No. 8, PP. 657-659, April 1991.

45) R. B. Dyott, J. Bello and V. A. Handerek, "Indium-Coated D-Shaped-Fiber Polariser", Opt. Lett., Vol. 12, No. 4, PP. 287-289, April 1987.

46) A. W. Snyder, D. J. Mitchell, L. Poladian, D. R. Rowland and V. Chen, "Physics of Nonlinear Coupler" J. Opt. Soc. A., Vol. 8, No. 10, PP. 2102-2118, Jan. 1991.

47) U. Trutschel, F. Lederer and M. Gloz, "Nonlinear Guided Waves in Multilayer Systems", IEEE J. Quant. Elect., Vol. 25, No. 2, PP. 194-200, Feb. 1989.

48) W. Biehlig, F. lederer, U. Trutscel, U. Langbein, D. Mihalache and A. D. Boardman, "TM polarized nonlinear guided waves in multilayer systems", IEEE J. of Quant. Elect., Vol. 27, No. 2, PP. 238-242, Feb. 1991.

49) D. Marcuse, "Light Transmission Optics", Van Nostrand Reinhold Company, 1982.

50) Jamid, H.A., "Absorption Loss in Graded-Index Metal-Clad Optical Waveguide", Ph.D. Dissertation, KFUPM, Dhahran, S.A., 1986.

51) J. Ctyroky and H.J. Henning, "Thin-Film Polariser for Ti:LiNbO3 Waveguides at $\lambda = 1.3\mu m$", Elect. Lett., Vol. 22, No. 14, PP. 756-758, July 1986.

52) Tadashi Takano and Joji Hamasaki, " Propagating Modes of a Metal-Clad-Dielectric-Slab Waveguide for Integrated Optics", IEEE J. Quant. Elect., Vol. 8, No. 2, PP. 206-212, Feb. 1972.

53) D.R. Hall, A. K. Gorton and R. M. Jenkins," $10-\mu m$ Propagation Losses in Hollow Dielectric Waveguides", J. of Applied Physics, Vol. 48, No. 3, PP. 1212-1216, March 1977.

54) W. A. Gambling and H. Matsumura, "Propagation of Radially-Inhomogeneous Single Mode Fiber", Optical and Quantum Electronics, Vol. 10, PP. 31-40, 1978.

55) T. Hidaka, T. Morikawa and J. Shimada, "Hollow-Core Oxide-Glass Cladding Optical Fibers for Middle Infrared Region", J. Appl. Phys., Vol. 52, No. 7, PP. 4467-4471, July 1981.

56) K. J. Blow and N. J. Doran, "Nonlinear Limits on Bandwidth at the Minimum Dispersion in Optical Fibers", Opt. Comm., Vol. 48, No. 3, PP. 181-184, Dec. 1893.

57) W. A. Gambling, H. Matsumura and C. H. Ragdale, "Wave Propagation in a Single-Mode Fiber with Dip in the Refractive Index", Optical and Quantum Electronics, Vol. 10, PP. 301-309, 1978.

58) K. J. Blow and N. J. Doran, " Nonlinear Effects in Optical Fibers and Fiber Devices", IEE proceeding, Vol. 134 Pt. J, No. 3, PP. 138-144, June 1987.

59) D. Gloge, "Weakly Guiding Fibers", Applied Optics, Vol. 10, No. 10, PP. 2252-2258, Oct. 1971.

60) G. I. Stegeman, E. M. Wright, N. Finlaysont, R. Zanoni and C. T. Seaton, "Third Order Nonlinear Integrated Optics", IEEE J. Light Wave Technology, Vol. 6, No. 6, pp. 953-970, June 1988.

61) K. MiKoshiba and H. Kajioka, " Transmission Characteristics of Multimode W-type Optical Fiber: Experimental Study of the Effect of Intermediate Layer", Applied Optics, Vol. 17 No. 17, PP. 1199-1206 Sep. 1978.

62) Stephen J. Grath and Colin Pask, "Polarization Rotation in Nonlinear Bimodal Optical Fibers", IEEE J. Light Wave Technology, Vol. 8, No. 2, pp. 129-137, June 1990.

63) C. T. Seaton, Xu Mai, G. I. Stegemen and H. G. Winful, "Nonlinear Guided Wave Applications", Optical Engineering, Vol. 24, No. 4, PP. 593-599, July/Aug. 1985

64) D. Mihalahe and Puo-Peng Wang, "Nonlinear Guided Waves in Multilayer System Bounded by Optically Nonlinear Media", J. Appl. Phys., Vol. 69, No. 4, PP. 1892-1900, Feb. 1991.

65) Wei Chen and A. A. Maradudin, "S-Polarized Guided and Surface Electromagnetic Waves Supported by a Nonlinear Dielectric Film", J. Opt. Soc. AM. B, Vol. 5, No. 2, PP. 529-538, Feb. 1988.

66) H. Khosravi, D. R. Tilley and R. Loudon, "Surface Polaritons in Cylindrical Optical Fibers", J. Opt. Soc. AM. B, Vol. 8, No. 1, PP. 112-122, Jan. 1991.

67) K. J. Blow, N. J. Doran, B. P. Nelson and David Wood, "Nonlinear Self-Guiding and Switching in All-Fiber Devices", IEEE J. of Quant. Elect., Vol. 23, No. 7, PP. 1108-1112, July 1987.

68) A. W. Snyder, D. J. Mitchell, L. Poladian, D. R. Rowland and Y. Chen, "Physics of Nonlinear Fiber Couplers", J. Opt. Soc. AM. B, Vol. 8, No. 10, PP. 2102-2118, Oct. 1991.

69) B. P. Nelson and David Wood, "Analyses of the Nonlinear Coaxial Coupler", IEEE J. of Quant. Elect., Vol. 24, No. 9, PP. 1915-1921, Sep. 1988.

70) A. A. Kolokolov, "Stability of the Dominant Mode of the Nonlinear Wave Equation in Cubic Medium", Translated from Zh. Prikl. Mekh. Tekh. Fiz., No. 3, pp. 152-155, May/June 1973.

71) E. Snitzer, "Cylindrical Dielectric Waveguide Modes", J. Opt. Soc. AM., Vol. 51, No. 5, PP. 491-498, May 1961.

72) David R. Rowland, "All Optical Devices Using Nonlinear Fiber Coupler", Journal of Lightwave Technology, Vol. 9, No. 9, pp. 1074-1082, 1991.

APPENDICES

```
C  THE FOLLOWING 3 PROGRAMS ARE USED TO OBTAIN THE RESULTS OF CHAPTER 4
C
C              ==========================
C                 PROGRAM 1 TEMC
C              ==========================
C
C  THIS PROGRAM SOLVES FOR THE COMPLEX MODE EFFECTIVE INDEX IN A 4 LAYER
C  CIRCULAR WAVEGUIDE STRUCTURE.  THE OUTER LAYER IS FORMED OF METAL
C  WITH COMPLEX PERMITTIVITY.   THE WAVEGUIDE PARAMETERS ARE DEFINED
C  AS FOLLOWS
C  R1=THE RADIUS OF THE INNERMOST LAYER
C  C= RATIO BETWEEN THE RADIUS OF THE SECOND LAYER TO THAT OF THE
C  INNERMOST LAYER.
C  DELR=THICKNESS OF THE BUFFER LAYER
C  REFSQ=THE SQUARE OF THE EFFECTIVE INDEX
C  EPSCO=DIELECTRIC CONSTANT OF THE INNERMOST LAYER
C  EPSCL=DIELECTRIC CONSTANT OF THE SECOND LAYER
C  EPSCL2=DIELECTRIC CONSTANT OF THE THIRD LAYER (THE BUFFER LAYER)
C  EPSCLO=DIELECTRIC CONSTANT OF THE OUTER METALLIC LAYER.
C  THE PROGRAM IS DEVELOPED TO WORK ON PC WITH M/S FORTRAN VER. 5.
C  THE SUBROUTINE FN IS USED FOR CALCULATING THE EIGENVALUE EQUATION
C  THE SUBROUTINE MULLER IS USED TO FIND THE EIGENVALUE.  IT IS CALLED
C  BY THE MAIN PROGRAM. AN INITIAL GUESS IS REQUIRED BY MULLER
C  TO FIND THE ROOT OF THE EIGENVALUE EQUATION.
C  THE FUNCTIONS BJN, BKN, BIN ARE COMPLEX BESSEL FUNCTION.  THESE
C  FUNCTION ARE CALLED BY THE SUBROUTINE FN.
C  THE SAME PROGRAM CAN BE USED TO SOLVE THE 3-LAYER STRUCTURE (DELR=0)
C  AND 2-LAYER STRUCTURE (C=1, DELR=0).
C  THE PROGRAM IS WRITTEN FOR TE MODES.
C  IT CAN ALSO BE USED TO PLOT THE FIELD PROFILE (EIGEN FUNCTION)
C  CORRESPONDING TO CERTAIN EIGENVALUE.
$DEBUG
$LARGE
      IMPLICIT REAL*8 (A-H,O-Z)
      COMPLEX*16 ZEROS(2),VALUE(2),NE
      EXTERNAL FN
      LOGICAL FNREAL
C     FNREAL=.FALSE.
      FNREAL=.TRUE.
C ENTER GUESS
      WRITE(*,*)'ENTER GUESS'
```

```
      READ(*,*)ZEROS(1)
      OPEN(UNIT=6,STATUS='OLD',FILE='OUT1')
C ENTER NUMBER OF ZEROS TO BE SEARCHED FOR.
      N=1
C ENTER THE NUMBER OF ZEROS PREVIOUSLY KNOWN
      NPREV=0
C ENTER THE MAXIMUM NUMBER OF FUNCTION EVALUATION FOR EACH ZERO.
      MAXIT=15
C ENTER THE MAXIMUM ERROR CONTROL PARAMETERS
      EP1=10.0D-30
      EP2=10.0D-40
      CALL MULLER (FN,FNREAL,ZEROS,N,NPREV,MAXIT,EP1,EP2)
      DO 312 I=1,N
      CALL FN(ZEROS(I),VALUE(I))
      WRITE(*,*)
      WRITE(*,*)ZEROS(I),VALUE(I)
      NE=CDSQRT(ZEROS(I))
      WRITE(*,*)NE
 312  CONTINUE
      STOP
      END
C =====================================
C  SUBROUTINE FN(REFSQ,FY)
C =====================================
      SUBROUTINE FN (REFSQ,FZ)
      IMPLICIT REAL*8 (A-H,O-Z)
      COMPLEX*16 B1(200),B2(200),ALPHA(200),ARG(200)
      COMPLEX*16 BJ01(200),BJ11(200),BJ02(200),BJ12(200)
      COMPLEX*16 EPHI(200),HZ(200),HR(200)
      COMPLEX*16 BY01(200),BY11(200),BY02(200),BY12(200)
      COMPLEX*16 EPS(200),COKSQ(200),REFSQ,BJN,BIN,BKN
      COMPLEX*16 EPSCL,BETASQ,BETA,BS2(3),BS1(3),BS3(3)
      COMPLEX*16 EPSCO,EPSCLO,H2,H3,H4,H5
      COMPLEX*16 FZ,X1,X2,X3,X4,BK1A,BK0A,G
      COMPLEX*16 T1,T2,Z1,Z2,Z3,Z8,Z9,F9
      DIMENSION DIS(200)
      PI=2.0D0*DASIN(1.0D0)
      R1=3.0D-6
      C=1.2D0
      K=200
      L=50
      WL=0.6328D-6
      C0=3.0D8
      U0=PI*4.0D-7
```

```
      DELR=0.220D-6
      G=DCMPLX(0.0D0,1.0D0)
      R2=C*R1+DELR
      EPSCL=DCMPLX(2.250D0,0.0D0)
C     EPSCL2=DCMPLX(1.69D0,0.0D0)
      EPSCL2=DCMPLX(2.89D0,0.0D0)
      EPSCO=DCMPLX(2.28010D0,0.0D0)
      EPSCLO=DCMPLX(-10.30D0,1.0D0)
C     EPSCLO=DCMPLX(-47.0D0,16.3D0)
      YY=L
      XX=R1/YY
      W=2.0D0*PI*(C0/WL)
      FSKSQ=((W/C0)**2.0D0)
      FSK=DSQRT(FSKSQ)
      BETASQ=REFSQ*FSKSQ
      BETA=CDSQRT(BETASQ)
      B1(1)=DCMPLX(0.1D0,0.0D0)
      B2(1)=DCMPLX(0.0D0,0.0D0)
      DO 55 I=1,50
      EPS(I)=EPSCO
 55   CONTINUE
      DO 65 I=51,60
      EPS(I)=EPSCL
 65   CONTINUE
      DO 75 I=1,60
      DIS(I)=XX+(I-1)*XX
 75   CONTINUE
      EPS(61)=EPSCL2
      DIS(61)=DIS(60)+DELR
      COKSQ(1)=FSKSQ*EPS(1)
      ALPHA(1)=COKSQ(1)-BETASQ
      ARG(1)=CDSQRT(ALPHA(1))
C     ================================================================
C     CALCULATIONS OF THE FIELDS FOR LAYERS BETWEEN 2 & K
      Z2=ARG(1)*DIS(1)
C     CALL DCBJNS(Z2,3,BS1)
      BS1(1)=BJN(0,Z2)
      BS1(2)=BJN(1,Z2)
      BJ01(1)=BS1(1)
      BJ11(1)=BS1(2)
      HZ(1)= B1(1)*BJ01(1)
      EPHI(1)=-(G*W*U0/ARG(1))*(B1(1)*BJ11(1))
      HR(1)=-(BETA/ARG(1))*(B1(1)*BJ11(1))
      WRITE(6,*)DIS(1),DIMAG(EPHI(1))
```

```
C ==========================================================
      DO 24 M=2,K
      COKSQ(M)=FSKSQ*EPS(M)
      ALPHA(M)=BETASQ-COKSQ(M)
      ARG(M)=CDSQRT(ALPHA(M))
      Z1=ARG(M)*DIS(M-1)
C  CALLING BESSEL FUNCTIONS I,K OF ORDERS 0,1
      BS2(1)=BIN(0,Z1)
      BS2(2)=BIN(1,Z1)
      H2=BKN(0,Z1)
      H3=BKN(1,Z1)
      BJ02(M)=BS2(1)
      BJ12(M)=BS2(2)
      BY02(M)=H2
      BY12(M)=H3
      T1=HZ(M-1)*BY12(M)-(ARG(M)/(G*W*U0))*BY02(M)*EPHI(M-1)
      T2=BJ12(M)*BY02(M)+BJ02(M)*BY12(M)
      B1(M)=T1/T2
      B2(M)=(HZ(M-1)-B1(M)*BJ02(M))/BY02(M)
      Z3=ARG(M)*DIS(M)
C     CALLING BESSEL FUNCTION I OF ORDER 0 AND 1
      BS3(1)=BIN(0,Z3)
      BS3(2)=BIN(1,Z3)
      H4=BKN(0,Z3)
      H5=BKN(1,Z3)
      BJ01(M)=BS3(1)
      BJ11(M)=BS3(2)
      BY01(M)=H4
      BY11(M)=H5
      HZ(M)= B1(M)*BJ01(M)+B2(M)*BY01(M)
      EPHI(M)=-(G*W*U0/ARG(M))*(B1(M)*BJ11(M)-B2(M)*BY11(M))
      HR(M)=-(BETA/ARG(M))*(B1(M)*BJ11(M)-B2(M)*BY11(M))
      WRITE(6,*)DIS(M),DIMAG(EPHI(M))
      IF(DABS(DIS(M)-R2).LT.1.0D-10)  GO TO 57
   24 CONTINUE
C ==========================================================
   57 F9=BETASQ-EPSCLO*FSKSQ
      Z8=CDSQRT(F9)
      Z9=Z8*DIS(M)
C  CALLING BESSEL FUNCTION K OF ORDERS 0,1 FOR THE LAST LAYER
      BK0A=BKN(0,Z9)
      BK1A=BKN(1,Z9)
C ==========================================================
C SOLVING THE EIGENVALUE EQUATION FOR TE MODES
```

```
      X1=B1(M)*BJ01(M)+B2(M)*BY01(M)
      X2=B1(M)*BJ11(M)-B2(M)*BY11(M)
      X3=Z8*BK0A
      X4=ARG(M)*BK1A
      FZ=1.0D0+(X2*X3)/(X1*X4)
C     FZ=(X2*X3)+(X1*X4)
C     FZ=(X1/X3)+(X2/X4)
      WRITE(*,*)FZ
      RETURN
      END
C     ================================================================
C  SUBROUTINE MULLER DETERMINES UP TO N ZEROS OF THE
C  FUNCTION SPECIFIED BY FN,USING QUADRATIC INTERPOLATION.
C  I.E.,MULLER'S METHOD.
C  LIST OF DEFINITION
C  FN=NAME OF A SUBROUTINE ,OF THE FORM FN(Z,FZ) WHICH.
C  FOR A GIVEN Z,RETURNS F(Z).MUST APPEAR IN AN EXTERNAL
C  STATEMENT IN THE CALLING PROGRAM.
C  FNREAL A LOGICAL VARIABLE.IF.TRUE.,ALL APPROXIMATIONS
C  ARE TAKEN TO BE REAL,ALLOWING THIS ROUTINE TO BE
C  USED EVEN IF F(Z) IS ONLY DEFINED FOR REAL Z.
C  ZEROS(1),...,ZEROS(NPREV) CONTAINS PREVIOUSLY FOUND
C  ZEROS (IF NPREV .GT. 0)
C  ZEROS(NPREV+1).....,ZEROS(N) CONTAINS FIRST GUESS FOR
C  THE ZEROS TO BE FOUND.
C  MAXIT MAXIMUM NUMBER OF FUNCTION EVALUATIONS ALLOWED
C  PER ZERO.
C  EP1 ITERATION IS STOPPED IF ABS(H) .LT. EP1*ABS(ZR).
C  WITH H=LATEST CHANGE IN ZERO ESTIMATE ZERO.
C  EP2 ALTHOUGH THE EP1 CRITERION IS NOT MET,ITERATION
C  IS STOPPED IF ABS(F(ZERO)).LT.EP2.
C  N TOTAL NUMBER OF ZEROS TO BE FOUND.
C  NPREV NUMBER OF ZEROS TO BE FOUND.
C  ZEROS(NPREV+1).....,ZEROS(N) APPROXIMATIONS TO ZEROS.
      SUBROUTINE MULLER (FN,FNREAL,ZEROS,N,NPREV,MAXIT,EP1,EP2)
      IMPLICIT REAL*8(A-H,O-Z)
      EXTERNAL FN
      LOGICAL FNREAL
      INTEGER MAXIT,N,NPREV,KOUNT
      COMPLEX*16 ZEROS(N),C,DEN,DIVDF1,DIVDF2,DVDF1P,FZR
      COMPLEX*16 FZRDFL,FZRPRV,H,ZERO,SQR
C     COMPLEX*16 FZRDFL,FZRPRV,H,ZERO,SQR
      EPS1 =DMAX1(EP1, 1.D-30)
      EPS2 =DMAX1(EP2, 1.D-40)
```

```
      DO 200 I=NPREV+1,N
      KOUNT=0
1     ZERO=ZEROS(I)
C  COMPUTE FIRST THREE ESTIMATES FOR ZERO AS
C  ZEROS(I)+.5D-6,ZEROS(I)-.5D-6,ZEROS(I).
      H=.5D-6
      CALL DFLATE(FN, ZERO+.5D-6,I,KOUNT,FZR,DVDF1P,ZEROS,*1)
C     CALL DFLATE(FN, ZERO+.5D-6,I,KOUNT,FZR,DVDFIP,ZEROS,*1)
      CALL DFLATE(FN,ZERO-.5D-6,I,KOUNT,FZR,FZRPRV,ZEROS,*1)
      HPREV=-1.0D-6
      DVDF1P=(FZRPRV-DVDF1P)/HPREV
      CALL DFLATE(FN,ZERO,I,KOUNT,FZR,FZRDFL,ZEROS,*1)
40    DIVDF1=(FZRDFL-FZRPRV)/H
      DIVDF2=(DIVDF1-DVDF1P)/(H+HPREV)
      HPREV=H
      DVDF1P=DIVDF1
      C=DIVDF1+H*DIVDF2
      SQR=C*C-4.*FZRDFL*DIVDF2
      IF (FNREAL .AND. REAL(SQR) .LT.0.) SQR=0.
      SQR=CDSQRT(SQR)
      IF (REAL(C)*REAL(SQR)+DIMAG(SQR) .LT. 0.) THEN
         DEN=C-SQR
      ELSE
         DEN=C+SQR
      END IF
      IF (CDABS(DEN) .LE. 0.0D0) DEN=1.0D0
      H=-2.*FZRDFL/DEN
      FZRPRV=FZRDFL
      ZERO=ZERO+H
      IF (KOUNT .GT. MAXIT)  GO TO 99
70    CALL DFLATE(FN,ZERO,I,KOUNT,FZR,FZRDFL,ZEROS,*1)
C  CHECK FOR CONVERGENCE.
      IF (CDABS(H) .LT. EPS1*CDABS(ZERO)) GO TO 99
      IF (DMAX1(CDABS(FZR),CDABS(FZRDFL)).LT.EPS2) GO TO 99
C  CHECK FOR CONVERGENCE.
      IF (CDABS(FZRDFL) .GE. 10.*CDABS(FZRPRV)) THEN
         H=H/2.
         ZERO=ZERO-H
                                  GO TO 70
      ELSE
                                  GO TO 40
      END IF
99    ZEROS(I)=ZERO
200   CONTINUE
```

```
      RETURN
      END
      SUBROUTINE DFLATE (FN,ZERO,I,KOUNT,FZERO,FZRDFL,ZEROS,* )
C  TO BE CALLED BY MULLER.
      IMPLICIT REAL*8 (A-H,O-Z)
      EXTERNAL FN
      INTEGER I,KOUNT,J
      COMPLEX*16  FZERO,FZRDFL,ZERO,ZEROS(I), DEN
      KOUNT=KOUNT+1
      CALL FN (ZERO,FZERO)
      FZRDFL=FZERO
      IF (I .LT. 2) RETURN
      DO 10 J=2,I
      DEN=ZERO-ZEROS(J-1)
      IF(CDABS(DEN).EQ.0.0D0) THEN
        ZEROS(I)=ZERO*1.001
                    RETURN1
      ELSE
        FZRDFL=FZRDFL/DEN
      END IF
10    CONTINUE
                    RETURN
      END
C     ================================================================
      COMPLEX*16 FUNCTION BJN(N,Z)
      COMPLEX*16 Z,T1,T2
      REAL *8 FCTN
      T1=-Z*Z/4
      K=0
      T2=1
      BJN=T2
200   K=K+1
      T2=T2*T1/K/(N+K)
      BJN=BJN+T2
      IF(CABS(T2).LT.1.E-19)GO TO 120
      GO TO 200
120   IF(N.GT.0)THEN
      FCTN=1.D0
      DO 130 I=1,N
130   FCTN=FCTN*I
      BJN=BJN*(Z/2)**N/FCTN
      END IF
      RETURN
      END
```

```
C ================================================================
      COMPLEX*16 FUNCTION BIN(N,Z)
      COMPLEX*16 Z,T1,T2
      REAL *8 FCTN
      T1=Z*Z/4
      K=0
      T2=1
      BIN=T2
200   K=K+1
      T2=T2*T1/K/(N+K)
      BIN=BIN+T2
      IF(CABS(T2).LT.1.E-19)GO TO 120
      GO TO 200
120   IF(N.GT.0)THEN
      FCTN=1.D0
      DO 130 I=1,N
130   FCTN=FCTN*I
      BIN=BIN*(Z/2)**N/FCTN
      END IF
      RETURN
      END
C ================================================================
      COMPLEX*16 FUNCTION BKN(N,Z)
      COMPLEX*16 Z,T,T1,T2,S1,S2,S3,Z2N,BIN
      REAL*8 FCTN,PK,PNK,PI,GAM
      PI=3.14159265358979323846D0
      GAM=0.57721 56649 01532 86060 D0
      Z2N=(Z/2)**N
      T=Z*Z/4
      IF(N.EQ.0)THEN
C
C ORDER 0
C
      K=1
      T1=T
      S1=T1
      PK=1
30    K=K+1
      T1=T1*(T)/K/K
      PK=PK+1.D0/K
      S1=S1+PK*T1
      IF(CABS(T1).LT.1.0E-19)GO TO 40
      GO TO 30
40    BKN=-(CDLOG(Z/2)+GAM)*BIN(0,Z)+S1
```

```
      ELSE
C
C  ORDER N
C  S2,S3
C
      K=0
      T2=1
      S2=T2
      PK=-GAM
      PNK=-GAM
      DO 50 I=1,N
50    PNK=PNK+1.D0/I
      S3=PK+PNK
200   K=K+1
      T2=T2*T/K/(N+K)
      PK=PK+1.0D0/K
      PNK=PNK+1.D0/(N+K)
      S2=S2+T2
      S3=S3+(PK+PNK)*T2
      IF(CABS(T2).LT.1.E-19)GO TO 120
      GO TO 200
120   FCTN=1.D0
      DO 130 I=1,N
130   FCTN=FCTN*I
C
C  S1
C
      T1=FCTN/N
      S1=T1
      IF(N.GT.1)THEN
      DO 150 I=1,N-1
      T1=T1*(-T)/I/(N-I)
150   S1=S1+T1
      END IF
C
C FIND BKN
C
      BKN=S1/2.D0/Z2N+((-1)**(N+1))*CDLOG(Z/2)*Z2N/FCTN*S2
     &  +((-1)**N)/2.D0*Z2N/FCTN*S3
      END IF
      RETURN
      END
c
C              ==========================
```

```
C                  PROGRAM 2 TMMC
C              ==========================
C
C  THIS SUBROUTINE IS SIMILAR TO THE SUBROUTINE FN USED IN THE FIRST
C  PROGRAM EXCEPT THAT IT IS WRITTEN FOR TM MODES. IT MUST BE USED
C  IN CONJUNCTION WITH MULLER'S SUBROUTINE AND BESSEL FUNCTIONS AS
C  EXPLAINED IN THE PREVIOUS PROGRAM.
C  ==========================
C SUBROUTINE FN(REFSQ,FY)
C  ==========================
      SUBROUTINE FN (REFSQ,FZ)
      IMPLICIT REAL*8 (A-H,O-Z)
      COMPLEX*16 B1(200),B2(200),ALPHA(200),ARG(200)
      COMPLEX*16 BJ01(200),BJ11(200),BJ02(200),BJ12(200)
      COMPLEX*16 HPHI(200),EZ(200),ER(200)
      COMPLEX*16 BY01(200),BY11(200),BY02(200),BY12(200)
      COMPLEX*16 EPS(200),COKSQ(200),REFSQ.BJN,BIN,BKN
      COMPLEX*16 EPSCL,BETASQ,BETA,BS2(3),BS1(3),BS3(3)
      COMPLEX*16 EPSCO,EPSCLO,H2,H3,H4,H5
      COMPLEX*16 FZ,X1,X2,X3,X4,BK1A,BK0A,G
      COMPLEX*16 T1,T2,Z1,Z2,Z3,Z8,Z9,F9
      DIMENSION DIS(200)
      PI=2.0D0*DASIN(1.0D0)
      R1=6.00D-6
      C=1.2D0
      DELR=0.000D-6
      R2=C*R1+DELR
      K=200
      L=50
      WL=0.6328D-6
      C0=3.0D8
      U0=PI*4.0D-7
      G=DCMPLX(0.0D0,1.0D0)
      EPSCL=DCMPLX(2.250D0,0.0D0)
      EPSCL2=DCMPLX(2.89D0,0.0D0)
      EPSCO=DCMPLX(2.28010D0,0.0D0)
      EPSCLO=DCMPLX(-10.30D0,1.0D0)
      YY=L
      XX=R1/YY
      W=2.0D0*PI*(C0/WL)
      FSKSQ=((W/C0)**2.0D0)
      FSK=DSQRT(FSKSQ)
      BETASQ=REFSQ*FSKSQ
      BETA=CDSQRT(BETASQ)
```

```
      B1(1)=DCMPLX(0.1D0,0.0D0)
      B2(1)=DCMPLX(0.0D0,0.0D0)
      DO 55 I=1,50
      EPS(I)=EPSCO
55    CONTINUE
      DO 65 I=51,60
      EPS(I)=EPSCL
65    CONTINUE
      DO 75 I=1,60
      DIS(I)=XX+(I-1)*XX
75    CONTINUE
      EPS(61)=EPSCL2
      DIS(61)=DIS(60)+DELR
      COKSQ(1)=FSKSQ*EPS(1)
      ALPHA(1)=COKSQ(1)-BETASQ
      ARG(1)=CDSQRT(ALPHA(1))
C     ================================================================
C     CALCULATIONS OF THE FIELDS FOR LAYERS BETWEEN 2 & K
      Z2=ARG(1)*DIS(1)
C     CALL BESSEL FUNCTION J OF ORDER 0,1
      BS1(1)=BJN(0,Z2)
      BS1(2)=BJN(1,Z2)
      BJ01(1)=BS1(1)
      BJ11(1)=BS1(2)
      EZ(1)= B1(1)*BJ01(1)
      HPHI(1)=((G*COKSQ(1))/(W*U0*ARG(1)))*(B1(1)*BJ11(1))
      ER(1)=-(BETA/ARG(1))*(B1(1)*BJ11(1))
      WRITE (6,*) DIS(1),DIMAG(HPHI(1))
C     ================================================================
      DO 24 M=2,K
      COKSQ(M)=FSKSQ*EPS(M)
      ALPHA(M)=BETASQ-COKSQ(M)
      ARG(M)=CDSQRT(ALPHA(M))
      Z1=ARG(M)*DIS(M-1)
C     CALLING BESSEL FUNCTIONS I,K OF ORDERS 0,1
      BS2(1)=BIN(0,Z1)
      BS2(2)=BIN(1,Z1)
      H2=BKN(0,Z1)
      H3=BKN(1,Z1)
      BJ02(M)=BS2(1)
      BJ12(M)=BS2(2)
      BY02(M)=H2
      BY12(M)=H3
      T1=EZ(M-1)*BY12(M)+((ARG(M)*W*U0)/(G*COKSQ(M)))*BY02(M)*HPHI(M-1)
```

```
      T2=BJ12(M)*BY02(M)+BJ02(M)*BY12(M)
      B1(M)=T1/T2
      B2(M)=(EZ(M-1)-B1(M)*BJ02(M))/BY02(M)
      Z3=ARG(M)*DIS(M)
C     CALLING BESSEL FUNCTIONS I AND K OF ORDER 0,1
      BS3(1)=BIN(0,Z3)
      BS3(2)=BIN(1,Z3)
      H4=BKN(0,Z3)
      H5=BKN(1,Z3)
      BJ01(M)=BS3(1)
      BJ11(M)=BS3(2)
      BY01(M)=H4
      BY11(M)=H5
      EZ(M)= B1(M)*BJ01(M)+B2(M)*BY01(M)
      HPHI(M)=((G*COKSQ(M))/(W*U0*ARG(M)))*(B1(M)*BJ11(M)-B2(M)*BY11(M))
      ER(M)=-(BETA/ARG(M))*(B1(M)*BJ11(M)-B2(M)*BY11(M))
      WRITE (6,*) DIS(M),DIMAG(HPHI(M))
      IF(DABS(DIS(M)-R2).LT.1.0D-10)  GO TO 57
 24   CONTINUE
C=====================================================================
 57   F9=BETASQ-EPSCLO*FSKSQ
      Z8=CDSQRT(F9)
      Z9=Z8*DIS(M)
C  CALLING BESSEL FUNCTIONS K OF ORDERS 0,1 FOR THE LAST LAYER
      BK0A=BKN(0,Z9)
      BK1A=BKN(1,Z9)
C=====================================================================
C SOLVING THE EIGENVALUE EQUATION FOR TE MODES
      X1=B1(M)*BJ01(M)+B2(M)*BY01(M)
      X2=EPS(M)*(B1(M)*BJ11(M)-B2(M)*BY11(M))
      X3=Z8*BK0A
      X4=EPSCLO*ARG(M)*BK1A
      FZ=1.0D0+(X1*X4)/(X2*X3)
C     FZ=1.0D0+(X2*X3)/(X1*X4)
C     FZ=(X2*X3)+(X1*X4)
C     FZ=(X1/X3)+(X2/X4)
      WRITE (*,*) FZ
      RETURN
      END
C
C              ==========================
C                 PROGRAM 3 HEMC
C              ==========================
C
```

```
C  THIS PROGRAM IS USED TO FIND THE COMPLEX EFFECTIVE INDEX OF THE HE11
C  MODE IN A 4-LAYER STRUCTURE SIMILAR TO THAT GIVEN IN PROGRAMS 1,2
C  GIVEN ABOVE.  IT IS USED IN CONJUNCTION WITH MULLER'S SUBROUTINE.
C  BESSEL FUNCTION J AND I USED IN THIS PROGRAM ARE CALLED FROM THE
C  IMSL LIBRARY OF THE DPC IN KFUPM.  THE K FUNCTION IS CALLED FROM THE
C  SUBROUTINE BESK WHICH IS SHOWN BELLOW.  THE WAVEGUIDE PARAMETERS
C  ARE DEFINED IN THE ABOVE TWO PROGRAMS (1,2).  THIS PROGRAM REQUIRES
C  AN INITIAL GUESS FOR THE EIGENVALUE.  IT ALSO NEEDS AN INITIAL VALUE
C  OF THE AMPLITUDE OF THE MAGNETIC FIELD HZ (B1(1)). THIS AMPLITUDE IS
C  REFINED BY CHANGING THE VALUE OF DELTA BY SMALL INCREMENTS.  WHEN
C  THE EIGENVALUES OBTAINED USING THE MATCHING OF EPHI AND THE MATCHING
C  HPHI ARE THE SAME, THIS IS CONSIDERED THE SOLUTION FOR THE HE11 MODE
C  AND THE AMPLITUDE B1(1) IS CONSIDERED THE PROPER AMPLITUDE OF THE
C  MAGNETIC FIELD CORRESPONDING TO THE INITIAL VALUE OF THE ELECTRIC
C  FIELD A1(1).
C
      IMPLICIT REAL*8 (A-H,O-Z)
      COMPLEX*16 ZEROS(20),VALUE(20),HH,NE
      EXTERNAL FN
      LOGICAL FNREAL
      FNREAL=.FALSE.
C ENTER GUESS
      WRITE(7,25)
 25   FORMAT(/// 'ENTER GUESS')
      READ(5,*)HH
      ZEROS(1)=HH
C ENTER NUMBER OF ZEROS TO BE SEARCHED FOR.
      N=1
C ENTER THE NUMBER OF ZEROS PREVIOUSLY KNOWN.
      NPREV=0
C ENTER THE MAXIMUM NUMBER OF FUNCTION EVALUATION FOR EACH ZERO.
      MAXIT=20
C ENTER THE MAXIMUM ERROR CONTROL PARAMETERS
      EP1=10.0**(-30)
      EP2=10.0**(-40)
      CALL MULLER (FN,FNREAL,ZEROS,N,NPREV,MAXIT,EP1,EP2)
      DO 312 I=1,N
      CALL FN(ZEROS(I),VALUE(I))
      WRITE(7,*)
      WRITE(7,*)ZEROS(I),VALUE(I)
      NE=CDSQRT(ZEROS(I))
      WRITE(7,*)NE
 312  CONTINUE
      STOP
```

```
      END
C  ==========================================
C  SUBROUTINE FN(REFSQ,FY)
C  ==========================================
      SUBROUTINE FN (REFSQ,FZ)
      IMPLICIT REAL*8 (A-H,O-Z)
      COMPLEX*16 A1(200),A2(200),BJ1P(200),BY1P(200)
      COMPLEX*16 BJ2P(200),BY2P(200),ER(200)
      COMPLEX*16 B1(200),B2(200),ALPHA(200),ARG(200)
      COMPLEX*16 BJ01(200),BJ11(200),BJ02(200),BJ12(200)
      COMPLEX*16 EZ(200),EPHI(200),HZ(200),ETSQ(200),HPHI(200)
      COMPLEX*16 BY01(200),BY11(200),BY02(200),BY12(200)
      COMPLEX*16 EPS(200),COKSQ(200),REFSQ,XY,X,AMP
      COMPLEX*16 EPSCL,BETASQ,BETA,BS2(3),BS1(3),BS3(3)
      COMPLEX*16 EPSCO,EPSCLO,H0,H1,H2,H3,H4,H5,EN,H6,H7
      COMPLEX*16 FZ,X1,X2,BKP,G,T3,T4,T5,X3,X4
      COMPLEX*16 T1,T2,Z1,Z2,Z3,Z8,Z9,F9,Z10,H8,H9,F10
      DIMENSION DIS(200)
      PI=2.0D0*DASIN(1.0D0)
      R1=3.0D-6
      C=1.2D0
      DELR=0.300D-6
      R2=C*R1+DELR
      K=200
      L=10
      WL=0.6328D-6
      C0=3.0D8
      U0=PI*4.0D-7
      G=DCMPLX(0.0D0,1.0D0)
      EPSCO=DCMPLX(2.2801D0,0.0D0)
      EPSCL=DCMPLX(2.250D0,0.0D0)
      EPSBF=DCMPLX(2.890D0,0.0D0)
      EPSCLO=DCMPLX(-10.3D0,1.0D0)
      ETA=120.0D0*PI
      EN=CDSQRT(REFSQ)
      YY=L
      XX=R1/YY
      W=2.0D0*PI*(C0/WL)
      FSKSQ=((W/C0)**2.0D0)
      FSK=DSQRT(FSKSQ)
      BETASQ=REFSQ*FSKSQ
      BETA=CDSQRT(BETASQ)
C  INTER AMPLITUDE OF ELECTRIC FIELD EZ
      V1=100.0D0
```

```
      A1(1)=DCMPLX(V1,0.0D0)
      A2(1)=DCMPLX(0.0D0,0.0D0)
C  INTER A GUESS FOR THE AMPLITUDE OF MAGNETIC FIELD HZ
      V2=V1*1.5D0/ETA
      DELTA=0.0022D0
      B1(1)=DCMPLX(V2,0.00D0)+DELTA
      B2(1)=DCMPLX(0.0D0,0.0D0)
      DO 55 I=1,L
      EPS(I)=EPSCO
   55 CONTINUE
      DO 65 I=L+1,L+2
      EPS(I)=EPSCL
   65 CONTINUE
      DO 75 I=1,12
      DIS(I)=XX+(I-1)*XX
   75 CONTINUE
      EPS(13)=EPSBF
      DIS(13)=DIS(12)+DELR
      COKSQ(1)=FSKSQ*EPS(1)
      ALPHA(1)=COKSQ(1)-BETASQ
      ARG(1)=CDSQRT(ALPHA(1))
C  ================================================================
      Z2=ARG(1)*DIS(1)
      CALL DCBJNS(Z2,3,BS1)
      CALL BESK(Z2,H0,H1)
      BJ01(1)=BS1(1)
      BJ11(1)=BS1(2)
      BY01(1)=H0
      BY11(1)=H1
C  CALCULATIONS OF THE FIELDS FOR LAYERS BETWEEN 1 & K
      EZ(1)=A1(1)*BJ11(1)+A2(1)*BY11(1)
      HZ(1)=B1(1)*BJ11(1)+B2(1)*BY11(1)
C  CALCULATIONS OF THE DERIVATIVES OF J & K FUNCTION
      BJ1P(1)=BS1(1)-(BS1(2)/Z2)
      BY1P(1)=-H0-(H1/Z2)
      EPHI(1)=(G/ALPHA(1))*(BETA*EZ(1)/DIS(1)+W*U0*B1(1)*ARG(1)*BJ1P(1))
      ER(1)=-(G/ALPHA(1))*(W*U0*HZ(1)/DIS(1)+BETA*ARG(1)*A1(1)*BJ1P(1))
      HPHI(1)=-(G/ALPHA(1))*((BETA*HZ(1)/DIS(1))+COKSQ(1)*A1(1)*BJ1P(1)*
     *ARG(1)/(W*U0))
C  ================================================================
      DO 24 M=2,K
      J=M-1
      COKSQ(M)=FSKSQ*EPS(M)
      ALPHA(M)=BETASQ-COKSQ(M)
```

```
      ARG(M)=CDSQRT(ALPHA(M))
      Z1=ARG(M)*DIS(M-1)
      CALL DCBINS(Z1,3,BS2)
      CALL BESK(Z1,H2,H3)
C  CALLING BESSEL FUNCTIONS I,K OF ORDERS 0,1
      BJ02(M)=BS2(1)
      BJ12(M)=BS2(2)
      BY02(M)=H2
      BY12(M)=H3
C   CALCULATIONS OF THE DERIVATIVES OF I & K FUNCTION
      BJ1P(M)=BS2(1)-(BS2(2)/Z1)
      BY1P(M)=-H2-(H3/Z1)
      T1=-(G*ALPHA(M)*HPHI(M-1)+(BETA*HZ(M-1)/DIS(M-1)))*BY12(M)
      T2=BJ1P(M)*BY12(M)-BJ12(M)*BY1P(M)
      T3=(COKSQ(M)*ARG(M)*EZ(M-1)*BY1P(M))/(W*U0)
      T4=-(G*ALPHA(M)*EPHI(M-1)-(BETA*EZ(M-1)/DIS(M-1)))*BY12(M)
      T5=(W*U0*ARG(M)*HZ(M-1)*BY1P(M))
      A1(M)=(T1-T3)/(T2*COKSQ(M)*ARG(M)/(W*U0))
      A2(M)=(EZ(M-1)-A1(M)*BJ12(M))/BY12(M)
      B1(M)=-(T4+T5)/(T2*ARG(M)*W*U0)
      B2(M)=(HZ(M-1)-B1(M)*BJ12(M))/BY12(M)
      Z3=ARG(M)*DIS(M)
      CALL DCBINS(Z3,3,BS3)
      CALL BESK(Z3,H4,H5)
      BJ01(M)=BS3(1)
      BJ11(M)=BS3(2)
      BY01(M)=H4
      BY11(M)=H5
C   CALCULATIONS OF THE DERIVATIVES OF I & K FUNCTIONS
      BJ2P(M)=BS3(1)-(BS3(2)/Z3)
      BY2P(M)=-H4-(H5/Z3)
      EZ(M)=(A1(M)*BJ11(M)+A2(M)*BY11(M))
      HZ(M)=(B1(M)*BJ11(M)+B2(M)*BY11(M))
      EPHI(M)=-(G/ALPHA(M))*((BETA/DIS(M))*EZ(M)+W*U0*ARG(M)*(B1(M)*BJ2P
     *(M)+B2(M)*BY2P(M)))
      HPHI(M)=+(G/ALPHA(M))*((COKSQ(M)*ARG(M)/(W*U0))*(A1(M)*BJ2P(M)+A2(
     *M)*BY2P(M))+(BETA/DIS(M))*HZ(M))
      ER(M)=+(G/ALPHA(M))*((BETA*ARG(M))*(A1(M)*BJ2P(M)+A2(M)*BY2P(M))+W
     **U0*HZ(M)/DIS(M))
      IF(DABS(DIS(M)-R2).LT.1.0D-10) GO TO 57
  24  CONTINUE
C     ================================================================
  57  F9=BETASQ-EPSCLO*FSKSQ
      F10=EPSCLO*FSKSQ
```

```
      Z8=CDSQRT(F9)
      Z9=Z8*DIS(M)
      S1=CDSQRT(EPSCLO)
C  CALLING BESSEL FUNCTIONS K OF ORDERS 0,1 FOR THE LAST LAYER
      CALL BESK(Z9,H6,H7)
C  CALCULATIONS OF THE DERIVATIVE OF K FUNCTION
      BKP=-H6-(H7/Z9)
      XY=-1.0D0-1.0D0/Z9
C  ==========================================================
C SOLVING THE EIGENVALUE EQUATION FOR HE11 MODE
      X1=-(G/F9)*((BETA/DIS(M))*EZ(M)+W*U0*Z8*HZ(M)*BKP/H7)
      X2=-(G/F9)*((BETA/DIS(M))*HZ(M)+(F10*Z8*EZ(M)*BKP/(H7*W*U0)))
C ========================
C     MATCHING OF EPHI
C ========================
C    FZ=1.0D0-(EPHI(M)/X1)
      FZ=EPHI(M)-X1
C ========================
C     MATCHING OF HPHI
C ========================
C    FZ=1.0D0+(HPHI(M)/X2)
C    FZ=HPHI(M)+X2
      WRITE(7,*)FZ
      RETURN
      END
C  ==========================================
C    SUBROUTINE BESK(Z,BK0,BK1)
C  ==========================================
      SUBROUTINE BESK(Z,BK0,BK1)
      IMPLICIT REAL*8 (A-H,O-Z)
      COMPLEX*16 Z,T,G0Z,G1Z,BK0,BK1,T2,T3,SUM2,SUM3,C2
      DIMENSION HS(12)
      C=0.5772156649D0
      PI=4.0D0*DATAN(1.0D0)
      T=1.D0/Z
      IF(CDABS(Z).LE.1.0D0)  GO TO 20
      G0Z=1.2533141D0-0.1566642D0*T+0.08811128D0*(T**2)-0.09139095D0*(T*
     **3)+0.1344596D0*(T**4)-0.2299850D0*(T**5)+0.3792410D0*(T**6)-0.524
     *7277D0*(T**7)+0.5575368D0*(T**8)-0.4262633D0*(T**9)+0.2184518D0*(T
     ***10)-0.06680977D0*(T**11)+0.009189338D0*(T**12)
C  ==========================================================
      G1Z=1.2533141D0+0.4699927D0*T-0.14685830D0*(T**2)+0.12804270D0*(T*
     **3)-0.1736432D0*(T**4)+0.2847618D0*(T**5)-0.4594342D0*(T**6)+0.628
     *3381D0*(T**7)-0.6632295D0*(T**8)+0.5050239D0*(T**9)-0.2581304D0*(T
```

```
     ***10)+0.07880001D0*(T**11)-0.010824200D0*(T**12)
      BK0=CDEXP(-Z)*CDSQRT(T)*G0Z
      BK1=CDEXP(-Z)*CDSQRT(T)*G1Z
      GO TO 30
20    SUM1=0.0D0
      DO 77 L=1,10
      V=L
      T1=1.D0/V
      SUM1=SUM1+T1
      HS(L)=SUM1
77    CONTINUE
      C2=(C+CDLOG(0.5D0*Z))
      SUM2=DCMPLX(0.0D0,0.0D0)
      DO 88 J=1,6
      T2=((0.5*Z)**(2*J))*(HS(J)-C2)/((DFAC(J))**2)
      SUM2=SUM2+T2
88    CONTINUE
      BK0=-C2+SUM2
      SUM3=DCMPLX(0.0D0,0.0D0)
      DO 44 I=1,8
      T3=(0.5*Z)**(2*I-1)*(0.5D0+I*(C2-HS(I)))/((DFAC(I))**2)
      SUM3=SUM3+T3
44    CONTINUE
      BK1=T+SUM3
30    RETURN
      END
C
c  THE FOLLOWING 4 PROGRAMS ARE USED TO OBTAIN THE RESULTS OF CHAPTER 5
c
C       ==========================================
C         PROGRAM 4 TENL RECURSIVE
C       ==========================================
C
C  THIS PROGRAM IS USED TO FIND THE EIGENVALUES AND EIGEN FUNCTIONS
C  OF TE MODES IN A FIBER HAVING NONLINEAR CORE AND LINEAR CLADDING.
C  THE PROGRAM IS DEVELOPED USING THE RECURSIVE SCHEME APPROACH.
C  IT IS USED IN CONJUNCTION WITH MULLER'S SUBROUTINE AND THE COMPLEX
C  BESSEL FUNCTIONS. IT REQUIRES THE MAGNETIC FIELD AMPLITUDE OF THE
C  INNERMOST LAYER IN ADDITION TO THE INITIAL GUESS FOR THE EIGENVALUE
C  THE PROGRAM ALSO CALCULATES THE TOTAL MODAL POWER PROPAGATED.
C  THE PARAMETERS USED ARE DEFINED AS FOLLOWS:
C  EPSCO = THE CORE DIELECTRIC CONSTANT (THE BACKGROUND VALUE)
C  EPSCL = THE LINEAR CLADDING DIELECTRIC CONSTANT
C      C = THE NONLINEAR COEFFICIENT
```

```
C      P = THE SATURATION PARAMETER
C     R1 = THE CORE RADIUS
C      L = THE NUMBER OF LAYERS IN THE NONLINEAR REGION
C  THE PROGRAM CAN BE MODIFIED TO SOLVE FOR THE EIGENVALUES AND
C  EIGEN FUNCTION IN THE CASE OF FIBER WITH LINEAR CORE AND NONLINEAR
C  CLADDING.  THE ONLY MODIFICATIONS REQUIRED IS TO REPLACE THE
C  THE DIS(I) AND EPS(J) THEIR NEW VALUES. THESE VALUES ARE LISTED
C  DIRECTLY BELOW THE OLD VALUES AND MARKED BY A COMMENT SIGN (C)
C  ALSO THE IF STATEMENT WHICH TERMINATES THE PROGRAM AT THE CORE-
C  CLADDING INTERFACE SHOULD BE REPLACED BY A ANOTHER ONE WHICH
C  TERMINATES THE PROGRAM AT DISTANCE LARGE ENOUGH TO MAKE THE EFFECT
C  OF THE ELECTRIC FIELD ON THE DIELECTRIC CONSTANT NEGLIGIBLE.
C  THIS DISTANCE IS VARIABLE AND IT DEPENDS ON THE INPUT FIELD
C  AMPLITUDE FOR THE SECOND FIBER STRUCTURE, THE  PROGRAM CALCULATES  LY THE
C  ONLY THE POWER PROPAGATED IN THE NONLINEAR CLADDING.  TO OBTAIN
C  THE TOTAL POWER OF THE MODE THE POWER PROPAGATED IN THE LINEAR
C  CORE SHOULD BE CALCULATED AND ADDED TO THAT OF THE CLADDING.
$DEBUG
$LARGE
      IMPLICIT REAL*8 (A-H,O-Z)
      COMPLEX*16 ZEROS(2),VALUE(2),NE
      EXTERNAL FN
      COMMON X
      LOGICAL FNREAL
C     FNREAL=.FALSE.
      FNREAL=.TRUE.
C ENTER AMPLITUDE OF HZ
      WRITE(*,*)'ENTER AMP.(HZ)'
      READ(*,*)X
C ENTER GUESS
      WRITE(*,*)'ENTER GUESS'
      READ(*,*)ZEROS(1)
      OPEN(UNIT=6,STATUS='OLD',FILE='OUT3')
C ENTER NUMBER OF ZEROS TO BE SEARCHED FOR.
      N=1
C ENTER THE NUMBER OF ZEROS PREVIOUSLY KNOWN
      NPREV=0
C ENTER THE MAXIMUM NUMBER OF FUNCTION EVALUATION FOR EACH ZERO.
      MAXIT=15
C ENTER THE MAXIMUM ERROR CONTROL PARAMETERS
      EP1=10.0D-30
      EP2=10.0D-40
      CALL MULLER (FN,FNREAL,ZEROS,N,NPREV,MAXIT,EP1,EP2)
      DO 312 I=1,N
```

```
      CALL FN(ZEROS(I),VALUE(I))
      WRITE(*,*)
      WRITE(*,*)ZEROS(I),VALUE(I)
      NE=CDSQRT(ZEROS(I))
      WRITE(*,*)NE
  312 CONTINUE
      STOP
      END
C ==========================================
C   SUBROUTINE FN(REFSQ,FY)
C ==========================================
      SUBROUTINE FN (REFSQ,FZ)
      IMPLICIT REAL*8 (A-H,O-Z)
      COMPLEX*16 B1(300),B2(300),ALPHA(300),ARG(300)
      COMPLEX*16 BJ01(300),BJ11(300),BJ02(300),BJ12(300)
      COMPLEX*16 EPHI(300),HZ(300),HR(300)
      COMPLEX*16 BY01(300),BY11(300),BY02(300),BY12(300)
      COMPLEX*16 EPS(300),COKSQ(300),REFSQ,BJN,BKN,BIN
      COMPLEX*16 EPSCL,BETASQ,BETA,BS2(3),BS1(3),BS3(3)
      COMPLEX*16 EPSCO,H2,H3,H4,H5,FZ
      COMPLEX*16 X1,X2,X3,X4,BK1A,BK0A,G
      COMPLEX*16 T1,T2,Z1,Z2,Z3,Z8,Z9,F9,Z10,H8,H9
      DIMENSION DIS(300),P1(300),ETSQ(300)
      COMMON X
      PI=2.0D0*DASIN(1.0D0)
      R1=4.0D-6
      K=300
      L=100
      WL=0.6328D-6
      C0=3.0D8
      U0=PI*4.0D-7
      G=DCMPLX(0.0D0,1.0D0)
      C=1.0D-8
      P=20.0D0
      EPSCL=DCMPLX(2.2500D0,0.0D0)
      EPSCO=DCMPLX(2.2550D0,0.0D0)
      YY=L
      XX=R1/YY
      W=2.0D0*PI*(C0/WL)
      FSKSQ=((W/C0)**2.0D0)
      FSK=DSQRT(FSKSQ)
      BETASQ=REFSQ*FSKSQ
      BETA=CDSQRT(BETASQ)
      B1(1)=DCMPLX(X,0.0D0)
```

```
      EPS(1)=EPSCO
      DO 75 I=1,K
      DIS(I)=XX+(I-1)*XX
C     DIS(I)=R1+(I-1)*XX
 75   CONTINUE
      COKSQ(1)=FSKSQ*EPS(1)
      ALPHA(1)=COKSQ(1)-BETASQ
      ARG(1)=CDSQRT(ALPHA(1))
C ==========================================================
C  CALCULATIONS OF THE FIELDS FOR LAYERS BETWEEN 1 & K
      Z2=ARG(1)*DIS(1)
C     CALLING BESSEL FUNCTION I OF ORDER 0,1
      BS1(1)=BJN(0,Z2)
      BS1(2)=BJN(1,Z2)
      BJ01(1)=BS1(1)
      BJ11(1)=BS1(2)
      HZ(1)= B1(1)*BJ01(1)
      EPHI(1)=-(G*W*U0/ARG(1))*(B1(1)*BJ11(1))
      HR(1)=-(BETA/ARG(1))*(B1(1)*BJ11(1))
C ==========================================================
      DO 24 M=2,K
      J=M-1
      ETSQ(J)=(CDABS(EPHI(J)))**2
      EPS(M)=EPSCO+(C*ETSQ(J))/(1.0D0+(C*P*ETSQ(J)))
C     EPS(M)=EPSCL+(C*ETSQ(J))/(1.0D0+(C*P*ETSQ(J)))
      COKSQ(M)=FSKSQ*EPS(M)
      ALPHA(M)=BETASQ-COKSQ(M)
      ARG(M)=CDSQRT(ALPHA(M))
      Z1=ARG(M)*DIS(M-1)
C  CALLING BESSEL FUNCTIONS I,K OF ORDERS 0,1
      BS2(1)=BIN(0,Z1)
      BS2(2)=BIN(1,Z1)
      H2=BKN(0,Z1)
      H3=BKN(1,Z1)
      BJ02(M)=BS2(1)
      BJ12(M)=BS2(2)
      BY02(M)=H2
      BY12(M)=H3
      T1=HZ(M-1)*BY12(M)-(ARG(M)/(G*W*U0))*BY02(M)*EPHI(M-1)
      T2=BJ12(M)*BY02(M)+BJ02(M)*BY12(M)
      B1(M)=T1/T2
      B2(M)=(HZ(M-1)-B1(M)*BJ02(M))/BY02(M)
      Z3=ARG(M)*DIS(M)
C  CALLING BESSEL FUNCTIONS I,K OF ORDERS 0,1
```

```
      BS3(1)=BIN(0,Z3)
      BS3(2)=BIN(1,Z3)
      H4=BKN(0,Z3)
      H5=BKN(1,Z3)
      BJ01(M)=BS3(1)
      BJ11(M)=BS3(2)
      BY01(M)=H4
      BY11(M)=H5
      HZ(M)=B1(M)*BJ01(M)+B2(M)*BY01(M)
      EPHI(M)=-(G*W*U0/ARG(M))*(B1(M)*BJ11(M)-B2(M)*BY11(M))
      HR(M)=-(BETA/ARG(M))*(B1(M)*BJ11(M)-B2(M)*BY11(M))
      ETSQ(M)=(CDABS(EPHI(M)))**2
      IF(DABS(DIS(M)-R1).LT.1.0D-10) GO TO 57
C     IF(DABS(DIS(M)-2.0D0*R1).LT.1.0D-10) GO TO 57
 24   CONTINUE
C ================================================================
 57   F9=BETASQ-EPSCL*FSKSQ
      Z8=CDSQRT(F9)
      Z9=Z8*DIS(M)
C  CALLING BESSEL FUNCTIONS K OF ORDERS 0,1 FOR THE LAST LAYER
      BK0A=BKN(0,Z9)
      BK1A=BKN(1,Z9)
C ================================================================
C SOLVING THE EIGENVALUE EQUATION FOR NONLINEAR TE MODES
      X1=B1(M)*BJ01(M)+B2(M)*BY01(M)
      X2=B1(M)*BJ11(M)-B2(M)*BY11(M)
      X3=Z8*BK0A
      X4=ARG(M)*BK1A
      FZ=1.0D0+(X2*X3)/(X1*X4)
C     FZ=1.0D0+(X1*X4)/(X2*X3)
C     FZ=X2*X3+X1*X4
C     FZ=(1.0D0/(X2*X3)+1.0D0/(X1*X4))
C     FZ=(X3/X4)+(X1/X2)
C     FZ=(X4/X3)+(X2/X1)
      DO 32 J=1,100
      WRITE(6,*)DIS(J)*(1.0D6),-DIMAG(EPHI(J))
 32   CONTINUE
      WRITE(*,*)FZ
C ================================
C     CALCULATION OF POWER
C ================================
      R=DIS(M)
      DO 51 I=M+1,M+100
      K2=I-M
```

```
      DELR=XX*0.10D0*K2
      R=R+DELR
      DIS(I)=R
      Z10=R*Z8
C  CALLING BESSEL FUNCTIONS K OF ORDERS 0,1 FOR THE LAST LAYER
      H8=BKN(0,Z10)
      H9=BKN(1,Z10)
      HZ(I)=HZ(M)*H8/BK0A
      EPHI(I)=EPHI(M)*H9/BK1A
      HR(I)=HR(M)*H9/BK1A
      R=R+DELR
   51 CONTINUE
      DO 52 I=1,M+100
      P1(I)=(CDABS(EPHI(I)))*(CDABS(HR(I)))*DIS(I)
   52 CONTINUE
      SUM=0.0D0
      DO 53 I=1,M+100-1
      P2=(P1(I)+P1(I+1))*(DIS(I+1)-DIS(I))*0.5D0
      SUM=SUM+P2
   53 CONTINUE
      PT=SUM*PI
      WRITE(6,*)PT
      WRITE(6,*)
      RETURN
      END
C
C     ==========================================
C       PROGRAM 5 TENL SELF-CONSISTENT
C     ==========================================
C
C  THIS PROGRAM IS USED TO FIND THE EIGENVALUES AND THE EIGEN FUNCTIONS
C  OF A FIBER HAVING NONLINEAR CORE AND LINEAR CLADDING
C  THE PROGRAM IS DEVELOPED USING THE SELF-CONSISTENT APPROACH.
C  IT IS USED IN CONJUNCTION WITH MULLER'S SUBROUTINE AND THE COMPLEX
C  BESSEL FUNCTIONS GIVEN IN PROGRAM 1.  TO START THE PROGRAM AN INITIAL
C  INTENSITY PROFILE IS REQUIRED IN ADDITION TO THE GUESS FOR THE MODE
C  EFFECTIVE INDEX. THE PRODUCED FIELD PROFILE IS USED INTERNALLY BY
C  THE PROGRAM TO MODIFY THE REFRACTIVE INDEX PROFILE AND PRODUCE
C  ANOTHER FIELD PROFILE AND SO ON.  THE NUMBER OF ITERATION REQUIRED
C  IS CHOSEN THROUGH THE INDEX OF THE DO LOOP WHICH IS 10 FOR THIS
C  EXAMPLE (DO 75 ...).  THE PROGRAM CAN ALSO BE USED FOR THE FIBER
C  STRUCTURE HAVING LINEAR CORE AND NONLINEAR CLADDING.  THE REQUIRED
C  MODIFICATION ARE SIMILAR TO THOSE MENTIONED IN PROGRAM 4 IN
C  ADDITION TO CHANGING THE INTERFACE VALUES FROM E(100) TO E(1)
```

```
C  AND FROM ETSQ(100) TO ETSQ (1)
$DEBUG
$LARGE
      IMPLICIT REAL*8 (A-H,O-Z)
      COMPLEX*16 ZEROS(2),VALUE(2),NE
      DIMENSION E(300),ETSQ(300)
C     COMMON E,ET
      COMMON E,ETSQ
      EXTERNAL FN
      LOGICAL FNREAL
C     FNREAL=.FALSE.
      FNREAL=.TRUE.
C ENTER GUESS
      WRITE(*,*)'ENTER GUESS'
      READ(*,*)ZEROS(1)
      OPEN(UNIT=5,STATUS='OLD',FILE='DATA1')
      OPEN(UNIT=6,STATUS='OLD',FILE='OUT1')
C ENTER NUMBER OF ZEROS TO BE SEARCHED FOR.
      N=1
C ENTER THE NUMBER OF ZEROS PREVIOUSLY KNOWN
      NPREV=0
C ENTER THE MAXIMUM NUMBER OF FUNCTION EVALUATION FOR EACH ZERO.
      MAXIT=15
C ENTER THE MAXIMUM ERROR CONTROL PARAMETERS
      EP1=10.0D-30
      EP2=10.0D-40
      DO 74 I=1,100
      READ(5,*)E(I)
 74   CONTINUE
      DO 75 I=1,10
      CALL MULLER (FN,FNREAL,ZEROS,N,NPREV,MAXIT,EP1,EP2)
      CALL FN(ZEROS(1),VALUE(1))
      NE=CDSQRT(ZEROS(1))
      WRITE(*,*)ZEROS(1),VALUE(1)
      WRITE(*,*)NE
      WRITE(*,*)
      DO 31 M=1,100
      E(M)=ETSQ(M)
 31   CONTINUE
      ZEROS(1)=NE**2
 75   CONTINUE
      DO 76 I=1,100
      WRITE(6,*)E(I)
 76   CONTINUE
```

```
 55  STOP
     END
C  ==========================
C  SUBROUTINE FN(REFSQ,FY)
C  ==========================
     SUBROUTINE FN (REFSQ,FZ)
     IMPLICIT REAL*8 (A-H,O-Z)
     COMPLEX*16 B1(300),B2(300),ALPHA(300),ARG(300)
     COMPLEX*16 BJ01(300),BJ11(300),BJ02(300),BJ12(300)
     COMPLEX*16 EPHI(300),HZ(300),HR(300)
     COMPLEX*16 BY01(300),BY11(300),BY02(300),BY12(300)
     COMPLEX*16 EPS(300),COKSQ(300),REFSQ,BJN,BIN,BKN
     COMPLEX*16 EPSCL,BETASQ,BETA,BS2(3),BS1(3),BS3(3)
     COMPLEX*16 EPSCO,H2,H3,H4,H5,FZ,ET(300)
     COMPLEX*16 X1,X2,X3,X4,BK1A,BK0A,G
     COMPLEX*16 T1,T2,Z1,Z2,Z3,Z8,Z9,F9
     DIMENSION DIS(300),E(300),ETSQ(300)
     COMMON E,ETSQ
     PI=2.0D0*DASIN(1.0D0)
     ES=3.200D6
     R1=4.0D-6
     K=300
     L=100
     WL=0.6328D-6
     C0=3.0D8
     U0=PI*4.0D-7
     G=DCMPLX(0.0D0,1.0D0)
     C=1.0D-8
     P=40.0D0
     EPSCL=DCMPLX(2.250D0,0.0D0)
     EPSCO=DCMPLX(2.2400D0,0.0D0)
     YY=L
     XX=R1/YY
     W=2.0D0*PI*(C0/WL)
     FSKSQ=((W/C0)**2.0D0)
     FSK=DSQRT(FSKSQ)
     BETASQ=REFSQ*FSKSQ
     BETA=CDSQRT(BETASQ)
     B1(1)=DCMPLX(2.00D0,0.0D0)
     EPS(1)=EPSCO
     DO 75 I=1,L
C    DIS(I)=R1+(I-1)*XX
     DIS(I)=XX+(I-1)*XX
 75  CONTINUE
```

```
      DO 72 M=1,100
      J=M+1
      ET(M)=E(M)*(ES/(E(100)))
C     ET(M)=E(M)*(ES/(E(1)))
C     EPS(J)=EPSCL+(C*ET(M))/(1.0D0+(C*P*ET(M)))
      EPS(J)=EPSCO+(C*ET(M))/(1.0D0+(C*P*ET(M)))
 72   CONTINUE
      COKSQ(1)=FSKSQ*EPS(1)
      ALPHA(1)=COKSQ(1)-BETASQ
      ARG(1)=CDSQRT(ALPHA(1))
C     ------------------------------------------------------------------
C     CALCULATIONS OF THE FIELDS FOR LAYERS BETWEEN 1 & K
      Z2=ARG(1)*DIS(1)
C     CALLING BESSEL FUNCTION J OF ORDER 0,1
      BS1(1)=BJN(0,Z2)
      BS1(2)=BJN(1,Z2)
      BJ01(1)=BS1(1)
      BJ11(1)=BS1(2)
      HZ(1)= B1(1)*BJ01(1)
      EPHI(1)=-(G*W*U0/ARG(1))*(B1(1)*BJ11(1))
      HR(1)=-(BETA/ARG(1))*(B1(1)*BJ11(1))
C     ------------------------------------------------------------------
      DO 24 M=2,K
      J=M-1
      COKSQ(M)=FSKSQ*EPS(M)
      ALPHA(M)=BETASQ-COKSQ(M)
      ARG(M)=CDSQRT(ALPHA(M))
      Z1=ARG(M)*DIS(M-1)
C     CALLING BESSEL FUNCTIONS I,K OF ORDERS 0,1
      BS2(1)=BIN(0,Z1)
      BS2(2)=BIN(1,Z1)
      H2=BKN(0,Z1)
      H3=BKN(1,Z1)
      BJ02(M)=BS2(1)
      BJ12(M)=BS2(2)
      BY02(M)=H2
      BY12(M)=H3
      T1=HZ(M-1)*BY12(M)-(ARG(M)/(G*W*U0))*BY02(M)*EPHI(M-1)
      T2=BJ12(M)*BY02(M)+BJ02(M)*BY12(M)
      B1(M)=T1/T2
      B2(M)=(HZ(M-1)-B1(M)*BJ02(M))/BY02(M)
      Z3=ARG(M)*DIS(M)
C     CALLING BESSEL FUNCTIONS I,K OF ORDERS 0,1
      BS3(1)=BIN(0,Z3)
```

```
      BS3(2)=BIN(1,Z3)
      H4=BKN(0,Z3)
      H5=BKN(1,Z3)
      BJ01(M)=BS3(1)
      BJ11(M)=BS3(2)
      BY01(M)=H4
      BY11(M)=H5
      HZ(M)=B1(M)*BJ01(M)+B2(M)*BY01(M)
      EPHI(M)=-(G*W*U0/ARG(M))*(B1(M)*BJ11(M)-B2(M)*BY11(M))
      HR(M)=-(BETA/ARG(M))*(B1(M)*BJ11(M)-B2(M)*BY11(M))
      IF(DABS(DIS(M)-1.0D0*R1).LT.1.0D-10)  GO TO 57
 24   CONTINUE
C ================================================================
 57   DO 78 I=1,100
      ETSQ(I)=(CDABS(EPHI(I)))**2
 78   CONTINUE
      DO 79 I=1,100
C     WRITE(6,*)DIS(I)*1.0D6,-DIMAG(EPHI(I)),DREAL(EPS(I))
      ETSQ(I)=ETSQ(I)*(ES/ETSQ(100))
C     WRITE(6,*)(ETSQ(I)*(ES/ETSQ(100))-E(I))/ETSQ(I)
 79   CONTINUE
      F9=BETASQ-EPSCL*FSKSQ
      Z8=CDSQRT(F9)
      Z9=Z8*DIS(M)
C  CALLING BESSEL FUNCTIONS K OF ORDERS 0,1 FOR THE LAST LAYER
      BK0A=BKN(0,Z9)
      BK1A=BKN(1,Z9)
C ================================================================
C SOLVING THE EIGENVALUE EQUATION FOR NONLINEAR TE MODES
      X1=B1(M)*BJ01(M)+B2(M)*BY01(M)
      X2=B1(M)*BJ11(M)-B2(M)*BY11(M)
      X3=Z8*BK0A
      X4=ARG(M)*BK1A
      FZ=1.0D0+(X2*X3)/(X1*X4)
C     FZ=1.0D0+(X1*X4)/(X2*X3)
C     FZ=((X2*X3)+(X1*X4))
C     FZ=(X3/X4)+(X1/X2)
C     FZ=(X4/X3)+(X2/X1)
C     WRITE(*,*)FZ
C     WRITE(6,*)
      RETURN
      END
C
C     ================================================
```

```
C          PROGRAM 6 TMNL RECURSIVE
C        ================================
C
C  THIS PROGRAM IS USED TO FIND THE EIGENVALUES AND EIGEN FUNCTIONS
C  OF TM MODES IN A FIBER HAVING NONLINEAR CORE AND LINEAR CLADDING.
C  THE PROGRAM IS DEVELOPED USING THE RECURSIVE SCHEME APPROACH.
C  IT IS USED IN CONJUNCTION WITH MULLER'S SUBROUTINE AND THE COMPLEX
C  BESSEL FUNCTIONS. THE COMMENTS ON THIS PROGRAM ARE THE SAME AS
C  THOSE STATED FOR PROGRAM 4.
$DEBUG
$LARGE
      IMPLICIT REAL*8 (A-H,O-Z)
      COMPLEX*16 ZEROS(2),VALUE(2),NE
      EXTERNAL FN
      LOGICAL FNREAL
C     FNREAL=.FALSE.
      FNREAL=.TRUE.
C ENTER GUESS
      WRITE(*,*)'ENTER GUESS'
      READ(*,*)ZEROS(1)
      OPEN(UNIT=6,STATUS='OLD',FILE='OUT1')
C ENTER NUMBER OF ZEROS TO BE SEARCHED FOR.
      N=1
C ENTER THE NUMBER OF ZEROS PREVIOUSLY KNOWN
      NPREV=0
C ENTER THE MAXIMUM NUMBER OF FUNCTION EVALUATION FOR EACH ZERO.
      MAXIT=15
C ENTER THE MAXIMUM ERROR CONTROL PARAMETERS
      EP1=10.0D-30
      EP2=10.0D-40
      CALL MULLER (FN,FNREAL,ZEROS,N,NPREV,MAXIT,EP1,EP2)
      DO 312 I=1,N
      CALL FN(ZEROS(I),VALUE(I))
      WRITE(*,*)
      WRITE(*,*)ZEROS(I),VALUE(I)
      NE=CDSQRT(ZEROS(I))
      WRITE(*,*)NE
  312 CONTINUE
      STOP
      END
C ================================
C SUBROUTINE FN(REFSQ,FY)
C ================================
      SUBROUTINE FN (REFSQ,FZ)
```

```
      IMPLICIT REAL*8 (A-H,O-Z)
      COMPLEX*16 B1(300),B2(300),ALPHA(300),ARG(300)
      COMPLEX*16 BJ01(300),BJ11(300),BJ02(300),BJ12(300)
      COMPLEX*16 HPHI(300),EZ(300),ER(300),ETSQ(300)
      COMPLEX*16 BY01(300),BY11(300),BY02(300),BY12(300)
      COMPLEX*16 EPS(300),COKSQ(300),REFSQ,BKN,BJN,BIN
      COMPLEX*16 EPSCL,BETASQ,BETA,BS2(3),BS1(3),BS3(3)
      COMPLEX*16 EPSCO,H2,H3,H4,H5,ET
      COMPLEX*16 FZ,X1,X2,X3,X4,G
      COMPLEX*16 T1,T2,Z1,Z2,Z3,Z8,Z9,F9,H6,H7,Z10,H8,H9
      DIMENSION DIS(300),P1(300)
      PI=2.0D0*DASIN(1.0D0)
      R1=4.0D-6
      K=300
      L=100
      WL=0.6328D-6
      C0=3.0D8
      U0=PI*4.0D-7
      G=DCMPLX(0.0D0,1.0D0)
      C=1.0D-8
      P=50.0D0
      EPSCL=DCMPLX(2.250D0,0.0D0)
      EPSCO=DCMPLX(2.265D0,0.0D0)
      YY=L
      XX=R1/YY
      W=2.0D0*PI*(C0/WL)
      FSKSQ=((W/C0)**2.0D0)
      FSK=DSQRT(FSKSQ)
      BETASQ=REFSQ*FSKSQ
      BETA=CDSQRT(BETASQ)
      B1(1)=DCMPLX(290.0D0,0.0D0)
      ET=(CDABS(B1(1)))**2
C     EPS(1)=EPSCL+((C*ET)/(1.0D0+(C*P*ET)))
      EPS(1)=EPSCO
      DO 75 I=1,K
C     DIS(I)=XX+(I-1)*XX
C     DIS(I)=R1+(I-1)*XX
      DIS(I)=R1+(I-1)*XX *2.0D0
 75   CONTINUE
      COKSQ(1)=FSKSQ*EPS(1)
      ALPHA(1)=COKSQ(1)-BETASQ
      ARG(1)=CDSQRT(ALPHA(1))
C =============================================================================
C  CALCULATIONS OF THE FIELDS FOR LAYERS BETWEEN 2 & K
```

```
      Z2=ARG(1)*DIS(1)
C     CALL DCBJNS(Z2,3,BS1)
      BS1(1)=BJN(0,Z2)
      BS1(2)=BJN(1,Z2)
      BJ01(1)=BS1(1)
      BJ11(1)=BS1(2)
      EZ(1)= B1(1)*BJ01(1)
      HPHI(1)=((G*COKSQ(1))/(W*U0*ARG(1)))*(B1(1)*BJ11(1))
      ER(1)=-(BETA/ARG(1))*(B1(1)*BJ11(1))
C ==========================================================
      DO 24 M=2,K
      J=M-1
      ETSQ(J)=((CDABS(EZ(J)))**2)+((CDABS(ER(J)))**2)
C     EPS(M)=EPSCO+(C*ETSQ(J))/(1.0D0+(C*P*ETSQ(J)))
      EPS(M)=EPSCL+(C*ETSQ(J))/(1.0D0+(C*P*ETSQ(J)))
      COKSQ(M)=FSKSQ*EPS(M)
      ALPHA(M)=BETASQ-COKSQ(M)
      ARG(M)=CDSQRT(ALPHA(M))
      Z1=ARG(M)*DIS(M-1)
C  CALLING BESSEL FUNCTIONS I,K OF ORDERS 0,1
      BS2(1)=BIN(0,Z1)
      BS2(2)=BIN(1,Z1)
      H2=BKN(0,Z1)
      H3=BKN(1,Z1)
      BJ02(M)=BS2(1)
      BJ12(M)=BS2(2)
      BY02(M)=H2
      BY12(M)=H3
      T1=EZ(M-1)*BY12(M)+((ARG(M)*W*U0)/(G*COKSQ(M)))*BY02(M)*HPHI(M-1)
      T2=BJ12(M)*BY02(M)+BJ02(M)*BY12(M)
      B1(M)=T1/T2
      B2(M)=(EZ(M-1)-B1(M)*BJ02(M))/BY02(M)
      Z3=ARG(M)*DIS(M)
      BS3(1)=BIN(0,Z3)
      BS3(2)=BIN(1,Z3)
      H4=BKN(0,Z3)
      H5=BKN(1,Z3)
      BJ01(M)=BS3(1)
      BJ11(M)=BS3(2)
      BY01(M)=H4
      BY11(M)=H5
      EZ(M)= B1(M)*BJ01(M)+B2(M)*BY01(M)
      HPHI(M)=((G*COKSQ(M))/(W*U0*ARG(M)))*(B1(M)*BJ11(M)-B2(M)*BY11(M))
      ER(M)=-(BETA/ARG(M))*(B1(M)*BJ11(M)-B2(M)*BY11(M))
```

```
      ETSQ(M)=((CDABS(EZ(M)))**2)+((CDABS(ER(M)))**2)
C     IF(DABS(DIS(M)-R1).LT.1.0D-10)  GO TO 57
      IF(DABS(DIS(M)-4.6D0*R1).LT.1.0D-10)  GO TO 57
 24   CONTINUE
C ==========================================================
 57   DO 71 I=1,M
      WRITE(6,*)DIS(I)*1E6,HPHI(I)
 71   CONTINUE
      F9=BETASQ-EPSCL*FSKSQ
      Z8=CDSQRT(F9)
      Z9=Z8*DIS(M)
C  CALLING BESSEL FUNCTIONS K OF ORDERS 0,1 FOR THE LAST LAYER
      H6=BKN(0,Z9)
      H7=BKN(1,Z9)
C ==========================================================
C SOLVING THE EIGENVALUE EQUATION FOR NONLINEAR TM MODES
      X1=B1(M)*BJ01(M)+B2(M)*BY01(M)
      X2=EPS(M)*(B1(M)*BJ11(M)-B2(M)*BY11(M))
      X3=Z8*H6
      X4=EPSCL*ARG(M)*H7
      FZ=1.0D0+(X2*X3)/(X1*X4)
C     FZ=1.0D0+(X1*X4)/(X2*X3)
C     FZ=(X2*X3)+(X1*X4)
C     FZ=(X2/X4)+(X1/X3)
      WRITE (*,*) FZ
C ==========================================================
C     CALCULATION OF POWER
C ==========================================================
      R=DIS(M)
      DO 51 I=M+1,M+100
      K2=I-M
      DELR=XX*0.03D0*K2
      R=R+DELR
      DIS(I)=R
      EPS(I)=EPSCL
      Z10=R*Z8
      H8=BKN(0,Z10)
      H9=BKN(1,Z10)
      EZ(I)=EZ(M)*H8/H6
      HPHI(I)=HPHI(M)*H9/H7
      ER(I)=ER(M)*H9/H7
 51   CONTINUE
      DO 52 I=1,M+100
      P1(I)=(CDABS(HPHI(I)))*(CDABS(ER(I)))*DIS(I)
```

```
 52   CONTINUE
      SUM=0.0D0
      DO 53 I=1,M+100-1
      P2=(P1(I)+P1(I+1))*(DIS(I+1)-DIS(I))*0.5D0
      SUM=SUM+P2
 53   CONTINUE
      PT=SUM*PI
      WRITE(6,*)PT
      WRITE(6,*)
      RETURN
      END
C
C       ==========================================
C         PROGRAM 7 TMNL SELF-CONSISTENT
C       ==========================================
C
C  THIS PROGRAM IS USED TO FIND THE EIGENVALUES AND THE EIGEN FUNCTIONS
C  FOR TM MODES OF A FIBER HAVING NONLINEAR CORE AND LINEAR CLADDING
C  THE PROGRAM IS DEVELOPED USING THE SELF-CONSISTENT APPROACH. IT IS
C  USED WITH MULLER'S SUBROUTINE AND THE COMPLEX BESSEL FUNCTIONS.
C  ALL THE COMMENTS STATED IN PROGRAM 5 ARE VALID FOR THIS PROGRAM.
C  THE ONLY DIFFERENCE IS THAT THE OUTPUT INTENSITY PROFILE
C  IS WRITTEN IN AN EXTERNAL FILE AND SHOULD BE TRANSFERRED TO THE INPUT
C  FILE EXTERNALLY.  THIS MAKES THE PROGRAM A LITTLE MORE TIME
C  CONSUMING BUT IT ENABLE THE USER TO LOOK AT THE FIELD IN EACH
C  IN EACH ITERATION WHICH IS NOT POSSIBLE FOR PROGRAM 5
$DEBUG
$LARGE
      IMPLICIT REAL*8 (A-H,O-Z)
      COMPLEX*16 ZEROS(2),VALUE(2),NE,E(200)
      EXTERNAL FN
      COMMON E
      LOGICAL FNREAL
      FNREAL=.TRUE.
C ENTER GUESS
      WRITE(*,*)'ENTER GUESS'
      READ(*,*)ZEROS(1)
      OPEN(UNIT=5,STATUS='OLD',FILE='DATA1')
      OPEN(UNIT=6,STATUS='OLD',FILE='OUT1')
C ENTER NUMBER OF ZEROS TO BE SEARCHED FOR.
      N=1
C ENTER THE NUMBER OF ZEROS PREVIOUSLY KNOWN
      NPREV=0
C ENTER THE MAXIMUM NUMBER OF FUNCTION EVALUATION FOR EACH ZERO.
```

```
      MAXIT=15
C ENTER THE MAXIMUM ERROR CONTROL PARAMETERS
      EP1=10.0D-30
      EP2=10.0D-40
      DO 77 I=1,100
      READ(5,*)E(I)
   77 CONTINUE
      DO 312 I=1,N
      CALL MULLER (FN,FNREAL,ZEROS,N,NPREV,MAXIT,EP1,EP2)
      CALL FN(ZEROS(I),VALUE(I))
      WRITE(*,*)
      WRITE(*,*)ZEROS(I),VALUE(I)
      NE=CDSQRT(ZEROS(I))
      WRITE(*,*)NE
  312 CONTINUE
      STOP
      END
C =============================
C  SUBROUTINE FN(REFSQ,FY)
C =============================
      SUBROUTINE FN (REFSQ,FZ)
      IMPLICIT REAL*8 (A-H,O-Z)
      COMPLEX*16 B1(300),B2(300),ALPHA(300),ARG(300)
      COMPLEX*16 BJ01(300),BJ11(300),BJ02(300),BJ12(300)
      COMPLEX*16 HPHI(300),EZ(300),ER(300),ETSQ(300)
      COMPLEX*16 BY01(300),BY11(300),BY02(300),BY12(300)
      COMPLEX*16 EPS(300),COKSQ(300),REFSQ,BKN,BJN,BIN
      COMPLEX*16 EPSCL,BETASQ,BETA,BS2(3),BS1(3),BS3(3)
      COMPLEX*16 EPSCO,H2,H3,H4,H5,ET(200)
      COMPLEX*16 FZ,X1,X2,X3,X4,G,E(200)
      COMPLEX*16 T1,T2,Z1,Z2,Z3,Z8,Z9,F9,H6,H7,Z10,H8,H9
      DIMENSION DIS(300),P1(300)
      COMMON E
      ES=3.5830D7
      PI=2.0D0*DASIN(1.0D0)
      R1=4.0D-6
      K=300
      L=100
      WL=0.6328D-6
      C0=3.0D8
      U0=PI*4.0D-7
      G=DCMPLX(0.0D0,1.0D0)
      C=1.0D-8
      P=50.0D0
```

```
      EPSCL=DCMPLX(2.250D0,0.0D0)
      EPSCO=DCMPLX(2.2750D0,0.0D0)
      YY=L
      XX=R1/YY
      W=2.0D0*PI*(C0/WL)
      FSKSQ=((W/C0)**2.0D0)
      FSK=DSQRT(FSKSQ)
      BETASQ=REFSQ*FSKSQ
      BETA=CDSQRT(BETASQ)
      B1(1)=DCMPLX(800.0D0,0.0D0)
C     EPS(1)=EPSCO+((C*E(1))/(1.0D0+(C*P*E(1))))
      EPS(1)=EPSCO
C     ================================================
      DO 75 I=1,K
C     DIS(I)=XX+(I-1)*XX
      DIS(I)=R1+(I-1)*XX
 75   CONTINUE
      DO 73 M=1,100
      J=M+1
C     ET(M)=(E(M))*(ES/(E(100)))
      ET(M)=(E(M))*(ES/(E(1)))
C     EPS(J)=EPSCO+(C*ET(M))/(1.0D0+(C*P*ET(M)))
      EPS(J)=EPSCL+(C*ET(M))/(1.0D0+(C*P*ET(M)))
 73   CONTINUE
      COKSQ(1)=FSKSQ*EPS(1)
      ALPHA(1)=COKSQ(1)-BETASQ
      ARG(1)=CDSQRT(ALPHA(1))
C     ================================================
C     CALCULATIONS OF THE FIELDS FOR LAYERS BETWEEN 2 & K
      Z2=ARG(1)*DIS(1)
      BS1(1)=BJN(0,Z2)
      BS1(2)=BJN(1,Z2)
      BJ01(1)=BS1(1)
      BJ11(1)=BS1(2)
      EZ(1)= B1(1)*BJ01(1)
      HPHI(1)=((G*COKSQ(1))/(W*U0*ARG(1)))*(B1(1)*BJ11(1))
      ER(1)=-(BETA/ARG(1))*(B1(1)*BJ11(1))
C     ================================================
      DO 24 M=2,K
      J=M-1
      ETSQ(J)=((CDABS(EZ(J)))**2)+((CDABS(ER(J)))**2)
C     EPS(M)=EPSCO+(C*ETSQ(J))/(1.0D0+(C*P*ETSQ(J)))
      COKSQ(M)=FSKSQ*EPS(M)
      ALPHA(M)=BETASQ-COKSQ(M)
```

```
      ARG(M)=CDSQRT(ALPHA(M))
      Z1=ARG(M)*DIS(M-1)
C  CALLING BESSEL FUNCTIONS I,K OF ORDERS 0,1
      BS2(1)=BIN(0,Z1)
      BS2(2)=BIN(1,Z1)
      H2=BKN(0,Z1)
      H3=BKN(1,Z1)
      BJ02(M)=BS2(1)
      BJ12(M)=BS2(2)
      BY02(M)=H2
      BY12(M)=H3
      T1=EZ(M-1)*BY12(M)+((ARG(M)*W*U0)/(G*COKSQ(M)))*BY02(M)*HPHI(M-1)
      T2=BJ12(M)*BY02(M)+BJ02(M)*BY12(M)
      B1(M)=T1/T2
      B2(M)=(EZ(M-1)-B1(M)*BJ02(M))/BY02(M)
      Z3=ARG(M)*DIS(M)
      BS3(1)=BIN(0,Z3)
      BS3(2)=BIN(1,Z3)
      H4=BKN(0,Z3)
      H5=BKN(1,Z3)
      BJ01(M)=BS3(1)
      BJ11(M)=BS3(2)
      BY01(M)=H4
      BY11(M)=H5
      EZ(M)= B1(M)*BJ01(M)+B2(M)*BY01(M)
      HPHI(M)=((G*COKSQ(M))/(W*U0*ARG(M)))*(B1(M)*BJ11(M)-B2(M)*BY11(M))
      ER(M)=-(BETA/ARG(M))*(B1(M)*BJ11(M)-B2(M)*BY11(M))
      ETSQ(M)=((CDABS(EZ(M)))**2)+((CDABS(ER(M)))**2)
      IF(DABS(DIS(M)-2.0D0*R1).LT.1.0D-10)  GO TO 57
 24   CONTINUE
C  ==========================================================
 57   DO 71 I=1,M
      WRITE(6,*)(ETSQ(I)*(ES/ETSQ(1))-E(I))/ETSQ(I)
 71   CONTINUE
      F9=BETASQ-EPSCL*FSKSQ
      Z8=CDSQRT(F9)
      Z9=Z8*DIS(M)
C  CALLING BESSEL FUNCTIONS K OF ORDERS 0,1 FOR THE LAST LAYER
      H6=BKN(0,Z9)
      H7=BKN(1,Z9)
C  ==========================================================
C SOLVING THE EIGENVALUE EQUATION FOR NONLINEAR TM MODES
      X1=B1(M)*BJ01(M)+B2(M)*BY01(M)
      X2=EPS(M)*(B1(M)*BJ11(M)-B2(M)*BY11(M))
```

```
      X3=Z8*H6
      X4=EPSCL*ARG(M)*H7
c     FZ=DREAL(X2*X3+X1*X4)+DIMAG(X2*X3+X1*X4)
      FZ=1.0D0+(X2*X3)/(X1*X4)
C     FZ=1.0D0+(X1*X4)/(X2*X3)
C     FZ=(X2*X3)+(X1*X4)
C     FZ=DREAL(X2*X3+X1*X4)
C     FZ=DIMAG(X2*X3+X1*X4)
C     FZ=(X2/X4)+(X1/X3)
      WRITE (*,*) FZ
      WRITE(6,*)
      RETURN
      END

C THE FOLLOWING 2 PROGRAMS ARE USED TO OBTAIN THE RESULTS OF CHAPTER 6
C
C       ==========================================
C         PROGRAM 8 HE11NL RECURSIVE
C       ==========================================
C
C  THIS PROGRAM IS USED TO FIND THE EIGENVALUE AND THE EIGEN FUNCTION
C  OF THE HE11 MODE IN A WAVEGUIDE HAVING A NONLINEAR CORE AND A LINEAR
C  CLADDING. THE PROGRAM IS USED IN CONJUNCTION WITH MULLER'S
C  SUBROUTINE AND THE COMPLEX BESSEL FUNCTIONS.
C  THE MATCHING TECHNIQUE BETWEEN THE TWO RESULTANT VALUES OF THE
C  EFFECTIVE INDEX IS SIMILAR TO THAT EXPLAINED IN PROGRAM 3.
C  HOWEVER, THIS PROGRAM IS WRITTEN TO BE MORE INTERACTIVE AND MORE
C  FASTER THAN PROGRAM 3.  THE PROGRAM CAN BE MODIFIED TO WORK FOR
C  A WAVEGUIDE HAVING LINEAR CORE AND NONLINEAR CLADDING.  THE SAME
C  MODIFICATION MENTIONED IN PROGRAM 4 ARE APPLIED TO THIS PROGRAM IN
C  ADDITION TO OMITTING ALL THE STEPS USED TO CALCULATE EPS(1). EPS(1)
C  FOR THIS CASE IS EQUAL TO EPSCO.
C  THE INPUTS FOR THIS PROGRAM ARE: THE AMPLITUDE OF THE AXIAL ELECTRIC
C  FIELD , THE VALUE OF DELTA REQUIRED FOR THE AMPLITUDE OF THE AXIAL
C  MAGNETIC FIELD , THE FUNCTION WHICH IS TO BE SOLVED FOR ITS ZEROS
C  (WHETHER THE ONE RESULTING FROM MATCHING EPHI OR THAT RESULTING
C  FROM MATCHING HPHI) AND THE GUESS REQUIRED FOR THE EFFECTIVE INDEX.
$DEBUG
$LARGE
      IMPLICIT REAL*8 (A-H,O-Z)
      COMPLEX*16 ZEROS(2),VALUE(2),NE
      EXTERNAL FN
      COMMON L1,C1,C2
      LOGICAL FNREAL
```

```
C     FNREAL=.FALSE.
      FNREAL=.TRUE.
C ENTER AMP(EZ)
      WRITE(*,*)'ENTER AMP.(EZ)'
      READ(*,*)C1
C ENTER DELTA
      WRITE(*,*)'ENTER DELTA'
      READ(*,*)C2
C ENTER FUNCTION
      WRITE(*,*)'ENTER FUNCTION'
      READ(*,*)L1
C ENTER GUESS
      WRITE(*,*)'ENTER GUESS'
      READ(*,*)ZEROS(1)
      OPEN(UNIT=6,STATUS='OLD',FILE='OUT1')
C ENTER NUMBER OF ZEROS TO BE SEARCHED FOR.
      N=1
C ENTER THE NUMBER OF ZEROS PREVIOUSLY KNOWN
      NPREV=0
C ENTER THE MAXIMUM NUMBER OF FUNCTION EVALUATION FOR EACH ZERO
      MAXIT=15
C ENTER THE MAXIMUM ERROR CONTROL PARAMETERS
      EP1=10.0D-30
      EP2=10.0D-40
      CALL MULLER (FN,FNREAL,ZEROS,N,NPREV,MAXIT,EP1,EP2)
      DO 312 I=1,N
      CALL FN(ZEROS(I),VALUE(I))
      WRITE(*,*)
      WRITE(*,*)ZEROS(I),VALUE(I)
      NE=CDSQRT(ZEROS(I))
      WRITE(*,*)NE
 312  CONTINUE
      STOP
      END
C ======================================
C  SUBROUTINE FN(REFSQ,FY)
C ======================================
      SUBROUTINE FN (REFSQ,FZ)
      IMPLICIT REAL*8 (A-H,O-Z)
      COMPLEX*16 A1(210),A2(210),BJ1P(210),BY1P(210)
      COMPLEX*16 BJ2P(210),BY2P(210),ER(300),BJN,BKN,BIN
      COMPLEX*16 B1(210),B2(210),ALPHA(210),ARG(210)
      COMPLEX*16 BJ01(210),BJ11(210),BJ02(210),BJ12(210)
      COMPLEX*16 EZ(300),EPHI(300),HZ(300),HPHI(300),HR(300)
```

```
      COMPLEX*16 BY01(210),BY11(210),BY02(210),BY12(210)
      COMPLEX*16 EPS(210),COKSQ(210),REFSQ,Y2,Y3,Y4,Y5
      COMPLEX*16 EPSCL,BETASQ,BETA,BS2(3),BS1(3),BS3(3)
      COMPLEX*16 EPSCO,H2,H3,H4,H5,H6,H7
      COMPLEX*16 X1,X2,BKP,G,T3,T4,T5,FZ,P3(300),P4(300)
      COMPLEX*16 T1,T2,Z1,Z2,Z3,Z8,Z9,F9,Z10,H8,H9,F10
      DIMENSION DIS(210),ETSQ(210),P1(210)
      COMMON L1,C1,C2
      PI=2.0D0*DASIN(1.0D0)
      R1=4.0D-6
      K=200
      L=100
      WL=0.6328D-6
      C0=3.0D8
      U0=PI*4.0D-7
      G=DCMPLX(0.0D0,1.0D0)
      C=1.0D-8
      P=20.0D0
      EPSCO=DCMPLX(2.2550D0,0.0D0)
      EPSCL=DCMPLX(2.250D0,0.0D0)
      ETA=120.0D0*PI
      YY=L
      XX=R1/YY
      W=2.0D0*PI*(C0/WL)
      FSKSQ=((W/C0)**2.0D0)
      FSK=DSQRT(FSKSQ)
      BETASQ=REFSQ*FSKSQ
      BETA=CDSQRT(BETASQ)
C  INTER AMPLITUDE OF ELECTRIC FIELD EZ
      V1=C1
      A1(1)=DCMPLX(V1,0.0D0)
      A2(1)=DCMPLX(0.0D0,0.0D0)
C  INTER A GUESS FOR THE AMPLITUDE OF MAGNETIC FIELD HZ
      CC=(DREAL(REFSQ))**0.5D0
      V2=(V1*1.5D0/ETA)+C2
      B1(1)=DCMPLX(V2,0.0D0)
      B2(1)=DCMPLX(0.0D0,0.0D0)
C = = = = = = = = = = = = = = = = = = = = = = = = = = = = = = = =
C  CALCULATION OF EPS(1)
C = = = = = = = = = = = = = = = = = = = = = = = = = = = = = = = =
      Y1=(CDABS(W*U0*B1(1)))**2.0D0+(CDABS(BETA*A1(1)))**2.0D0
      Y2=(C*P*Y1/FSKSQ)-EPSCO-REFSQ
      Y3=EPSCO*REFSQ-(C*Y1/FSKSQ)*(P*EPSCO+1.0D0)
      Y4=(-Y2+CDSQRT(Y2**2.0-4.0*Y3))/2.0D0
```

```
      Y5=(-Y2-CDSQRT(Y2**2.0-4.0*Y3))/2.0D0
      EPS(1)=Y4
C     WRITE(6,*)EPS(1),Y5
C ==========================================
C     EPS(1)=EPSCO
      DO 75 I=1,K
      DIS(I)=XX+(I-1)*XX
C     DIS(I)=R1+(I-1)*XX
 75   CONTINUE
      COKSQ(1)=FSKSQ*EPS(1)
      ALPHA(1)=COKSQ(1)-BETASQ
      ARG(1)=CDSQRT(ALPHA(1))
C ==========================================
      Z2=ARG(1)*DIS(1)
      BJ01(1)=BJN(0,Z2)
      BJ11(1)=BJN(1,Z2)
      BS1(1)=BJ01(1)
      BS1(2)=BJ11(1)
C  CALCULATIONS OF THE FIELDS FOR LAYERS BETWEEN 1 & K
      EZ(1)=A1(1)*BJ11(1)
      HZ(1)=B1(1)*BJ11(1)
C  CALCULATIONS OF THE DERIVATIVES OF J & K FUNCTION
      BJ1P(1)=BS1(1)-(BS1(2)/Z2)
      EPHI(1)=(G/ALPHA(1))*(BETA*EZ(1)/DIS(1)+W*U0*B1(1)*ARG(1)*BJ1P(1))
      HR(1)=-((COKSQ(1)/(W*U0))*EZ(1)/DIS(1)+BETA*B1(1)*ARG(1)*BJ1P(1))
     **(G/ALPHA(1))
      ER(1)=-(G/ALPHA(1))*(W*U0*HZ(1)/DIS(1)+BETA*ARG(1)*A1(1)*BJ1P(1))
      HPHI(1)=-(G/ALPHA(1))*((BETA*HZ(1)/DIS(1))+COKSQ(1)*A1(1)*BJ1P(1)*
     *ARG(1)/(W*U0))
      ETSQ(1)=((CDABS(EZ(1)))**2.0)+((CDABS(EPHI(1)))**2.0)+((CDABS(ER(1
     *)))**2.0)
C ==========================================
      DO 24 M=2,K
      J=M-1
      EPS(M)=EPSCO+((C*ETSQ(J))/(1.0D0+C*P*ETSQ(J)))
C     EPS(M)=EPSCL+((C*ETSQ(J))/(1.0D0+C*P*ETSQ(J)))
      COKSQ(M)=FSKSQ*EPS(M)
      ALPHA(M)=BETASQ-COKSQ(M)
      ARG(M)=CDSQRT(ALPHA(M))
      Z1=ARG(M)*DIS(M-1)
C CALLING BESSEL FUNCTIONS I,K OF ORDERS 0,1
      BS2(1)=BIN(0,Z1)
      BS2(2)=BIN(1,Z1)
      H2=BKN(0,Z1)
```

```
      H3=BKN(1,Z1)
      BJ02(M)=BS2(1)
      BJ12(M)=BS2(2)
      BY02(M)=H2
      BY12(M)=H3
C  CALCULATIONS OF THE DERIVATIVES OF I & K FUNCTION
      BJ1P(M)=BS2(1)-(BS2(2)/Z1)
      BY1P(M)=-H2-(H3/Z1)
      T1=-(G*ALPHA(M)*HPHI(M-1)+(BETA*HZ(M-1)/DIS(M-1)))*BY12(M)
      T2=BJ1P(M)*BY12(M)-BJ12(M)*BY1P(M)
      T3=(COKSQ(M)*ARG(M)*EZ(M-1)*BY1P(M))/(W*U0)
      T4=-(G*ALPHA(M)*EPHI(M-1)-(BETA*EZ(M-1)/DIS(M-1)))*BY12(M)
      T5=(W*U0*ARG(M)*HZ(M-1)*BY1P(M))
      A1(M)=(T1-T3)/(T2*COKSQ(M)*ARG(M)/(W*U0))
      A2(M)=(EZ(M-1)-A1(M)*BJ12(M))/BY12(M)
      B1(M)=-(T4+T5)/(T2*ARG(M)*W*U0)
      B2(M)=(HZ(M-1)-B1(M)*BJ12(M))/BY12(M)
      Z3=ARG(M)*DIS(M)
      BS3(1)=BIN(0,Z3)
      BS3(2)=BIN(1,Z3)
      H4=BKN(0,Z3)
      H5=BKN(1,Z3)
      BJ01(M)=BS3(1)
      BJ11(M)=BS3(2)
      BY01(M)=H4
      BY11(M)=H5
C  CALCULATIONS OF THE DERIVATIVES OF I & K FUNCTIONS
      BJ2P(M)=BS3(1)-(BS3(2)/Z3)
      BY2P(M)=-H4-(H5/Z3)
      EZ(M)=(A1(M)*BJ11(M)+A2(M)*BY11(M))
      HZ(M)=(B1(M)*BJ11(M)+B2(M)*BY11(M))
      EPHI(M)=-(G/ALPHA(M))*((BETA/DIS(M))*EZ(M)+W*U0*ARG(M)*(B1(M)*BJ2P
     *(M)+B2(M)*BY2P(M)))
      HPHI(M)=+(G/ALPHA(M))*((COKSQ(M)*ARG(M)/(W*U0))*(A1(M)*BJ2P(M)+A2(
     *M)*BY2P(M))+(BETA/DIS(M))*HZ(M))
      ER(M)=+(G/ALPHA(M))*((BETA*ARG(M))*(A1(M)*BJ2P(M)+A2(M)*BY2P(M))+W
     **U0*HZ(M)/DIS(M))
      HR(M)=((COKSQ(M)/(W*U0))*EZ(M)/DIS(M)+BETA*ARG(M)*(B1(M)*BJ2P(M)+
     *B2(M)*BY2P(M)))*(G/ALPHA(M))
      ETSQ(M)=((CDABS(EZ(M)))**2.0)+((CDABS(EPHI(M)))**2.0)+((CDABS(ER(M
     *)))**2.0)
      IF(DABS(DIS(M)-R1).LT.1.0D-10)  GO TO 57
C     IF(DABS(DIS(M)-2.0D0*R1).LT.1.0D-10)  GO TO 57
 24   CONTINUE
```

```
C ==========================================================
 57   F9=BETASQ-EPSCL*FSKSQ
      F10=EPSCL*FSKSQ
      Z8=CDSQRT(F9)
      Z9=Z8*DIS(M)
      S1=CDSQRT(EPSCL)
C  CALLING BESSEL FUNCTIONS K OF ORDERS 0,1 FOR THE LAST LAYER
      H6=BKN(0,Z9)
      H7=BKN(1,Z9)
C   CALCULATIONS OF THE DERIVATIVE OF K FUNCTION
      BKP=-H6-(H7/Z9)
C ==========================================================
C SOLVING THE EIGENVALUE EQUATION FOR THE HE11 MODE
      X1=-(G/F9)*((BETA/DIS(M))*EZ(M)+W*U0*Z8*HZ(M)*BKP/H7)
      X2=-(G/F9)*((BETA/DIS(M))*HZ(M)+(F10*Z8*EZ(M)*BKP/(H7*W*U0)))
C    ====================
      IF (L1.EQ.1) THEN
C    ====================
C ====================================
C    MATCHING OF EPHI
C ====================================
      FZ=1.0D0-(EPHI(M)/X1)
C     FZ=DREAL(EPHI(M)-X1)+DIMAG(EPHI(M)-X1)
C     FZ=EPHI(M)-X1
C    ========
      ELSE
C ====================================
C    MATCHING OF HPHI
C ====================================
      FZ=1.0D0+(HPHI(M)/X2)
C     FZ=DREAL(HPHI(M)+X2)+DIMAG(HPHI(M)+X2)
C     FZ=HPHI(M)+X2
C ================
      END IF
C ================
      DO 32 I=1,L
      WRITE(6,*)ETSQ(I)
C     WRITE(6,*)DIS(I)*1E6,DIMAG(EPHI(I)),ETSQ(I)
  32  CONTINUE
      WRITE(*,*)FZ
C ====================================
C    CALCULATION OF POWER
C ====================================
C CALLING BESSEL FUNCTIONS K OF ORDERS 0,1 FOR THE LAST LAYER
```

```
      R=DIS(M)
      DO 51 I=M+1,M+100
      K2=I-M
      DELR=XX*0.10D0*K2
      R=R+DELR
      DIS(I)=R
      EPS(I)=EPSCL
      Z10=R*Z8
      H8=BKN(0,Z10)
      H9=BKN(1,Z10)
      HZ(I)=HZ(M)*H9/H7
      EZ(I)=EZ(M)*H9/H7
C  CALCULATIONS OF THE DERIVATIVES OF K FUNCTION
      BY1P(I)=-H8-(H9/Z10)
      EPHI(I)=-(G/F9)*((BETA*EZ(I)/R)+W*U0*HZ(M)*Z8*BY1P(I)/H7)
      HR(I)=(G/F9)*((F10/W*U0)*(EZ(I)/R)+BETA*HZ(M)*Z8*BY1P(I)/H7)
      ER(I)=(G/F9)*((W*U0*HZ(I)/R)+BETA*EZ(M)*Z8*BY1P(I)/H7)
      HPHI(I)=(G/F9)*((BETA*HZ(I)/R)+(F10/(W*U0))*EZ(M)*Z8*BY1P(I)/H7)
 51   CONTINUE
      DO 52 I=1,M+100
      P4(I)=(DREAL(EPHI(I))+DIMAG(EPHI(I)))*(DREAL(HR(I))-DIMAG(HR(I)))
      P3(I)=(DREAL(HPHI(I))-DIMAG(HPHI(I)))*(DREAL(ER(I))+DIMAG(ER(I)))
      P1(I)=DREAL(P4(I)-P3(I))*DIS(I)
 52   CONTINUE
      SUM=0.0D0
      DO 53 I=1,M+100-1
      P2=(P1(I)+P1(I+1))*(DIS(I+1)-DIS(I))*0.5D0
      SUM=SUM+P2
 53   CONTINUE
      PT=SUM*PI
      WRITE(6,*)
      WRITE(6,*)PT
      RETURN
      END
C
C     ==========================================
C       PROGRAM 9 HE11NL SELF-CONSISTENT
C     ==========================================
C
C  THIS PROGRAM IS USED TO FIND THE EIGENVALUE AND THE EIGEN FUNCTION
C  OF THE HE11 MODE IN A WAVEGUIDE HAVING A NONLINEAR CORE AND A LINEAR
C  CLADDING.  THE PROGRAM IS BASED ON THE SELF-CONSISTENT APPROACH.
C  IT IS USED WITH MULLER'S ROUTINE AND THE COMPLEX BESSEL FUNCTIONS.
C  THE MATCHING TECHNIQUE BETWEEN THE TWO RESULTANT VALUES
```

```
C  OF THE EFFECTIVE INDEX IS SIMILAR TO THAT EXPLAINED IN PROGRAM 8.
C  THE PROGRAM CAN BE MODIFIED TO WORK FOR A WAVEGUIDE HAVING LINEAR
C  CORE AND NONLINEAR CLADDING IN A MANNER SIMILAR TO THAT EXPLAINED
C  IN THE PROGRAM 8.  IN ADDITION TO THE MODIFICATION OF PROGRAM 8.
C  THE INTERFACE INTENSITY VALUES E(100) AND ETSQ(100) SHOULD BE
C  REPLACED BY THE NEW INTERFACE VALUES E(1) AND ETSQ(1)
C  THE INPUTS FOR THIS PROGRAM ARE: THE AMPLITUDE OF THE AXIAL ELECTRIC
C  FIELD , THE VALUE OF DELTA REQUIRED FOR THE AMPLITUDE OF THE AXIAL
C  MAGNETIC FIELD , THE FUNCTION WHICH IS TO BE SOLVED FOR ITS ZEROS
C  (WHETHER THE ONE RESULTING FROM MATCHING EPHI OR THAT RESULTING
C  FROM MATCHING HPHI) AND THE GUESS REQUIRED FOR THE EFFECTIVE INDEX.
C  AN INITIAL INTENSITY PROFILE IS REQUIRED TO START THE PROGRAM AND
C  PRODUCE THE FIRST EIGENVALUE AND THE FIRST EIGEN FIELD. THIS EIGEN
C  FIELD IS FED BACK TO THE MAIN PROGRAM TO PRODUCE A NEW FIELD AND
C  SO ON. THE PROGRAM IS TERMINATED AFTER NUMBER OF RUNS ENOUGH FOR
C  THE EIGEN VALUE TO BE STABILIZED.
$DEBUG
$LARGE
      IMPLICIT REAL*8 (A-H,O-Z)
      COMPLEX*16 ZEROS(2),VALUE(2),NE
      DIMENSION E(300),ETSQ(300)
      COMMON E,ETSQ,L1,C1,C2
      EXTERNAL FN
      LOGICAL FNREAL
      FNREAL=.TRUE.
      OPEN(UNIT=5,STATUS='OLD',FILE='DATA1')
      OPEN(UNIT=6,STATUS='OLD',FILE='OUT1')
      DO 74 I=1,100
      READ(5,*)E(I)
 74   CONTINUE
C ENTER AMP(EZ)
      WRITE(*,*)'ENTER AMP.(EZ)'
      READ(*,*)C1
C ENTER DELTA
      WRITE(*,*)'ENTER DELTA'
      READ(*,*)C2
C ENTER FUNCTION
      WRITE(*,*)'ENTER FUNCTION'
      READ(*,*)L1
C ENTER GUESS
      WRITE(*,*)'ENTER GUESS'
      READ(*,*)ZEROS(1)
C ENTER NUMBER OF ZEROS TO BE SEARCHED FOR.
      N=1
```

```
C ENTER THE NUMBER OF ZEROS PREVIOUSLY KNOWN
      NPREV=0
C ENTER THE MAXIMUM NUMBER OF FUNCTION EVALUATION FOR EACH ZERO.
      MAXIT=15
C ENTER THE MAXIMUM ERROR CONTROL PARAMETERS
      EP1=10.0D-30
      EP2=10.0D-40
      DO 75 I=1,10
      CALL MULLER (FN,FNREAL,ZEROS,N,NPREV,MAXIT,EP1,EP2)
      CALL FN(ZEROS(1),VALUE(1))
      NE=CDSQRT(ZEROS(1))
      WRITE(*,*)ZEROS(1),VALUE(1)
      WRITE(*,*)NE
      WRITE(*,*)
      DO 31 M=1,100
      E(M)=ETSQ(M)
 31   CONTINUE
      ZEROS(1)=NE**2
 75   CONTINUE
      DO 76 I=1,100
      WRITE(6,*)E(I)
 76   CONTINUE
      STOP
      END
C =====================================
C SUBROUTINE FN(REFSQ,FY)
C =====================================
      SUBROUTINE FN (REFSQ,FZ)
      IMPLICIT REAL*8 (A-H,O-Z)
      COMPLEX*16 A1(210),A2(210),BJ1P(210),BY1P(210)
      COMPLEX*16 BJ2P(210),BY2P(210),ER(300),BJN,BKN,BIN
      COMPLEX*16 B1(210),B2(210),ALPHA(210),ARG(210)
      COMPLEX*16 BJ01(210),BJ11(210),BJ02(210),BJ12(210)
      COMPLEX*16 EZ(300),EPHI(300),HZ(300),HPHI(300),HR(300)
      COMPLEX*16 BY01(210),BY11(210),BY02(210),BY12(210)
      COMPLEX*16 EPS(210),COKSQ(210),REFSQ
      COMPLEX*16 EPSCL,BETASQ,BETA,BS2(3),BS1(3),BS3(3)
      COMPLEX*16 EPSCO,H2,H3,H4,H5,H6,H7
      COMPLEX*16 X1,X2,BKP,G,T3,T4,T5,FZ,ET(300)
      COMPLEX*16 T1,T2,Z1,Z2,Z3,Z8,Z9,F9,F10
      DIMENSION DIS(210),ETSQ(300),E(300)
      COMMON E,ETSQ,L1,C1,C2
      PI=2.0D0*DASIN(1.0D0)
      ES=3953.0D0
```

```
      R1=4.0D-6
      K=200
      L=100
      WL=0.6328D-6
      C0=3.0D8
      U0=PI*4.0D-7
      G=DCMPLX(0.0D0,1.0D0)
      C=1.0D-8
      P=20.0D0
      EPSCO=DCMPLX(2.2550D0,0.0D0)
      EPSCL=DCMPLX(2.250D0,0.0D0)
      ETA=120.0D0*PI
      YY=L
      XX=R1/YY
      W=2.0D0*PI*(C0/WL)
      FSKSQ=((W/C0)**2.0D0)
      FSK=DSQRT(FSKSQ)
      BETASQ=REFSQ*FSKSQ
      BETA=CDSQRT(BETASQ)
C  INTER AMPLITUDE OF ELECTRIC FIELD EZ
      V1=C1
      A1(1)=DCMPLX(V1,0.0D0)
      A2(1)=DCMPLX(0.0D0,0.0D0)
C  INTER A GUESS FOR THE AMPLITUDE OF MAGNETIC FIELD HZ
      CC=(DREAL(REFSQ))**0.5D0
      V2=(V1*CC/ETA)+C2
C     V2=(V1*1.5D0/ETA)+C2
      B1(1)=DCMPLX(V2,0.0D0)
      B2(1)=DCMPLX(0.0D0,0.0D0)
C  ==========================================
      DO 75 I=1,K
      DIS(I)=XX+(I-1)*XX
 75   CONTINUE
      DO 72 M=1,100
      J=M+1
      ET(M)=(E(M))*(ES/(E(100)))
C     ET(M)=(E(M))*(ES/(E(1)))
      EPS(J)=EPSCO+((C*ET(M))/(1.0D0+C*P*ET(M)))
C     EPS(J)=EPSCL+((C*ET(M))/(1.0D0+C*P*ET(M)))
 72   CONTINUE
C  ==========================
C  CALCULATION OF EPS(1)
C  ==========================
      EPS(1)=EPSCO+((C*ET(1))/(1.0D0+C*P*ET(1)))
```

```
      COKSQ(1)=FSKSQ*EPS(1)
      ALPHA(1)=COKSQ(1)-BETASQ
      ARG(1)=CDSQRT(ALPHA(1))
      Z2=ARG(1)*DIS(1)
      BJ01(1)=BJN(0,Z2)
      BJ11(1)=BJN(1,Z2)
      BS1(1)=BJ01(1)
      BS1(2)=BJ11(1)
C  CALCULATIONS OF THE FIELDS FOR LAYERS BETWEEN 1 & K
      EZ(1)=A1(1)*BJ11(1)
      HZ(1)=B1(1)*BJ11(1)
C  CALCULATIONS OF THE DERIVATIVES OF J & K FUNCTION
      BJ1P(1)=BS1(1)-(BS1(2)/Z2)
C     BJ1P(1)=BJ01(1)-(BJ11(1)/Z2)
      EPHI(1)=(G/ALPHA(1))*(BETA*EZ(1)/DIS(1)+W*U0*B1(1)*ARG(1)*BJ1P(1))
      HR(1)=-((COKSQ(1)/(W*U0))*EZ(1)/DIS(1)+BETA*B1(1)*ARG(1)*BJ1P(1))
     **(G/ALPHA(1))
      ER(1)=-(G/ALPHA(1))*(W*U0*HZ(1)/DIS(1)+BETA*ARG(1)*A1(1)*BJ1P(1))
      HPHI(1)=-(G/ALPHA(1))*((BETA*HZ(1)/DIS(1))+COKSQ(1)*A1(1)*BJ1P(1)*
     *ARG(1)/(W*U0))
      ETSQ(1)=((CDABS(EZ(1)))**2.0)+((CDABS(EPHI(1)))**2.0)+((CDABS(ER(1
     *)))**2.0)
C  ==========================================================
      DO 24 M=2,K
      J=M-1
      COKSQ(M)=FSKSQ*EPS(M)
      ALPHA(M)=BETASQ-COKSQ(M)
      ARG(M)=CDSQRT(ALPHA(M))
      Z1=ARG(M)*DIS(M-1)
C  CALLING BESSEL FUNCTIONS I,K OF ORDERS 0,1
      BS2(1)=BIN(0,Z1)
      BS2(2)=BIN(1,Z1)
      H2=BKN(0,Z1)
      H3=BKN(1,Z1)
      BJ02(M)=BS2(1)
      BJ12(M)=BS2(2)
      BY02(M)=H2
      BY12(M)=H3
C  CALCULATIONS OF THE DERIVATIVES OF I & K FUNCTION
      BJ1P(M)=BS2(1)-(BS2(2)/Z1)
      BY1P(M)=-H2-(H3/Z1)
      T1=-(G*ALPHA(M)*HPHI(M-1)+(BETA*HZ(M-1)/DIS(M-1)))*BY12(M)
      T2=BJ1P(M)*BY12(M)-BJ12(M)*BY1P(M)
      T3=(COKSQ(M)*ARG(M)*EZ(M-1)*BY1P(M))/(W*U0)
```

```
      T4=-(G*ALPHA(M)*EPHI(M-1)-(BETA*EZ(M-1)/DIS(M-1)))*BY12(M)
      T5=(W*U0*ARG(M)*HZ(M-1)*BY1P(M))
      A1(M)=(T1-T3)/(T2*COKSQ(M)*ARG(M)/(W*U0))
      A2(M)=(EZ(M-1)-A1(M)*BJ12(M))/BY12(M)
      B1(M)=-(T4+T5)/(T2*ARG(M)*W*U0)
      B2(M)=(HZ(M-1)-B1(M)*BJ12(M))/BY12(M)
      Z3=ARG(M)*DIS(M)
      BS3(1)=BIN(0,Z3)
      BS3(2)=BIN(1,Z3)
      H4=BKN(0,Z3)
      H5=BKN(1,Z3)
      BJ01(M)=BS3(1)
      BJ11(M)=BS3(2)
      BY01(M)=H4
      BY11(M)=H5
C  CALCULATIONS OF THE DERIVATIVES OF I & K FUNCTIONS
      BJ2P(M)=BS3(1)-(BS3(2)/Z3)
      BY2P(M)=-H4-(H5/Z3)
      EZ(M)=(A1(M)*BJ11(M)+A2(M)*BY11(M))
      HZ(M)=(B1(M)*BJ11(M)+B2(M)*BY11(M))
      EPHI(M)=-(G/ALPHA(M))*((BETA/DIS(M))*EZ(M)+W*U0*ARG(M)*(B1(M)*BJ2P
     *(M)+B2(M)*BY2P(M)))
      HPHI(M)=+(G/ALPHA(M))*((COKSQ(M)*ARG(M)/(W*U0))*(A1(M)*BJ2P(M)+A2(
     *M)*BY2P(M))+(BETA/DIS(M))*HZ(M))
      ER(M)=+(G/ALPHA(M))*((BETA*ARG(M))*(A1(M)*BJ2P(M)+A2(M)*BY2P(M))+W
     **U0*HZ(M)/DIS(M))
      HR(M)=((COKSQ(M)/(W*U0))*EZ(M)/DIS(M)+BETA*ARG(M)*(B1(M)*BJ2P(M)+
     *B2(M)*BY2P(M)))*(G/ALPHA(M))
      ETSQ(M)=((CDABS(EZ(M)))**2.0)+((CDABS(EPHI(M)))**2.0)+((CDABS(ER(M
     *)))**2.0)
      IF(DABS(DIS(M)-R1).LT.1.0D-10)  GO TO 57
C     IF(DABS(DIS(M)-2.0D0*R1).LT.1.0D-10)  GO TO 57
 24   CONTINUE
C  ==========================================================
 57   F9=BETASQ-EPSCL*FSKSQ
      F10=EPSCL*FSKSQ
      Z8=CDSQRT(F9)
      Z9=Z8*DIS(M)
      S1=CDSQRT(EPSCL)
C  CALLING BESSEL FUNCTIONS K OF ORDERS 0,1 FOR THE LAST LAYER
      H6=BKN(0,Z9)
      H7=BKN(1,Z9)
C  CALCULATIONS OF THE DERIVATIVE OF K FUNCTION
      BKP=-H6-(H7/Z9)
```

```
C ==========================================================
C SOLVING THE EIGENVALUE EQUATION FOR THE HE11 MODE
      X1=-(G/F9)*((BETA/DIS(M))*EZ(M)+W*U0*Z8*HZ(M)*BKP/H7)
      X2=-(G/F9)*((BETA/DIS(M))*HZ(M)+(F10*Z8*EZ(M)*BKP/(H7*W*U0)))
C ==========================
      IF (L1.EQ.1) THEN
C ==========================
      FZ=1.0D0-(EPHI(M)/X1)
C     FZ=EPHI(M)-X1
C ==========================================
      ELSE
      FZ=1.0D0+(HPHI(M)/X2)
C     FZ=HPHI(M)+X2
C ==========================================
      END IF
C ==========================================
      DO 32 I=1,L
      ETSQ(I)=ETSQ(I)*(ES/ETSQ(100))
C     WRITE(6,*)ETSQ(I)
C     WRITE(6,*)DIS(I)*1E6,DIMAG(EPHI(I)),ETSQ(I)
   32 CONTINUE
      WRITE(*,*)FZ
      RETURN
      END
```